

AD-A018 047

DEVELOPMENT OF A MINIATURE GAS-BEARING CRYOGENIC
TURBO REFRIGERATOR

R. B. Fleming, et al

General Electric Corporate Research and Development

Prepared for:

Army Mobility Equipment Research and Development Center

October 1975

DISTRIBUTED BY:

NTIS

National Technical Information Service
U. S. DEPARTMENT OF COMMERCE

343134

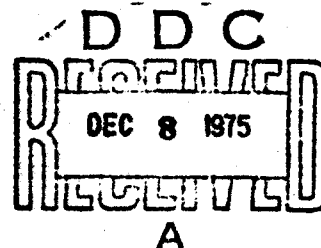
Contract No. DAAK02-71-C0026

DEVELOPMENT OF A MINIATURE GAS-BEARING CRYOGENIC TURBO REFRIGERATOR

ADA 018047

R. B. Fleming, et al.
Power Generation and Propulsion Laboratory
Corporate Research and Development
General Electric Company
Schenectady, New York 12301

19 November 1975



Final Report for Period 15 January 1971 - 1 October 1975

Approved for public release; distribution unlimited.

Prepared for

U. S. Army Mobility Equipment
Research and Development Center
Fort Belvoir, Virginia

Reproduced by
NATIONAL TECHNICAL
INFORMATION SERVICE
US Department of Commerce
Springfield, VA. 22151

REPRODUCED FROM
BEST AVAILABLE COPY

SRD-75-097

Unclassified

SECURITY CLASSIFICATION OF THIS PAGE (When Data Entered)

REPORT DOCUMENTATION PAGE		READ INSTRUCTIONS BEFORE COMPLETING FORM
1. REPORT NUMBER	2. GOVT ACCESSION NO.	3. RECIPIENT'S CATALOG NUMBER
4. TITLE (and Subtitle) Development of a Miniature Gas-Bearing Cryogenic Turbo Refrigerator		5. TYPE OF REPORT & PERIOD COVERED Final Report 15 January 1971-October 1975
7. AUTHOR(s) R. B. Fleming, D. B. Colyer, R. K. Terbush, B. B. Gamble, R. O. Oney		6. PERFORMING ORG. REPORT NUMBER SRD-75-097
9. PERFORMING ORGANIZATION NAME AND ADDRESS Corporate Research and Development General Electric Company Schenectady, New York 12301		8. CONTRACT OR GRANT NUMBER(s) DAAK02-71-C-0026
11. CONTROLLING OFFICE NAME AND ADDRESS U.S. Army Mobility Equipment Research and Development Center Fort Belvoir, Virginia 22060		10. PROGRAM ELEMENT, PROJECT, TASK AREA & WORK UNIT NUMBERS
14. MONITORING AGENCY NAME & ADDRESS (if different from Controlling Office)		12. REPORT DATE October 1975
		13. NUMBER OF PAGES 211 229
		18. SECURITY CLASS. (of this report) Unclassified
		15. DECLASSIFICATION/DOWNGRADING SCHEDULE
16. DISTRIBUTION STATEMENT (of this Report) Approved for public release; distribution unlimited.		
17. DISTRIBUTION STATEMENT (of the abstract entered in Block 20, if different from Report)		
18. SUPPLEMENTARY NOTES		
19. KEY WORDS (Continue on reverse side if necessary and identify by block number) Cryogenics, Refrigerator, Turboalternator, Heat Exchanger		
20. ABSTRACT (Continue on reverse side if necessary and identify by block number) The work described in this report was undertaken to advance the develop- ment of miniature cryogenic refrigerators that have high reliability, long life, minimum maintenance requirements, and no mechanical vibration. The type of system investigated utilized the Claude cycle for the production of refrigeration at 4.4°K. Temperatures at this level are suitable for numerous applications of superconductivity. (Continued on reverse side)		

DD FORM 1 JAN 73 1473

EDITION OF 1 NOV 65 IS OBSOLETE

Unclassified
SECURITY CLASSIFICATION OF THIS PAGE (When Data Entered)

Unclassified

SECURITY CLASSIFICATION OF THIS PAGE(When Data Entered)

Block 20

A distinguishing feature of the equipment under development is the use of high-speed dynamic compressors and turboalternators, in which all rotating parts are suspended on self-acting gas bearings. Such a system avoids sliding contact and wear during operation and avoids the contamination problems associated with oil lubricated compressors used in conventional cryogenic refrigerators.

The work described in this report was directed finally to the development of a system consisting of three cryogenic turboalternators, six helium centrifugal compressor stages, and a cryogenic heat exchanger with seven heat exchanger modules. Work was limited to the turboalternators and heat exchangers. A cryogenic turboalternator was developed and successfully tested to temperatures in the range of 80° to 100°K. In a parallel contract, a similar turboalternator was tested, with no load, at a temperature of 0.8°K.

The contract effort fell short of its goals because of difficulties encountered by a vendor in the construction of the heat exchanger assembly. The heat exchanger was designed and constructed using a novel approach that promised a significant advance in the technology of cryogenic heat exchangers and a sizable reduction in size and weight. However, it was found unexpectedly that not all development problems had been solved before construction began, and after a two year delay in delivery, the heat exchanger was found to be unusable for its intended function.

The work reported on the turboalternator represents an advance in the technology of cryogenic refrigeration. It is expected that heat exchanger development problems can be solved with further effort.

Unclassified

SECURITY CLASSIFICATION OF THIS PAGE(When Data Entered)

FOREWORD

This final technical report covers development work performed under Contract No. DAAK02-71-C-0026 with the U.S. Army Mobility Equipment Research and Development Center, Fort Belvoir, Virginia. The work was performed by the Power Generation and Propulsion Laboratory in the Research and Development Center of the General Electric Company in Schenectady, New York. The work described herein covers the period from January 1971 to October 1975.

The program was under the direction of Dr. L.I. Amstutz, of the Mobility Equipment Research and Development Center; this report was submitted in October 1975.

The General Electric Program Manager was Dr. R.B. Fleming.

The principal contributors to this program were:

R. B. Fleming
D. B. Colyer
R. K. Terbush
B. B. Gamble
W. R. Oney

TABLE OF CONTENTS

<u>Section</u>		<u>Page</u>
1	SUMMARY	1
2	INTRODUCTION.	3
	Objective	3
	Background.	4
	Accomplishments.	5
3	REFRIGERATION SYSTEM	7
	System Description.	7
	Original System.	7
	Systems Considered	7
	Positive Displacement Compressor.	7
	Hybrid Cycle.	7
	Split Cycle	9
	Final System Selection	10
	Cycle Analysis.	12
	Computer Program.	12
	System Design Criteria.	12
	System Weight.	12
	Results for 5-Watt System.	14
	Off-Design Calculations.	17
	Results for 3-Watt System.	18
	Off-Design Calculations.	22
	Experimental System Design	23
	General	23
	Radiation Shield.	23
	Cryogenic Piping	25
	Joule-Thomson Valve	25
	Liquid Nitrogen Cooler	26
	Cold End Cooler.	28
	Heat Leak.	28
	Layout of Cryogenic Section.	29
4	TURBOALTERNATOR.	31
	General	31
	Turboalternator Designs	32
	Preliminary Designs.	32
	Final Design of the 14°K Turboalternator	32
	Alternator Design.	34
	Gas Bearing Analysis and Design	36
	Assembly Procedure.	36
	Turboalternator Performance.	36
	Turboalternator Manufacture	36
	Turboalternator Performance Data Reduction Program	37

Preceding page blank

TABLE OF CONTENTS (Cont'd)

<u>Section</u>		<u>Page</u>
4	TURBOALTERNATOR (Cont'd)	
	Journal Bearing Material	43
	Very Low Temperature Test	43
	MERDC Turboalternator Assembly	53
	Preliminary Turboalternator Test	55
	MERDC Turboalternator Open-Cycle Tests	56
	Final Turboalternator Open-Cycle Tests	60
	Performance Test Results	63
5	CRYOGENIC HEAT EXCHANGERS	69
	General	69
	Design and Construction	69
	Test Results -- Kinergetics	69
	Test Results -- General Electric	69
	General Electric Test Facility	70
	Test Method	70
	Test Results	73
	Discussion of the Test Results	75
6	RECOMMENDATIONS	79
	Turboalternators	79
	Cryogenic Heat Exchangers	79
	Compressors	80
	Systems	80
 <u>Appendix</u>		
1	PRELIMINARY TURBOALTERNATOR DESIGNS	81
	Turboalternator Design Goals	82
	Design for 14°K Turboalternator	84
	Design for 55°K Turboalternator	85
	Design for 170°K Turboalternator	83
	Mechanical Arrangement	100
	Turbine Wheel Stress and Deflection Analysis	101
	14°K Unit	101
	55°K Unit	103
	170°K Unit	103
II	GAZ-BEARING ANALYSIS AND DESIGN	105
	Bearing Design Requirements	105
	Bearing Type Selections	105
	Journal Bearing Design	109
	Procedure	109

TABLE OF CONTENTS (Cont'd)

<u>Appendix</u>		<u>Page</u>
II	GAS-BEARING ANALYSIS AND DESIGN (Cont'd)	
	Performance	111
	Thrust Bearing Design	128
	Procedure	128
	Performance	129
III	TURBOALTERNATOR ASSEMBLY PROCEDURES	147
	Preliminary Cleaning and Handling	147
	Clean Room Assembly	147
	Initial Wheel-to-Shaft Assembly	149
	Balancing the Rotating Assembly	151
	Inner Thrust Bearing Assembly (Part 22)	151
	Outer Thrust Bearing Assembly (Part 13)	153
	Preliminary Journal Bearing Assembly and Stator Installation	153
	Shaft Housing Assembly	155
	Nozzle Assemblies	157
	Preliminary Thrust Bearing Shimming	157
	Installation of Thrust Proximity Probe	160
	Final Journal Bearing Pad Adjustments	162
	Turboalternator Operation	164
	Magnetizing Shaft Magnet	168
	Shaft Balance Equipment	169
	Parts List for Assembly Drawings	170
IV	SPECIFICATIONS FOR A SET OF SEVEN CRYOGENIC HEAT EXCHANGERS	173
	Specifications	173
	Thermal Performance and Pressure Drop	175
	Structure	175
	General Configuration	176
	Attachment to Flange	176
	Support of Components	176
	Structural Heat Leak	177
	Leakage	177
	Design Life	177
	Cleanliness	177
	Testing Procedures -- Thermal	177
	Cryogenic Tests	177
	Data Extrapolation	178
	Testing Procedures -- Pressure Drop	178
	Flow Tests	178
	Data Extrapolation	178
	Thermal Cycling	178

TABLE OF CONTENTS (Cont'd)

<u>Appendix</u>		<u>Page</u>
IV	SPECIFICATIONS FOR A SET OF SEVEN CRYOGENIC HEAT EXCHANGERS (Cont'd)	
	Testing Procedures -- Leakage	179
	Stream-to-Stream Leakage	179
	External Leakage	179
	Witness Testing	179
	Design Review	179
	Schedule	179
	Deliverable Items	180
V	KINERGETICS INCORPORATED FINAL REPORT	181
VI	HEAT EXCHANGER ANALYSIS	209
	Relating Results to Design Conditions	209
	Heat Transfer Data	209
	Pressure Drop Data	210
	Data Reduction Computer Program	210
	Effect of Helium Leakage, Thermal Radiation, and Axial Conduction on Heat Exchanger Performance	215
	Stream-to-Stream Leakage	215
	Leakage to Casing	215
	Thermal Radiation and Axial Conduction	216
VII	REFERENCES	219

LIST OF ILLUSTRATIONS

<u>Figure</u>		<u>Page</u>
1	Hybrid-Cycle System (Schematic Diagram)	8
2	Split-Cycle System (Schematic Diagram)	10
3	Claude-Cycle System (Schematic Diagram -- Corresponds to Computer Run 479)	11
4	Turboalternator Cryogenic Performance Power Output Versus Speed	16
5	Design Point for System with 3-Watt Capacity at 4.4°K (Run 479)	19
6	Input Power Versus Turbine Inlet Temperature	21
7	Cryosection (Schematic Diagram)	24

LIST OF ILLUSTRATIONS (Cont'd)

<u>Figure</u>		<u>Page</u>
8	Cooling System (Schematic Diagram)	26
9	Temperature Distribution	27
10	Helium-to-Nitrogen Heat Exchanger	27
11	Cryogenic Section.	30
12	Partial-Admission Radial-Impulse Turboalternator	31
13	Single-Stage Radial Impulse Turboalternator.	33
14	Turboalternator Parts.	38
15	Principal Turboalternator Instrumentation	39
16	Typical Single MERDC Data Point at Cryogenic Temperature.	41
17	Test Reduction Program	44
18	Open-Cycle Turboalternator Temperature Program.	45
19	TA Assembly Drawing 55SE477.	54
20	Shaft Orbits of MERDC Turboalternator Assembly, Operating at Room Temperature, No Load, and 100,000 RPM.	56
21	MERDC Turboalternator Assembly, Operating at Room Temperature, No Load, and 100,000 RPM	57
22	Alternator, 3-Phase, Line-to-Line Voltage Output of MERDC Turboalternator, Operating at Room Temperature, No Load, and 100,000 RPM	58
23	Alternator, 3-Phase, Line-to-Neutral Voltage Output of MERDC Turboalternator, Operating at Room Temperature, 8.5-Watt Resistive Load, and 100,000 RPM.	58
24	Shaft Orbits of MERDC Turboalternator Operating in Second Open-Cycle Test with 80°K Gas, 11-Watt Load, and 100,000 RPM.	60
25	MERDC Turboalternator Operating in the Same Conditions as Figure 24.	61
26	Shaft Orbits of MERDC Turboalternator Operating with 82°K Gas, 60.1-Watt Load, and 188,940 RPM with Nozzle Pressure Ratio of 2.4.	62

LIST OF ILLUSTRATIONS (Cont'd)

<u>Figure</u>		<u>Page</u>
27	MERDC Turboalternator Operating in the Same Conditions as Figure 26.	62
28	Overall Efficiency Versus Velocity Ratio	64
29	Wheel Efficiency Versus Velocity Ratio	64
30	Flow Factor Versus Velocity Ratio	65
31	Corrected Torque Versus Velocity Ratio	65
32	Flow Factor Versus Corrected Speed.	66
33	Electrical Output Power Versus Speed.	66
34	MERDC Run 103, Data Point 1, Data Obtained with Housing Bleed Valve Closed.	67
35	MERDC Run 103, Data Point 2, Data Obtained with Housing Bleed Valve Open, but not Corrected for Housing Leakage Flow.	68
36	Heat Exchanger Test (Schematic Diagram)	71
37	Heat Exchanger During Assembly	72
38	Design for 14°K Turboalternator.	86
39	Design for 55°K Turboalternator.	91
40	Design for 170°K Turboalternator, 0.625-inch Wheel	94
41	Design for 170°K Turboalternator, 1.00-inch Wheel.	97
42	First-Stage Wheel	101
43	Cold-Condition Effective Stress Contours.	102
44	Deflections for Wheel in Cold Condition	103
45	Pivoted-Pad Journal Bearing (Schematic Diagram).	106
46	Cryogenic Turboalternator Tilting-Pad Journal Bearing	107
47	Gimbal-Mounted Spiral-Groove Thrust Bearing.	108
48	Spiral-Groove Thrust Bearing (Schematic Diagram).	108
49	Design for 2.0-g Gas-Lubricated Journal Bearings	114
50	Design for 1.0-g Gas-Lubricated Journal Bearings	117
51	Design for 0.0-g Gas-Lubricated Journal Bearings	121
52	Journal Bearing Performance as a Function of G-Loading.	124

LIST OF ILLUSTRATIONS (Cont'd)

<u>Figure</u>		<u>Page</u>
53	Journal Bearing Performance as a Function of G-Loading	125
54	Journal Bearing Design Clearance and Pad Frequency Versus Spring-Pad Spring Rate	126
55	Thrust Bearing Groove Depth Versus Clearance	130
56	Helium-Lubricated Spiral-Groove Thrust Bearing, Design Run No. 4791003, Ratio of Outside to Inside Diameter 2.0	131
57	Helium-Lubricated Spiral-Groove Thrust Bearing, Design Run No. 4791004, Ratio of Outside to Inside Diameter 2.0	136
58	Helium-Lubricated Spiral-Groove Thrust Bearing, Ratio of Outside to Inside Diameter = 2.00, Design Run No. 4791003	139
59	Helium-Lubricated, Spiral-Groove Thrust Bearing, 1220-Microinch Groove Depth, Performance as a Function of Loaded Side Clearance	141
60	Helium-Lubricated, Spiral-Groove Thrust Bearing, 610-Microinch Groove Depth, Performance as a Function of Loaded Side Clearance	142
61	Helium-Lubricated, Spiral-Groove Thrust Bearing, 948-Microinch Groove Depth, Low-Temperature Performance as a Function of Loaded Side Clearance	143
62	Helium-Lubricated, Spiral-Groove Thrust Bearing, 948-Microinch Groove Depth, Room-Temperature Performance as a Function of Loaded Side Clearance	145
63	Turboalternator Assembly Tools and Fixtures	148
64	Turboalternator Parts	148
65	Wheel Pusher Assembly	150
66	Turboalternator Shaft Assembly Balance Specifications	151
67	Turboalternator Inner Thrust Bearing Assembly	152
68	Turboalternator Outer Thrust Bearing Assembly	153
69	Cryogenic Turboalternator Tilting-Pad Journal Bearing, Viewing Shaft from Thrust End	154
70	First-Stage Wheel Puller (d)	156
71	Turboalternator Dimensions for Shimming Thrust Bearing Position	158

LIST OF ILLUSTRATIONS (Cont'd)

<u>Figure</u>		<u>Page</u>
72	Thrust Clearance Ring Positioned in Inner and Outer Thrust Bearing Assemblies	159
73	Open-Cycle Test Station for Turboalternator.	161
74	Turboalternator Assembly on Open-Cycle Test Stand	164
75	Principal Turboalternator Instrumentation.	165
76	Open-Cycle Turboalternator Test Station	166
77	Open-Cycle Turboalternator Inlet Gas Instrumentation	167
78	Modified Model MV-6 Balancer.	169
79	Balancing Cradle Assembly	170
80	Claude Cycle System (Schematic Diagram)	174
81	Pressure and Temperatures Throughout System	175
82	Sample Data Run	212
83	Stream-to-Stream Leakage	215
84	Leakage to Casing	216
85	Radiation and Conduction.	217

LIST OF TABLES

<u>Table</u>		
1	Heat Loads for Hybrid-Cycle System	9
2	System Design Calculations -- 5 Watts at 4.4°K.	15
3	Design-Point and Off-Design-Point Computer Results.	22
4	Estimates of Heat Conduction Rates.	29
5	Alternator Design and Calculated Performance	35
6	Comparison of Wheel and Nozzle Characteristics.	36
7	MERDC Turboalternator Flow Test.	55
8	Heat Exchanger Test Results	73
9	Leakage Measurements	74
10	Turboalternator Designs	81

LIST OF TABLES (Cont'd)

<u>Table</u>		<u>Page</u>
11	Turboalternator Design Summary	83
12	Design Variations for 14°K Turboalternator	85
13	Design Variations for 55°K Turboalternator	89
14	Design Variations for 170°K Turboalternator.	90
15	Designs with a Maximum Operating Speed of 250,000 RPM	111
16	Design Speed Performance at 2.0 G.	112
17	Gas Bearing Performance Summary	113
18	Turboalternator Tilting-Pad Journal Gas-Bearing Design Summary	127
19	Thrust Bearing Design Comparison.	140
20	Turboalternator Spiral-Groove Thrust Bearing Design Summary	144
21	Axial Shimming Measurements for Turboalternator	158
22	Parts List for Single-Stage Radial Impulse Turboalternator.	171
23	Parts List for Inner Thrust Gimbal Assembly.	172
24	Parts List for Outer Thrust Gimbal Assembly.	172

Section 1

SUMMARY

The work described in this report was undertaken to advance the development of miniature cryogenic refrigerators that have high reliability, long life, minimum maintenance requirements, and no mechanical vibration. The type of system investigated utilized the Claude cycle for the production of refrigeration at 4.4°K. Temperatures at this level are suitable for numerous applications of superconductivity.

A distinguishing feature of the equipment under development is the use of high-speed dynamic compressors and turboalternators, in which all rotating parts are suspended on self-acting gas bearings. Such a system avoids sliding contact and wear during operation and avoids the contamination problems associated with oil lubricated compressors used in conventional cryogenic refrigerators.

The work described in this report was directed finally to the development of a system consisting of three cryogenic turboalternators, six helium centrifugal compressor stages, and a cryogenic heat exchanger with seven heat exchanger modules. Work was limited to the turboalternators and heat exchangers. A cryogenic turboalternator was developed and successfully tested to temperatures in the range of 80° to 100°K. In a parallel contract, a similar turboalternator was tested, with no load, at a temperature of 9.8°K.

The contract effort fell short of its goals because of difficulties encountered by a vendor in the construction of the heat exchanger assembly. The heat exchanger was designed and constructed using a novel approach that promised a significant advance in the technology of cryogenic heat exchangers and a sizable reduction in size and weight. However, it was found unexpectedly that not all development problems had been solved before construction began, and after a two year delay in delivery, the heat exchanger was found to be unusable for its intended function.

The work reported on the turboalternator represents an advance in the technology of cryogenic refrigeration. It is expected that heat exchanger development problems can be solved with further effort.

Section 2

INTRODUCTION

The application of superconductivity has been considered to reduce the size and weight of several types of electrical equipment. Since superconductivity requires temperatures in the range of 4° to 10°K, cryogenic refrigeration must be provided. A reduction in the overall electrical system size and weight can be realized only if the size and weight of the refrigerator is sufficiently small. At present, there is a need to reduce the size, weight, and maintenance requirements of cryogenic refrigerators, and to improve their reliability. With such advancements, the promise of superconducting apparatus and other cryogenic devices can be realized.

OBJECTIVE

The objective of this contract was to advance the development of high-reliability, maintenance-free, cryogenic refrigerators. This advancement was to be accomplished by the design, construction, and experimental evaluation of a 4.4°K refrigerator, based upon the Claude cycle principle, utilizing high-speed compressors and turboalternators with all rotating parts suspended on gas-lubricated bearings.

The tasks that were originally to be accomplished under this contract are outlined in the following four line items:

Line Items 0001 and 0002

- Conduct refrigerator cycle studies.
- Design, construct, and test 10°K turboalternator.
- Design, construct, and test transformer-rectifier.
- Assemble and test 80°K refrigerator (two-stage reversed Brayton cycle).

Line Items 0003 and 0004

- Design, construct, and test two regenerative motor-compressors for the first and second stages of a three-stage system.
- Design, construct, and test two power conditioners and transformer-rectifiers for the two new motor compressors.
- Modify 10°K and 80°K turboalternators to satisfy both the interim and final 4.4°K refrigerator specifications.
- Design, construct, and test a 4.4°K interim refrigerator using positive displacement compressors.

Preceding page blank

- Construct a final 4.4°K refrigerator by replacing positive displacement compressors with three single-stage dynamic compressors.

As the work progressed, these original tasks were modified, as will be described in the following paragraphs.

BACKGROUND

The present contract was preceded by an earlier Mobility Equipment Research and Development Center (MERDC) contract (No. DAAK02-68-C-0320), and was conducted in parallel with an Air Force contract (No. F33615-71-C-1003). The technology and some parts and equipment from both these contracts were utilized in the present contract. In this report, references will be made to reports from these other contracts (Refs. 1 through 5).

As the present contract was originally constituted, the system was to have included three helium regenerative compressor stages, two turboalternators, and a set of five cryogenic heat exchangers. Of these components, one compressor stage and one turboalternator were to have been made available as Government furnished equipment from previous MERDC contracts. The set of heat exchangers were to have been obtained from a previous General Electric funded development program. The refrigeration capacity using these components had previously been estimated to be between 1 and 2 watts at 4.4°K.

When detailed cycle studies were performed early in this program, it was found that the system then being considered would produce only a fraction of one watt. In order to increase the probability of reaching the required temperature of 4.4°K, it was considered necessary to construct a system with higher refrigeration capacity as its design goal.

A number of system changes were considered to improve capacity, such as:

- additional regenerative compressor stages
- positive displacement compressors for higher pressure ratios
- heat exchangers with higher effectiveness
- different cycle arrangements

During the time these systems investigations were being carried out, all work on the contract was stopped except for cycle studies. A stop work order was in effect from 31 March 1971 to 1 November 1971.

After consideration of a number of alternatives, the final system selected had a larger refrigeration capacity (3 watts at 4.4°K), six centrifugal compressor stages (instead of three regenerative compressor stages), and three turboalternators (instead of two).

Late in 1973, MERDC decided to cut back on the scope of the contract, and to eliminate most of the work in Line Items 0003 and 0004. In December 1973, the contract was modified to cover just the following tasks:

- Conduct refrigerator cycle studies.
- Design, construct, and test a 10°K turboalternator.
- Design and construct a cryosection consisting of a set of heat exchangers, a Joule-Thomson loop, a vacuum vessel for thermal insulation, and necessary piping and instrumentation.
- Test the turboalternator and the Joule-Thomson loop at final operating temperatures, using liquid nitrogen for precooling, and a positive displacement compressor.

The heat exchanger described in Section 5 was designed and constructed by a vendor who used a novel approach for design and construction. Unfortunately, not all the development problems had been worked out prior to construction, and a number of unexpected difficulties were encountered by the vendor during construction. The exchanger was delivered almost two years late, and upon testing, it was found that the thermal effectiveness was too low to permit cooldown and test of the turboalternator near its design temperature.

ACCOMPLISHMENTS

The work described in this report advanced the development of cryogenic refrigeration systems using miniature high-speed turboalternators with self-acting gas bearings.

Designs were derived for systems that tended toward minimum weight and input power, within certain constraints of component sizes and refrigeration capacity. System designs are described under Section 3, "Refrigeration System."

A turboalternator was constructed and was tested at temperatures in the range of 80° to 100°K. Extensive measurements of performance parameters were made at those temperatures.

To determine the behavior of the turboalternator at even lower temperatures, a unit was constructed using the identical parts that were tested under the MERDC contract, with the exception of the turbine nozzle and the alternator. This unit was tested under a program sponsored by the Advanced Research Projects Agency to a temperature of 9.8°K (possibly the lowest temperature at which a turboalternator with self-acting gas bearings had been tested). Details of turboalternator construction and testing are given in Section 4, "Turboalternator."

The cryogenic heat exchanger development was not fully completed under this contract. However, a number of design and construction advances were

made toward the development of a cryogenic heat exchanger that has the potential of sizable reductions in size, weight, and cost, compared with presently available heat exchangers. Details of the heat exchanger development are given in Section 5, "Cryogenic Heat Exchangers."

Section 3

REFRIGERATION SYSTEM

SYSTEM DESCRIPTIONORIGINAL SYSTEM

As discussed in Section 2, "Introduction," the original system that was to be constructed under the contract consisted of three regenerative compressor stages, two turboalternators, and a set of five cryogenic heat exchangers. The detailed cycle analysis conducted early in the program showed that the refrigeration capacity at 4.4°K was only a fraction of one watt, rather than the 1 to 2 watts that had been estimated in earlier, less precise calculations. With a predicted capacity of only a fraction of one watt, the risk of not being able to reach the desired temperature of 4.4°K was considered too high. Therefore, means to achieve higher capacities, using as many already available components as possible, were sought. Some of the alternatives that were considered are discussed in the following paragraphs.

SYSTEMS CONSIDEREDPositive Displacement Compressor

One means of increasing the refrigeration capacity is to increase the pressure ratio of the compressor. The addition of more regenerative compressor stages was considered to be too costly; therefore, positive displacement compressors were considered. The compressors had to be noncontaminating, small, and lightweight. MERDC personnel carried out this investigation. In their search, no positive displacement compressors were found that were compatible with the system goals of small size and light weight.

Hybrid Cycle

During the investigation of positive displacement compressors, a cycle that takes advantage of higher pressure ratios was considered. The Claude cycle results showed that higher pressure ratios benefited the cycle performance because of higher Joule-Thomson coefficients, but at the expense of degraded turbine performance. A hybrid cycle (Figure 1) was considered in an attempt to overcome this problem. Each of the compressors shown is assumed to be a single-stage, positive displacement compressor. This cycle is a combination of a two-stage reversed Brayton cycle and a Joule-Thomson cycle.

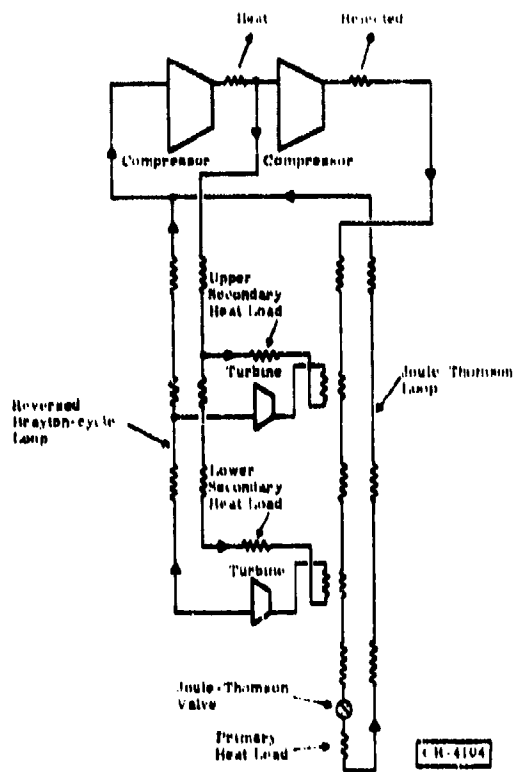


Figure 1. Hybrid-Cycle System
(Schematic Diagram)

In the analysis, the pressure levels were first established arbitrarily:

- Compressor suction -- 1.2 atm
- Intermediate -- 2.6 atm
- Compressor discharge -- 5.0 atm

Heat-exchanger pressure drops were ignored.

Next, the flow rate through the Joule-Thomson loop was calculated to be 2.14 g/sec, to produce the required 5-watt refrigeration capacity at 4.4°K. Next, the heat that must be removed from the Joule-Thomson loop at the 16°K cooling station was calculated to be 16.0 watts. The corresponding heat load at the 75°K level was 36.0 watts. A summary of heat loads is given in Table 1.

Next, a computer cycle calculation was carried out for a reversed Brayton-cycle system with the total heat loads given in Table 2. The flow rate for the reversed Brayton cycle was 11.7 g/sec, giving a total flow rate in the first-stage compressor of 2.14 plus 11.7, or 13.8 g/sec.

Table 1
HEAT LOADS FOR HYBRID-CYCLE SYSTEM

Temperature (°K)	Useful Capacity (watts)	Joule-Thomson Load (watts)	Total Load on Reversed Brayton Cycle (watts)
4.4	5.0	--	--
16.0	10.0	16.0	26.0
75.0	20.0	36.0	56.0

The power inputs were:

<u>Stage</u>	<u>kw</u>
First	12.4
Second	<u>1.6</u>
Total	14.0

This input power is about seven percent lower than the power for an equivalent Claude cycle.

Split Cycle

Another cycle variation that was considered, the "split cycle," is shown in Figure 2. This system is similar to the hybrid cycle above. However, in the split cycle, the refrigerant fluids in the two sides of the system are entirely separate; the only communication between the reversed Brayton and the Joule-Thomson cycles is by means of the two counterflow heat exchangers, which transfer heat from the high pressure stream of the Joule-Thomson system to the cooling stations of the reversed Brayton cycle.

There are several advantages of this arrangement. First, the compressor for the Joule-Thomson system provides the motive force for circulating the helium through the cooling passages in the primary heat load. This arrangement is less complicated and more reliable than the use of a pump for circulating a secondary fluid at the 4.4°K level.

Another advantage is that the helium gas in the reversed Brayton cycle system can be completely sealed and maintained at a high purity level. High purity is particularly needed in this part of the system because of the close tolerances in the gas bearings. Opening up and recharging helium in the primary heat load would not affect the helium charge of the reversed Brayton cycle.

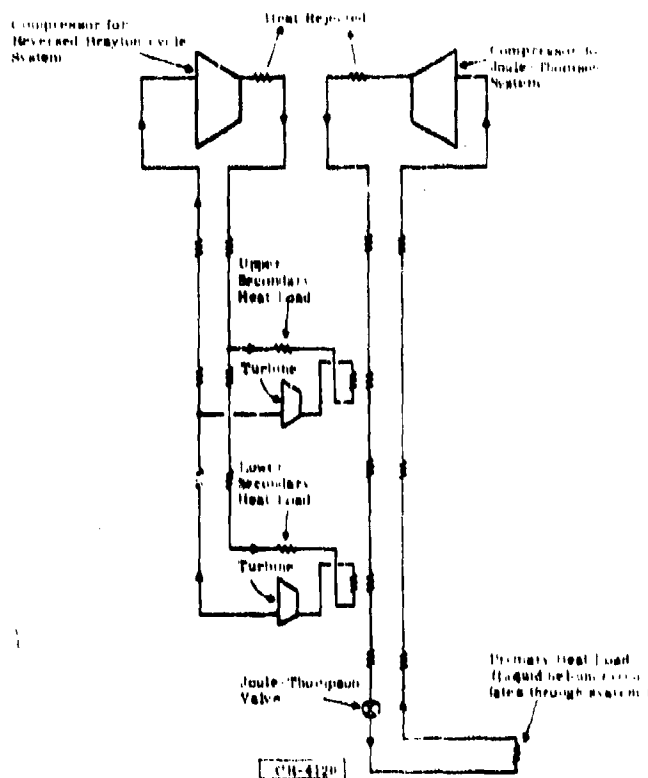


Figure 2. Split-Cycle System (Schematic Diagram)

A further advantage is that the turbomachinery of the reversed Brayton cycle is compatible with low pressures, high volume flow rates, and low pressure ratios. In contrast, the Joule-Thomson cycle requires high pressure-ratios and only small volume-flow rates; these requirements are more compatible with positive displacement compressors. The optimum system may, therefore, consist of turbocompressors in the reversed Brayton cycle and positive displacement compressors in the Joule-Thomson cycle.

It was concluded that neither the split cycle nor the hybrid cycle would be suitable because of the unavailability of satisfactory positive displacement compressors and because of the extra weight and size associated with additional compressor stages.

FINAL SYSTEM SELECTION

After investigation of systems with 5- to 10-watt capacity, it was concluded that contract goals could be met best with a Claude cycle system of 3-watt capacity at 4.4°K. Instead of the original three regenerative compressor stages, the compressor selected has six centrifugal compressor stages. Two centrifugal stages are mounted on a single shaft, one on either

side of the drive motor. There will, therefore, be three compressor modules, with two compressor stages per module. The centrifugal compressors were chosen in place of the regenerative compressors because, in larger sizes, centrifugal compressors are much more efficient than regenerative compressors.

In place of the original two turboalternators, there are three. The number of turboalternators had to be increased to three in order to increase system capacity without resorting to a larger turboalternator frame size.

The heat exchanger selected consists of seven heat exchanger modules.

A schematic diagram of the final system selected, based on computer Run 479, is given in Figure 3. Details of the system analysis, and the basis for the final system selection, are given below under "Cycle Analysis."

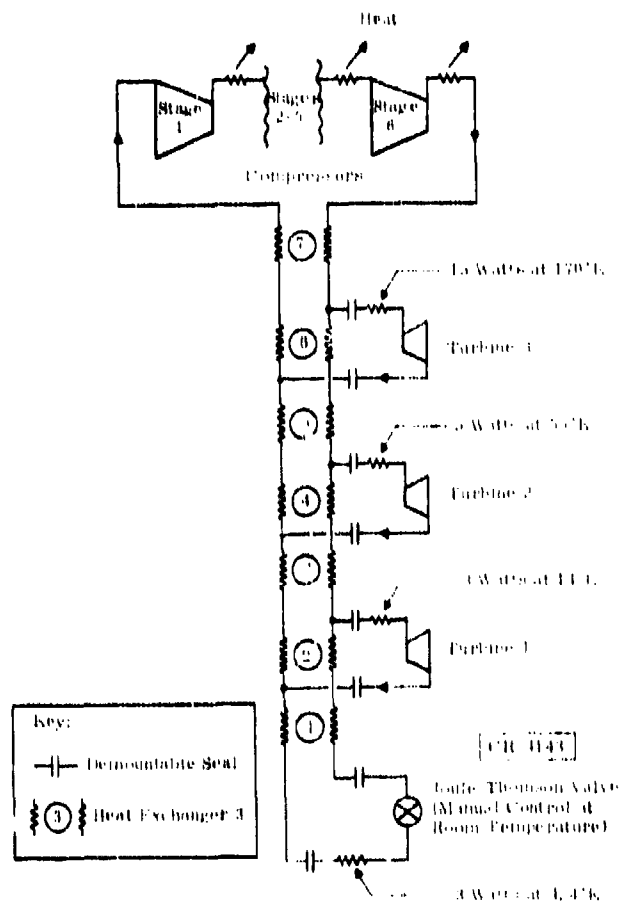


Figure 3. Claude-Cycle System (Schematic Diagram -- Corresponds to Computer Run 479)

CYCLE ANALYSIS

COMPUTER PROGRAM

The computer program, "REFRIG," that was used for cycle analysis, is described in detail by D. B. Colyer et al. (Ref. 3, Vol. 1, pp. 9-28).

SYSTEM DESIGN CRITERIA

The principal design criteria were reliability and total system weight and size. Other criteria were cost and input power.

The goals for total system weight (not including dewar or interface with the system to be cooled) were:

- For a 5-watt capacity at 4.4°K, the goal was 400 pounds or less.
- For a 10-watt capacity at 4.4°K, the goal was 500 pounds or less.

For design, the maximum heat-exchanger effectiveness was set at 98.5 percent, a conservative design goal giving reasonable assurance that the performance could be achieved.

The centrifugal compressor impeller tip speed was set at less than 520 m/sec (1700 ft/sec).

The compressor suction pressure was set at above one atmosphere.

At the time the cycle studies were being made, there were two turbo-alternator frame sizes being designed under contract with the Air Force (Ref. 3). (The "small" and "large" turboalternator frame sizes in this section refer to these Air Force sizes.) It was desired to design the MERDC turboalternator to the small frame size, which is the size previously designed and constructed for MFRDC (Ref. 2). It was believed the development risk would be higher with the large frame size.

SYSTEM WEIGHT

A complete analysis of system weight was impossible without knowing the exact system design. However, an approximate weight calculation was developed and applied to the system calculation as a means of evaluating designs.

An approximate weight was first developed for all components, based on electrical power input to the conditioner-controller. These weights were estimated by General Electric engineers, based upon compressor modules of about a two-kw power level, each module having two compressor stages and one motor:

<u>Component</u>	<u>Weight</u>
Compressor subsystem (two stages in each module)	
Power conditioner-controller	4 lb/kw*
Motor	5 lb/kw
Compressor (frame, impeller, etc.)	7 lb/kw
Aftercooler (for transfer of heat from helium to cooling fluid)	2 lb/kw
Heat rejector (for final rejection of heat from cooling fluid to air)	<u>7 lb/kw</u>
Total compressor subsystem	25 lb/kw
Heat-exchanger core	(Calculated by computer)
Heat-exchanger headers	(10% of core weight)
Turboalternator (including piping and filter)	10 lb/turboalternator
Dewar (not included in system weight calculations)	70 pounds

It is apparent that basing the compressor subsystem weight purely on the basis of input power is a crude approximation. A report by P. G. Wapato presented much more detailed compressor weight estimates (Ref. 6). In some cases, the Wapato report estimates differed considerably from those given above; in those instances averages were generally taken between the estimates by Wapato and by the General Electric Company. In the summary of the resulting weight calculation, which appears below, the following symbols are used:

<u>Symbol</u>	<u>Meaning</u>
N	Number of compressor modules, each having two centrifugal compressor stages and one motor.
P_i	Electrical input power to power conditioner-controller, for the <i>i</i> th compressor module (kw)
W_c	Weight of a single compressor module, with two compression stages, not including motor (pounds)
W_h	Total weight of compressor aftercoolers and heat rejector, for one compressor module (pounds)

*Assumes conversion from 60 to 1500 hertz; also assumes water cooling. (Estimated weight for air-cooled power conditioner-controller is 11 lb/kw.)

<u>Symbol</u>	<u>Meaning</u>
W_m	Weight of motor in one compressor module (pounds)
W_p	Weight of power conditioner-controller for one compressor module (pounds)
W_t	Weight of total compressor subsystem (pounds)

For the motor, the weight was calculated to be:

$$W_m = 4.0 P_i^{2/3} \quad (1)$$

The compressor weight was:

$$W_c = 20 \quad (2)$$

The weight of the power conditioner-controller was the same as above:

$$W_p = 4 P_i \quad (3)$$

The aftercooler and heat-rejector weight was also the same as above:

$$W_h = 9 P_i \quad (4)$$

Adding all these weights together gives, for the total weight of the compressor subsystem:

$$W_t = 20 N + \sum_{i=1}^N (4.0 P_i^{2/3} + 13 P_i) \quad (5)$$

This equation was used to estimate system weights in the analysis that follows.

RESULTS FOR 5-WATT SYSTEM

A number of systems were studied, with refrigeration capacities of 5 watts at 4.4°K and secondary loads totaling 30 watts at higher temperatures. A summary of the results is presented in Table 2.

The total system weight is the sum of the compressor subsystem, the heat exchanger core weight with ten percent of the core weight added for headers, and 10.0 pounds for each turbine (including piping and filters). Dewar and radiation shield weight are not included in the system weight because these weights will be shared by the system to be cooled.

As mentioned previously, there are two turboalternator frame sizes, large and small. The frame size can be determined by Figure 4, which was taken from Colyer and Oney, Figure 4.2.3-1 (Ref. 1). A large-frame

Table 2
SYSTEM DESIGN CALCULATIONS -- 5 WATTS AT 4.4°K

Run	Compressor Stages	Turbines	Refrigerator Capacity (w/ Temperature (°K))					Turbine Stages (Cold to Warm) ⁽¹⁾	Input Power (kw)	Compressor Subsystem Weight (lb)	Heat Exchanger Core Weight (lb)	Total System Weight (lb)
			Station 1	Station 2	Station 3	Station 4	Station 5					
394	6	4	5/4.4	5/12	10/60	15/100	0/100	L-S-S-S	15.0	290	164	510
395	6	4	5/4.4	5/15	10/65	15/100	0/120	S-S-S-S	16.8	316	210	597
397	4	4	5/4.4	5/15	10/65	15/100	0/100	L-L-S-L	22.8	376	653	1135
399	6	4	5/4.4	5/12	10/60	15/110	0/210	L-L-L-S	15.8	276	330	606
401	4	3	5/4.4	5/14	10/60	15/170	--	L-L-S	18.8	320	325	706
402	4	3	5/4.4	5/12	10/60	15/170	--	L-L-S	17.0	294	260	554
403	4	3	5/4.4	5/10	10/60	15/170	--	L-L-S	18.0	326	326	711
404	4	3	5/4.4	5/12	10/60	15/100	--	L-L-L	16.5	277	194	530
405	4	3	5/4.4	5/10	10/60	15/100	--	L-L-L	17.4	290	214	565
416	6	3	5/4.4	5/14	10/60	15/170	--	S-L-S	16.6	313	165	563
411	6	3	5/4.4	5/14	10/50	15/170	--	L-L-L	16.3	300	144	497
412	6	3	5/4.4	5/12	10/50	15/170	--	L-L-L	16.1	300	139	489
433	6	3	5/4.4	5/12	10/60	15/100	--	L-S-L	15.9	303	107	451
436	6	3	5/4.4	5/14	10/60	15/100	--	S-S-L	16.6	313	119	474
437	6	3	5/4.4	5/14	10/60	15/170	--	L-L-L	16.6	313	156	513
438	6	3	5/4.4	5/14	10/55	15/170	--	L-L-L	16.4	310	140	503
439	6	3	5/4.4	5/14	10/55	15/170	--	S-S-S	13.9	274	154	474
440	5	3	5/4.4	5/14	10/55	15/170	--	L-L-L	19.9	300	101	508
414	6	2	5/4.4	10/16	20/80	15/170	--	L-L	26.4	300	129	530
415	6	2	5/4.4	10/14	20/80	--	--	L-L	26.1	304	124	521
416	6	2	5/4.4	10/14	20/80	--	--	L-L	26.3	307	114	512
424	6	2	5/4.4	10/13	20/80	--	--	L-L	26.4	309	215	515
425	6	2	5/4.4	10/14	20/100	--	--	L-L	22.2	306	170	602
427	4	2	5/4.4	10/14	20/100	--	--	L-L	26.2	467	300	826
428	4	2	5/4.4	10/14	20/80	--	--	L-L	24.5	401	285	734
430	4	2	5/4.4	10/12	20/80	--	--	L-L	27.3	441	325	810
430	4	2	5/4.4	10/16	20/80	--	--	L-L	23.0	441	368	810
431	4	2	5/4.4	10/16	20/70	--	--	L-L	29.3	489	352	876
432	4	2	5/4.4	10/14	20/70	--	--	L-L	23.9	382	258	686

1) 'L' indicates "Large"; 'S' indicates "Small".

2) Optimum for four compressor stages

3) Optimum for six compressor stages

4) Exchanger effectiveness is 90.9%

5) Exchanger effectiveness is 90.9%

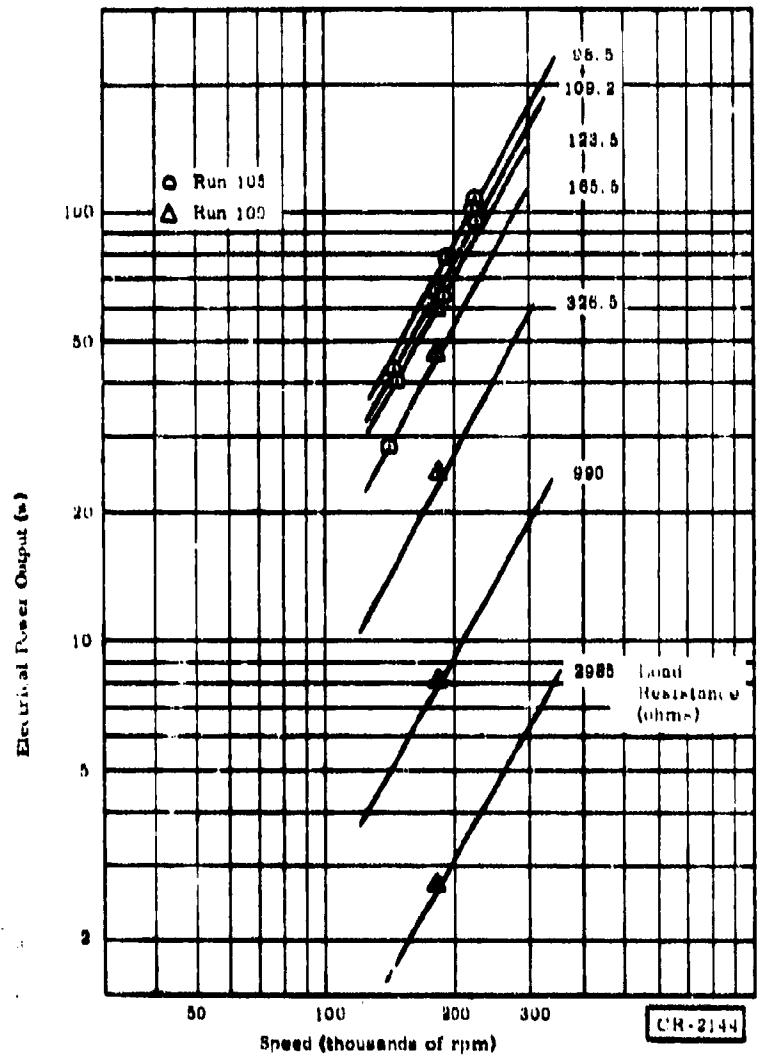


Figure 4. Turboalternator Cryogenic Performance Power Output Versus Speed

turboalternator is considered to be a unit whose speed-power characteristic falls above the highest curve in the figure, while a small-frame turboalternator falls on or below that highest curve. For example, a unit with a speed of 180,000 rpm and a power output of 50 watts would require a small frame, while a unit of the same speed with a power output of 100 watts would require a large frame.

Many of the computer runs were made in attempts to produce a system design with all turbines of a small frame size. This was found not to be possible with the refrigeration capacities chosen. In all runs, at least one of the three turbines exceeded the small frame size.

It was concluded, on the basis of only a few runs, that there was no advantage in four-turbine systems and that the additional complexity was not justified. Two-turbine systems (Runs 414 through 432) showed larger system weight than three-turbine systems. The choice was therefore a three-turbine system, with either four or six compressor stages (two- or three-compressor modules). Most of the runs were made on three-turbine systems.

For systems with four compressor stages and three turbines, the optimum system was represented by Run 404, with a system weight of 530 pounds.

For six compressor stages and three turbines, the optimum system was represented by Run 433 (system weight 451 pounds). This system comes close to the goal of 400 pounds for a system having a 5-watt capacity at 4.4°K.

Off-Design Calculations

Present computer programs are "design" programs in that, generally speaking, system performance is specified as program input and component geometry is calculated and presented as output. A true off-design program would do the opposite: It would accept geometry as input and would calculate system performance over a range of values for various parameters.

Such calculations were beyond the scope of the present contract; however, pseudo off-design calculations were performed using the present design program. Starting with the system of Run 433 (six compressor stages and three turbines), the heat-exchanger effectiveness was lowered to 98.0 percent to determine the effect of missing the heat exchanger design goal of 98.5 percent. At the same time, in Run 442 (not listed in Table 2), the two coldest heat loads were lowered to a level that would maintain the same total helium mass flow rate (10.4 g/sec) as in the original design (Run 433). The resulting heat loads required to maintain this flow rate were 3 watts at the 4.4° and 12°K levels (compared to the original design of 5 watts at each temperature station). The heat exchanger and turbine designs of Run 442 changed only slightly from the original design of Run 433, and the compressor design was unaffected because the flow rate and pressure ratio were the same.

The same pseudo off-design procedure was applied to design Run 404 (four compressor stages and three turbines). In Run 445 (not given in Table 2), the two coldest heat loads were found to drop to 2.8 watts each (from the original design of 5 watts) as a result of the heat-exchanger effectiveness dropping from 98.5 percent to 98.0 percent.

In Run 451, the same off-design procedure was applied to design Run 404, but this time the turbine nozzle coefficients for all three turbines were lowered from the design value of 0.90 to 0.85, which dropped the turbine efficiency about five percent. The two coldest heat loads were found to drop from the original 5 watts each to 3.8 watts.

Likewise, the same drop in nozzle coefficients was used in Run 459, applied to design Run 433. The two coldest loads dropped from the original 5 watts each to 3.8 watts.

Next, starting with design Run 433, the heat-exchanger efficiencies were lowered to 98.0, and the nozzle coefficients were dropped to 0.85 at the same time, in off-design Run 466. The two coldest loads dropped from the original 5 watts each to 2.2 watts.

Likewise, starting with design Run 404, the same parameters were changed the same amounts in off-design Run 470, and the two coldest loads dropped to 1.98 watts.

It can therefore be seen that systems with four or six compressor stages have about the same sensitivity to changes in heat exchanger and turbine performance and that the design for 5 watts at the coldest station appears adequate to maintain some capacity even in the event of depressed heat exchanger and turbine performance.

RESULTS FOR 3-WATT SYSTEM

All attempts to design a system with 5-watt capacity at 4.4°K and with three turboalternators of small frame size failed. It was found that the capacity at 4.4°K had to be reduced to 3 watts in order to achieve the desired small frame size for all three turboalternators.

Figure 5 is a printout of Run 470, which represents a system having 3-watt capacity at 4.4°K. There are six compressor stages (three compressor modules) and three turbines. All three turboalternators are of the small frame size. This run was selected as the system design basis. (See Figure 3 for a schematic diagram of the system.)

The Run 470 system has a compressor subsystem of three modules, with two centrifugal stages each (a total of six stages), and three turboalternators.

The total system weight was calculated to be 388 pounds:

<u>Component</u>	<u>Weight (pounds)</u>
Compressor subsystem	262.7
Heat-exchanger core	84.9
Heat-exchanger headers (10% of core)	8.5
Turboalternators (including filters and piping), at 10 pounds each	<u>30.0</u>
Total	388

The dewar and radiation shield weights are not included in the above calculation.

Before Run 470 was finally selected, a number of computer cycle calculations were made in an attempt to optimize the system. First, the temperature into the coldest turbine was varied. The results are shown in Figure 6,

*Using Equation 5

RUN

REFRIG 11137EST 12/15/71

RUN NUMBER 479

ITERATIONS * * * * *
* * * * * 24

ELEMENT SEQUENCE = 4 2 2 2 1

LOCATION	LOAD(W)	TEMP(K)	FLOW(G/SEC)
1	3.000	4.400	2.106
2	3.000	14.00	3.360
3	5.000	55.00	1.486
4	15.00	170.0	0.7343

CYCLE DESIGN POINTS ? YES

LOC.	P(ATM)	TEMP(K)	LOC.	P(ATM)	TEMP(K)
1 1	2.800	5.747	1 2	1.180	4.406
1 3	1.174	4.400	2 2	2.814	12.57
2 1	2.828	13.54	2 4	1.174	4.400
2 3	2.800	5.747	2 6	1.157	12.95
2 5	1.142	12.45	3 2	2.842	49.27
2 7	2.814	14.00	3 4	1.157	12.95
3 1	2.856	54.35	3 6	1.139	52.73
3 3	2.828	13.54	4 2	2.871	155.3
3 5	1.145	48.73	4 4	1.139	52.73
3 7	2.842	55.00	4 6	1.122	163.5
4 1	2.885	166.1	5 2	2.885	166.1
4 3	2.856	54.35	5 4	1.100	332.4
4 5	1.128	153.8			
4 7	2.871	170.0			
5 1	2.914	335.0			
5 3	1.122	163.5			

TURBOALTERNATORS ? YES

-----TURBOALTERNATORS-----				
LOC.	DIA(IN)	PWR(W)	EFFIC.	RPM
2	0.5000	27.14	0.3730	118022.
3	0.7000	48.47	0.3746	161695.
4	1.000	61.89	0.3062	186765.

CR-4132

Figure 5. Design Point for System with 3-Watt Capacity at 4.4°K (Run 479)
(Sheet 1 of 3)

LOC.	ADM.FRACT.	W.LOSS(W)	FLG.FAC.	SP.VEL.RAT.
2	0.3056	0.7241	1.588	0.3773
3	0.1670	1.701	1.378	0.3609
4	0.1074	4.772	1.185	0.3349

LOC.	T.BRG.NB.	T.LD CØ.	T.MIN F.(IN)	BRG.PWR.(W)
2	0.3790F-01	0.1382E-01	0.1160E-02	0.3647
3	0.1269	0.1445E-01	0.1160E-02	1.552
4	0.3117	0.1621E-01	0.1160E-02	4.102

LOC.	J.BRG.NB.	J.LD CØ.	BL.HT./CUT.DIA.
2	0.7863	0.4741E-01	2.065
3	1.677	0.4959E-01	2.210
4	2.000	0.5561E-01	1.380

USE HRDWR PROGRAM ? YES

-----HEAT EXCHANGER DESIGN-----

LOC.	WT(LBS)	LENGTH(CM)	VOL(CU.FT.)	EFFECT
2 B	1.243	11.50	0.2035E-01	0.9850
2 U	0.1509	1.395	0.2469E-02	0.9123
3 B	12.90	47.32	0.2604	0.9851
3 U	0.6474	4.017	0.1613E-01	0.9035
4 B	29.20	58.51	0.6707	0.9849
4 U	1.671	4.629	0.3586E-01	0.8738
5 B	38.89	60.68	0.9383	0.9851
TOTALS	84.91		1.944	

CENTRIFUGAL COMPRESSOR? YES

-----CENTRIFUGAL COMPRESSOR-----

POWER TO CONDIT-CONTROL (KW)	13.12		
AMBIENT TEMPERATURE (K)	322.0		
PRESSURE RATIO	2.649		
MASS FLOW (G/SEC)	7.686		
MODULE IN.	POWER(KW)	RPM	ROT.SPD.(FPS)
1	4.829	0.9100E+05	667.2
2	4.391	0.9100E+05	667.2
3	3.903	0.9100E+05	667.2

BEARINGS

CR-4182

Figure 5. Design Point for System with 3-Watt Capacity at 4.40K (Run 479) (Sheet 2 of 3)

MODULE	T.BRG.NO.	T.LD.CO.	T.MIN F.(IN)	BRG.PWR.(W)
1	6.332	0.4618E-01	0.1323E-02	453.7
2	4.435	0.3345E-01	0.1323E-02	474.2
3	3.274	0.2585E-01	0.1323E-02	517.4

MODULE	J.BRG.NO.	J.LD.CO.	J.MIN F.(IN)	CRIT.SPEED
1	2.000	0.7605E-01	0.1223E-02	0
2	2.000	0.5507E-01	0.1223E-02	0
3	2.000	0.4257E-01	0.1223E-02	0

STAGE	SP.SPEED	AERD.EFF.	TIP SPD(FPS)	DIA. (IN)
1	0.4338E-01	0.6367	1696.	4.271
2	0.4060E-01	0.6153	1696.	4.271
3	0.3969E-01	0.6077	1629.	4.100
4	0.3907E-01	0.6022	1563.	3.936
5	0.3863E-01	0.5983	1501.	3.779
6	0.3842E-01	0.5964	1441.	3.628

STAGE	PRESS.RATIO	COOL.EFFCTV.
1	1.214	0.7662
2	1.204	0.7765
3	1.184	0.7620
4	1.166	0.7469
5	1.150	0.7311
6	1.136	0.7148

CR-4132

Figure 5. Design Point for System with 3-Watt Capacity at 4.4°K (Run 479)
(Sheet 3 of 3)

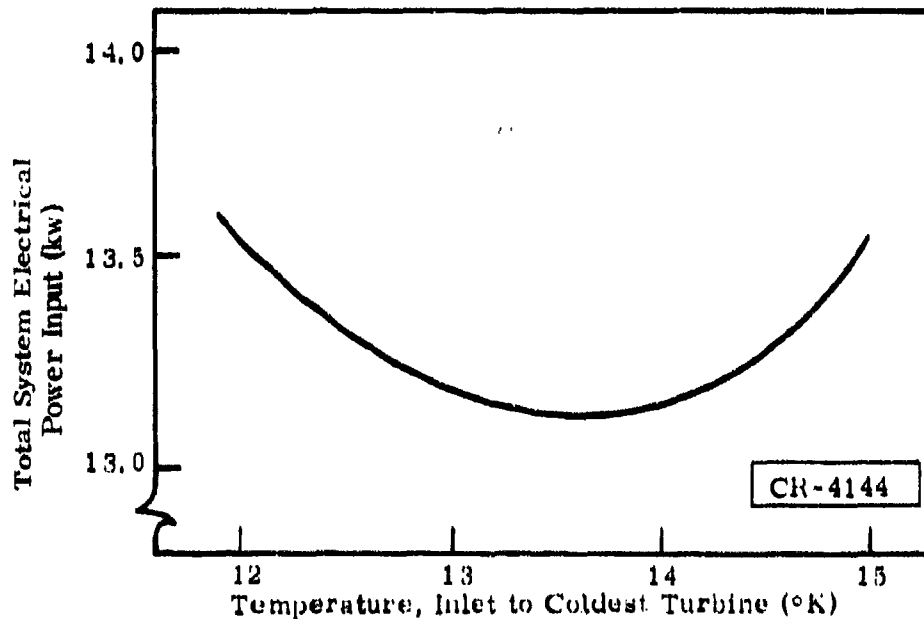


Figure 6. Input Power Versus Turbine Inlet Temperature

which indicates that the temperature of 14°K is optimum from an input power standpoint.

Several additional calculations were made with variations in the warmer two turbine temperatures. While slightly lower input powers could be achieved by changing those temperatures, changes in temperatures in a direction to attain lower input powers also caused at least one turbine to exceed the maximum power level of a turboalternator with small frame size. The requirement of small frame size therefore imposes the temperatures used in Run 479 for the warmer two turbines.

Off-Design Calculations

Pseudo off-design calculations were applied to design-point Run 479, to determine the effect of degraded performance of cryogenic heat exchangers and turboalternators. Table 3 shows the results of design-point Run 479 and three off-design-point runs. The total flow rate that was held approximately constant for all these runs was the design-point value of 7.69 g/sec.

Table 3
DESIGN-POINT AND OFF-DESIGN-POINT COMPUTER RESULTS

Characteristic	Run			
	479	482	490	478
Parameter degraded	No degradation (design point)	Turbine nozzle coefficient	Heat exchanger thermal effectiveness	Both turbine nozzle coefficient and heat-exchanger effectiveness
Turbine nozzle coefficient (all three turbine), dimensionless	0.90	0.85	0.90	0.85
Heat exchanger thermal effectiveness, all four balanced flow exchangers (1, 2, 3, and 4), dimensionless	0.985	0.98	0.980	0.980
Total helium flow rate (grams/sec)	7.69	7.69	7.73	7.68
Refrigeration capacity at each of the two coldest refrigeration stations (watts)	3.00	2.27	1.85	1.15

GE-1145

The drop in turbine-nozzle coefficient from 0.90 to 0.85 caused approximately a five-percent drop in overall turbine efficiency. As can be seen from the table, even in the unlikely event that both turbine and heat-exchanger performance were degraded by the amounts shown, there would still be more than one watt of refrigeration capacity at each of the two coldest refrigeration stations.

EXPERIMENTAL SYSTEM DESIGNGENERAL

The experimental system included only the coldest turboalternator and a heat exchanger that was to be cooled by a liquid nitrogen stream that takes the place of the warmer turboalternators, as shown in the schematic of Figure 7.

The design goals for the experimental system that were used as guides during the design phase of this program were:

- Refrigerator Maintenance-Free Life. This goal was to demonstrate the potential for long life (ultimately perhaps 10,000 hours or more). The contract goal was given as 2500 hours.
- Shock and Vibration. The refrigerator was not to be subjected to shock or vibration loading, except during normal handling and shipping while the refrigerator was not operating.
- Acceleration Loading. The refrigerator was not to be subjected to acceleration loading beyond normal gravity loading; however, to be conservative, all structural design and turboalternator bearing design were based upon a steady acceleration loading, in any direction, of twice the acceleration of gravity.
- Temperature Capability. The unit was to be designed so there would be at least a 0.8 probability of reaching the design temperature of 4.4°K, with no useful refrigeration load at that temperature.

RADIATION SHIELD

Calculations were made to determine whether the thermal radiation shield should be thermally connected to the 170°K or the 55°K refrigeration load station. It was found that if the shield is connected to the 170°K station, as much as 130 watts could be radiated inward to the lower-temperature regions of the cryosection; this condition would have necessitated multilayer reflective insulation both inside and outside the radiation shield -- an undesirable complication.

With the shield connected to the 55°K station, the inward radiation was found to be less than 1.4 watts, eliminating the need for insulation inside the shield.

With the shield at 55°K, the external heat load on the shield was conservatively estimated to be less than 4 watts, if a 5-cm thickness of reflective multilayer insulation were used outside the shield (such a thickness would contain 60 to 80 layers of insulation). This heat load would be the major constituent of the 5-watt load at 55°K, assumed in the cycle studies.

CRYOGENIC PIPING

Cryogenic piping is required to carry gas between turbines and heat exchangers with an acceptably low pressure drop. Calculations were made for pipe diameters, with the following assumptions:

- For each pipe carrying gas either to or from a turbine, the ratio of pressure drop to average pressure must not exceed 0.001.
- Pressure losses caused by wall friction are negligible, compared with losses caused by bends or elbows in the pipes.
- In each pipe to or from a turbine, there are four right-angle bends and a total pressure loss corresponding to four times the velocity head.

These assumptions are somewhat conservative because in some pipes there are fewer than four bends and there is probably less than one velocity head loss in each bend.

Results of the pressure-drop calculations showed that a 1/2-inch nominal pipe size, schedule 5S, would be adequately large for all cryogenic piping, from a pressure-drop standpoint. This pipe has an inside diameter of 18.0 mm (0.710 inch) and an outside diameter of 21.3 mm (0.840 inch).

Because this pipe size is reasonably small, yet large enough for mechanical support of the turboalternators, this size was tentatively selected for all piping to and from the turbines and to and from the Joule-Thomson valve.

JOULE-THOMSON VALVE

The simplest approach for the construction of a Joule-Thomson valve is to use a standard needle valve and to modify it with the addition of a long stem sealed within a vacuum-tight sheath. The valve could thereby be manually controlled at the warm end. The stem screw threads were initially located at the warm end, but in a later design change, the threads were relocated to the cold end.

Choked flow of an ideal gas through a sharp-edged orifice was assumed for sizing the valve orifice. A Whitey Company valve, Model 2RF4-316, with an orifice diameter of 2.36 mm (0.093 inch) was selected. An orifice of this size, with an upstream temperature and pressure corresponding to cycle design-point conditions, would result in a calculated helium flow rate of 6.9 g/sec.

The cycle-design flow rate through the Joule-Thomson valve is 2.1 g/sec. It is believed that this ratio of flow rates is adequately large to assure control at the design point, despite uncertainties in the calculation (the greatest uncertainty of course results from the assumption of an ideal gas). The valve gives nearly linear control from the closed to the fully opened stem position.

LIQUID NITROGEN COOLER

As indicated above, a liquid nitrogen cooler was needed to take the place of the warmer turboalternators, to depress the temperature at the cold end of the warmest heat exchanger.

The method selected to accomplish this while attaining a small stream-to-stream temperature difference at the cold end of the warmest heat exchanger is to unbalance the flow between the two streams by providing a larger flow to the colder stream. This unbalance can be accomplished as shown in Figure 8. The resulting temperature distribution is shown in Figure 9.

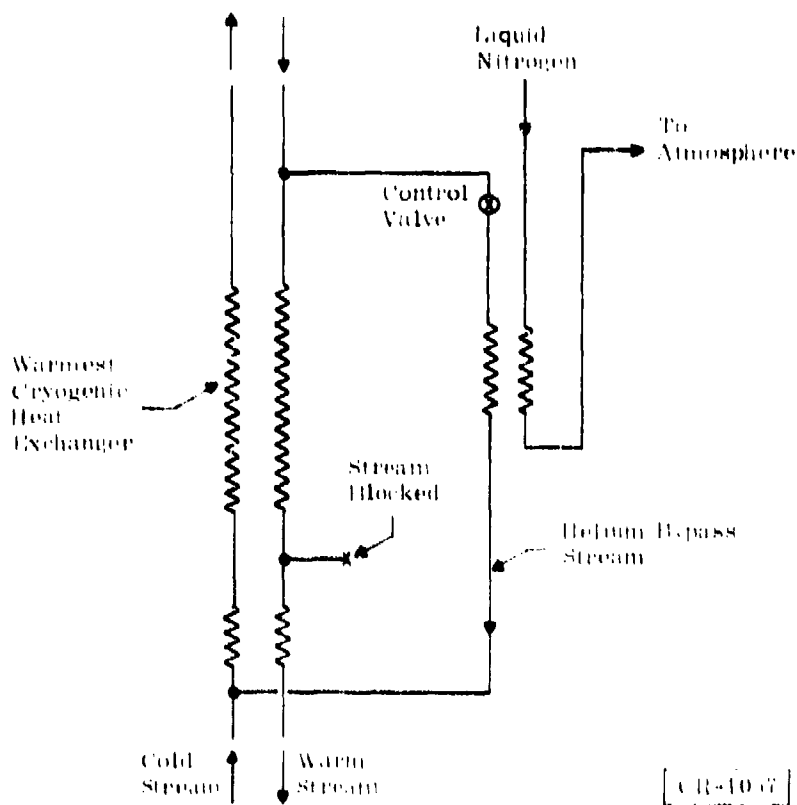


Figure 8. Cooling System (Schematic Diagram)

The advantage of this arrangement is that the control valve can be a warm valve with conventional (but leak-tight) packing and the helium-to-nitrogen heat exchanger can be located outside the vacuum space. This arrangement is shown in Figure 10.

The cold end, stream-to-stream temperature difference shown in Figure 9 can be calculated as follows, using the definitions, equations, and nomenclature of Kays and London (Ref. 7, pp. 15-17). Several iterations showed

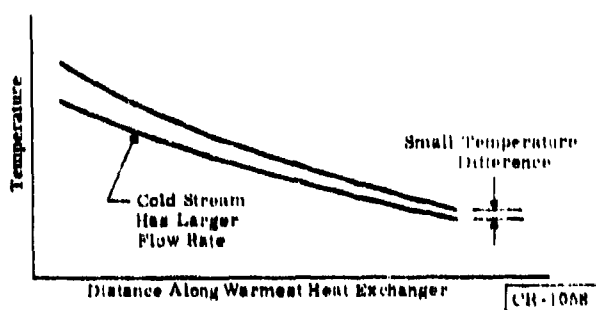


Figure 9. Temperature Distribution

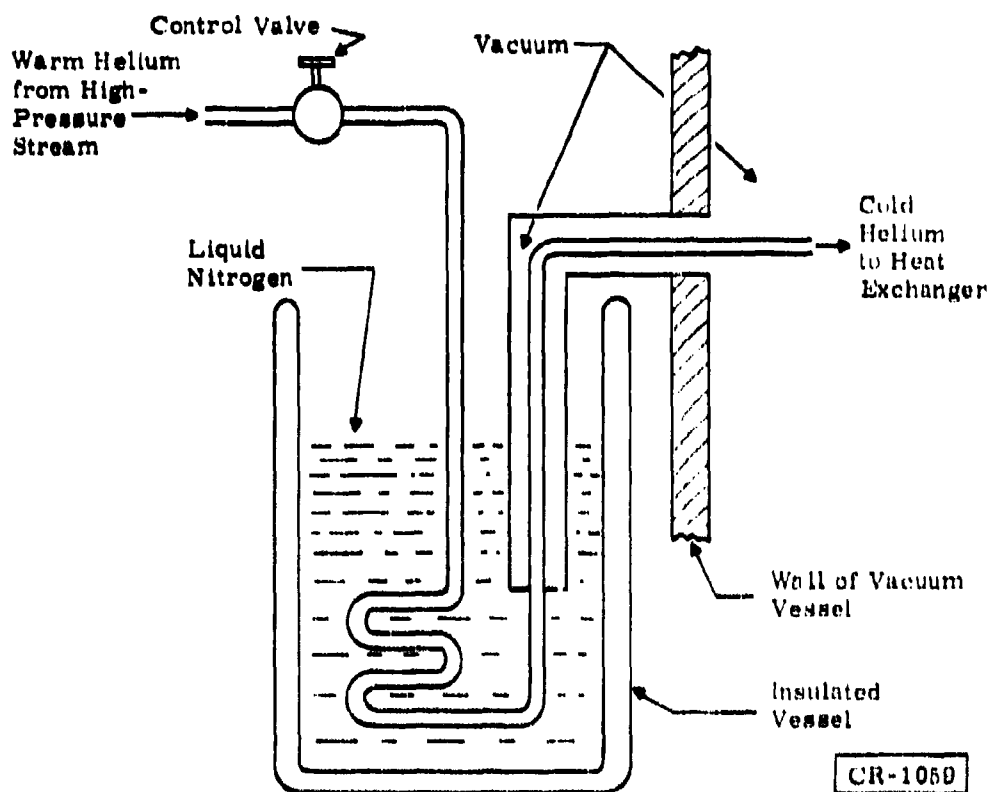


Figure 10. Helium-to-Nitrogen Heat Exchanger

that a helium flow rate through the control valve of 0.3 g/sec provides a sufficiently large flow unbalance between the two streams. The warm-stream flow rate (Figure 8) is 5.47 g/sec (the sum of the flow rates through the Joule-Thomson valve and the 14°K turboalternator). The cold-stream flow rate is therefore 5.47 + 0.3, or 5.77 g/sec. The capacity-rate ratio, C' , is calculated to be the ratio of mass flows for equal heat capacities:

$$C' = \frac{C_{\min}}{C_{\max}} = \frac{5.47}{5.77} = 0.95$$

The heat transfer effectiveness for a counterflow arrangement is:

$$e = \frac{1 - e^{-NTU(1 - C)}}{1 - Ce^{-NTU(1 - C)}}$$

For number of transfer units (NTU) of 86 (the design value of the warmest heat exchanger), the effectiveness is calculated from the above equation to be 0.998, and the cold-end stream-to-stream temperature difference is calculated to be 0.44°K. This value is sufficiently small to match the stream-to-stream temperature difference at the warm end of the adjacent colder heat exchanger.

COLD END COOLER

A method for cooling the cold end of the system was devised. As shown in Figure 7 a small diameter tube leads helium from just upstream of the Joule-Thomson valve, through a room temperature control valve, and finally back to the low pressure side of the compressor system. The purpose of this gas bleed was to remove at least part (if not all) of the warm helium stream returning through the counterflow heat exchangers during the cooldown process. If allowed to pass through the heat exchangers, this warm return stream would transfer heat to the incoming cold stream, thereby lengthening the cooldown process. Once the Joule-Thomson valve dropped to below the inversion temperature and produced cooling, the bleed stream valve would be closed, and all of the gas would return through the heat exchanger system.

HEAT LEAK

The cryosection design concept was to mount all cryosection components (turboalternators, Joule-Thomson valve, filters, and radiation shield) directly on the heat exchanger or on the liquid nitrogen cooling stage. Thus, no structural supports between room temperature and cryogenic temperatures would be needed, and all conducted heat leakage would be through instrumentation leads and through the Joule-Thomson valve stem.

A summary of calculated heat leaks is given in Table 4.

The above heat leaks do not include conduction through liquid nitrogen tubes, which will be installed to expedite rapid cooldown of the cold end of the heat exchanger system.

The bases for the heat leak calculations were:

- The coaxial cable assumed is Microdot, Incorporated, No. 250-4013. This cable contains seven strands of 0.0041-inch-diameter copper wire in the inner conductor, and 64 strands of 0.0033-inch-diameter copper wire in the shield. A length of 1.2 meters was assumed.

Table 4
ESTIMATES OF HEAT CONDUCTION RATES

Thermal Conductor	Calculated Rate of Heat Conduction (w)	
	To 14°K Level	To 4.4°K Level
Seven coaxial cables for proximity probes	0.275	--
Three alternator power leads (includes Joule heat)	0.072	--
Leads for three platinum resistance thermometers (four leads for each thermometer)	0.056	0.028
Three pairs of thermocouple leads	0.020	0.010
Two pressure lines	0.007	--
Joule-Thomson valve stem	--	<u>0.063</u>
	0.430	0.101

The total of 0.275 watt given in Table 4 is for all seven cables. If the cables were thermally connected to the 80°K level, with a 1-meter length between that temperature and the 14°K level, the heat leak could be reduced to about 0.13 watt.

- The turboalternator power leads were optimized by the method of McFee (Ref. 8). The conductor diameter was calculated to be 0.41 mm (0.016 in.) for an assumed length of 1.0 meter.
- It was assumed that two platinum resistance thermometers would be used at the 14°K level (one at the inlet and one at the outlet of the turboalternator) and that one thermometer would be used at the discharge of the Joule-Thomson valve.
- Copper constantan thermocouples would be mounted at the same positions. These sensors would be used for monitoring cooldown only (their sensitivity would not be adequate for sensing the final steady-state temperatures).
- Pressure lines were assumed to be stainless steel lines 1.6 mm. (0.062 in.) outside diameter and 0.81 mm. (0.032 in.) inside diameter, 1.2 meters long.

LAYOUT OF CRYOGENIC SECTION

A layout of the cryogenic section showing the location of all cryogenic components is shown in Figure 11.

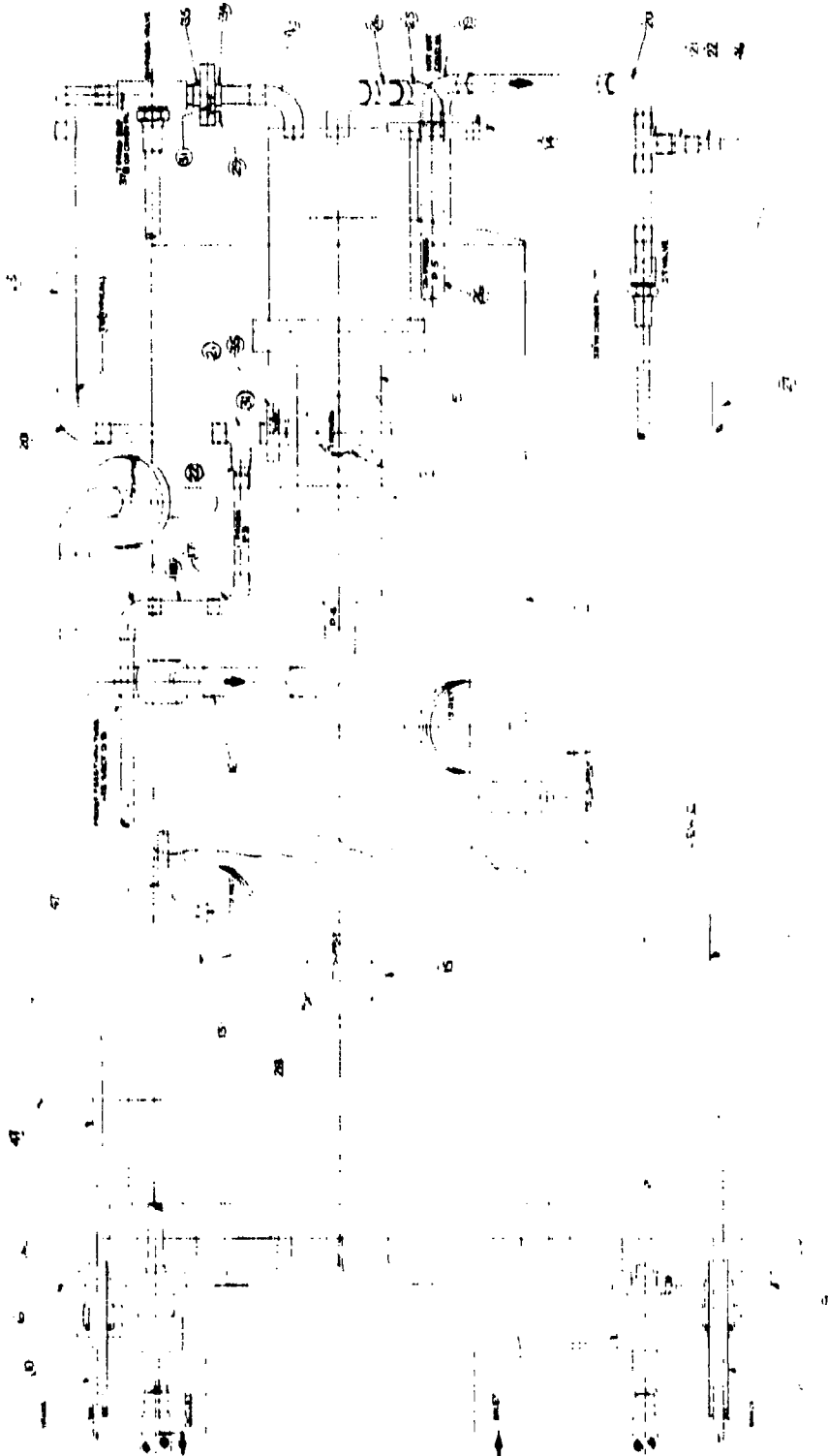


Figure 11. Cryogenic Section

Section 4

TURBOALTERNATOR

GENERAL

The turboalternator arrangement used in this program is shown in Figure 12. It comprises a high speed, radial inflow, impulse turbine mounted on a permanent magnet alternator shaft. The shaft is supported and positioned on self-acting, gas-lubricated bearings. Operating tests at speeds up to 400,000 rpm have been conducted on this type of turboalternator. The bearing, windage, and electromagnetic parasitic losses are reasonably low. The high speed alternator has proven to be of both sound design and high efficiency. Tests with electrical loads up to 109 watts have been conducted with electromagnetic efficiencies of 98 percent. The bearing system allows operation in any orientation, free from gas bearing and rotor instabilities sometimes found in other bearing systems.

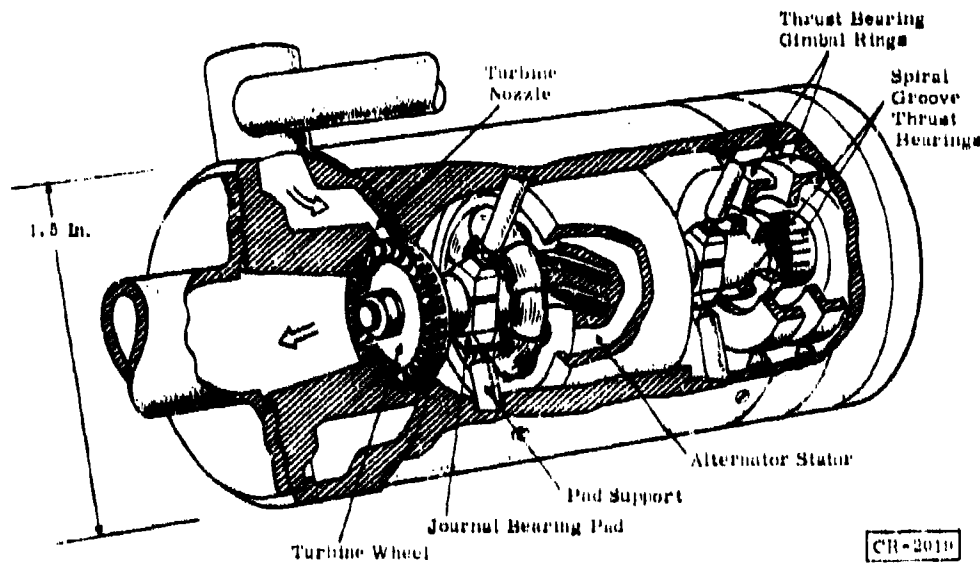


Figure 12. Partial-Admission Radial-Impulse Turboalternator

The turbine rotor is mounted on gas-lubricated journal bearings. Three hardened pads at each journal bearing support the 1/4-inch-diameter shaft with an operating gas film thickness of about 300 microinches. These journal bearings are of the self-acting, tilting pad type. They were incorporated to ensure stable operation throughout the operating range and at any attitude.

Two inward pumping spiral grooved thrust bearings position the shaft axially. Like the journal bearings, the thrust bearings are gas lubricated, typically using a 500 microinch film thickness.

The entire bearing system is self-aligning because the thrust bearings are gimbal mounted and the tilting-pad journal bearings are self-aligning. Satisfactory operation of the complete bearing system is independent of the accuracy with which adjacent parts are manufactured.

The turbine energy is absorbed by the permanent magnet alternator. This compact alternator is the most practical device for extracting energy at cryogenic temperatures when that energy will be expended at ambient temperatures. The two-pole magnet operates within the stator which is wound 3-phase within low-loss iron laminations. These laminations have been made by conventional die punching and by photoetching, a method which eliminates crimped edges. The alternator rotor consists of a high field-strength platinum-cobalt magnet. The rotor is constructed by brazing the magnet to shaft ends. The ground magnet surface has the same diameter as the shaft.

TURBOALTERNATOR DESIGNS

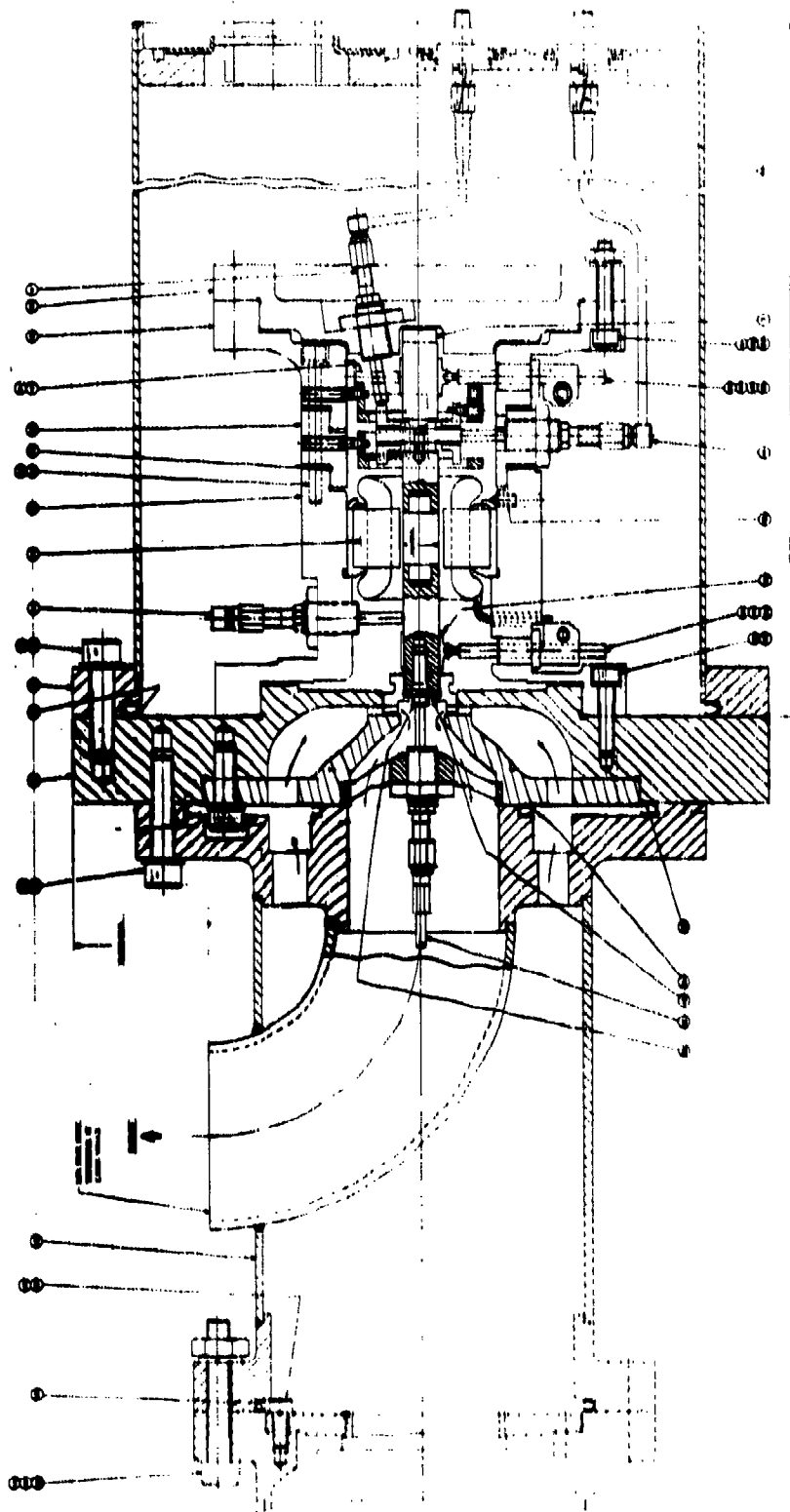
PRELIMINARY DESIGNS

Preliminary designs of the three turboalternators needed for the refrigeration system were made (Appendix I, "Preliminary Turboalternator Designs"). The final designs of the two warmer turboalternators were not completed because it was decided to manufacture and test only the coldest turboalternator. The final design of the coldest turboalternator is discussed in the following section.

FINAL DESIGN OF THE 14°K TURBOALTERNATOR

The overall mechanical configuration design of the turboalternator is shown in Figure 13 (excerpted from General Electric Drawing 588E477). The active components, turbine, alternator, and bearings are mounted on a base-plate (Part 18), which allows simple attachment of the assembled turboalternator to the remainder of the refrigeration system.

All enclosure seals are indium-coated C rings. The base material of the C rings is 304 stainless steel, to match the thermal coefficient of expansion of the flanges. The low mass of the seals coupled with the excellent thermal contact between the seal and flange, established by the soft indium coating that essentially becomes bonded to the flange surfaces, ensures geometric temperature uniformity in the seal area during system temperature excursions. Relative motion between the seal and the flange faces is thus prevented. Although the thermal coefficient of expansion of the indium coating is almost twice that of the base metal, the spring loading of the C ring coupled with the extreme softness of the indium overcomes this mismatch.



CR-2225

Figure 13. Single-Stage Radial Impulse Turboalternator

Axial positioning of the turboalternator shaft is accomplished by spiral-groove gas bearings. The bearings are self-aligning, because of their gimbal mounting. The bearing material is beryllium-copper alloy, which is compatible with the nitrided thrust runner at the low unit loading present (in contrast with the journal bearing pads where the high loading at start and stop, due to line contact between the journal and pad, precludes the use of this material). The grooves are photoetched into the bearing surface.

For monitoring bearing performance as well as for initial bearing adjustment, provision is made for seven capacitance-type displacement probes with the placements proceeding from the turbine end of the shaft:

<u>Probes</u>	<u>Function</u>
1	Axial shaft movement
2	Shaft orbital movement
2	Shaft orbital (periphery of thrust collar)
1	Journal bearing pad movement
1	Outer thrust bearing movement

The turbine wheel is 1/2 inch in diameter and is made of aluminum. The wheel is secured to the shaft by an interference fit. Proper selection of the fit diameters and wheel shape allows the assembled rotor to be operated at design temperature, at safe stress levels. Experience has shown that turbine wheels can be removed from the shaft and can be replaced without disturbing the rotor balance.

ALTERNATOR DESIGN

The alternator design is similar to previous designs but, because of the required design-point values of speed and power, greater advantage can be taken of the very high copper conductivity at the 14°K inlet temperature than in earlier designs. Because of this high conductivity, the armature current can be high for this alternator, which allows the terminal voltage to be lowered at the required power. Thus the flux density can be lowered and the air gap can be increased.

Decreased flux density reduces core losses. The large air gap coupled with a tooth width of 0.050 inch reduces the slot harmonics and associated losses to a negligible level.

Table 5 shows the calculated features and performance of the alternator. Electromagnetic efficiency is estimated to be 99.4 percent, which is higher than the efficiency for previous designs.

Table 5
 ALTERNATOR DESIGN AND CALCULATED PERFORMANCE
 (14°K inlet temperature)

Parameter	Performance (Computer Design D-2300C)
<u>Stator</u>	
Outside diameter punching (in.)	0.840
Inside diameter (in.)	0.281
Length (in.)	0.415
Material (in.)	0.004 Hymu 80
Number of slots	12
Spiral (deg)	21
Tooth width (in.)	0.080
Circuits	1
Connection	Wye
Pitch (%)	83.3
Conductors per slot	50
Wire	1 - 0.0008 in. HF
Turns in series per phase	100
Pitch factor	0.988
Distribution factor	0.988
Skew factor	0.993
Stacking factor	0.92
Resistance, 20° C (Ω)	4.68
Leakage reactance (Ω)	0.64 at 1500 Hz
<u>Rotor Field</u>	
Diameter (in.)	0.261
Length (in.)	0.375
Material	Co-Pt
Air gap (in.)	0.016
<u>Performance (18° K)</u>	
Speed (rpm)	90,000
Power factor	1.0
Output (w)	29.92
Line-to-line volts -- no load	30.0
Line-to-line volts -- full load	28.8
Resistance at 18° K (Ω)	0.032
Current (amp)	0.800
Current density (amp/in ²)	11.800
Core loss (w)	0.13
Copper loss (w)	0.03
Electromagnetic efficiency (%)	99.4

CR-0187

GAS BEARING ANALYSIS AND DESIGN

The gas bearing analysis and design is presented in Appendix II, "Gas-Bearing Analysis and Design."

ASSEMBLY PROCEDURE

The procedure for assembling the turboalternator is presented in Appendix III. This appendix is reproduced from a separate document titled Instruction Manual: Turboalternator Assembly Procedures.

TURBOALTERNATOR PERFORMANCE

TURBOALTERNATOR MANUFACTURE

During the course of this program, it was decided to utilize a turboalternator made available from a terminated U. S. Air Force contract.* The important dimensions of the wheel and nozzle are almost identical to the unit designed for MERDC, and calculations indicate that the Air Force turbine would meet the requirements of the MERDC tests.

A comparison of the wheel and nozzle characteristics for the MERDC and Air Force units is given in Table 6. The Air Force unit was originally designed for two turbine wheels on one shaft. In the MERDC tests, only the smaller of the two wheels was used.

Table 6

COMPARISON OF WHEEL AND NOZZLE CHARACTERISTICS

	Air Force	MERDC
Wheel Diameter (inch)	0.500	0.500
Blade Height (inch)	0.0609	0.0700
Number of Blades	37	23
Design Speed (rpm)	80,000	90,000
Nozzle Admission Arc (fraction)	0.2518	0.2714
Nozzle Flow Factor (c/√T ₀ /sec-atm)	4.41	4.49

Nozzle Flow Factor $\frac{(\text{Mass Flow} \times \sqrt{\text{Temperature}})}{\text{Pressure (Upstream of Nozzle)}}$

An alternator was designed and built for the MERDC turboalternator with 1/3 fewer turns per slot than the Air Force alternator to reduce the operating voltage and improve its efficiency at 14°K. Since this alternator also fit the Air Force housing, it was used in the MERDC turboalternator assembly.

*Contract No. F33615-71-C-1003

A new nozzle flange was designed and fabricated to permit disassembly of the turboalternator housing. (The Air Force unit was designed for welding, which made disassembly inconvenient.)

The parts used in the MERDC assembly are shown in Figure 14; with the exception of the alternator and the nozzle flange, essentially all of the other parts were previously assembled and tested on Air Force contract, as in Build 10. The operation of this first stage Air Force turboalternator, Build 10, is described on pages 108-111 of the Air Force final Technical Report (Ref. 5).

The report also includes the following information pertinent to the MERDC turboalternator:

The turboalternator open-cycle tests and procedures are described on pages 83-86.

The results of open-cycle performance tests on the first stage, 0.5-inch-diameter turbine wheel at room temperature and 177°K are described on pages 111-155. In reviewing these data, the fact that the MERDC alternator has 1/3 fewer conductors in the windings must be kept in mind. This reduces the output voltages and affects the total power. The alternator phase winding resistance is also reduced approximately 1/3, thus reducing the power loss per phase and the total power loss, and affecting the electromagnetic efficiency.

TURBOALTERNATOR PERFORMANCE DATA REDUCTION PROGRAM

A data reduction program was used to reduce the open-cycle data on both the Air Force and MERDC programs. This data reduction program was prepared to evaluate single-stage turboalternator performance. The alternator voltages and currents, thermocouple voltages, turbine pressures, and alternator frequency are the data recorded and used in the computer program. Perfect gas relationships are used throughout the program. Any perfect gas can be used in this program with suitable input of:

- Gas constants
- Rotometer constants
- Alternator housing leakage constants

The program is now set up only for helium and nitrogen.

The open-cycle turboalternator temperature (OCTRM'T) program was prepared for open-cycle tests conducted at room and cryogenic temperatures, using FORTRAN IV computer language. Ice is used for the room-temperature thermocouple reference junction and liquid nitrogen is used for the cryogenic temperature test reference junction. All principal turboalternator instrumentation is shown schematically in Figure 15.

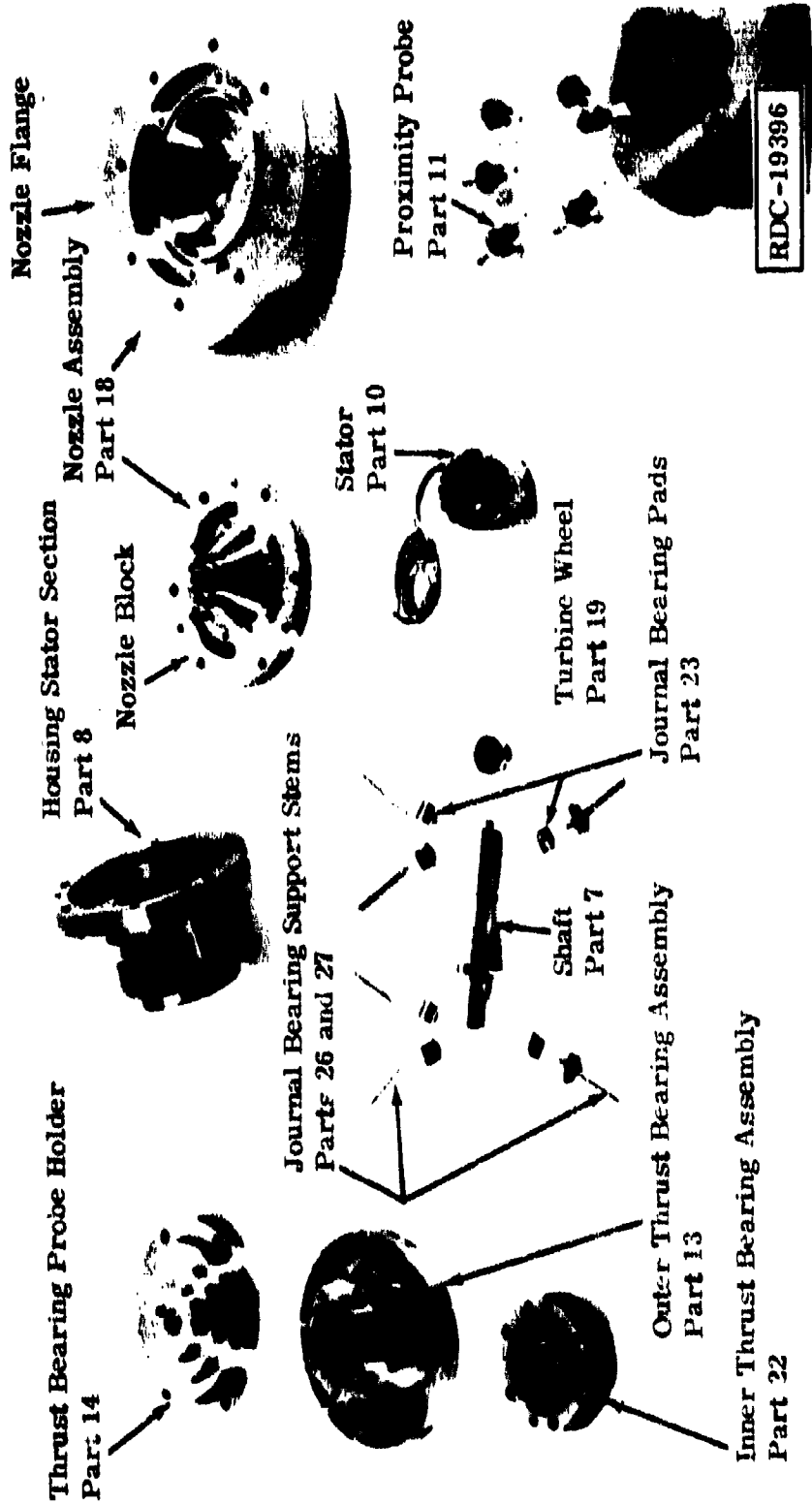
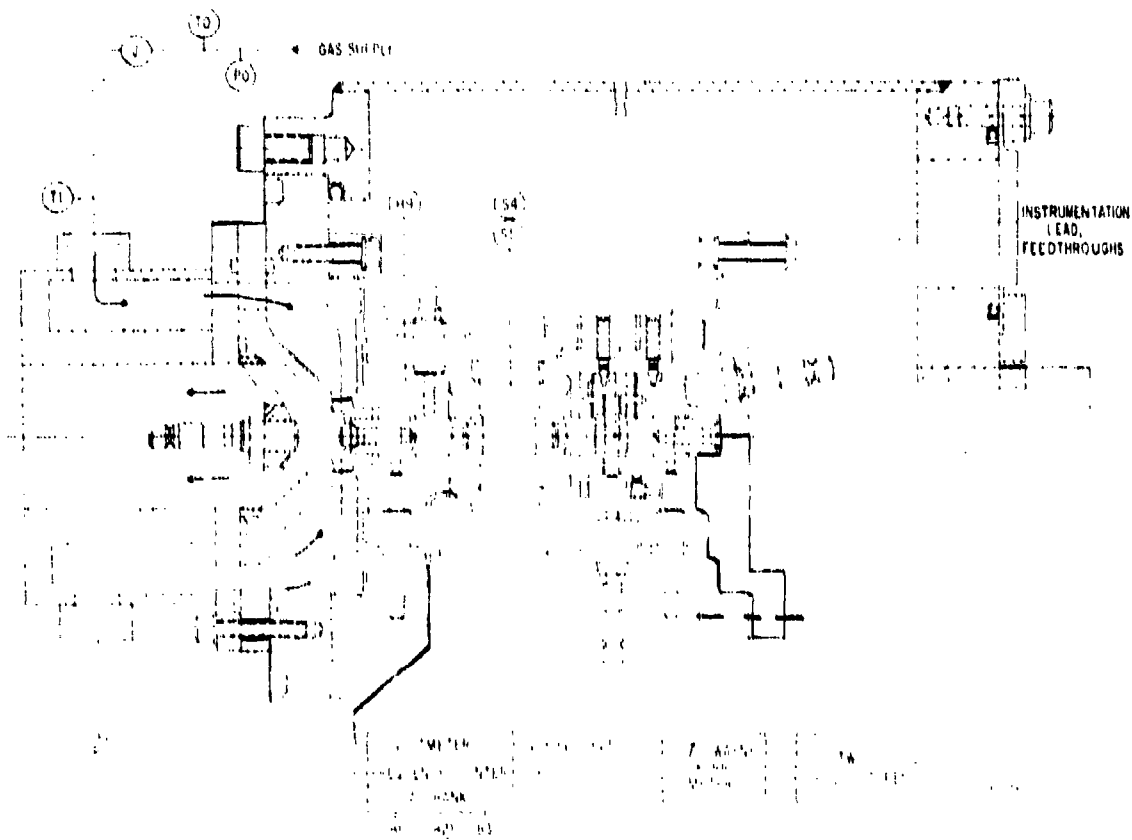


Figure 14. Turboalterator Parts



- C1 Alternator Frequency (hertz)
- P0 Flowmeter Pressure (psig)
- P1 Nozzle Inlet Pressure (in. mercury)
- J Flowmeter Reading
- H0 Housing Pressure (in. water)
- R1 Load Resistance per Phase (ohms)
- V1 Voltage, Line to Neutral (volts)
- V2 Voltage, Line to Neutral (volts)
- V3 Voltage, Line to Neutral (volts)
- B1 Shunt Voltage (volts)
- B2 Shunt Voltage (volts)
- B3 Shunt Voltage (volts)
- T0 Gas Temperature at Flowmeter
- T1 Gas Temperature into Nozzle
- S4 Alternator Winding Temperature
- S5 Alternator Winding Temperature

Figure 15. Principal Turboalternator Instrumentation

Results of the data reduction program for a typical MERDC data point at cryogenic temperature using the OC TRMP program is shown on Figure 16. The data reduction program used to reduce the Air Force data was modified to eliminate the alternator housing leakage flow, since the MERDC open cycle tests were conducted with the turboalternator installed into a sealed housing. These data reduction results are based on:

- Data obtained directly during tests.
- Test data conversion, such as thermocouple voltages converted to absolute temperatures.
- Test data manipulated to provide performance factors, such as overall efficiency and individual losses.

Methods used and entries on each line of the output data reduction sheet are:

- Line 1 - The first entry is the title and lists the ambient temperature and gas used in testing.
- Line 2 - The second entry identifies the data point, run, and date.
- Line 3 - The third entry shows overall performance. The total electrical power is the sum of the three phase powers. The speed is obtained from the frequency counter. The overall efficiency is the actual total electrical power output over the isentropic power input. The isentropic power is based on the flow across the turbine wheel, not the total flow through the nozzle. The corrected speed is the rotating speed over the square root of the absolute inlet temperature.
- Line 4 - The next entry shows the load voltages, as obtained from the line to neutral terminals from the data sheet. The load resistance is derived from the calibrated test load bank. The frequency is the rotational frequency in hertz.
- Line 5 - The three phase currents are obtained by measurement of voltage drops across the load bank current shunt in each leg. Also listed is the core loss, based on frequency, which is in turn based on a pre-determined relationship, based on the average slot temperature.
- Line 6 - Power of each phase is shown from the product of phase current and voltage. The sum of the three phase powers is shown on Line 2. The electromagnetic efficiency results from the core and pole losses relative to the total input power.

*****TEST REFERENCE*****

POINT	RUN	MONTH	DAY
4	101	11	1

*****OVERALL PERFORMANCE*****

TOT EL PWR.	SPD,RPM	OVALL EFF.	CORR.SPD.
37.3915	187680.	0.3708	15339.2

*****ELECTROMAGNETIC PERFORMANCE*****

PHASE VOLTAGE,VOLTS	LOAD RES (L-N)	FREQ,CPS
35.10 35.10 35.10	9R.5	3128.0

*****PHASE CURRENT,AMPS*****	CORR LOSS,WATTS
0.3550 0.3550 0.3550	0.460349

*****PHASE PWR,WATTS*****	FLMAG. EFF.
12.4605 12.4605 12.4605	0.9712

*****JOULE LOSS/PHASE,WATTS*****	TOTAL JOULE LOSS,WATTS
0.2155 0.2155 0.2155	0.6465

*****SLOT TEMPS,*****	AVG SLOT T,R	WDG RES/PH
187.568 190.679	189.124	1.7100

*****TURBINE PERFORMANCE*****

TUR IN T,R	TUR EX T,R	ACT T DR,R	IN./EX. P.R.
149.70	136.88	12.82	1.9292174

WHL. PWR.	WHL. EFF.	WIND PWR.	BRQ. PWR.
44.5525	0.4419	0.9043	5.1599

CORR. TORQ.	T.D. EFF.	TIP SPEED	VFL. RATIO
0.2996E-03	0.3708	409.5	0.2793

TOT. FLOW	IN./V0Z.P.R.	V0Z./EX.P.R.	FLOW FACT.
8.007	1.6604312	1.1612753	1.7467

JNL.PWR.	PIV.FIL.CL.	TH.L0.PWR.	TH.L0.CL.
0.6377	250.00	1.9423	200.00

Figure 18. Typical Single MERDC Data Point at Cryogenic Temperature

- Line 7 -- Joule (I^2R) losses are shown for the separate phases and the total of these losses. These losses were determined from the measured current and phase winding resistance, which is a function of the average slot temperature.
- Line 8 -- Two slot temperatures are tabulated along with the average slot temperature. The temperature is measured from thermocouples positioned 120 degrees apart in the stator slots. The winding resistance is a function of the average slot temperature.
- Line 9 -- Performance factors and characteristics of the turbine are shown. The turbine inlet temperature is measured at the nozzle inlet. The exit temperature is calculated from the calculated temperature drop across the turbine wheel. The temperature drop is calculated from the input power and actual flow across the turbine wheel. The inlet/exhaust pressure ratio is the total pressure ratio across the turbine.
- Line 10 -- The wheel power is the power input of the turbine wheel to the shaft. It is determined by adding the total electrical power to the sum of the losses. The wheel efficiency is the wheel power over the isentropic power across the turbine wheel. The windage power is the sum of the shaft and wheel parasitic losses deduced from the design computer program and is a function of speed, temperature, and ambient pressure. The bearing friction power is calculated from relationships generated from the design computer program and is a function of speed, temperature, and pressure. Both journals and both sides of the thrust bearing are included. The corrected torque is the torque (in. -lb) divided by the absolute inlet pressure in inches of mercury.
- Line 11 -- The temperature drop efficiency is the calculated temperature drop over the isentropic temperature drop. It represents the potential efficiency if there were no flow leakage loss. The tip speed is the turbine wheel tip speed. Shown next is the velocity ratio of the tip speed to the spouting velocity.
- Line 12 -- Next listed is the total measured flow through the turbine nozzle from one of the rotometers. Prior calibration of the rotometer provided the proper constant for the flow equation. The inlet/nozzle pressure ratio is the inlet pressure to nozzle exit pressure ratio. The nozzle/exhaust pressure ratio is the nozzle exit pressure to turbine exit pressure ratio. The flow factor is a grouping of flow, temperature, and pressure, which is a turbine nozzle performance characteristic.
- Line 13 -- Next listed are bearing performance factors. The journal bearing power for one set of three tilting pads is determined from the measured assembly average pivot film clearance listed. The friction power for the loaded side of the thrust bearing is also determined from the thrust bearing loaded side clearance. Both the

assembled journal pivot film thickness and the load side thrust bearing clearance are listed in microinches.

A listing and flow chart of the open-cycle data reduction computer program used to reduce the MERDC cryogenic turboalternator data are given in Figures 17 and 18.

JOURNAL BEARING MATERIAL

As described in the Air Force Final Report (Ref. 5), problems were encountered in manufacturing and operation of turboalternators using tilting pad journal pads made of nitrided 304L stainless steel. Air Force turboalternator assemblies, Builds 8, 9, and 10, were made with a new design of tilting pad journal bearings, fabricated from a promising new material, Kentanium, Grade 165. Since Build 10 is the one used for MERDC tests (with the exception of the nozzle flange and alternator), the MERDC unit used Kentanium bearing material.

VERY LOW TEMPERATURE TEST

Results of the preliminary open-cycle tests made on the Air Force turboalternator assembly, Build 10, were very encouraging. However, the Air Force contract was terminated before further tests could be completed. Since similar tilting pad bearings would be required in a turboalternator assembly being designed on an ARPA contract (No. DAHC-15-720C-0235), a special open-cycle experimental test was conducted on the ARPA contract, using the Air Force turboalternator assembly, Build 10, to operate at temperatures approaching liquid helium. The turboalternator was installed into a sealed housing and operated in the normal manner on the open-cycle system at approximately 100,000 rpm, with a 9-watt load, until the assembly reached 90°K. Then, with a valving arrangement, the turboalternator was gradually changed to operate on cold helium gas supplied directly from a pressurized liquid helium dewar. The turboalternator continued to operate satisfactorily with a minimum turbine exhaust temperature of 9.8°K obtained. Essentially, no performance data were taken during this test because of the limited amount of liquid helium in the pressurized dewar. The main purpose of the test was to observe the operation of the bearings, by monitoring the proximity probe signals, at the low temperatures. As mentioned previously, the unit tested at 9.8°K was identical to the MERDC unit, with the exception of the nozzle flange and alternator.

This experiment was successful and a significant milestone was achieved in the development of turboalternators for cryogenic refrigeration. This was, perhaps the lowest temperature ever achieved with a turboexpander operating on self-acting gas bearings. It is the first step in establishing the feasibility of turboalternator operation with gas-lubricated bearings, using very low viscosity helium. The 9.8°K helium gas is probably the lowest viscosity fluid ever used in a hydrodynamic bearing system.

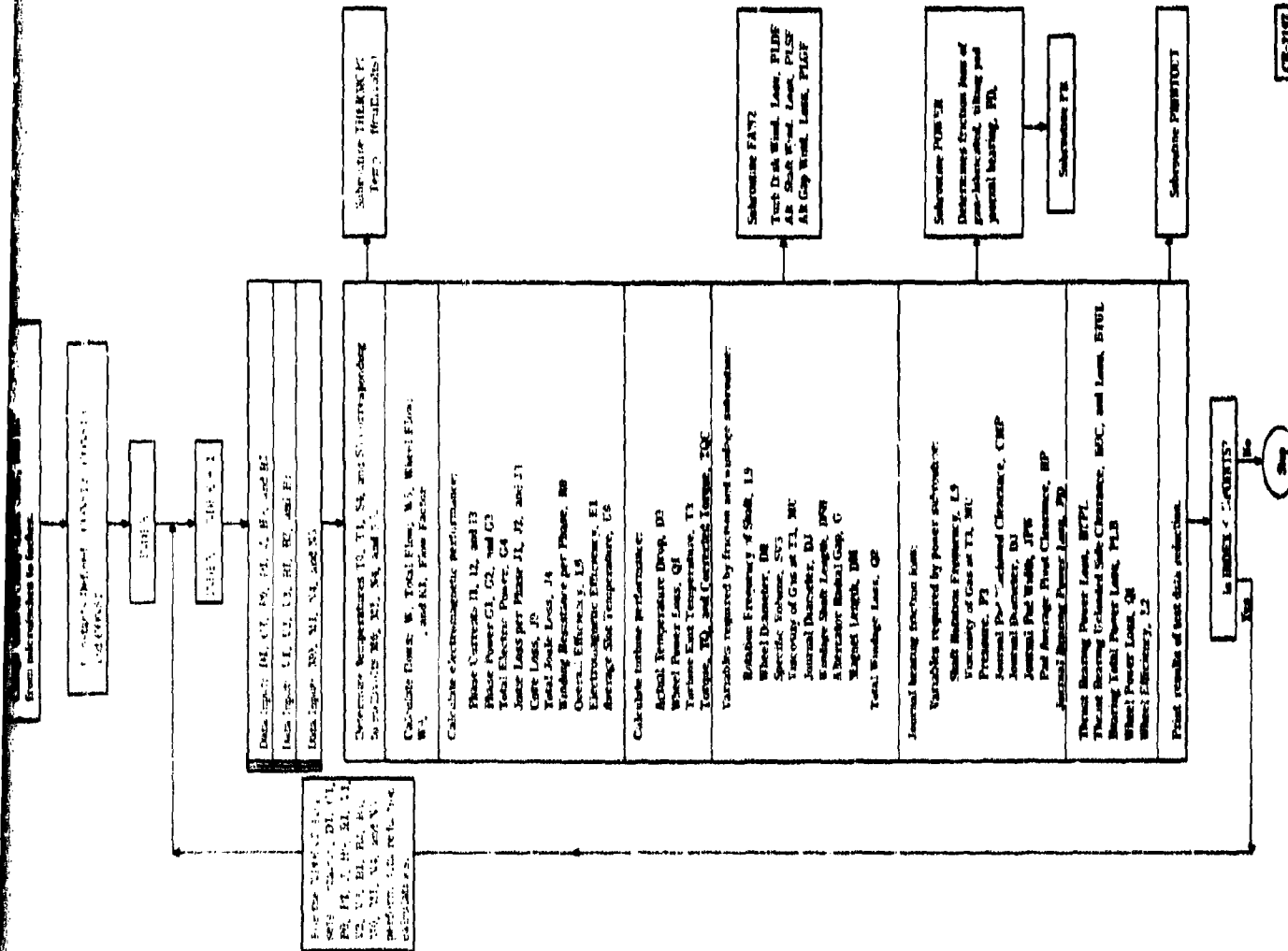


Figure 17. Test Reduction Program

CB-2147

ECRMT 01/03/75

```

1000 ***** D.G. COLYER'S PROGRAM*****
1200 PROGRAM TO EVALUATE TEST DATA FROM OPEN-CYCLE, SINGLE-STAGE
1400 TURBOALTERNATOR, ROOM-TEMPERATURE AND CRYOGENIC TEMPERATURE
1410 PERFORMANCE, ANY PERFECT GAS.
1450 THIS PROGRAM HAS BEEN MODIFIED TO TEST WITH NO LEAKAGE FROM
1460 HOUSING TO ATMOSPHERE. THIS HAS MADE OBSOLETE (NOW "C")
1470 LINES: 964,965,967,968,1520,1620
1500 MODIFIED LINES REQUIRED TO CHANGE THE PROGRAM INCLUDE: 220,
1510 240,4300,4350,7700,8550,8650
1550 NEW LINES TO MODIFY PROGRAM INCLUDE: 1382,1384,1386,1388
1600
180 COMMON C1,D1,D2,D3,D4,D5,D6,D7,D8,D9,E1,E2,E3,E4
200 COMMON I1,I2,I3,J1,J2,J3,J4,J5,J6,J7,J8,J9,K1,L0,L1,L9
220 COMMON Q1,Q2,Q3,Q4,R0,R1,PNPE,S4,S5,T1,T3,U,U0
240 COMMON V1,V2,V3,V5,W,PIP,N,K,PLM
260 COMMON PD,HP,TRC,RLC,NST,TCC,RTPL,LR
265 COMMON DUMMY
280 FILENAME GAS,REFJ,ROTAM,WORD
3000
3010 *****FILENAME MUST BE IN ODD LOCATION WITH RESPECT TO COMMON
3020 VARIABLES*****
320 FILELIST "OCTR0A1"
340 IO FORMAT(V)
360 II FORMAT(I3,I4,A8,I4,A3,I4,A1)
380 INTEGER D1,D2,D3,D4
400 REAL I1,I2,I3,J1,J2,J3,J4,J5,J6,J7,J8,J9,K,K1
420 REAL L0,L1,L2,L3,M0,M1,N4,N5
440 REAL L,MU,NKED,NREG,NREJ,NST,JPW
480 DATA PI/3.141593/
5390
5400 FLOWMETER CONSTANTS
5600 -----
5800 S/N 6107A4692R1 TUBE 3/4-270-10/80 FL. TA 9VT-54 USE QR=11.0
6000 S/N 6207A2779R1 TUBE 1/2-270-10/80 FL. TA 5VT-44 USE QR=4.6
6200 S/N 7107A1289A2 TUBE 3/4-270-10/85 FL. QV9VT59TA0 QR=19.8
6400 S/N 7107A1289A1 TUBE 1/2-270-10/85 FL. QV9VT48ATA0 QR=6.25
660 READ(1,11) LNG,GAS,REFJ,ROTAM
6700 LEAK CALIBRATED CONSTANT W9CON APPLIES TO SPECIFIC
6710 TURBINE WHEEL DIAMETER.
680 IF(GAS .NE. "HELIUM") GO TO 800
700 RMU=5.01E-111 REV=0.6461 K=1.6671 R=386.11 GO TO 950
720 800 IF(GAS .NE. "NITROGEN") GO TO 850
740 RMU=1.101E-111 REV=0.8701 K=1.401 R=55.11 GO TO 950
760 850 PRINT," BAD INPUT GAS IS NEITHER HELIUM NOR NITROGEN."
780 STOP
800 950 IF(REFJ .NE. "ICE") GO TO 700
820 IREFJ=2 J GO TO 775
840 700 IF(REFJ .NE. "LN2") GO TO 725
860 IREFJ=1 J GO TO 775
880 725 PRINT," BAD INPUT REFERENCE JUNCTION IS NEITHER ICE NOR LN2"

```

Figure 1B. Open-Cycle Turboalternator Temperature Program (Sheet 1 of 9)

OC TAMI 01/03/75

```

9000 STOP
920 7/5 IF(ROTAM .EQ. "A") QR=11.0
925 IF(ROTAM .EQ. "B") QR=4.6
930 IF(ROTAM .EQ. "C") QR=19.8
935 IF(ROTAM .EQ. "D") QR=6.25
945 LNO=LNO
960 READ(1,10) LNO,SL,DJ,DT,DR,DR,RB
9640 IF(GAS .EQ. "HELIUM") .AND. (DR .EQ. 0.5) W9CON=4.60
9650 IF(GAS .EQ. "NITROGEN") .AND. (DR .EQ. 0.5) W9CON=20.2
9670 IF(GAS .EQ. "HELIUM") .AND. (DR .EQ. 1.1) W9CON=4.5
9680 IF(GAS .EQ. "NITROGEN") .AND. (DR .EQ. 1.1) W9CON=13.92
980 READ(1,10) LNO,CMP,JPW,ODM,DA
990 CMP=1.E-6*CMP
1000 READ(1,10) LNO,D2,D3,D4,R
1020 READ(1,10) LNO,IRI,RLC,HP
1040 IRI=1.E-6*IRI RLC=1.E-6*RLC HP=1.E-6*HP
1060 READ(1,10) LNO,NPCINTS
1080 DO 1000 INDEX=1,NPCINTS
1100 READ(1,10) LNO,O1,C1,P0,P1,J,H9,R1
1120 READ(1,10) LNO,V1,V2,V3,R1,R2,R3
1140 READ(1,10) LNO,M0,M1,N4,N5
11590
11600 CONSTANTS
1180 CONST1=.001*CI
1200 CONST2=(K-1.)/K
1220 CONST3=K/(K-1.)
1240 CONST5=33000.*60.
12590
12600 *****PERFORMANCE DATA REDUCTION*****
1300 L9=.6).*CI
1360 J=PI+QR*L9/720.
1380 SUM=PI+B
13820 INLET%02. PRESS. RATIO
1384 PI*V*(PI+B)/((H9/13.6)*R)
13860 NO2./EXIT PRESS. RATIO
1388 INPE=((H9/13.6)*R)/B
1400 V=SUM/B
1420 T=1.0*(CONST2)-1.
1440 CALL THERMOPL(IREFJ,M0,10)
1445 V=177.0*QR*.J*SQRT((P0+.49)*R)/(R*T0)
1460 CALL THERMOPL(IREFJ,M1,11)
1480 CALL THERMOPL(IREFJ,N4,S4)
1500 CALL THERMOPL(IREFJ,N5,S5)
15200 W9=W9CON*SQRT(H9*R/T1)
1540 T5=T-W9
1560 CONST16=W5*R*747.
16200 R9=W9/W
1640 J0=0.5*(S4+S5)
1680 I1=R1/R8
1700 I2=R2/R8

```

Figure 18. Open-Cycle Turboalternator Temperature Program (Sheet 2 of 9)

QCTRM1 01/03/75

```

1740 J3=H3/RH
1740 G1=V1*11
1760 G2=V2*12
1780 G3=V3*13
1800 G4=G1+G2+G3
1810 D9=G4*CONST5/(CONST3*CONST6)
1815 T3=T1-D9
1820 J9=.0477*CONST14+.0318*CONST4**2
1830 CONST=00/1800.
1840 R0=(6.37/1.14)*(-.34*6.8*CONST-6.2*CONST**2)
1860 J1=R0*11**2
1880 J2=R0*12**2
1900 J3=R0*13**2
1920 J4=J1+J2+J3
1940 E1=G4/(G4+J4+J9)
1960 H7=CONST3*R*T1*(Y/(Y+1.))
1980 Z=T1*Y/(Y+1.)
2000 L1=D9/Z
2020 I=H7*747./((3600.*550.))
2040 L0=I4/I
2060 V5=J/SQRT((64.4*H7))
2080 K1=H*SQRT(T1)/SUM
2085 NS1=L9/SQRT(T1)
2090 T0=H4*33000.*12./((L9*747.*2.*PI))
2095 T0C=T0/(PI+9)
2099C
2100C WHEEL POWER
2120 W1=D9*CONST3*CONST6/CONST5
2140 DSH=SL-2.*JPW-DM-2.*DA
2160 MU=RMU*1.3**REV
2180 P3=0.491*R
2200 SVJ=R*T1/(P3*144.)
2220 CALL FAW2(L9,DM,SVJ,MU,DJ,DSH,DJ,G,PLDF,PLDF,PLSF,GN,NRFJ,
2240 & CMO,CDS,COI,NRFJ,NREG,DM)
2259C
2260C TOTAL WINDAGE LOSSES
2280 W2=PLDF+PLSF+PLGF
2299C
2300C JOURNAL BEARING FRICTION FROM POWER SUPP. (REVISED TPWATS)
2320 CALL POWER(L9,MU,P3,CMP,DJ,JPW,HP,PD)
2380 BUC=18T-BLC
2400 H1PL=9.02F-5*MU*(L9**2)*(DT**4)*(1.-DR**4)/BLC
2420 B1PL=B1PL*H1PL/BUC
2439C
2440C TOTAL BEARING FRICTION
2460 PLB=2.*PD+B1PL+B1UL
2479C
2480C WHEEL POWER
2490 J1=G4+J9+J4+Q2+PLB
2495C WHEEL EFFICIENCY

```

Figure 18. Open-Cycle Turboalternator Temperature Program (Sheet 3 of 8)

OCTRMI 01/03/75

```

2500 L2=J1/1
2520 CALL PRNTOU(GAS,REFT)
2540 T000 CONTINUE
2560 STOP
2580 OPTION LOAD
2600 END
3900 SUBROUTINE THERMOPL(INEFJ,MV,DEGR)
3910 REAL MV
3940 X=MV
3945 N0=10*(200,100),INEFJ
3950 T00=DEGR*(31.967400+X*(46.833212+X*(1.3093682)
3951C POLYNOMIAL REPRESENTATION OF COPPER-CONSTANTAN THERMOPLCOEFF
3952C CHARACTERISTIC POLYNOMIAL X IS MILLIVOLTS.
3955 G0=10*900
4100 T00=DEGR*(76.920643+X*(61.974432+X*(-13.244225+X*(7.0956986
4101C +X*(-0.34096114+X*(0.14044993*X))))
4110 DEGR=DEGR-273.15
4115 DEGR=DEGR*(DEGR/5.+32.0
4150 T00=DEGR*(460.+DEGR)
4160 RETURN
4170 END
4180 SUBROUTINE PRNTOU(GAS,REFT)
4200 COMMON C1,D1,D2,D3,D4,D5,D6,D7,D8,D9,F1,G1,G2,G3,G4
4250 COMMON I1,I2,I3,J1,J2,J3,J4,J5,K1,L0,L1,L9
4300 COMMON U1,U2,U3,U4,U5,U6,U7,U8,U9,V1,V2,V3,V4,V5,W,P1,P2,X,PLR
4350 COMMON M0,M1,M2,M3,M4,M5,M6,M7,M8,M9,N0,N1,N2,N3,N4,N5,N6,N7,N8,N9
4360 COMMON P0,P1,P2,P3,P4,P5,P6,P7,P8,P9,Q0,Q1,Q2,Q3,Q4,Q5,Q6,Q7,Q8,Q9
4362 COMMON DUMMY
4363 REAL I1,I2,I3,J1,J2,J3,J4,J5,K1,L0,L1,L9,L2
4365 FILENAME(GAS,REFT,ROTAM,WORD)
4400 1 FORMAT(IH)
4450 2 FORMAT(IH)
4500 3 FORMAT(IH-)
4550 4 FORMAT(10X,53H-----)
4551 PRINT 4PRINT 3PRINT 3
4552 PRINT 3
4554 PRINT 6
4555 6FORMAT(24X,26HSINGLE STAGE TURBOALTERNATOR)
4556 PRINT 4,GAS
4557 8FORMAT(14X,26HOPEN CYCLE PERFORMANCE WITH ,A9,4H GAS)
4558 IF(NEFT.EQ."IC") PRINT 10
4559 10FORMAT(24X,3HA1,4HROOM,12H TEMPERATURE)
4660 IF(NEFT.EQ."LV2") PRINT 11
4661 11FORMAT(24X,3HA1,9HCRYOGENIC,12H TEMPERATURE)
4750 PRINT 2
4800 PRINT 12
4850 12FORMAT(10X,15H*****.14HTFST REFERENCE,21H*****
4900 8*****
4950 PRINT 1
5000 PRINT 14

```

Figure 18. Open-Cycle Turboalternator Temperature Program (Sheet 4 of 9)

OCPRMT 01/03/75

```

5050 14FORMAT(10X,5HP0INT,10X,3HRUN,11X,5HM0NTH,11X,7MDAY)
5100 PRINT 16,D1,D2,D3,DA
5150 16FORMAT(10X,13,11X,15,7X,16,12X,14)
5200 PRINT 1
5250 PRINT 18
5300 18FORMAT(10X,11H*****,19HOVRALL PERFORMANCE,
5350 22IH*****))
5400 PRINT 4
5450 PRINT 1
5500 PRINT 20
5550 20FORMAT(10X,11HT0T EL PWR.,4X,7HSPD,RPM,8X,10HOVALL EFF.,
5600 4 5X,9HCOXK,SPD.)
5650 PRINT 22,G4,L9,L0,NST
5700 22FORMAT(10X,F9.4,6X,G10.6,8X,F8.4,6X,G10.6)
5750 PRINT 1
5800 PRINT 24
5850 24FORMAT(10X,10H*****,27HELECTROMAGNETIC PERFORMANCE,
5900 21SH*****))
5950 PRINT 4
6000 PRINT 26
6050 26FORMAT(10X,26H***PHASE VOLTAGE,VOLTS***,3X,14HLOAD RFS (L-V),
6051 8 1X,8HFLW,CPS)
6100 PRINT 28,V1,VR,V3,RI,C1
6150 28FORMAT(10X,F6.2,2X,F6.2,3X,F6.2,6X,F6.1,10X,F8.1)
6200 PRINT 1
6250 PRINT 30
6300 30FORMAT(10X,30H*****PHASE CURRENT,AMPS***** ,8X,
6350 21SHCOXK LOSS,WATTS)
6400 PRINT 32,11,12,13,J9
6450 32FORMAT(10X,F8.4,6X,F7.4,7X,F7.4,9X,F12.6)
6500 PRINT 1
6550 PRINT 34
6600 34FORMAT(10X,38H*****PHASE PWR,WATTS***** ,6X,
6650 21HELMAN. EFF.)
6700 PRINT 36,B1,G2,G3,E1
6750 36FORMAT(10X,4(F8.4,6X))
6800 PRINT 2
6850 PRINT 38
6900 38FORMAT(10X,36H*****JULE LOSS/PHASE,WATTS***** ,4X,
6950 22HTOTAL JULE LOSS,WATTS)
7000 PRINT 40,J1,J2,J3,J4
7050 40FORMAT(10X,4(F8.4,6X))
7100 PRINT 1
7150 PRINT 42
7200 42FORMAT(10X,51H*****SL0T TEMPS,R*****  AVG SL0T T,R  W00 RFS/P0
7250 PRINT 44,S4,S5,U0,H0
7300 44FORMAT(10X,3(F9.3,5X),1X,F9.4)
7350 PRINT 2
7400 PRINT 46
7450 46FORMAT(10X,52H*****TURBINE PERFORMANCE*****

```

Figure 18. Open-Cycle Turboalternator Temperature Program (Sheet 5 of 8)

OCIRMI 01/03/75

```

7500 PRINT 4
7550 PRINT 1
7600 PRINT 48
7650 48FORMAT(10X,10HTUR IN T,R,6X,10HTUR EX T,R,6X,10HACT T DR,R,
7700 87X,12MIN./EX.P.R.)
7750 PRINT 50,11,T3,D9,X
7800 50 FORMAT(10X,3(F9.2,7X),F12.7)
7850 PRINT 1
7900 PRINT 52
7950 52FORMAT(10X,9HWHL. PWR.,7X,9HWHL. EFF.,7X,9HWIND PWR.,7X,
7951 89HBR11. PWR.)
8000 IF(L2.GT.1.) L2=0.0
8050 PRINT 54,J1,L2,02,PLB
8100 54FORMAT(10X,FB.4,6X,FB.4,9X,F11.4,10X,FB.4)
8150 PRINT 1
8200 PRINT 56
8250 56FORMAT(10X,11CONN. TORQ.,5X,9HT.D. EFF.,7X,9HTIP SPEED,9X,
8300 810HVML. RATIO)
8350 PRINT 58,FUC,L1,U,V5
8400 58FORMAT(8X,011.4,6X,FB.4,10X,09.4,10X,FB.4)
8450 PRINT 1
8500 PRINT 60
8550 60FORMAT(10X,9HTOT. FLOW,5X,12MIN./NOZ.P.R.,5X,12HNOZ./EX.P.R.6X,
8600 810HFLOW FACT.)
8650 PRINT 62,W,PIPN,PVPE,K1
8700 62FORMAT(10X,F10.3,6X,F10.7,7X,F10.7,7X,FB.4)
8705 PRINT 1
8710 PRINT 64
8715 64 FORMAT(10X,8HJNL.PWR.,6X,11MPIV.FIL.GL.,5X,10HT4.LO.PWR.,
8716 8 9X,9HTH.LO.GL.)
8717 WORD1=1.E6*HP; WORD2=1.E6*PLC
8720 PRINT 66,PD,WORD1,BTPL,WORD2
8725 66FORMAT(10X,F11.4,5X,F0.2,6X,F10.4,10X,FB.2)
8730 PRINT 31PRINT 41PRINT 1
8750 RETURN
8800 END
10000 SUBROUTINE POWER(SPEED,VISD,PA,C,DIA,R,HP,PD)
10010 DIMENSION FRICM(6,7),PLN(A),HPD(A),P(2),Y(2),COFF(A)
10020 DATA FRICM(1,1),FRICM(2,1),FRICM(3,1),FRICM(4,1),FRICM(5,1),
10030 8FRICM(6,1)/.79548335E-01,17.997757,-1.0442957,18.725119,
10040 4-21.215130,4.2838538/
10050 DATA FRICM(1,2),FRICM(2,2),FRICM(3,2),FRICM(4,2),FRICM(5,2),
10060 8FRICM(6,2)/.53573563E-01,16.320037,1.7129676,-7.1244876,
10070 815.269540,-10.607818/
10080 DATA FRICM(1,3),FRICM(2,3),FRICM(3,3),FRICM(4,3),FRICM(5,3),
10090 8FRICM(6,3)/.41118604E-01,14.632700,-1.3671661,5.4194476,
10100 82.2727448,-6.5721933/
10110 DATA FRICM(1,4),FRICM(2,4),FRICM(3,4),FRICM(4,4),FRICM(5,4),
10120 8FRICM(6,4)/.46567553E-01,11.296766,1.3254786,-1.9497037,
10130 8-3.8823788,2.8164330/

```

Figure 18. Open-Cycle Turboalternator Temperature Program (Sheet 6 of 11)

001RMI 01/03/75

```

10140 DATA FRICM(1,5),FRICM(2,5),FRICM(3,5),FRICM(4,5),FRICM(5,5),
10150 &FRICM(6,5)/.16495614E-01,10.145229,-6.5322911,18.324597,
10160 &-21.139634,8.9724413/
10170 DATA FRICM(1,6),FRICM(2,6),FRICM(3,6),FRICM(4,6),FRICM(5,6),
10180 &FRICM(6,6)/.21405743E-01,8.2584829,-1.5153738,5.5441763,
10190 &-5.1637303,1.6683671/
10200 DATA FRICM(1,7),FRICM(2,7),FRICM(3,7),FRICM(4,7),FRICM(5,7),
10210 &FRICM(6,7)/.11773073E-01,7.0436074,-2.2367598,6.1213670,
10220 &-6.0091956,2.4735195/
102300 PROGRAM TPWATS APL 1971 JTMCC OF J20-C2947-01
102400 THIS PROGRAM OBTAINS THE POWER LOSS IN WATTS OF A TP JOURNAL BE
102500 CONSISTING OF THREE 100 DEG SHOES PIVOTED AT .65 AND LINE@
102600 WITH HELIUM GAS
102700
102800 INPUT DESCRIPTION
102900 SPEED = ROTATIONAL SPEED,RPM
103000 FEMP0 = GAS FEMP,DEGR (FEMP AT SPEED)
103100 SPDMAX = MAXIMUM ROTATIONAL SPEED,RPM
103200 FEMP1 = GAS FEMP AT SPDMAX,DEGR
103300 PA = AMBIENT PRESS.,PSIA (CONST FOR BOTH SPEEDS)
103400 DIA = JOURNAL DIAMETER,IN.
103500 DATA SEGMENTS (COEFF. OF POLY)
103600 1) FRICTION VS LAMBDA AT CONST HP
103700 2) LAMBDA MIN VS (LAMBDA MAX)/(LAMBDA MIN)
103800 3) HP VS JOURNAL DIA
103900 R=DIA/2.
104000 VISD=5.E-11*(FEMP0)**.646
10410 PLAMD=6.*VISD*SPEED*(R/2)**2*(4.55*PA)
10420 WALLS=0.0114193*PA*R*R*C*SPEED
10430 H=HP/20
10440 V= .35261157*PLAMD/(1.+005263156*PLAMD)
10450 IPATH=0
10460 IF(CH.LF..2)GO TO 70
10470 IF(CH.GI..75)GO TO 90
10480 IF(CH.GI..2).AND.(CH.LF..25)CALL FR(FRICM,1,.2,.25,V,P,Y,IPW
10490 IF(IPATH .EQ. 4)GO TO 500
10500 IF(CH.GI..25).AND.(CH.LF..3)CALL FR(FRICM,2,.25,.3,V,P,Y,IPW
10510 IF(IPATH .EQ. 4)GO TO 500
10520 IF(CH.GI..3).AND.(CH.LF..4)CALL FR(FRICM,3,.3,.4,V,P,Y,IPAW
10530 IF(IPATH .EQ. 4)GO TO 500
10540 IF(CH.GI..4).AND.(CH.LF..5)CALL FR(FRICM,4,.4,.5,V,P,Y,IPAW
10550 IF(IPATH .EQ. 4)GO TO 500
10560 IF(CH.GI..5).AND.(CH.LF..6)CALL FR(FRICM,5,.5,.6,V,P,Y,IPAW
10570 IF(CH.GI..6).AND.(CH.LF..75)CALL FR(FRICM,6,.6,.75,V,P,Y,IPW
10580 GO TO 500
10590 70 GO TO I=1,C
10600 COEF(I)=FRICM(I,I)
10610 79 CONTINUE
10620 K=V
10630 IPATH=3

```

Figure 18. Open-Cycle Turboalternator Temperature Program (Sheet 7 of 8)

GCPRM1 11/03/75

```

10640      80 TO 100
10650      80 PD=EVAL*WATTS*3.
10660      90 TO 600
10670      90 99 I=1.6
10680      COEFF(1)=FRICM(1,7)
10690      99 CONTINUE
10700      N=V
10710      IPATH=3
10720      100 EVAL=0.
10730      90 101 K=1.5
10740      IHAL=7-K
10750      EVAL=(EVAL+COEFF(IAL))*K
10760      101 CONTINUE
10770      EVAL=EVAL+COEFF(1)
10780      60 TO (80,80,80),IPATH
10790      50 A=(P(1)-P(2))*(Y(1)-H)/(Y(2)-Y(1))
10800      PD=(A+P(1))*WATTS*3.
10810      600 RETURN
10820      END
11000      SUBROUTINE FRICFRICM,K,X1,X2,V,P,Y,IPATH)
11010      DIMENSION FRICM(6,7),P(2),Y(2),L(2)
11020      L(1)=K
11030      L(2)=K+1
11040      Y(1)=X1
11050      Y(2)=X2
11060      90 20 I=1,2
11070      P(1)=0.
11080      JJ=L(1)
11090      90 10 J=1,5
11100      IHAL=7-J
11110      P(1)=(P(1)+FRICM(IHAL,JJ))*V
11120      10 CONTINUE
11130      P(1)=P(1)+FRICM(1,JJ)
11140      20 CONTINUE
11150      IPATH=4
11160      RETURN
11170      END
120000     ** FRICTION AND WINDAGE LOSSES **
120100     FACTOR IS FACTOR RE-PROGRAMMED APRIL, 1972 BY A. WARNER
120200     SUBROUTINE FAWR(N,D,SV3,MU,NJ,DSH,DS,G,PLGF,PLDF,PLSF,DD,NREF,
120300     RCM,DG,DDG,NREF,DM)
120400     VARIABLES REQUIRFD,DD,DDJ,DM,DSH,G,MU,N,SV3
120500     VARIABLES FURNISHEDDGD,DDG,DDM,DD,NREF,NREF,NREF,PLDF,PLSF,PLGF
120600     REAL D,MU,NREF,NREF,NREF,N3
120700     CDS=1.45V3*MU
120800     DSH=DD*DJ N3=N**3
120900     NREF IS TURBINE DISC REYNOLDS NUMBER
121000     NREF=0.367*N**0.5/(9.55E6*CONST1)
121100     DM IS TURBINE DISC DRAG COEFFICIENT
121200     IF(NREF.LT.75000.) DM=3.566*NREF**(-.5235)

```

Figure 1B. Open-Cycle Turboalternator Temperature Program (Sheet 8 of 9)

QCRMT

01/03/75

```

12130 IF(NRED .GE. 7500.) CMD=.1158*NRED**(-.2205)
12140C PLDF IS TURBINE DISC WINDAGE LOSS
12150 700 PLDF=2.645*CMD*N3*(D**5)/(SV3*R7.F10)
12160 IF(NRED .LT. 12000.) GFUN=1.8182*NRED**(-.4793)
12170 IF(NRED .GE. 12000.) GFUN=55.33E-4*NRED**(.1366)
12180C GD IS WHEEL BACKSIDE OPTIMUM GAP
12190 1000 GD=0.5*GFUN*D
12200C NREJ IS JOURNAL DIAM. REYNOLDS NUMBER
12210 NREJ=0.367*N*DJSQ/(9.55E6*CONST1)
12220C CDS IS JOURNAL DIAMETER DRAG COEFFICIENT
12230 CDS=0.0889/(NREJ**0.25)
12240C PLSF IS ALTERNATOR SHAFT WINDAGE LOSS.
12250 PLSF=3.3*DSH*CDS*N3*DJSQ*DJSQ/(870.F8*SV3)
12260C NREG IS ???
12270 NREG=N*DG*G/(9.55*33.3E4*CONST1)
12280 CONST3=(G/DG)**0.25
12290 IF(NREG .LT. 10000.) CDG=0.546*CONST3/SORT(NREG)
12300 IF(NREG .GE. 10000.) CDG=0.0867*CONST3/(NREG**0.7)
12310C CDG IS ALTERNATOR GAP MOMENT COEFFICIENT
12320C PLGF IS ALTERNATOR GAP WINDAGE LOSS
12330 PLGF=0.0332*CDG*DM*N3*DG**4/(8.7F8 *SV3)
12340C TOTAL WINDAGE LOSSES: PLDF+PLSF+PLGF
12350 RETURN
12360 END

```

Figure 18. Open-Cycle Turboalternator Temperature Program
(Sheet 9 of 9)

MERDC TURBOALTERNATOR ASSEMBLY

An assembly drawing of the MERDC turboalternator is shown in Figure 19.

Upon transfer of the Air Force turboalternator, Build 10, to the MERDC contract, the unit was completely disassembled. All critical parts to be re-used were carefully examined under a microscope. The shaft (part 7) journal bearing surfaces and the Kentalum journal bearing pads (part 23) were lightly relapped to remove slight indications of wear. The housing section (part 13) was drilled and tapped to reposition the journal bearing proximity probe (part 11) to adjust the probe angle for viewing the larger Kentalum journal bearing pad. New thrust bearing gimbal pivots were installed in the thrust bearing assemblies (parts 13 and 22). The new pivots have mating ball and socket fits to reduce the play in the thrust bearing assemblies, as noted in the Air Force turboalternator, Build 10.

The nozzle seal inspection test was made with the nozzle block and new nozzle flange to ensure a uniform metal-to-metal seal at the nozzle diameter. This test is described above under turboalternator open-cycle tests and procedures.

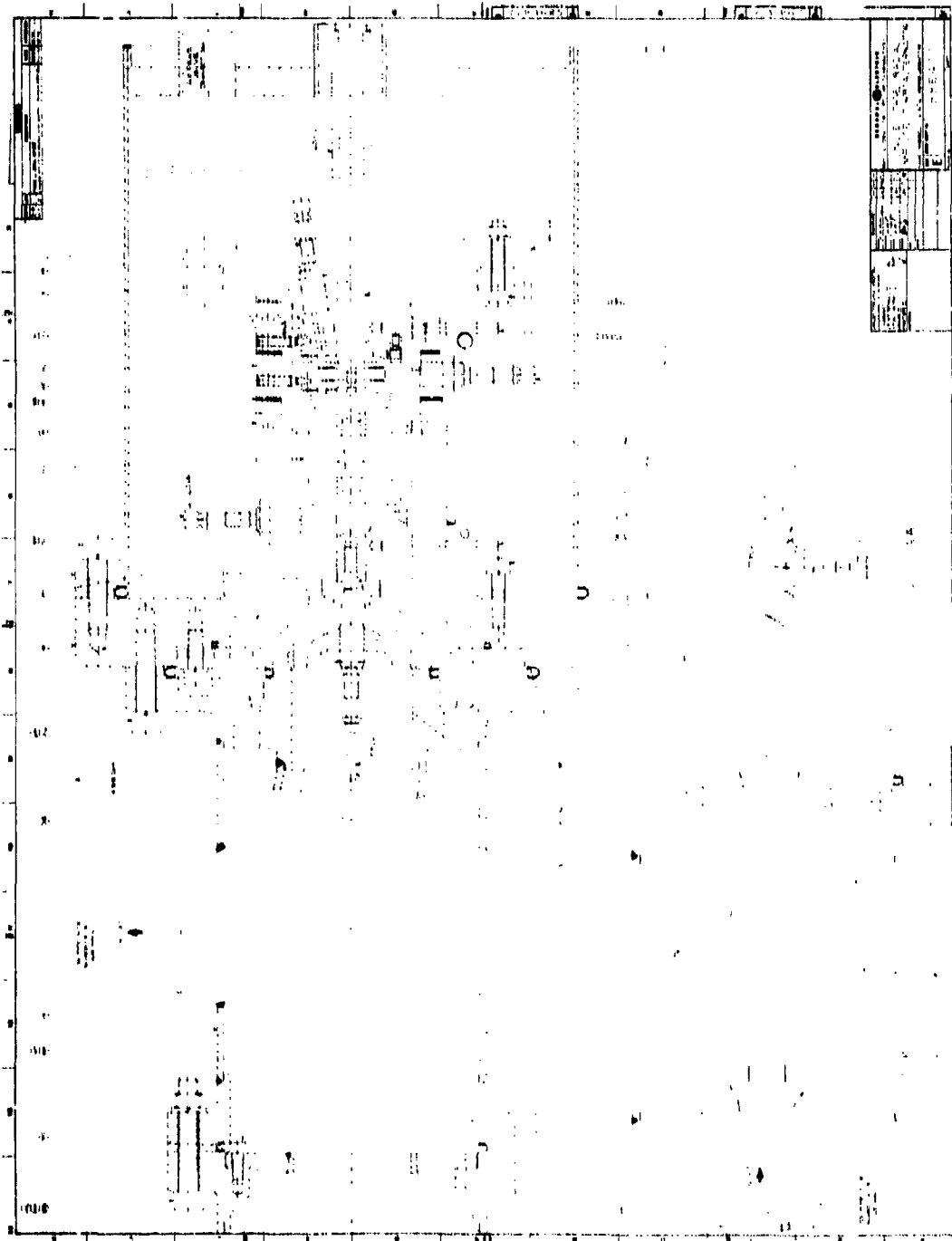


Figure 19. TA Assembly Drawing 588E477

All of the turboalternator parts were ultrasonically cleaned and sealed in clean plastic prior to assembly in a clean room as outlined in Appendix III, "Turboalternator Assembly Procedures."

The thrust bearings were shimmed to give a total axial shaft travel of 0.6-thousandth of an inch between thrust bearings and to provide a 1.5- to 2.0-thousandth of an inch turbine wheel to nozzle axial clearance. The journal bearings were adjusted for 260-microinch radial clearance.

PRELIMINARY TURBOALTERNATOR TEST

The turboalternator flow tests described in the Air Force Report (Ref. 5) and results plotted in Figures 75 and 76 of that report were repeated on the MERDC assembly. Results of the tests are shown in Table 7.

Table 7

MERDC TURBOALTERNATOR FLOW TEST

Test	Gas	% Agreement
Nozzle calibration (no turbine wheel)	He	<2
Nozzle calibration (no turbine wheel)	N ₂	<3
Zero speed (with turbine wheel)	He	<3
Zero speed (with turbine wheel)	N ₂	<6

Initial room temperature operational tests (October 1973) on the turboalternator assembly with the shaft magnet unmagnetized and magnetized gave excellent results. Tests were made at speeds in the area of 100,000 rpm. The proximity probes indicated very stable operation, and the shaft orbit probe signals produced exceptionally small orbits of 30 to 40 microinches at each end of the shaft, very similar to Build 10. The thrust, journal bearing, and outer gimbal ring proximity probes also showed very stable operation, with a slight once per revolution oscillation noted. Figures 20 and 21 show the proximity probe signals obtained. (The faint shadow or double images in the oscilloscope traces are caused by background noise in the proximity probe instrumentation.)

Alternator Winding Test. Room temperature resistance measurements were made on the MERDC alternator 3-phase windings. The average winding resistance was $9.135\Omega \pm 0.15\%$. The Air Force average winding resistance was 12.52Ω at room temperature and 1.64Ω at liquid nitrogen temperature. Since



Figure 20. Shaft Orbits of MERDC Turboalternator Assembly, Operating at Room Temperature, No Load, and 100,000 RPM. (Oscilloscope Sensitivity of proximity probe signals - 200 μ in/cm.)

the same wire was used in both windings, a resistance ratio of 7.65 would apply to both windings.

Figures 22 and 23 show the sinusoidal, 3-phase voltage outputs from the alternator. (The oscilloscope vertical sensitivity is 10 volts per centimeter and the sweep is 0.1 millisecond per centimeter in both figures.) These photographs verify, to a degree, the low voltage regulation and the freedom from harmonics one would predict from past similar experiences. The terminal voltage appears approximately as it should for the conditions of this test.

MERDC Turboalternator Open-Cycle Tests

Since considerable room temperature test data had been obtained on the Air Force program, it was decided to test this assembly at temperatures approaching that of liquid nitrogen, with helium gas, in the open-cycle test station. In this test, the turboalternator is installed into a sealed housing with feedthroughs for the electrical connections. The helium gas to the turbine is precooled by flowing the gas through a coil immersed in liquid nitrogen. Strips of plastic material were attached to the turboalternator support strand, to direct the cold nozzle exhaust gas around the turboalternator sealed housing, cooling the whole assembly. A bell jar was placed over the turboalternator assembly, to isolate the system from ambient moisture. The turbine exhaust gas still expands to atmosphere.

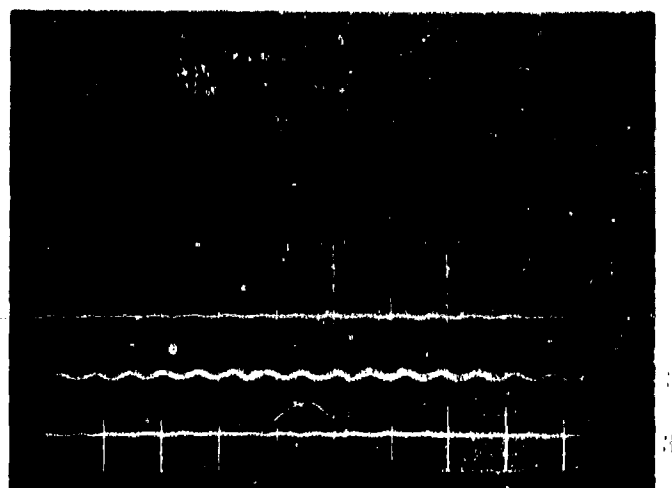


Figure 21. MERDC Turboalternator Assembly, Operating at Room Temperature, No Load, and 100,000 RPM. (Trace 1 is the thrust probe, axial shaft motion between thrust bearings; Trace 2 is the journal bearing pad motion; Trace 3 is the outer thrust bearing gimbal ring motion. Oscilloscope sensitivity of proximity probe signal 400 μ in/cm vertically; horizontal sweep 1.0 ms/cm.)

The performance measurements can be obtained and the effective average nozzle pressure can be measured in conjunction with other performance factors. The effective average nozzle pressure would be the pressure in the sealed housing. The three pressure ratios obtained from combinations of the inlet, nozzle, and exit pressures will vary with the velocity ratio in a characteristic manner.

The turboalternator was operated for one hour at room temperature, 100,000 rpm, and no load, to purge the system with cylinders of helium gas. The dew point of the helium was -65°F . The gas pressure tap connecting the sealed housing was disconnected to purge the turboalternator housing and the sealed housing. Then, in order to cool the turboalternator assembly at a slow rate, liquid nitrogen was slowly added to a dewar containing the cooling coil.

After 2-1/4 hours of cooling, the gas temperature at the nozzle inlet reached 109°K, and the alternator winding temperature was 165°K. The turboalternator operated satisfactorily at speeds in the order of 100,000 rpm with an 11-watt load on the alternator.

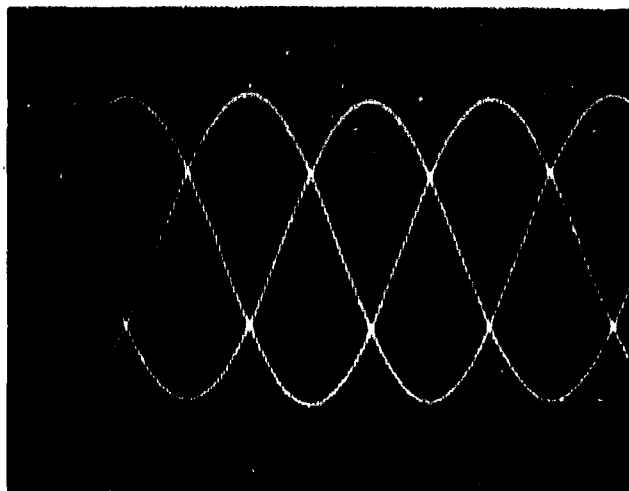


Figure 22. Alternator, 3-Phase, Line-to-Line Voltage Output of MERDC Turboalternator, Operating at Room Temperature, No Load, and 100,000 RPM

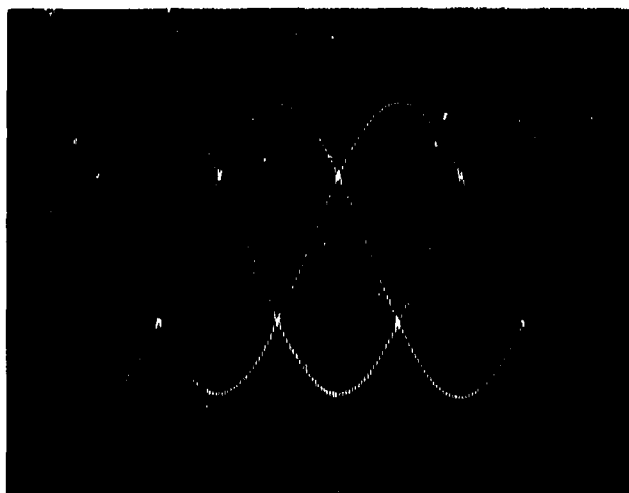


Figure 23. Alternator, 3-Phase, Line-to-Neutral Voltage Output of MERDC Turboalternator, Operating at Room Temperature, 8.5-Watt Resistive Load, and 100,000 RPM

The only problem encountered during cooldown was that the leads from the orbit proximity probes failed and the operation of the turboalternator had to be monitored by the remaining probes.

The test plan was to check the operation of the turboalternator and to obtain performance data by operating the turboalternator in a vertical position, thrust end up, with the nozzle-inlet-to-exhaust pressure ratios of 1.4, 1.9, and 2.4 (pressure ratio of 2.4 was the design condition).

Tests were conducted by adjusting the gas flow through the nozzle to obtain a given pressure ratio, and the turboalternator speed was controlled by varying the resistive load on the alternator with speeds ranging from low operating speeds up to 200,000 rpm. Nine data points were obtained on MERDC Run 100 with a pressure ratio of 1.4 and speeds ranging from 69,300 to 211,320 rpm.

The nozzle pressure ratio was then adjusted to 1.9, and 5 data points were obtained on MERDC Run 101 with the turboalternator speeds ranging from 118,320 to 196,240 rpm. As the turboalternator speed was adjusted towards 180,000 rpm slight roughness was noted on the thrust probe, the journal bearing probe, and the outer gimbal ring proximity probe signals. This indicated that the shaft may have been just touching the thrust bearing surface, but in general, this did not affect the operation. At this pressure ratio and speed, the sealed housing pressure was 64 inches of water above atmospheric.

As the turboalternator flow was gradually increased for the 2.4 pressure ratio, the proximity probe signals became rough and the turbine speed decreased. Increasing the gas flow continued to decrease the turbine speed. Then, the turbine stopped. Attempts to restart the turbine failed.

The turboalternator was allowed to warm up to room temperature. There appeared to be considerable moisture present in the turboalternator, as evidenced by the fact that tapping the support stand did not move the shaft as it does normally. After purging the turboalternator with a low flow of helium gas for approximately one hour longer, the turbine started. Its operation was rough at first, but smoothed out quickly. All of the proximity probe signals were identical to those obtained before starting the cold tests.

There are two possible explanations for unsatisfactory operation at the higher pressure ratio. First, the vessel in which the unit was tested did not permit a bleed of gas from the alternator region to the discharge side of the turbine. For this reason, increased pressure on the back side of the turbine wheel may have overloaded the inner thrust bearing. (The final installation of the turboalternator included a gas bleed to counteract this effect.)

A second explanation is that moisture was deposited in the turboalternator and caused the shutdown. There was some evidence of this; as the unit was being warmed up and purged with dry gas, the bearings appeared sticky on the oscilloscope traces, which would be the case if moisture were present. This effect was present until some time after the unit was fully warmed up.

FINAL TURBOALTERNATOR OPEN-CYCLE TESTS

To complete the open-cycle testing, a second series of tests was conducted in December 1974.

A number of gas supply systems were considered to eliminate the possibility of moisture causing the above problem. It was decided to use helium gas from a trailer containing 40,000 standard cubic feet of helium. The purity was guaranteed to be 99.995 percent or better, with a dew point less than -110°F (less than 2 ppm water by volume).

A bleed line and valve were also connected to the turboalternator sealed housing to reduce the housing pressure during the open-cycle tests if required.

The proximity probe feedthroughs were adjusted to improve the contact with the mating lead connectors and prevent opening during cooldown.

The second open-cycle test was started using the same procedures for purging and cooling as described above. The turboalternator operated very well during cooldown, and this time the orbit proximity probe leads did not open. Figures 24 and 25 show the proximity probe signals obtained with the turboalternator operating with the nozzle gas inlet temperature of 89°K , 11-watt load and at 100,000 rpm. The proximity probe signals are very similar to the room temperature, no load operation shown in Figures 19 and 20.

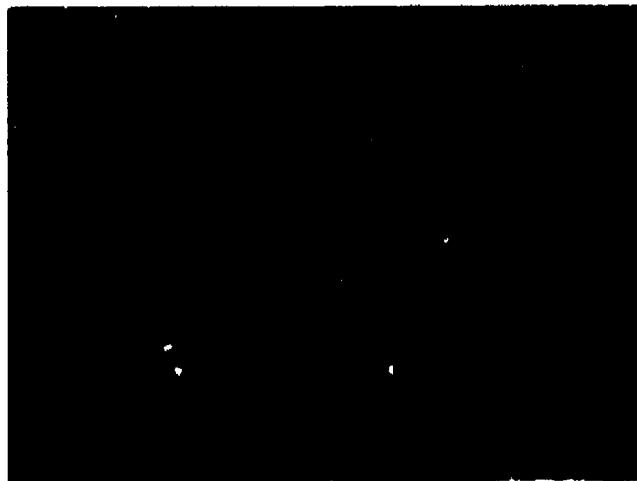


Figure 24. Shaft Orbits of MERDC Turboalternator Operating in the Second Open-Cycle Test with 89°K Gas, 11-Watt Load, and 100,000 RPM. (Oscilloscope Sensitivity of Proximity Probe Signals 200 $\mu\text{in/cm}$.)

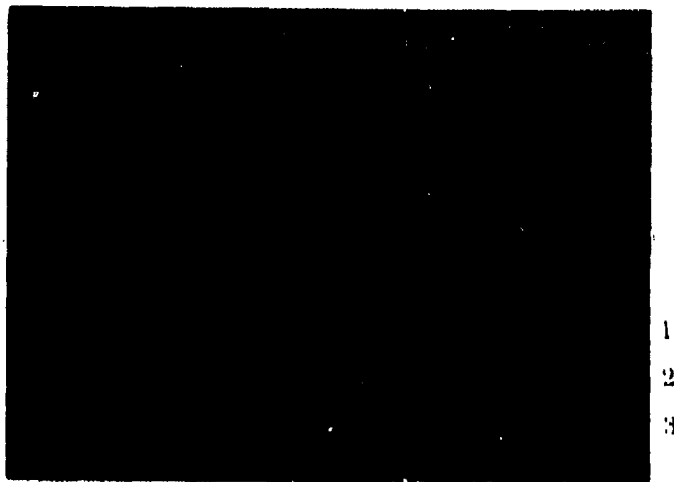


Figure 25. MERDC Turboalternator Operating in the Same Conditions as Figure 24. (Trace 1 is the thrust probe, axial shaft motion between thrust bearings; Trace 2 is the journal bearing pad motion; Trace 3 is the outer thrust bearing gimbal ring motion. Oscilloscope sensitivity of proximity probe signal = 400 μ in/cm vertically; horizontal sweep = 1.0 ms/cm.)

As a comparative check, two data points were repeated in MERDC Run 102 with the nozzle inlet to exhaust pressure ratio of 1.4. There was no noticeable change in the operation of the turboalternator. The nozzle pressure ratio was then increased to 1.9, and one of the lower speed data points was repeated in MERDC Run 103, with the nozzle inlet gas at 83°K, 29.5-watt alternator load, and 117,000 rpm. This data point also repeated very well; however, the thrust proximity probe indicated that the shaft thrust was just barely touching the thrust bearing. It was, therefore, decided to reduce the housing pressure from 59 inches of water to 27 inches by opening the housing bleed valve, since this condition would become worse at higher speeds and higher nozzle pressure ratio. The reduced housing pressure corrected the thrust operation and the data point was repeated with lower housing pressure being the only difference. The nozzle pressure ratio was then increased to 2.4 to be certain that the housing bleed was sufficient. The turboalternator operated well; four data points were taken during this MERDC Run 104 with speeds ranging from 166,500 to 188,940 rpm and loads from 57.7 to 60.1 watts. The fixed three-phase, "Y" connected, resistive load points were the limiting factor in varying the speed and load over a wider range. Figures 26 and 27 show the proximity probe signals obtained with the turboalternator operating at 188,940 rpm and 60.1-watt load. Figure 27 shows a slight oscillation of the shaft between the thrust bearings, but there was no indication of touching or

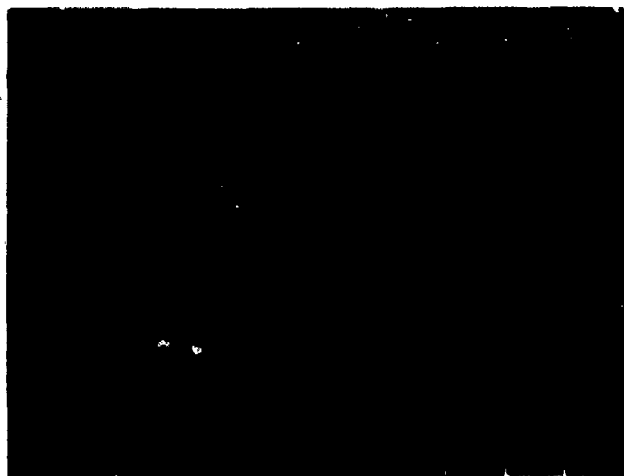


Figure 26. Shaft Orbits of MERDC Turboalternator Operating with 82°K Gas, 60.1-Watt Load, and 188,940 RPM with Nozzle Pressure Ratio of 3.4. (Oscilloscope sensitivity of proximity probe signals = 200 μ in/cm.)

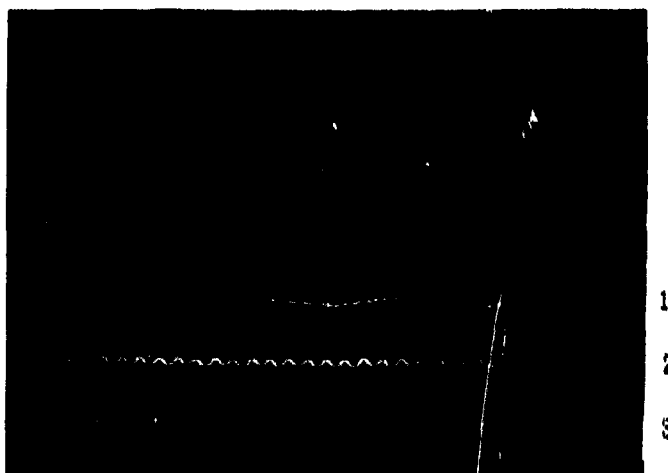


Figure 27. MERDC Turboalternator Operating in the Same Conditions as Figure 26. (Trace 1 is the thrust probe, axial shaft motion between thrust bearings; Trace 2 is the journal bearing pad motion; Trace 3 is the outer thrust bearing gimbal ring motion. Oscilloscope sensitivity of proximity probe signals = 400 μ in/cm vertically; horizontal sweep = 1.0 ms/cm).

rough operation. Since the housing bleed did not have to be readjusted at the higher pressure ratio, three additional data points were taken for MERDC Run 103, pressure ratio 1.9, at higher speeds.

After the above data points were taken, the turboalternator was stopped and restarted cold without any difficulty.

The operation of the turboalternator was very successful during the second open-cycle test. Results of this test with very dry gas gave evidence that moisture was the cause of the turbine stopping during the first cold test, and that the sealed housing bleed will be required in the cryosection to reduce the housing pressure when operating the turboalternator with nozzle pressure ratios greater than 1.8.

PERFORMANCE TEST RESULTS

The data obtained in the first and second cryogenic open-cycle tests were reduced and the performance test parameters were plotted in Figures 28 through 33.

The data reduction program was not modified to reflect the operation with the housing bleed line open, since only four new data points were obtained in the second open-cycle test, with the nozzle pressure ratio of 2.4. A rather lengthy program would be required to establish the correct parameters over this wide temperature range. Therefore, the points obtained with the bleed line open are identified in the curves, and their values should be considered as trends, not actual values. An indication of the effect on the data, caused by the housing bleed valve, can be seen by comparing the reduced data from MERDC Run 103, data points 1 and 2. Data point 1, shown in Figure 34, was obtained with the bleed valve closed. Data point 2, shown in Figure 35, was obtained with the same resistive load and with the turboalternator operating at approximately the same pressure ratio and speed, but with the bleed valve open to reduce the housing pressure from 59 to 27 inches of water.

Also, the equation used in the data reduction program to calculate the alternator winding resistance per phase versus temperature was derived for the Air Force alternator and was not modified for the lower resistance windings of the MERDC alternator; therefore, the winding resistance per phase, the joule loss per phase, and total joule loss shown in Figures 34 and 35 would be approximately one third less. This would increase the electromagnetic efficiency slightly.

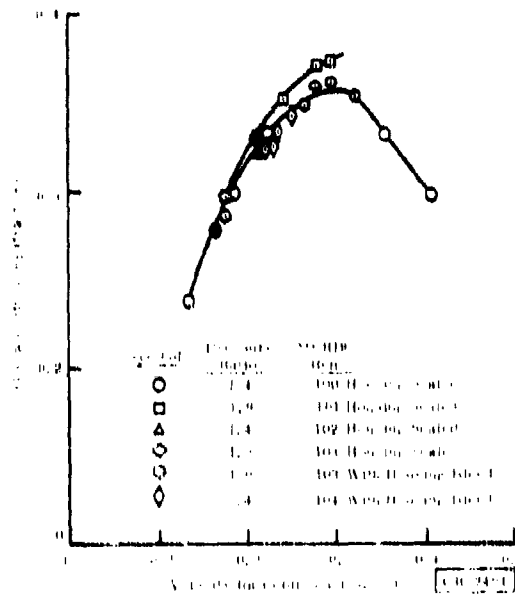


Figure 28. Overall Efficiency Versus Velocity Ratio (Helium Gas at 83° K)

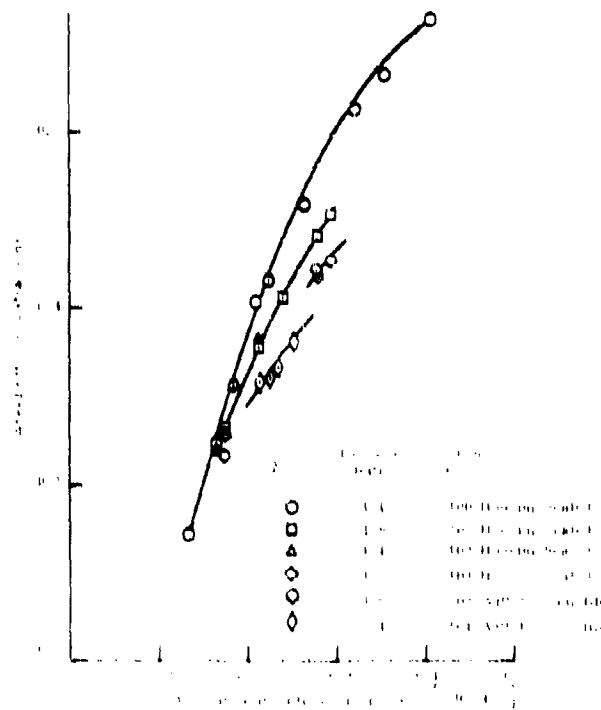


Figure 29. Wheel Efficiency Versus Velocity Ratio (Helium Gas at 83° K)

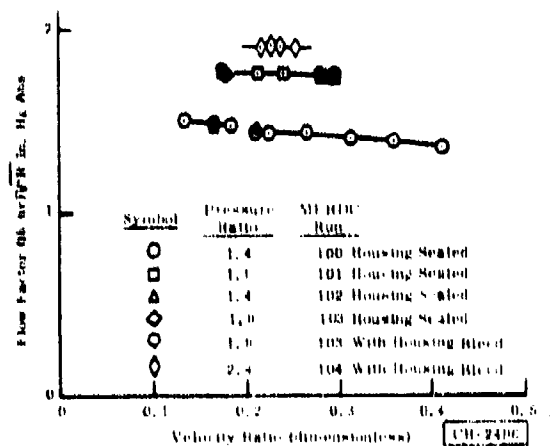


Figure 30. Flow Factor Versus Velocity Ratio (Helium Gas at 83°K)

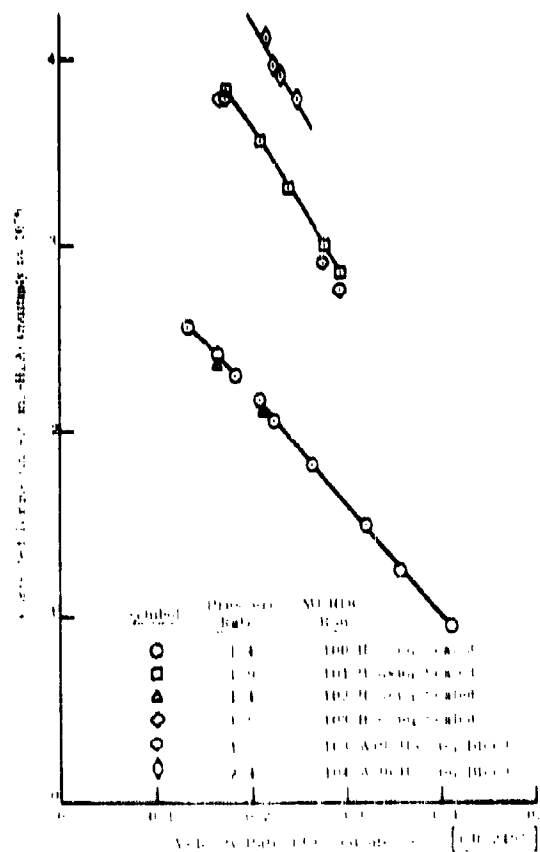


Figure 31. Corrected Torque Versus Velocity Ratio (Helium Gas at 83°K)

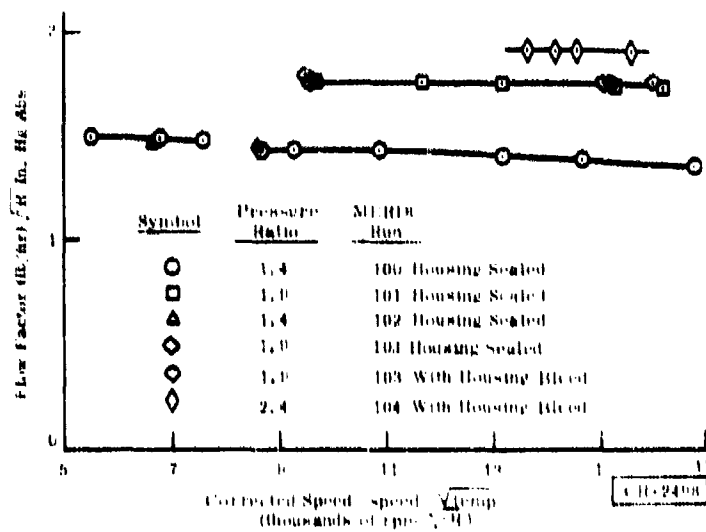


Figure 32. Flow Factor Versus Corrected Speed (Helium Gas at 83° K)

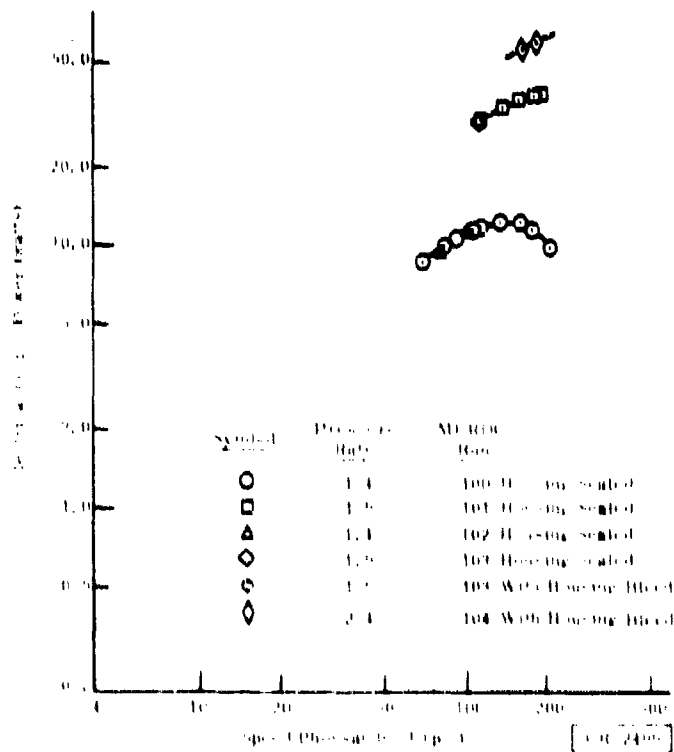


Figure 33. Electrical Output Power Versus Speed (Helium Gas at 83° K)

SINGLE STAGE TURBOALTERNATOR
OPEN CYCLE PERFORMANCE WITH HELIUM GAS
AT CRYOGENIC TEMPERATURE

*****TEST REFERENCE*****

POINT RUN MONTH DAY
1 103 12 4

*****OVERALL PERFORMANCE*****

TOT EL PWR. SPD, RPM OVAL EFF. CORR. SPD.
29.4574 117000. 0.2960 9596.89

*****ELECTROMAGNETIC PERFORMANCE*****

PHASE VOLTAGE, VOLTS LOAD REF (L-N) FREQ, CPS
21.30 21.30 21.30 45.7 1950.0

*****PHASE CURRENT, AMPS***** OMR LOSS, WATTS
0.4610 0.4610 0.4610 0.213974

*****PHASE PWR, WATTS***** FL MAG. EFF.
9.8193 9.8193 9.8193 0.9579

*****JOULE LOSS/PHASE, WATTS***** TOTAL JOULE LOSS, WATTS
0.3597 0.3597 0.3597 1.0792

*****SLOT TEMP, ***** AVG SLOT T/R WDR PER/PH
186.553 189.677 186.115 1.6927

*****TURBINE PERFORMANCE*****

TUR IN TOR TOR EX TOR NET TOR IN. ZFK. P.P.S.
136.63 136.63 0.95 1.9987513

WHL. PWR. WHL. EFF. RIND PWR. RPP. PWR.
32.7651 0.3292 0.2609 1.7535

CORR. TORQ. T.D. EFF. TIP SPEED VFL. RATIO
0.3776E+03 0.2960 255.1 0.1744

TOT. FLUX IN. ZFK. P.P.S. NOZ. ZFK. P.P.S. FLOW FACT.
3.133 1.7558590 1.1024366 1.7615

JNL. PWR. PLY. FL. CL. FLY. PWR. TOL. CL.
0.2233 150.31 0.2190 250.33

Figure 34. MERDC Run 103, Data Point 1, Data Obtained with Housing Bleed Valve Closed

SINGLE PHASE CORROALTERNATOR
 OPEN CYCLE PERFORMANCE WITH HELIUM GAS
 AT CRYOGENIC TEMPERATURE

*****TEST*****

POINT 2 RUN 103 MONTH 12 DAY 4

*****OVERALL PERFORMANCE*****

LINE FL. EFF. SPD. RPM. OVAL. EFF. CORR. SPD.
 27.1934 11492.0 9.885 9470.95

*****ELECTROMAGNETIC PERFORMANCE*****

PHASE VOLTAGE, VOL. (RMS) LOAD EFF. (LINE) KW/PHASE
 1.20 21.20 45.7 133.0

PHASE CURRENT, AMP. CORE LOSS, WATT
 0.459 0.459 0.459 0.210856

PHASE IND. REACTANCE, OHM. RMAG. EFF.
 2.730 8.730 8.730 0.9637

RESULTS/PHASE, WATT. INITIAL DOUBLE LINE WATT
 0.266 0.266 0.266 0.4881

LINE VOLTAGE, VOLT. LINE CURRENT, AMP. LINE REACTOR
 171.22 171.22 171.22 1.2052

*****LINE PERFORMANCE*****

LINE EFF. LINE REACTOR EFF. LINE REACTOR WATT
 1.000 1.000 1.000 1.200000

LINE EFF. LINE REACTOR EFF. LINE REACTOR WATT
 1.000 1.000 1.000 1.200000

LINE EFF. LINE REACTOR EFF. LINE REACTOR WATT
 1.000 1.000 1.000 1.200000

LINE EFF. LINE REACTOR EFF. LINE REACTOR WATT
 1.000 1.000 1.000 1.200000

LINE EFF. LINE REACTOR EFF. LINE REACTOR WATT
 1.000 1.000 1.000 1.200000

Figure 35. MERIC Run 103, Data Point 2, Data Obtained with Housing Bleed Valve Open, but not Corrected for Housing Leakage Flow

Section 5

CRYOGENIC HEAT EXCHANGERS

GENERAL

Refrigeration cycles which employ dynamic rotating machinery operate at lower pressure ratios than cycles which employ positive displacement machinery. For a given refrigeration load, this requires a higher mass flow. These conditions place a requirement on the cryogenic heat exchangers for high thermaleffectiveness and large heat transfer surface area. An effectiveness of 98.5% is required in the warmest heat exchanger of the selected cycle. An effectiveness this high implies an extremely large number of transfer units, 66, which also implies an extremely high lateral thermal conductance. A conflicting requirement is that while the heat exchangers must have high thermal conductances, they must also have small pressure drops because of the low pressure ratio of the cycle.

A type of heat exchanger considered to be well suited for this application was the stacked screen heat exchanger. The perforated plate heat exchanger was considered, but the required plate porosity and hole size would have made manufacturing extremely difficult. Since stacked screen heat exchangers had been successfully constructed in small sizes by Kinergetics Incorporated, the decision was made to purchase the heat exchangers.

Specifications for the heat exchangers were selected based on analysis of the cycle. These are presented in Appendix IV, "Specifications for a Set of Seven Cryogenic Exchangers."

DESIGN AND CONSTRUCTION

The design and construction of the heat exchangers is discussed in the vendor report enclosed as Appendix V, "Kinergetics Incorporated -- Final Report." Because the vendor was unable to prevent stream-to-stream leakage in the cold exchanger, it was decided to make this exchanger inactive. This was accomplished by blocking it off at the joint between the aluminum header and the wire mesh header section at the warm end of this exchanger.

TEST RESULTS -- KINERGETICS

The portion of the testing which was completed by Kinergetics is presented in Appendix V.

TEST RESULTS -- GENERAL ELECTRIC

The difficulties encountered at Kinergetics Incorporated resulted in a delay of 23 months from the specified date. It was concluded in conjunction

with MERDC, that it was in the best interest of the Government to accept delivery of the heat exchangers and complete the testing at General Electric.

GENERAL ELECTRIC TEST FACILITY

The Research and Development helium test facility consists of a positive displacement compressor, aftercoolers, and leak-tight plumbing necessary for the testing of high efficiency heat exchangers and turbomachinery. It was decided to use this facility to test the heat exchanger.

The compressor is an Ingersoll Rand Company unit, Class ESH-1 N1-2, which has a solid lubricated piston. The bore is 17 inches in diameter and the stroke is 9 inches long, and the unit can be operated either in the single or double acting mode. The motor is 60 horsepower, 1800 rpm.

With the suction pressure above one atmosphere, the unit is single acting. Under these conditions, the rated performance for helium gas is:

<u>Characteristic</u>	<u>Performance</u>
Inlet pressure	0.121 MN/m ² (17.6 psia)
Discharge pressure	0.358 MN/m ² (52 psia)
Inlet temperature	332°K (136°F)
Volume flow at inlet	0.187 m ³ /sec (396 cfm)
Helium density at inlet	0.175 kg/m ³
Helium mass flow	32.7 g/sec

This mass flow of 32.7 grams per second, and the pressure ratio of 2.95, are more than adequate for testing the heat exchanger.

TEST METHOD

The physical arrangement of the heat exchanger test is shown in Figure 36. Helium is supplied from the facilities compressor. It passes through the high pressure side of heat exchanger 7 before flowing out supply 7 to the liquid nitrogen dewar. The lines to and from the liquid nitrogen dewar are insulated. A valve is included for controlling the returning stream pressure. The helium returns from the dewar, flows in return 5, and flows through exchangers 6 and 7, before returning to the compressor. Heat exchanger 6 has flow only through the low pressure passages. Although exchanger 6 does contribute to the low pressure-stream pressure drop, it does not contribute to the stream-to-stream heat transfer. There is a bleed from return 1 for use during cooldown.

The temperatures of the two streams are measured before entering and after leaving the heat exchanger, with copper-constantan thermocouples inserted in the streams. There is also a thermocouple on the bleed line near

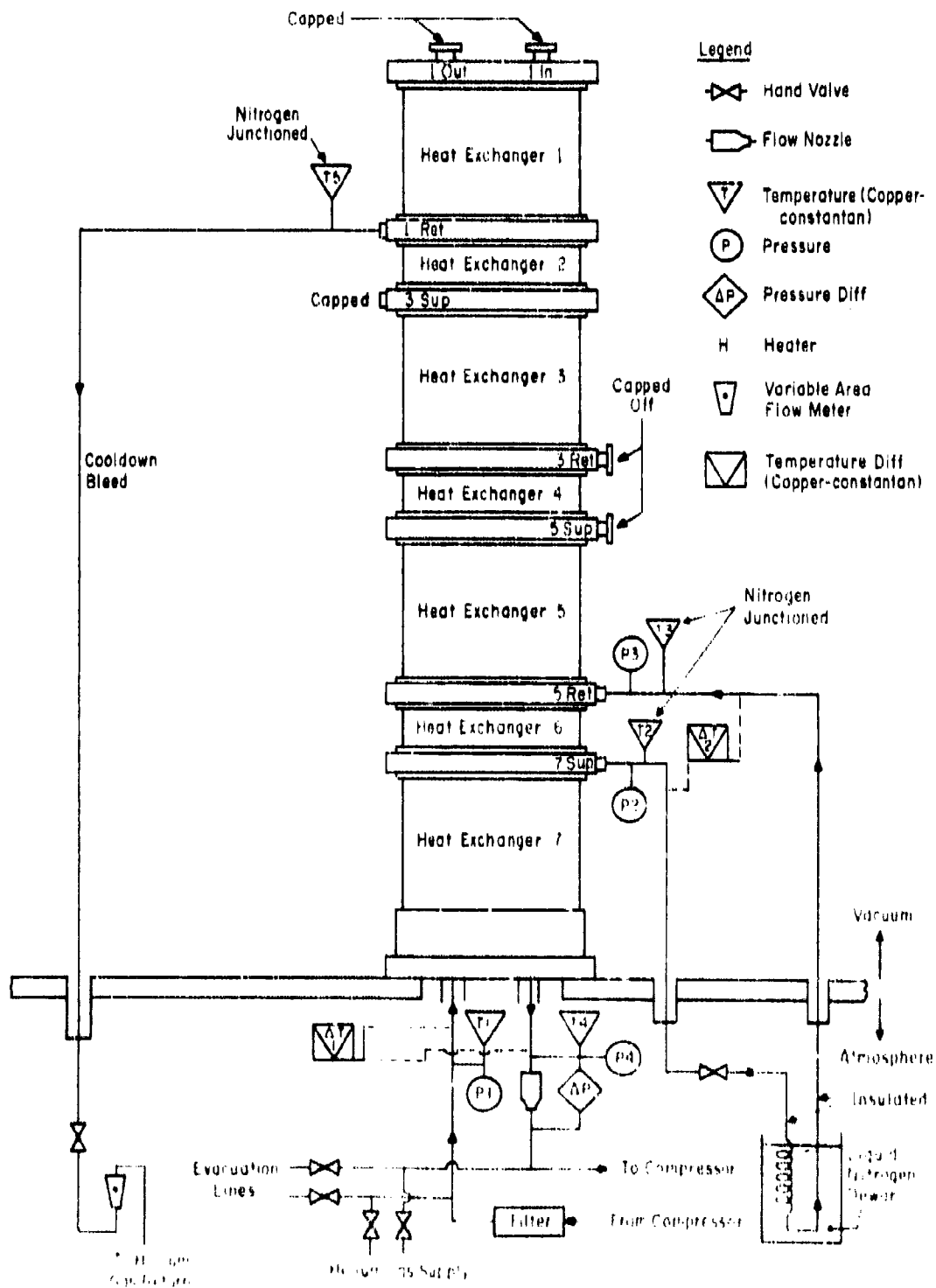


Figure 36. Heat Exchanger Test System (No Flow)

return 1. The reference junction of the thermocouples used to measure the warm end temperatures of the heat exchanger are in an ice bath, and all others are in a liquid nitrogen bath. Figure 36 shows temperature difference measurements, ΔT_1 and ΔT_2 , but these measurements were not taken because grounding of the thermocouples during installation made them inoperable in the temperature-difference mode of operation.

Pressures are measured at points indicated in Figure 36 with pressure gauges. The ΔP measurement indicates the pressure drop past an A. S. M. E. nozzle of known diameter to provide a mass flow measurement.

Figure 37 depicts the heat exchanger during assembly. In this figure, the vacuum bell jar is not yet in place over the exchanger on the base plate. The tubing to and from the cold end of the heat exchanger can be seen to be curved in two planes at the connections to the heat exchanger. This is to ensure good thermal mixing of the gas in the tubing before the temperature measurements are made. The nitrogen dewar is on the right and the cryogenic valve in the cold helium stream can be seen to the lower left of the nitrogen dewar. The tubing leading to and from the nitrogen dewar was later insulated with 1-inch thick foam rubber.



Figure 37. Heat Exchanger During Assembly

After the six points in Test 1 were taken, an attempt was made to measure the leakage from stream-to-stream. It was found that the leakage had increased so that it was above the range of the instrumentation.

Because of this high leakage rate, it was decided to attempt to increase the loading on the heat exchanger tension rod. It was discovered that the rod was under tension well under one-third of the design value. The rod tension was then increased to the design value (15,800 lb warm).

During Test 2, additional flow meters were used to allow measurement of interstream leakage over a range of several orders of magnitude. The stream-to-stream leakage was then measured during the Test 2 cooldown. Table 9 presents the leakage data as the heat exchanger was cooled.

Table 9
LEAKAGE MEASUREMENTS

Test No.	T2 (°K)	T5 (°K)	DP (psi)	ML (g/sec)	ML/DP (g/sec/psi)
Test 1	298	298	5.6	7.677×10^{-5}	1.37×10^{-5}
Test 2	300	300	5.1	3.3×10^{-5}	6.48×10^{-6}
			5.6	3.56×10^{-5}	6.36×10^{-6}
			9.4	6.44×10^{-5}	6.86×10^{-6}
			9.8	7.13×10^{-5}	7.27×10^{-6}
	204	300	10.8	3.03×10^{-5}	2.81×10^{-5}
			11.8	3.63×10^{-5}	3.08×10^{-5}
	154	297.5	6.5	2.02×10^{-5}	3.12×10^{-5}
			7.2	2.71×10^{-5}	3.76×10^{-5}
	120	221.5	4	8.07×10^{-5}	2.01×10^{-2}
			4.5	1.02×10^{-1}	2.27×10^{-2}
			5.5	1.24×10^{-1}	2.2×10^{-2}
	123	130°K	3	2.42×10^{-1}	3.07×10^{-2}
			3	2.42×10^{-1}	3.07×10^{-2}
	98	202°K	5	1.10×10^{-1}	3.835×10^{-2}
			10	3.77×10^{-1}	3.77×10^{-2}
12.5			5.11×10^{-1}	4.09×10^{-2}	

no flow through the bleed

After cooldown, the efficiency and pressure drop were again measured. These are the two points listed under Test 2 in Table 8. The first was taken near the design pressures, and the second was taken with the valve in the tubing leading to the nitrogen dewar wide open.

DISCUSSION OF THE TEST RESULTS

The data taken during this test were taken at temperatures lower than the design condition temperatures. The section titled "Relating the Results to Design Condition," in Appendix VI, "Heat Exchanger Analysis," presents an analysis of heat transfer and pressure drop in the heat exchanger. Equations for scaling the data to the design condition are developed.

The specified pressure drops through heat exchanger 7 are .019 atm (.279 psi) on the high pressure side and .022 atm (.3234 psi) on the low pressure side at the rated flow of 7.686 g/sec. The measured high pressure side drop can be seen in Table 8 to be in the range from 1.7 to 1.9 psi.

As a result, at least in part, of leakage, the heat exchanger will not meet the 98.5% specification for effectiveness. The measured effectiveness at design pressures never exceeded 92.6%. When the stream-to-stream pressure difference was reduced from the design condition, an improved effectiveness as high as 94.9% was observed. This indicates that stream-to-stream leakage is at least in part causing the low heat exchanger effectiveness.

The method used to calculate effectiveness and NTU from the data is described in the section titled, "Data Reduction Computer Program," in Appendix VI. The effectiveness calculation is based on the average of the temperature differences between streams at the warm and cold end of the heat exchanger.

$$\text{Effectiveness} = \frac{1}{1 + \frac{(\Delta T_1 + \Delta T_2)/2}{(T_1 + T_4 - T_2 - T_3)/2}}$$

The effect of leakage on the heat exchanger effectiveness is analyzed in the section titled, "Effect of Helium Leakage, Thermal Radiation, and Axial Conduction on Heat Exchange Performance," in Appendix VI. The effect of stream-to-stream leakage is shown to increase the cold end temperature difference (ΔT_2) and to have little effect on the warm end temperature difference (ΔT_1). A leak to the casing of the heat exchanger bypasses the low pressure side of the heat exchanger and increases the temperature difference on both ends. The following approximate equations are developed in the same section of Appendix VI.

$$\frac{\Delta T_1}{T_1 - T_2} \approx \frac{M_1}{M} \quad \text{for leakage to the casing}$$

$$\frac{\Delta T_1}{\Delta T_2} \sim 1 - \frac{M_L}{M} \text{ for stream to stream leakage}$$

Applying these equations to the data in Table 8 yields some information about the leaks in the heat exchanger. In Test 1, the large difference in the temperature differences at the two ends of the heat exchanger indicates that there was a large stream-to-stream leak. This leak appears to be substantially less in Test 2 after tension on the bolt has been increased. This can be seen from the fact that the temperature differences at the two ends of the heat exchanger are closer together. A comparison of the warm end temperature difference in the two cases indicates that the leakage to the casing was not affected substantially by the tightening of the bolt.

The two data points in Test 2 show the effect of decreasing the stream-to-stream leakage on the stream-to-stream temperature differences. The ratio $\Delta T_1/\Delta T_2$ is much larger in the second data point, where the pressures in the low and high pressure sides of the heat exchanger were brought closer together. This would be expected from the preceding equation.

The first Test 2 data point was taken at the design pressures for the heat exchanger. When the temperature differences are applied to the preceding two equations, a stream-to-stream leakage of approximately 1/3 the mass flow and a leakage to the casing of 1/20 the mass flow are indicated.

The specification for the heat exchanger stream-to-stream leakage was 10^{-3} atm cc/sec at 20 psi pressure differential, which corresponds to approximately 1.6×10^{-2} g/sec. The leakage test results in Table 9 indicate that the heat exchanger exceeds the specified maximum stream-to-stream leakage at room temperature.

Several features of the leakage from stream-to-stream are indicated by the data in Table 9. The room temperature leakage decreased after the rod was loaded, as was indicated by the thermal data. The leakage increases dramatically with decreasing temperature. The leakage was experimentally found to be linearly dependent on the stream-to-stream pressure difference. This indicates that the leak is laminar. The dependence of the leak on temperature can be derived from the laminar equation for the friction factor,

$$f \propto 1/Re \quad \text{where } f = \text{friction factor} = \frac{4 \Delta P}{(L/D) (M_L^2 / 2cA)}$$

$$M_L \propto P \sqrt{T} \quad \text{Re} = \frac{(M_L / A) D}{\rho}$$

D hydraulic diameter

ρ density

M_L leakage

- μ - viscosity
- A - cross section
- l - length

The leakage increases faster with decreasing temperature than can be explained by the increase in density and the decrease in viscosity considered in the above equation. This indicates that the hole through which the leakage is occurring changes geometry with decreasing temperature.

The last two data points in Table 9 indicate that the stream-to-stream leakage is more sensitive to the temperature of the cold heat exchangers (which are pressurized but through which there is no flow) than it is to the cold end temperature of heat exchanger 7. This indicates that the stream-to-stream leak is in one of the colder heat exchangers. Since the other heat exchangers have lower design operating temperatures, the stream-to-stream leakage would probably be much worse when cooled down to design conditions.

The next to last data point indicates that the heat exchanger would leak approximately 1/4 the mass flow from stream to stream when operating at the design mass flow and pressures. This agrees fairly well with the previous estimate of the leakage based on the warm and cold temperature differences.

The leakage to the casing could be in any of the heat exchangers, and there is nothing in the data to indicate where it is. If this leak is also in one of the colder heat exchangers, it will increase at the actual operating temperatures.

Section 6

RECOMMENDATIONS

TURBOALTERNATORS

Miniature turboalternators with self-acting gas bearings have been developed under this contract and other contracts to the point that they appear well suited for those applications where reliability and long life are of primary importance. Provided that a noncontaminating system can be developed, it appears that the only drawback to the type of turboalternator tested under this contract is the relatively high cost. It is, therefore, recommended that further effort be devoted to cost reduction in the area of turboalternators.

CRYOGENIC HEAT EXCHANGERS

The difficulties with development of a heat exchanger of the plastic and wire mesh type are described in this report. Unfortunately, the causes of the construction and leakage problems were not identified in this project. It is, therefore, difficult to make recommendations for further work on this type of exchanger except to propose a more fundamental approach, with a detailed analytical and experimental investigation of plastic-to-metal bonding and differential thermal contraction. Further recommendations can be made after the next development phase, now being conducted under another contract, is completed.

Other types of plastic and metal exchangers are the perforated-plate type and the expanded metal types. The perforated plate type was rejected for use in this contract because of its high cost compared with the wire mesh. However, the perforated plate heat exchanger has already been partly developed and found to be relatively leaktight. Perhaps further work on production of perforated plates with lower cost would be justified. Expanded metal is a low cost heat transfer surface that has already been investigated for use in heat exchangers. Preliminary development results indicate that sealing is not a problem with this material.

The ideal heat exchanger would avoid the use of plastics altogether, thus alleviating problems of sealing and differential contraction. An all-metal exchanger using wire mesh bonded to thin-wall stainless steel tubing has been partially developed. This type of exchanger would be especially useful in systems with the higher pressure ratios that are characteristic of positive displacement compressors; in those systems, longitudinal heat conduction and flow maldistribution in heat exchangers are not as severe a problem as they are in systems with low pressure ratios. It is recommended that further development of all-metal wire mesh exchangers be conducted. This development would be concerned primarily with metal joining techniques, especially in the beader region, and with constructing and testing full-sized units.

APPENDIX I

PRELIMINARY TURBOALTERNATOR DESIGNS

Cycle-study computer Run 479, Figure 5, established the turboalternator requirements shown in Table 10. Also shown in this table are principal turboalternator design parameters given by the same run. The three power outputs and overall efficiencies must match the cycle requirements. These turboalternators, of course, were not optimized in the cycle study; hence, the wheel tip diameter, admission, and speed are shown only for reference purposes.

Complete turboalternator design studies were conducted for all three of the stages for the required cycle conditions. The best operating geometries

Table 10
TURBOALTERNATOR DESIGNS
From Cycle Study Run 479

Cycle Study Parameters	Turboalternator Inlet Temperature		
	14°K	55°K	170°K
<u>Inputs</u>			
Inlet temperature (°R)	25.2	99.0	306.0
Inlet pressure (psia)	41.2	41.7	42.1
Inlet pressure (atm)	2.814	2.842	2.871
Outlet pressure (psia)	17.22	16.82	16.57
Outlet pressure (atm)	1.162	1.145	1.128
Mass flow (lb./hr)	26.64	11.80	5.81
Mass flow (lb./sec)	0.0074	0.00327	0.001614
Mass flow (g./sec)	3.36	1.486	0.7343
<u>Results</u>			
Refrigerator power output (watts)	27.14	48.45	61.39
Overall refrigerator efficiency (fraction)	0.3730	0.3746	0.3062
Wheel tip diameter (inch)	0.500	0.700	1.00
Admission (fraction)	0.3036	0.1970	0.1034
Speed (rpm)	118,000	101,500	75,800

GE 2104

were established. The 0.625-inch-diameter turbine-wheel size was evaluated for the 170°K turbine. An initial assembly-drawing layout was made, and the expected mechanical arrangement was established. The tilting-pad journal-bearing designs were examined for all three stages, and considerations for the thrust-bearing designs were reviewed. Limiting conditions on the turbine wheel were examined for stress and deflection for all three wheels, and a complete analysis was made for the 0.50-inch-diameter turbine wheel of the 14°K turbine. A review was then made of the two alternate approaches for designing and constructing the 170°K turboalternator stage, and consideration was given to the use of an existing Government-furnished unit.

The three designs that were recommended are shown in Table 11. A 0.625-inch-diameter wheel design is also shown for the 170°K turbine. The U. S. Army turbine referred to is the unit previously constructed under U. S. Army Contract No. DAAK02-68-C-0320. This unit has a wheel diameter of 0.625 inch.

TURBOALTERNATOR DESIGN GOALS

One goal for the turboalternator designs was to use identical parts wherever possible in all three turboalternators. Further, the design of the existing small frame size turboalternator, constructed under a U. S. Air Force contract, was used wherever possible, to limit the need for new drawings. Geometry aspects of the small frame size were incorporated, wherever possible, in the cycle studies and the subsequent actual design of the individual turboalternators. It was thereby hoped that only the nozzle and turbine wheels would be different from unit to unit. The purpose of the design approach used was to maintain low design-point speed, so the higher initial operating speed at room temperature would provide a reasonably large power output for fast cooldown. Holding the design speed low can also reduce the bearing losses because bearing losses increase with speed and will vary with individual unit assemblies. Adequately checking the bearing settings and assuring that they are of the desired design clearances is still uncertain. Hence, if the design speed is low, the risk of incurring a large bearing loss from a particular assembly should not be as great.

No allowances were made for axial thrust caused by axial gas force on the rotating assembly. Past experience has indicated that there often can be a net gas force, usually on the back side of the turbine wheel, that increases the thrust bearing load in one direction. However, from experience with different assemblies for the same design, it has been found that this thrust can be in either direction, and the resultant force is relatively small. A contingency allowance for thrust bearing load capability should therefore be added.

¹ U. S. Air Force Contract No. F-36(3)-71-C-100, Air Force Research and Development Command, Air Force Flight Directorate, Fort Belvoir, WPAFB, Ohio.

The design approach anticipated for the turboalternators has been to use the laminar-flow, radial-impulse turbine blades that have a converging flow passage. This flow passage is considerably different from that previously used on the early General Electric and U. S. Army turbine wheels. These early turbine wheels used a constant cutter diameter to form the blade profiles, and therefore there was a constant-flow, cross-sectional area between the turbine blades. This cutter diameter enters into the design program calculations and also the performance of the overall turboalternator and is a significant computer-program design variable. All the turboalternator designs were therefore considered with a nominal cutter diameter, so the trend in efficiencies could be seen along with the blade-height-to-cutter-diameter ratio. This ratio is a significant consideration because it is an index to how time-consuming and costly it is to cut the particular turbine wheel with the miniature-tracer milling system used.

DESIGN FOR 14K TURBOALTERNATOR

A number of runs were conducted using the design-point computer program that designs partial-admission radial-impulse turboalternators. Overall results are shown in Table 12, where various nozzle angles were used in conjunction with a 0.50-inch-diameter turbine wheel. For the coldest turbine, it is desirable to maintain a small turbine-wheel diameter, to keep the design operating speed up to a reasonable level; however, previous experience in manufacturing and assembly has indicated that the turbine wheel diameter should not be below 0.50 inch. In this particular design, there is no apparent reason that the turbine-wheel diameter should be larger to decrease the design speed further. This table shows the variety of changes within the design before the final design basis was adopted; 90,000 rpm is the best design speed, along with a nozzle angle of 80 degrees. The overall efficiency is a few percent higher than the design requirement, providing a design contingency. A configuration of 23 blades is best for high efficiency, which also results in a blade height-diameter ratio of 2.0. The fact that the 23-blade configuration is the most efficient one is contrary to what has been seen on other designs, where a larger number of blades can improve efficiency. The last two columns show the change in axial clearance efficiency. An efficiency gain of about two percent can be obtained by decreasing the axial clearance from 2.0 to 1.0 mil.

Table 12 indicates that there is a trade-off between the nozzle angle, speed, and blade height-to-diameter ratio. The larger nozzle angle increases the blade height to accommodate the flow.

A complete printout of the adopted design point, computer run 4791007, is shown in Figure 3B, which shows all of the significant input and output information. The journal-bearing clearance and power loss compare reasonably well with that for a similar run with the tilting-pad gas-bearing selector program of the Franklin Institute Research Laboratories. Of course

Table 12

DESIGN VARIATIONS FOR 14°K TURBOALTERNATOR

Design Parameters	Run 1	Run 2	Run 3	Run 4	Run 6	Run 7	Run 8
Nozzle angle (deg)	78	78	78	78	80	80	80
Speed (rpm)	90,000	85,000	95,000	90,000	90,000	90,000	90,000
Overall efficiency (fraction)	0.4070	0.4061	0.4059	0.4127	0.4140	0.4164	0.4330
Number of blades	23	23	23	23	27	23	23
Nominal cutter diameter (in.)	0.03051	0.03051	0.03051	0.03051	0.0271	0.03051	0.03051
Blade height (in.)	0.0595	0.0595	0.0595	0.0641	0.0701	0.0701	0.0698
Blade-height-to-cutter-diameter Ratio	1.70	1.70	1.70	1.86	2.59	2.00	1.99
Axial clearance (in.)	0.002	0.002	0.002	0.002	0.002	0.002	0.001

*Adopted as preliminary design point.

CR-21 68

there should be a good correlation, because the design-point computer program for the turboalternator incorporates the tilting-pad gas journal-bearing selector program. However, there is a slight difference in the value of the turboalternator design-point program, which shows a journal friction of 0.09007 watt, while the bearing-selector program shows a power loss of 0.0875 watt. The actual total power is, of course, the sum of both sides of the thrust bearing and both journal bearings. In the design-point computer program, only the one loaded side of the thrust bearing has been included. Both the thrust- and journal-bearing film thicknesses do show reasonable values: the thrust-bearing film thickness (loaded side) is around 400 micro-inches, and the journal pivot-film thickness is shown to be about 140 micro-inches.

DESIGN FOR 55°K TURBOALTERNATOR

The first series of design studies was conducted with a 0.70-inch-diameter wheel, as was used in the cycle-design program. With an 80-degree nozzle angle, the best speed was determined for a 43-blade turbine wheel (Table 13). A worthwhile increase in efficiency could be obtained by decreasing the speed from the 161,700 rpm calculated by the cycle computer program, because the cycle program optimizes the turbine on the basis of aerodynamic efficiency, and the parasitic losses are not included in this optimization. Inclusion of the parasitic losses lowers the predicted speed. It can be seen that with a 0.70-inch-diameter turbine wheel, the efficiency can easily exceed the cycle-design requirement of 0.374. At 130,000 rpm the predicted efficiency is 0.403.

A second wheel diameter was investigated with the possible prospect of adapting the existing U. S. Army turboalternator with a wheel diameter of 0.625 inch. Table 13 shows the turboalternator design results representative of different speeds with different numbers of blades. It is seen that the computer program predicts efficiencies greater than the cycle-design

TURBOALTERNATOR PARTIAL ADMISSION RADIAL IMPULSE
DESIGN POINT COMPUTER OUTPUT

DESIGN CASE	4791007
REFRIGERATION PWR OUT (WATTS)	0.2992E+02
ELECTRICAL POWER OUTPUT (WATTS)	0.2992E+02
SPEED (RPM)	0.9000E+05
OVERALL EFFICIENCY (FRACTION)	0.4164E+00
TEMPERATURES, PRESSURES, FLOW	
INLET TEMPERATURE (K)	0.2520E+02
INLET TEMPERATURE (K)	0.1400E+02
OVERALL TEMPERATURE DROP (K)	0.3101E+01
OVERALL TEMPERATURE DROP (K)	0.1723E+01
OUTLET TEMPERATURE EXIT (K)	0.2210E+02
OUTLET TEMPERATURE EXIT (K)	0.1228E+02
INLET PRESSURE (PSIA)	0.4120E+02
INLET PRESSURE (ATM)	0.2803E+01
OUTLET PRESSURE (PSIA)	0.1722E+02
OUTLET PRESSURE (ATM)	0.1172E+01
PRESSURE RATIO	0.2393E+01
FLOW (LB/SEC)	0.7400E+02
FLOW (LB/HR)	0.2664E+02
FLOW (G/SEC)	0.3360E+01
PRIMARY DIMENSIONS	
WHEEL TIP DIAMETER (IN)	0.5000E+00
NUMBER OF BLADES	0.2400E+02
BLADE HEIGHT (IN)	0.7007E-01
THRUST BEARING	
LOAD (LBS.)	0.5935E-01
OUTSIDE DIAMETER (IN)	0.5740E+00
DIAMETER RATIO	0.5002E+00
CLEAR. TO DIA. RATIO	0.7000E-03
LOAD COEFFICIENT	0.1514E-01
BEARING NUMBER	0.2319E+00
CLEARANCE, LOADSIDE (IN)	0.4018E-03
FRICITION POWER (WATTS)	0.9563E-01
JOURNAL BEARING	
LOAD (LBS.)	0.2967E-01
LOAD COEFFICIENT	0.5059E-01
BEARING NUMBER	0.6027E+00
CLEAR. TO DIA. RATIO	0.7400E-03
MACHINED CLEARANCE (IN)	0.1931E-03
PIV. FILM THICK (IN)	0.1416E-03
FRICITION POWER (WATTS)	0.9007E-01

CR-2189-1

Figure 38. Design for 14°K Turboalternator (Sheet 1 of 3)

DESIGN CASE	4791007
PRIMARY LOSSES	
ALTERNATOR TOTAL (WATTS)	0.2124E+00
SUM OF FRICTION LOSSES (WATTS)	0.6367E+00
TWO STAGE PERFORMANCE	
OTHER STAGE IN TEMP (K)	0.1400E+02
TOTAL HEAT LEAK (WATTS)	0.
EXIT TEMPERATURE (K)	0.1222E+02
SHAFT HEAT LEAK (WATTS)	0.
HOUSG HEAT LEAK (WATTS)	0.
GAS BEARINGS	
ROTATING ASSEMBLY WEIGHT (LBS)	0.5935E-01
ACCELERATION OF GRAVITY ("G")	0.1000E+01
TOT. BEARING FRICTION (WATTS)	0.2758E+00
PERFORMANCE TERMS	
ISENTROPIC HEAD (FT)	0.7154E+04
HYDRAULIC EFF., FIRST TERM	0.5963E+00
HYDRAULIC EFF., SECOND TERM	0.1010E+00
HYDRAULIC EFF., THIRD TERM	0.3120E-04
TIP CLEARANCE EFF. CORRECTION	0.9563E+00
TRAIL EDGE EFF. CORRECTION	0.8991E+00
BLADE RE. NO. EFF. CORR.	0.1005E+01
ALTERNATOR GAP FLUX (KGAUSS)	
ALTERNATOR CORE LOSS COEFF.	0.3357E+01
ALTERNATOR COPPER LOSS COEFF.	0.2542E+01
ALTERNATOR COPPER LOSS COEFF.	0.7133E+02
TEMPERATURE WHEEL EXIT GAS (R)	
NOZ. DISC. VOLUME FLOW CFS	0.2201E+02
TURBINE BLADE DISC VOL. FLOW (CFS)	0.2207E-01
TURBINE BLADE DISC VOL. FLOW (CFS)	0.2532E-01
PERFORMANCE FACTORS	
TIP SPEED TO SPOUTING VEL. RATIO	0.2395E+00
BLADE INCIDENCE ANGLE (DEGREES)	0.1052E+02
NOZZLE COEFFICIENT	0.9030E+00
SPECIFIC SPEED	0.1759E+02
SPECIFIC DIAMETER	0.2405E+01
FLOW FACTOR	0.1594E+01
WHEEL EFFICIENCY (FRACTION)	
HYDRAULIC EFFICIENCY (FRACTION)	0.4282E+00
ELECTROMAGNET EFF. (FRACTION)	0.4953E+00
ELECTROMAGNET EFF. (FRACTION)	0.9930E+00
ISENTROPIC POWER (WATTS)	
WHEEL POWER OUTPUT (WATTS)	0.7184E+02
SHAFT POWER OUTPUT (WATTS)	0.3076E+02
SHAFT POWER OUTPUT (WATTS)	0.3013E+02

CR-2160-2

Figure 38. Design for 14°K Turboalternator (Sheet 2 of 3)

DESIGN CASE

4791007

PARASITIC LOSSES (WATTS)	
TURBINE DISC FRICTION	0.1243E+00
JOURNAL DIAM SHAFT FRICTION	0.2192E+00
ALTERNATOR GAP FRICTION	0.1752E-01
BEARING FRICTION	0.2758E+00
GEOMETRY	
WHEEL TIP CLEARANCE (IN)	0.2000E-02
BLADE PASSAGE OUTER DIAMETER (IN)	0.3015E-01
BLADE TRAILING EDGE THICKNESS (IN)	0.4000E-02
ADMISSION ARC (FRACTION)	0.2714E+00
ADMISSION ARC (DEGREES)	0.9772E+02
NOZZLE ANGLE (DEGREES)	0.8000E+02
BLADE ANGLE (DEGREES)	0.6480E+02
BLADE CHORD (IN)	0.9909E-01
WHEEL INSIDE DIAMETER (IN)	0.3018E+00
BLADE PRESSURE SURFACE RADIUS (IN)	0.5476E-01
BLADE SUCTION SURFACE RADIUS (IN)	0.2461E-01
TOTAL MACHINE SHAFT LENGTH (IN)	0.2660E+01
JOURNAL SHAFT DIAMETER (IN)	0.2610E+00
JOURNAL FREE SHAFT LENGTH (IN)	0.1366E+01
ALTERNATOR DIAMETER (IN)	0.2610E+00
ALTERNATOR MAGNET LENGTH (IN)	0.3336E+00
ALTERNATOR PERIF. SPEED (P.P.S.)	0.1026E+03
ALTERNATOR RADIAL GAP (IN)	0.1501E-01
STATOR OVERHANG (IN)	0.4502E-01
STATOR LAMINATION DIA. (IN)	0.9448E+00
WHEEL BACK SIDE OPTIMUM GAP (IN)	0.8670E-02
VELOCITIES	
SPOUTING VELOCITY (FPS)	0.6788E+03
NOZZLE DISCHARGE VELOCITY (FPS)	0.6109E+03
BLADE INLET RELATIVE VELOCITY (FPS)	0.1097E+03
BLADE INLET RADIAL VELOCITY (FPS)	0.1061E+03
BLADE INLET RELATIVE MACH NUMBER	0.1740E+00
REYNOLDS NUMBERS	
BLADE PASSAGE REYNOLDS NO.	0.6590E+05
TURBINE DISC REYNOLDS NO.	0.6340E+06
JOURNAL DIAMETER REYNOLDS NO.	0.1845E+06
ALTERNATOR GAP REYNOLDS NO.	0.8776E+05
DRAG COEFFICIENTS	
TURBINE DISC DRAG COEFF.	0.6139E-02
JOURNAL DIAMETER DRAG COEFF.	0.4278E-02
ALTERNATOR GAP MOMENT COEFF.	0.1396E-02

CR-2169-3

Figure 38. Design for 14°K Turboalternator (Sheet 3 of 3)

Table 13
 DESIGN VARIATIONS FOR 55°K TURBOALTERNATOR

Run	Nozzle Angle (deg)	Speed (rpm)	Overall Efficiency (fraction)	No. Blades	Nominal Cutter Diameter (in.)	Blade Height (in.)	Blade-height-to-cutter-diameter Ratio	Axial Clearance (in.)
<u>Wheel Diameter: 0.70 Inch</u>								
1	80	160,000	0.3740	43	0.02157	0.0659	3.06	0.002
2	80	155,000	0.3837	43	0.02157	0.0658	3.05	0.002
3	80	150,000	0.3900	43	0.02157	0.0657	3.05	0.002
4	80	145,000	0.3965	43	0.02157	0.0657	3.05	0.002
5	80	140,000	0.4006	43	0.02157	0.0656	3.04	0.002
6	80	135,000	0.4031	43	0.02157	0.0656	3.04	0.002
7	80	130,000	0.4033	43	0.02157	0.0656	3.04	0.002
<u>Wheel Diameter: 0.625 Inch</u>								
8	80	130,000	0.3945	37	0.02253	0.0658	2.92	0.002
9	80	135,000	0.3970	37	0.02253	0.0657	2.92	0.002
10	80	140,000	0.3983	37	0.02253	0.0657	2.92	0.002
11	80	145,000	0.3985	37	0.02253	0.0657	2.92	0.002
12	80	145,000	0.3011	31	0.02767	0.0657	2.38	0.002
13	80	145,000	0.3865	29	0.02985	0.0658	2.20	0.002
<u>Wheel Diameter: 0.75 Inch</u>								
14	80	135,000	0.3996	47	0.02107	0.0657	3.12	0.002
15	80	130,000	0.4024	47	0.02107	0.0656	3.12	0.002
16	80	125,000	0.4045	47	0.02107	0.0656	3.12	0.002
17*	80	120,000	0.4038	47	0.02107	0.0654	3.12	0.002
18	80	120,000	0.4051	53	0.01823	0.0656	3.60	0.002
19	80	120,000	0.4016	43	0.0234	0.0657	2.80	0.002
20	80	120,000	0.4234	47	0.02107	0.0654	3.12	0.001

*Adopted as preliminary design point

CR-2174

requirements, but not as great as in the larger 0.70-inch turbine wheel design. Operating at a higher speed is also not as desirable.

A third wheel diameter was considered for this second-stage turboalternator, as shown at the bottom of Table 13. With a 0.75-inch turbine wheel diameter, a variety of computer runs was made, with a varying number of blades and some changes in design speed. It is seen on the table that slight variations will produce the expected trends of slightly increased efficiency, with a larger number of blades. There is no compelling reason to choose one of these designs over the other; however, it is desirable to maintain low design speed, to minimize bearing losses and provide an adequate speed margin for much faster refrigerator-system cool-down. The recommended

design is shown in Table 13, Run 17, where 47 blades are required for a 0.75-inch-diameter turbine wheel operating at 120,000 rpm. A complete printout of the design for this 55 K turboalternator is shown in Figure 39.

DESIGN FOR 170°K TURBOALTERNATOR

Table 14 shows a summary of the turboalternator computer-program designs conducted. The first set of computer design results is shown for a 0.625-inch-diameter turbine wheel. This wheel diameter was selected because of the possibility of using the existing U. S. Army turboalternator. The design shows that the required efficiency of 0.3062 apparently can be met with a small margin but with a very high design speed of 230,000 rpm. Of course this design speed allows little opportunity for a wide margin from an initial cooldown speed on the order of 250,000 rpm. Figure 40 shows a complete design-program computer printout.

Table 14
DESIGN VARIATIONS FOR 170°K TURBOALTERNATOR

Run	Nozzle Angle (deg)	Speed (rpm)	Overall Efficiency (fraction)	No. Blades	Nominal Cutter Diameter (in.)	Blade Height (in.)	Blade-height-to-cutter-diameter Ratio	Axial Clearance (in.)
<u>Wheel Diameter: 0.625 Inch</u>								
1	80	200,000	0.3133	37	0.02253	0.0618	3.64	0.002
2	80	210,000	0.3165	37	0.02253	0.0618	3.64	0.002
3	80	220,000	0.3184	37	0.02253	0.0618	3.64	0.002
4	80	230,000	0.3188	37	0.02253	0.0618	3.64	0.002
<u>Wheel Diameter: 1.00 Inch</u>								
5	80	180,000	0.2883	43	0.0325	0.0621	1.91	0.002
6	80	170,000	0.3036	43	0.0325	0.0618	1.91	0.002
10	80	150,000	0.3155	43	0.0325	0.0618	1.91	0.002
11	80	160,000	0.3121	43	0.0325	0.0618	1.91	0.002
13	80	150,000	0.3210	47	0.0294	0.0617	2.10	0.002
14	80	150,000	0.3261	53	0.0256	0.0617	2.41	0.002
15	80	150,000	0.3282	59	0.0226	0.0617	2.73	0.002
16	80	150,000	0.3277	67	0.0194	0.0617	3.18	0.002

CR-2175

A 1.0-inch-diameter turbine wheel was then evaluated to satisfy the same requirements, but to operate at a much lower design operating speed. The computer runs show that with some variation in the number of turbine blades and speeds, a best operating condition can be 150,000 rpm with a 57-blade turbine wheel and with a reasonable blade-height-to-cutter-diameter ratio. This condition is shown as Run 16 in Table 14. Figure 41 shows a complete printout of the design-program output.

TURBOALTERNATOR PARTIAL ADMISSION RADIAL IMPULSE
DESIGN POINT COMPUTER OUTPUT

DESIGN CASE	4792017
REFRIGERATION PWR OUT (WATTS)	0.5206E+02
ELECTRICAL POWER OUTPUT (WATTS)	0.5206E+02
SPEED (RPM)	0.1200E+06
OVERALL EFFICIENCY (FRACTION)	0.4038E+00
TEMPERATURES, PRESSURES, FLOW	
INLET TEMPERATURE (K)	0.9900E+02
INLET TEMPERATURE (K)	0.5500E+02
OVERALL TEMPERATURE DROP (K)	0.1221E+02
OVERALL TEMPERATURE DROP (K)	0.6741E+01
OUTLET TEMPERATURE EXIT (K)	0.5679E+02
OUTLET TEMPERATURE EXIT (K)	0.4822E+02
INLET PRESSURE (PSIA)	0.4170E+02
INLET PRESSURE (ATM)	0.2838E+01
OUTLET PRESSURE (PSIA)	0.1662E+02
OUTLET PRESSURE (ATM)	0.1145E+01
PRESSURE RATIO	0.2479E+01
FLOW (LB/SEC)	0.3270E+02
FLOW (LB/HR)	0.1177E+02
FLOW (G/SEC)	0.1485E+01
PRIMARY DIMENSIONS	
WHEEL TIP DIAMETER (IN)	0.7500E+00
NUMBER OF BLADES	0.1700E+02
BLADE HEIGHT (IN)	0.6564E-01
THRUST BEARING	
LOAD (LBS.)	0.6075E-01
OUTSIDE DIAMETER (IN)	0.5740E+00
DIAMETER RATIO	0.5002E+00
CLEAR. TO DIA. RATIO	0.7000E-03
LOAD COEFFICIENT	0.1587E-01
BEARING NUMBER	0.7636E+00
CLEARANCE, LOADSIDE (IN)	0.4018E-03
FRICTION POWER (WATTS)	0.4101E+00
JOURNAL BEARING	
LOAD (LBS.)	0.3038E-01
LOAD COEFFICIENT	0.5302E-01
BEARING NUMBER	0.1477E+01
CLEAR. TO DIA. RATIO	0.3591E-03
MACHINED CLEARANCE (IN)	0.2242E-03
PIV. FILM THICK (IN)	0.1416E-03
FRICTION POWER (WATTS)	0.3606E+00

CR-2167-1

Figure 30. Design for 55°K Turboalternator (Sheet 1 of 3)

DESIGN CASE	4792017
PRIMARY LOSSES	
ALTERNATOR TOTAL (WATTS)	0.1141E+01
SUM OF FRICTION LOSSES (WATTS)	0.2087E+01
TWO STAGE PERFORMANCE	
OTHER STAGE IN TEMP (K)	0.5503E+02
TOTAL HEAT LEAK (WATTS)	0.
EXIT TEMPERATURE (K)	0.4422E+02
SHAFT HEAT LEAK (WATTS)	0.
HOUSG HEAT LEAK (WATTS)	0.
GAS BEARINGS	
ROTATING ASSEMBLY WEIGHT (LBS)	0.6079E+01
ACCELERATION OF GRAVITY ("G")	0.1000E+01
TOT. BEARING FRICTION (WATTS)	0.1131E+01
PERFORMANCE TERMS	
ISENTRIC HEAD (FT)	0.2906E+05
HYDRAULIC EFF., FIRST TERM	0.6017E+00
HYDRAULIC EFF., SECOND TERM	0.5652E-01
HYDRAULIC EFF., THIRD TERM	0.4403E-04
TIP CLEARANCE EFF. CORRECTION	0.9008E+00
TRAIL EDGE EFF. CORRECTION	0.8724E+00
BLADE RE. NO. EFF. CORR.	0.9310E+00
ALTERNATOR GAP FLUX (KGAUSS)	0.5900E+01
ALTERNATOR CORE LOSS COEFF.	0.1704E+01
ALTERNATOR COPPER LOSS COEFF.	0.1100E+02
TEMPERATURE WHEEL EXIT GAS (K)	0.8604E+02
NOZ. DISC. VOLUME FLOW (CF)	0.3880E-01
TURBINE BLADE DISC VOL. FLOW (CF)	0.4477E-01
PERFORMANCE FACTORS	
TIP SPEED TO SPOUTING VEL. RATIO	0.2873E+00
BLADE INCIDENCE ANGLE (DEGREES)	0.1057E+02
NOZZLE COEFFICIENT	0.9000E+00
SPECIFIC SPEED	0.1101E+02
SPECIFIC DIAMETER	0.3857E+01
FLOW FACTOR	0.1379E+01
WHEEL EFFICIENCY (FRACTION)	0.4846E+00
HYDRAULIC EFFICIENCY (FRACTION)	0.5151E+00
ELECTROMAGNET EFF. (FRACTION)	0.9790E+00
ISENTRIC POWER (WATTS)	0.1289E+03
WHEEL POWER OUTPUT (WATTS)	0.5529E+02
SHAFT POWER OUTPUT (WATTS)	0.5120E+02

CR-2167-2

Figure 30. Design for 55°K Turboalternator (Sheet 2 of 3)

DESIGN CASE	4792017
PARASITIC LOSSES (WATTS)	
TURBINE DISC FRICTION	0.7233E+00
JOURNAL DIAM SHAFT FRICTION	0.2130E+00
ALTERNATOR GAP FRICTION	0.1936E-01
BEARING FRICTION	0.1131E+01
GEOMETRY	
WHEEL TIP CLEARANCE (IN)	0.2000E-02
BLADE PASSAGE OUTER DIAMETER (IN)	0.2107E-01
BLADE TRAILING EDGE THICKNESS (IN)	0.4000E-02
ADMISSION ARC (FRACTION)	0.1686E+00
ADMISSION ARC (DEGREES)	0.6068E+02
NOZZLE ANGLE (DEGREES)	0.8000E+02
BLADE ANGLE (DEGREES)	0.6480E+02
BLADE CHORD (IN)	0.8093E-01
WHEEL INSIDE DIAMETER (IN)	0.5381E+00
BLADE PRESSURE SURFACE RADIUS (IN)	0.4472E-01
BLADE SUCTION SURFACE RADIUS (IN)	0.2365E-01
TOTAL MACHINE SHAFT LENGTH (IN)	
JOURNAL SHAFT DIAMETER (IN)	0.2610E+00
JOURNAL FREE SHAFT LENGTH (IN)	0.1366E+01
ALTERNATOR DIAMETER (IN)	0.2610E+00
ALTERNATOR MAGNET LENGTH (IN)	0.3427E+00
ALTERNATOR PERIF. SPEED(R.P.S.)	0.1363E+03
ALTERNATOR RADIAL GAP (IN)	0.1501E-01
STATOR OVERHANG (IN)	0.4502E-01
STATOR LAMINATION DIA. (IN)	0.9443E+00
WHEEL BACK SIDE OPTIMUM GAP (IN)	0.1109E-01
VELOCITIES	
SPRUITING VELOCITY (FPS)	0.1164E+04
NOZZLE DISCHARGE VELOCITY (FPS)	0.1231E+04
BLADE INLET RELATIVE VELOCITY (FPS)	0.2211E+03
BLADE INLET RADIAL VELOCITY (FPS)	0.2139E+03
BLADE INLET RELATIVE MACH NUMBER	0.1778E+00
REYNOLDS NUMBERS	
BLADE PASSAGE REYNOLDS NO.	0.1041E+05
TURBINE DISC REYNOLDS NO.	0.2127E+06
JOURNAL DIAMETER REYNOLDS NO.	0.2576E+05
ALTERNATOR GAP REYNOLDS NO.	0.1212E+05
DRAG COEFFICIENTS	
TURBINE DISC DRAG COEFF.	0.7944E-02
JOURNAL DIAMETER DRAG COEFF.	0.7017E-02
ALTERNATOR GAP MOMENT COEFF.	0.2528E-02

CR-2167-3

Figure 30. Design for 55° Turboalternator (Sheet 3 of 3)

TURBOALTERNATOR PARTIAL ADMISSION RADIAL IMPULSE
DESIGN POINT COMPUTER OUTPUT

DESIGN CASE	4793004
REFRIGERATION PWR OUT (WATTS)	0.6411E+02
ELECTRICAL POWER OUTPUT (WATTS)	0.6324E+02
SPEED (RPM)	0.2300E+06
OVERALL EFFICIENCY (FRACTION)	0.3188E+00
TEMPERATURES, PRESSURES, FLOW	
INLET TEMPERATURE (K)	0.3060E+03
INLET TEMPERATURE (K)	0.1700E+03
OVERALL TEMPERATURE DROP (K)	0.3006E+02
OVERALL TEMPERATURE DROP (K)	0.1670E+02
OUTLET TEMPERATURE EXIT (K)	0.2759E+03
OUTLET TEMPERATURE EXIT (K)	0.1533E+03
INLET PRESSURE (PSIA)	0.4210E+02
INLET PRESSURE (ATM)	0.2865E+01
OUTLET PRESSURE (PSIA)	0.1657E+02
OUTLET PRESSURE (ATM)	0.1128E+01
PRESSURE RATIO	0.2541E+01
FLOW (LB/SEC)	0.1614E-02
FLOW (LB/HR)	0.5810E+01
FLOW (G/SEC)	0.7328E+00
PRIMARY DIMENSIONS	
WHEEL TIP DIAMETER (IN)	0.6250E+00
NUMBER OF BLADES	0.3700E+02
BLADE HEIGHT (IN)	0.6174E-01
THRUST BEARING	
LOAD (LBS.)	0.5916E-01
OUTSIDE DIAMETER (IN)	0.5740E+00
DIAMETER RATIO	0.5002E+00
CLEAR. TO DIA. RATIO	0.7000E-03
LOAD COEFFICIENT	0.1568E-01
BEARING NUMBER	0.3109E+01
CLEARANCE/LOADSIDE (IN)	0.4018E-03
FRICTION POWER (WATTS)	0.3153E+01
JOURNAL BEARING	
LOAD (LBS.)	0.2958E-01
LOAD COEFFICIENT	0.5241E-01
BEARING NUMBER	0.2000E+01
CLEAR. TO DIA. RATIO	0.1483E-02
MACHINED CLEARANCE (IN)	0.3870E-03
PIV. FILM THICK (IN)	0.1416E-03
FRICTION POWER (WATTS)	0.2516E+01

CR-2165-1

Figure 40. Design for 170°K Turboalternator, 0.625-inch Wheel (Sheet 1 of 3)

DESIGN CASE	4793004
PRIMARY LOSSES	
ALTERNATOR TOTAL (WATTS)	0.2749E+01
SUM OF FRICTION LOSSES (WATTS)	0.9981E+01
TWO STAGE PERFORMANCE	
OTHER STAGE IN TEMP (K)	0.5500E+02
TOTAL HEAT LEAK (WATTS)	0.8673E+00
EXIT TEMPERATURE (K)	0.1531E+03
SHAFT HEAT LEAK (WATTS)	0.2212E+00
HOUSG HEAT LEAK (WATTS)	0.6461E+00
GAS BEARINGS	
ROTATING ASSEMBLY WEIGHT (LBS)	0.5916E-01
ACCELERATION OF GRAVITY ("G")	0.1000E+01
TOT. BEARING FRICTION (WATTS)	0.8186E+01
PERFORMANCE TERMS	
ISENTROPIC HEAD (FT)	0.9181E+05
HYDRAULIC EFF., FIRST TERM	0.5627E+00
HYDRAULIC EFF., SECOND TERM	0.7023E-01
HYDRAULIC EFF., THIRD TERM	0.2944E-04
TIP CLEARANCE EFF. CORRECTION	0.7454E+00
TRAIL EDGE EFF. CORRECTION	0.8903E+00
BLADE RE. NO. EFF. CORR.	0.9117E+00
ALTERNATOR GAP FLUX (KGAUSS)	0.5473E+01
ALTERNATOR CORE LOSS COEFF.	0.1226E+01
ALTERNATOR COPPER LOSS COEFF.	1.2356E+01
TEMPERATURE WHEEL EXIT GAS (K)	0.2699E+03
NOZ. DISC. VOLUME FLOW (CMS)	0.0965E-01
TURBINE BLADE DISC VOL. FLOW (CMS)	0.7042E-01
PERFORMANCE FACTORS	
TIP SPEED TO SPOUTING VEL. RATIO	0.2082E+00
BLADE INCIDENCE ANGLE (DEGREES)	0.1123E+02
NOZZLE COEFFICIENT	0.9000E+00
SPECIFIC SPEED	0.1105E+02
SPECIFIC DIAMETER	0.3416E+01
FLOW FACTOR	0.1135E+01
WHEEL EFFICIENCY (FRACTION)	0.3778E+00
HYDRAULIC EFFICIENCY (FRACTION)	0.4925E+00
ELECTROMAGNET EFF. (FRACTION)	0.9600E+00
ISENTROPIC POWER (WATTS)	0.2011E+03
WHEEL POWER OUTPUT (WATTS)	0.7577E+02
SHAFT POWER OUTPUT (WATTS)	0.6599E+02

CR-2165-2

Figure 40. Design for 170°K Turboalternator, 0.625-Inch Wheel (Sheet 2 of 3)

DESIGN CASE

4793004

PARASITIC LOSSES (WATTS)	
TURBINE DISC FRICTION	0.1089E+01
JOURNAL DIAM SHAFT FRICTION	0.6427E+00
ALTERNATOR GAP FRICTION	0.6347E-01
BEARING FRICTION	0.8186E+01
GEOMETRY	
WHEEL TIP CLEARANCE (IN)	0.2000E-02
BLADE PASSAGE CUTTER DIAMETER (IN)	0.2253E-01
BLADE TRAILING EDGE THICKNESS (IN)	0.4000E-02
ADMISSION ARC (FRACTION)	0.1860E+00
ADMISSION ARC (DEGREES)	0.6695E+02
NOZZLE ANGLE (DEGREES)	0.3000E+02
BLADE ANGLE (DEGREES)	0.6480E+02
BLADE CHORD (IN)	0.8324E-01
WHEEL INSIDE DIAMETER (IN)	0.4585E+00
BLADE PRESSURE SURFACE RADIUS (IN)	0.4600E-01
BLADE SUCTION SURFACE RADIUS (IN)	0.2347E-01
TOTAL MACHINE SHAFT LENGTH (IN)	
JOURNAL SHAFT DIAMETER (IN)	0.2610E+00
JOURNAL FREE SHAFT LENGTH (IN)	0.1366E+01
ALTERNATOR DIAMETER (IN)	0.2610E+00
ALTERNATOR MAGNET LENGTH (IN)	0.2837E+00
ALTERNATOR PERIF. SPEED (F.P.S.)	0.2621E+03
ALTERNATOR RADIAL GAP (IN)	0.1501E-01
STATOR OVERHANG (IN)	0.4503E-01
STATOR LAMINATION DIA. (IN)	0.9448E+00
WHEEL BACK SIDE OPTIMUM GAP (IN)	0.7413E-02
VELOCITIES	
SPOOTING VELOCITY (FPS)	0.2432E+04
NOZZLE DISCHARGE VELOCITY (FPS)	0.2188E+04
BLADE INLET RELATIVE VELOCITY (FPS)	0.3918E+03
BLADE INLET RADIAL VELOCITY (FPS)	0.3802E+03
BLADE INLET RELATIVE MACH NUMBER	0.1799E+00
REYNOLDS NUMBERS	
BLADE PASSAGE REYNOLDS NO.	0.2861E+04
TURBINE DISC REYNOLDS NO.	0.4246E+05
JOURNAL DIAMETER REYNOLDS NO.	0.7404E+04
ALTERNATOR GAP REYNOLDS NO.	0.3484E+04
DRAG COEFFICIENTS	
TURBINE DISC DRAG COEFF.	0.1347E-01
JOURNAL DIAMETER DRAG COEFF.	0.7534E-02
ALTERNATOR GAP MOMENT COEFF.	0.4530E-02

CR-2165-3

Figure 40. Design for 170°K Turboalternator, 0.625-inch Wheel (Sheet 3 of 3)

TURBOALTERNATOR PARTIAL ADMISSION RADIAL IMPULSE
DESIGN POINT COMPUTER OUTPUT

DESIGN CASE	4793019
REFRIGERATION PWR OUT (WATTS)	0.6600E+02
ELECTRICAL POWER OUTPUT (WATTS)	0.5514E+02
SPEED (RPM)	0.1500E+06
OVERALL EFFICIENCY (FRACTION)	0.3282E+00
TEMPERATURES, PRESSURES, FLOW	
INLET TEMPERATURE (R)	0.3060E+03
INLET TEMPERATURE (K)	0.1700E+03
OVERALL TEMPERATURE DROP (R)	0.3096E+02
OVERALL TEMPERATURE DROP (K)	0.1720E+02
OUTLET TEMPERATURE EXIT (R)	0.2750E+03
OUTLET TEMPERATURE EXIT (K)	0.1528E+03
INLET PRESSURE (PSIA)	0.4210E+02
INLET PRESSURE (ATM)	0.2865E+01
OUTLET PRESSURE (PSIA)	0.1657E+02
OUTLET PRESSURE (ATM)	0.1128E+01
PRESSURE RATIO	0.2541E+01
FLOW (LB/SEC)	0.1614E+02
FLOW (LB/HR)	0.5810E+01
FLOW (G/SEC)	0.7328E+00
PRIMARY DIMENSIONS	
WHEEL TIP DIAMETER (IN)	0.1000E+01
NUMBER OF BLADES	0.5900E+02
BLADE HEIGHT (IN)	0.6166E-01
THRUST BEARING	
LOAD (LBS.)	0.6273E-01
OUTSIDE DIAMETER (IN)	0.5740E+00
DIAMETER RATIO	0.5032E+00
CLEAR. TO DIA. RATIO	0.7003E-03
LOAD COEFFICIENT	0.1665E-01
BEARING NUMBER	0.2024E+01
CLEARANCE, LOADSIDE (IN)	0.4018E-03
FRICTION POWER (WATTS)	0.1339E+01
JOURNAL BEARING	
LOAD (LBS.)	0.3139E-01
LOAD COEFFICIENT	0.5562E-01
BEARING NUMBER	0.2000E+01
CLEAR. TO DIA. RATIO	0.1193E-02
MACHINED CLEARANCE (IN)	0.3126E-03
PIV. FILM THICK (IN)	0.1416E-03
FRICTION POWER (WATTS)	0.1104E+01

CR-2166-1

Figure 41. Design for 170°K Turboalternator, 1.00-inch Wheel (Sheet 1 of 3)

DESIGN CASE	4793015
PRIMARY LOSSES	
ALTERNATOR TOTAL (WATTS)	0.6303E+01
SUM OF FRICTION LOSSES (WATTS)	0.6197E+01
TWO STAGE PERFORMANCE	
OTHER STAGE IN TEMP (K)	0.5500E+02
TOTAL HEAT LEAK (WATTS)	0.8673E+00
EXIT TEMPERATURE (K)	0.1526E+03
SHAFT HEAT LEAK (WATTS)	0.2212E+00
HOUSG HEAT LEAK (WATTS)	0.6461E+00
GAS BEARINGS	
ROTATING ASSEMBLY WEIGHT (LBS)	0.6278E-01
ACCELERATION OF GRAVITY ("G")	0.1000E+01
TOT. BEARING FRICTION (WATTS)	0.3547E+01
PERFORMANCE TERMS	
ISENTROPIC HEAD (FT)	0.9181E+05
HYDRAULIC EFF., FIRST TERM	0.5754E+00
HYDRAULIC EFF., SECOND TERM	0.8413E-01
HYDRAULIC EFF., THIRD TERM	0.4596E-04
TIP CLEARANCE EFF. CORRECTION	0.9453E+00
TRAIL EDGE EFF. CORRECTION	0.9100E+00
BLADE RE. NO. EFF. CORR.	0.9125E+00
ALTERNATOR GAP FLUX (KGAUSS)	0.8725E+01
ALTERNATOR CORE LOSS COEFF.	0.1226E+01
ALTERNATOR COPPER LOSS COEFF.	0.2356E+01
TEMPERATURE WHEEL EXIT GAS (R)	0.2692E+03
NOZ. DISC. VOLUME FLOW (CFS)	0.5965E-01
TURBINE BLADE DISC VOL. FLOW (CFS)	0.7023E-01
PERFORMANCE FACTORS	
TIP SPEED TO SPOUTING VEL. RATIO	0.2694E+00
BLADE INCIDENCE ANGLE (DEGREES)	0.1098E+02
NOZZLE COEFFICIENT	0.9000E+00
SPECIFIC SPEED	0.7333E+01
SPECIFIC DIAMETER	0.5474E+01
FLOW FACTOR	0.1185E+01
WHEEL EFFICIENCY (FRACTION)	0.3856E+00
HYDRAULIC EFFICIENCY (FRACTION)	0.4013E+00
ELECTROMAGNET EFF. (FRACTION)	0.9200E+00
ISENTROPIC POWER (WATTS)	0.2011E+03
WHEEL POWER OUTPUT (WATTS)	0.7754E+02
SHAFT POWER OUTPUT (WATTS)	0.7134E+02

CR-2166-2

Figure 41. Design for 170°K Turboalternator, 1.00-inch Wheel (Sheet 2 of 3)

DESIGN CASE

4793015

PARASITIC LOSSES (WATTS)
 TURBINE DISC FRICTION 0.2424E+01
 JOURNAL DIAM SHAFT FRICTION 0.1987E+00
 ALTERNATOR GAP FRICTION 0.2772E-01
 BEARING FRICTION 0.3547E+01

GEOMETRY

WHEEL TIP CLEARANCE (IN) 0.2000E-02
 BLADE PASSAGE CUTTER DIAMETER (IN) 0.2262E-01
 BLADE TRAILING EDGE THICKNESS (IN) 0.4000E-02
 ADMISSION ARC (FRACTION) 0.1164E+00
 ADMISSION ARC (DEGREES) 0.4190E+02
 NOZZLE ANGLE (DEGREES) 0.3000E+02
 BLADE ANGLE (DEGREES) 0.6480E+02
 BLADE CHORD (IN) 0.8789E-01
 WHEEL INSIDE DIAMETER (IN) 0.8242E+00
 BLADE PRESSURE SURFACE RADIUS (IN) 0.4857E-01
 BLADE SUCTION SURFACE RADIUS (IN) 0.2595E-01

TOTAL MACHINE SHAFT LENGTH (IN) 0.2660E+01
 JOURNAL SHAFT DIAMETER (IN) 0.2610E+00
 JOURNAL FREE SHAFT LENGTH (IN) 0.1366E+01
 ALTERNATOR DIAMETER (IN) 0.2610E+00
 ALTERNATOR MAGNET LENGTH (IN) 0.3606E+00
 ALTERNATOR PERIF. SPEED(F.P.S.) 0.1710E+03
 ALTERNATOR RADIAL GAP (IN) 0.1501E-01
 STATOR OVERHANG (IN) 0.4502E-01
 STATOR LAMINATION DIA. (IN) 0.9448E+00
 WHEEL BACK SIDE OPTIMUM GAP (IN) 0.1273E-01

VELOCITIES

SHOOTING VELOCITY (FPS) 0.2432E+04
 NOZZLE DISCHARGE VELOCITY (FPS) 0.2148E+04
 BLADE INLET RELATIVE VELOCITY (FPS) 0.3923E+03
 BLADE INLET RADIAL VELOCITY (FPS) 0.3302E+03
 BLADE INLET RELATIVE MACH NUMBER 0.1801E+00

REYNOLDS NUMBERS

BLADE PASSAGE REYNOLDS NO. 0.2884E+04
 TURBINE DISC REYNOLDS NO. 0.7121E+05
 JOURNAL DIAMETER REYNOLDS NO. 0.4351E+04
 ALTERNATOR GAP REYNOLDS NO. 0.2332E+04

DRAG COEFFICIENTS

TURBINE DISC DRAG COEFF. 0.1023E-01
 JOURNAL DIAMETER DRAG COEFF. 0.1065E-01
 ALTERNATOR GAP MOMENT COEFF. 0.5597E-02

CR-2166-3

Figure 41. Design for 170°K Turboalternator, 1.00-inch Wheel (Sheet 3 of 3)

Between the two different turbine-wheel diameters, the obvious preference would be the 1.0-inch wheel diameter, where there is about a one-percent efficiency advantage; the largest overall advantage would be in operating at a design-point speed of 150,000 rpm, rather than 230,000 rpm.

MECHANICAL ARRANGEMENT

A mechanical-arrangement layout was made for the 14°K unit, based on the design approach used in the small Air Force turboalternator frame size.

The turboalternator was designed to incorporate elements that could readily be developed to provide suitable performance and that could be adaptable to quantity production. A layout of this turboalternator is shown in Figure 13.

The turboalternator is mounted on gas-lubricated journal bearings. Three hardened pads at each journal bearing support the 0.25-inch-diameter shaft with an operating gas-film thickness on the order of 200 microinches. These journal bearings are of the self-acting tilting-pad type and are capable of stable operation throughout the operating range and at any attitude.

Two inward-pumping, self-acting, spiral-grooved, thrust bearings position the shaft axially. Like the journal bearings, the thrust bearings are gas-lubricated and typically operate with a 500-microinch gas-film thickness. The entire bearing system is self-aligning because the thrust bearings are gimbal-mounted and the journal tilting pads are individually self-aligning. Satisfactory operation of the complete bearing system can therefore be somewhat independent of the accuracy with which adjacent parts are manufactured.

The radial-inflow impulse turbine wheel is 0.50 inch in diameter. The radial-inflow wheel is convenient for close blade-tip axial clearances to minimize leakage. The turbine nozzle will be designed for partial admission.

The turbine energy is absorbed by a two-pole permanent-magnet alternator. This compact alternator is a very practical device for extracting energy at cryogenic temperatures when that energy will be dissipated at a remote location. The two-pole magnet operates within the stator, which is wound three-phase in a core of low-loss iron laminations.

A vacuum-type enclosure is welded for the final assembly. Proximity probes are installed to monitor the position of the rotor and gas-bearing elements.

TURBINE WHEEL STRESS AND DEFLECTION ANALYSIS

14°K UNIT

The 14°K unit turbine wheel is shown in Figure 42. The wheel is made of 6061-T6 aluminum and fits onto a stainless-steel shaft. The extreme operating conditions for the wheel are:

<u>Condition</u>	<u>Temperature</u>	<u>Speed (rpm)</u>
Cold	14°K	90,000
Warm	323°K	250,000

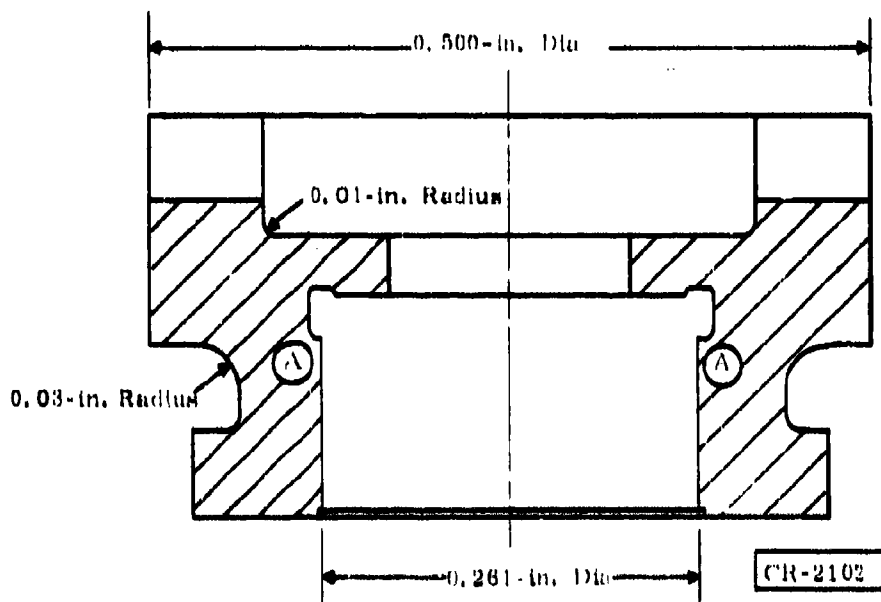


Figure 42. First-Stage Wheel

The coefficient of thermal expansion of aluminum is greater than that of steel. The wheel-shaft assembly is made at room temperature; therefore, as the warm condition is approached, the wheel expands more than the shaft and becomes loose on the shaft unless the wheel shaft assembly is made with a slight interference fit at room temperature.

The stresses caused by the interference fit are increased as the temperature is lowered. The thermal stresses are therefore very much higher for the cold condition than for the warm condition. Because the wheel is small, the centrifugal stresses are very small. At 250,000 rpm, the peak centrifugal stresses are only about one-third of the thermal stresses at 14°K. From the standpoint of stress, the cold condition is therefore the critical condition. The process followed in the analysis of this wheel was to determine the room-temperature interference required to maintain wheel-to-shaft contact in the warm

condition and then to perform a stress analysis for the cold condition with this interference fit.

The interference fit required is 0.05 mil on the radius or 0.1 mil on the diameter. This fit is sufficient to offset the differential thermal expansion and the small centrifugal force, tending to separate the wheel and shaft in a warm condition. The wheel stress was analyzed for the cold condition, using this value of interference fit. A plot of the effective stress contours is shown in Figure 43. Note that the stress levels are low everywhere except in region A, and even in region A, the stress level is acceptable. Actually there is no contact with the shaft in region A, because the shaft is slightly relieved to aid in piloting the wheel for assembly.

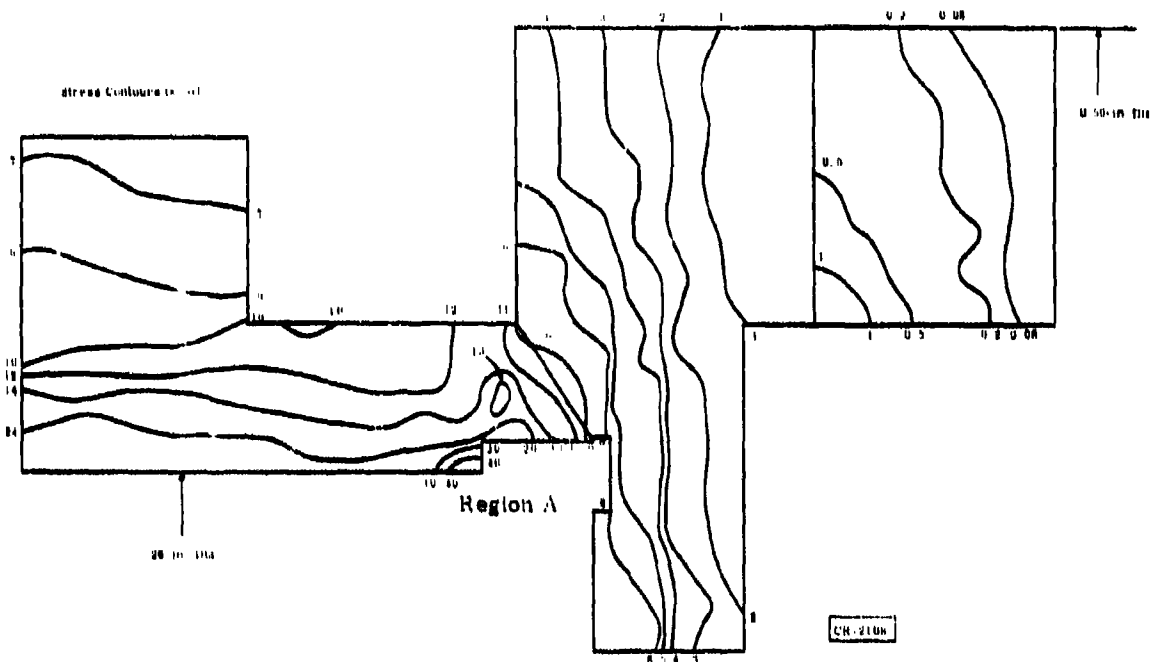


Figure 43. Cold-Condition Effective Stress Contours

Because centrifugal effects are small for this wheel, there is almost no bending, so the tip deflections are very low. Deflections for the wheel in the cold condition are shown in Figure 44. Deflections for the warm condition were not calculated but are expected to also be small, because the centrifugal stresses are small.

Because the 0.1-percent creep-stress limit at 70°F for 30,000 hours is 40,000 psi, the wheel design is considered acceptable. Creep data at cryogenic temperatures are not available.

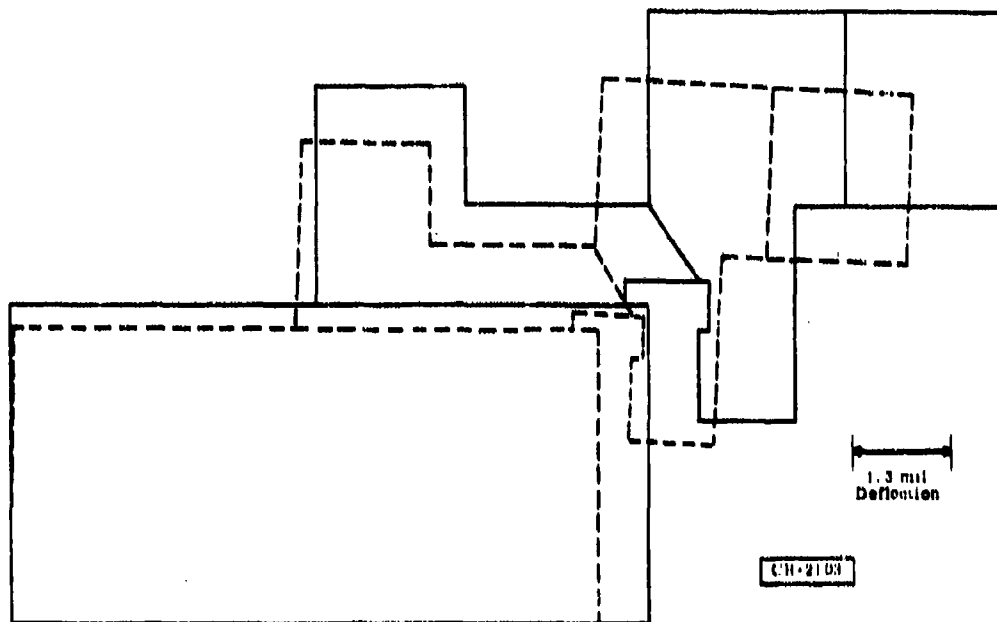


Figure 44. Deflections for Wheel in Cold Condition

The actual design range on this aluminum-wheel interference fit is 0.2- to 0.4-mil diametral interference, to assure that the wheel is attached at all times and can resist the operating torque.

55°K UNIT

The 55°K wheel design is 0.75 inch in diameter. The extreme operating conditions for the wheel are expected to be:

<u>Condition</u>	<u>Temperature</u>	<u>Speed (rpm)</u>
Cold	55°K	120,000
Warm	322°K	250,000

The wheel may be made of either 6061-T6 aluminum or 0 Al-4V titanium, a trade-off between:

- Ease of making the aluminum wheel, but possibly limiting the maximum speed below the target of 250,000 rpm.
- Using titanium, but ensuring that the target upper speed limit of 250,000 rpm can be obtained.

170°K UNIT

The 170°K wheel design is 1.0 inch or 0.625 inch in diameter. The extreme operating conditions expected for the two different wheels are:

Condition	Temperature	Speed	
		1.0-inch Wheel	0.625-inch Wheel
Cold	170°K	150,000 rpm	230,000 rpm
Warm	322°K	250,000 rpm	250,000 rpm

From prior results, such as the work completed for the U. S. Air Force, it is expected that: the 1.0-inch-diameter wheel must be made of 6 Al-4Vn titanium to achieve the target warm speed of 250,000 rpm, and the 0.625-inch-diameter wheel probably can be made of aluminum, with no problem.

Design considerations for a titanium wheel are somewhat different from those for an aluminum wheel. The coefficient of thermal expansion is less than that of stainless steel. The wheel-shaft assembly is made at room temperature; therefore, as the cold condition is approached, the wheel contracts less than the shaft and becomes loose on the shaft unless the wheel-shaft assembly is made with an interference fit at room temperature. The stresses caused by the interference fit are relieved as the temperature is lowered and are increased as the temperature is raised. The thermal stresses are therefore very much higher for the warm condition than for the cold condition. Because the warm condition also has a higher speed, it is the critical condition from the standpoint of stress.

The process to be followed in the analysis is to determine the room-temperature interference fit required to maintain wheel-to-shaft contact in the cold condition and then to perform a stress analysis for the warm condition, with this interference fit.

The design of a 1.1-inch-diameter turbine wheel is described in the progress report to Wright-Patterson Air Force Base (Ref. 4, Vol. I, Section 5).

Appendix II

GAS-BEARING ANALYSIS AND DESIGN**BEARING DESIGN REQUIREMENTS**

The overall design requirements for the journal and thrust bearings are:

Lubricant -- Helium gas from cycle working fluid

Contract design life goal -- 2500 hours

Ultimate design life goal -- 10,000 hours and more

Shock and vibration loads -- None while operating; normal handling while not operating

Acceleration load -- None while operating, but design for 2.0 g in any direction while operating

Design temperature -- 14°K (25.2°R)

Maximum operating temperature -- 125°F (585°R)

Starting -- Many start-stop cycles

Orientation -- Both vertical and horizontal

Additional requirements, as a consequence of the operating environment, include a constant bearing ambient pressure 1.19×10^5 newtons per square meter (17.22 psia) and a maximum speed of 200,000 rpm. This maximum speed will be experienced only at the maximum operating temperature at the start of system cooldown. After cooldown has started, the speed will be gradually decreased until the design speed of 90,000 rpm is reached at the design temperature of 14°K.

BEARING TYPE SELECTIONS

Only self-acting gas bearings were considered for this design.

Externally pressurized bearings were not seriously considered for the following reasons:

- Refrigerator cycle efficiency requires a low ambient pressure, near atmospheric, in the rotor housings.
- Refrigerator cycle efficiency would be lowered because a portion of the cycle gas would have to be diverted through the bearings.
- Ducting the bearing exhaust gas involves a mechanical and thermal heat-leak complication that is considered impractical.

- The bearings must be isolated from the rotor cavity by noncontacting seals. The design of the seals could be as complicated as the design of the bearing itself.

Tilting-pad journal bearings (Figures 45 and 46) were selected for the journals because of:

- Confidence in ultimate success
- Prior manufacturing and cryogenic test experience
- Broad stability range
- Inherent self-alignment
- Reasonable tolerance to dirt ingestion and thermal distortion

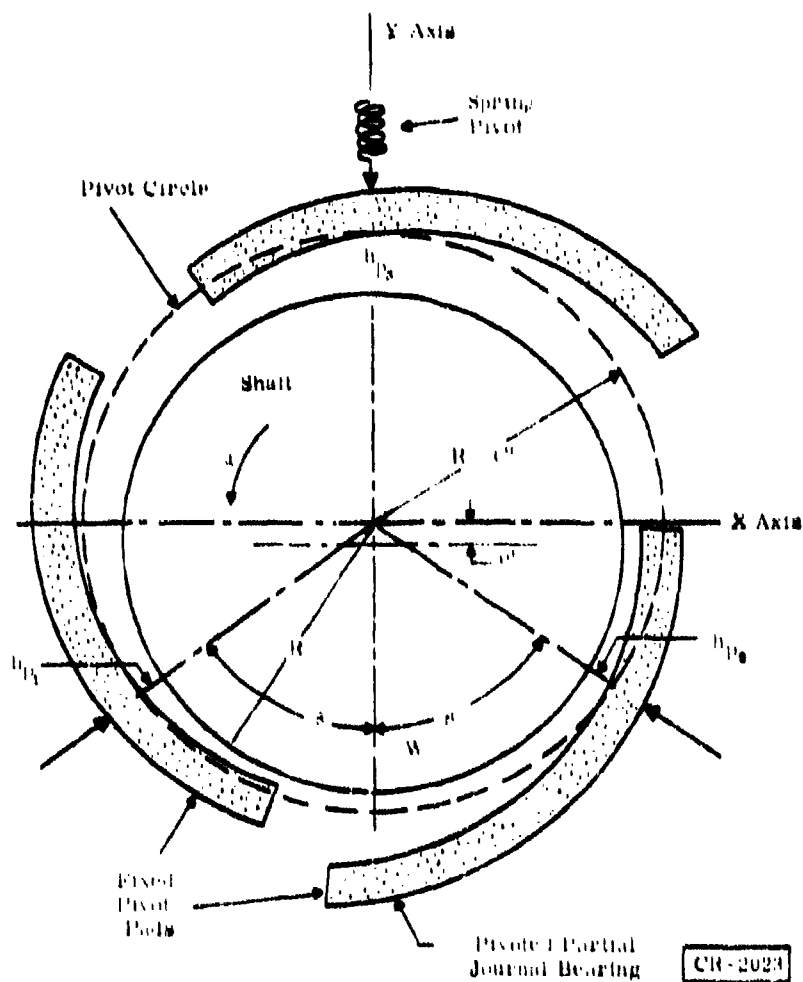


Figure 45. Pivoted-Pad Journal Bearing (Schematic Diagram)

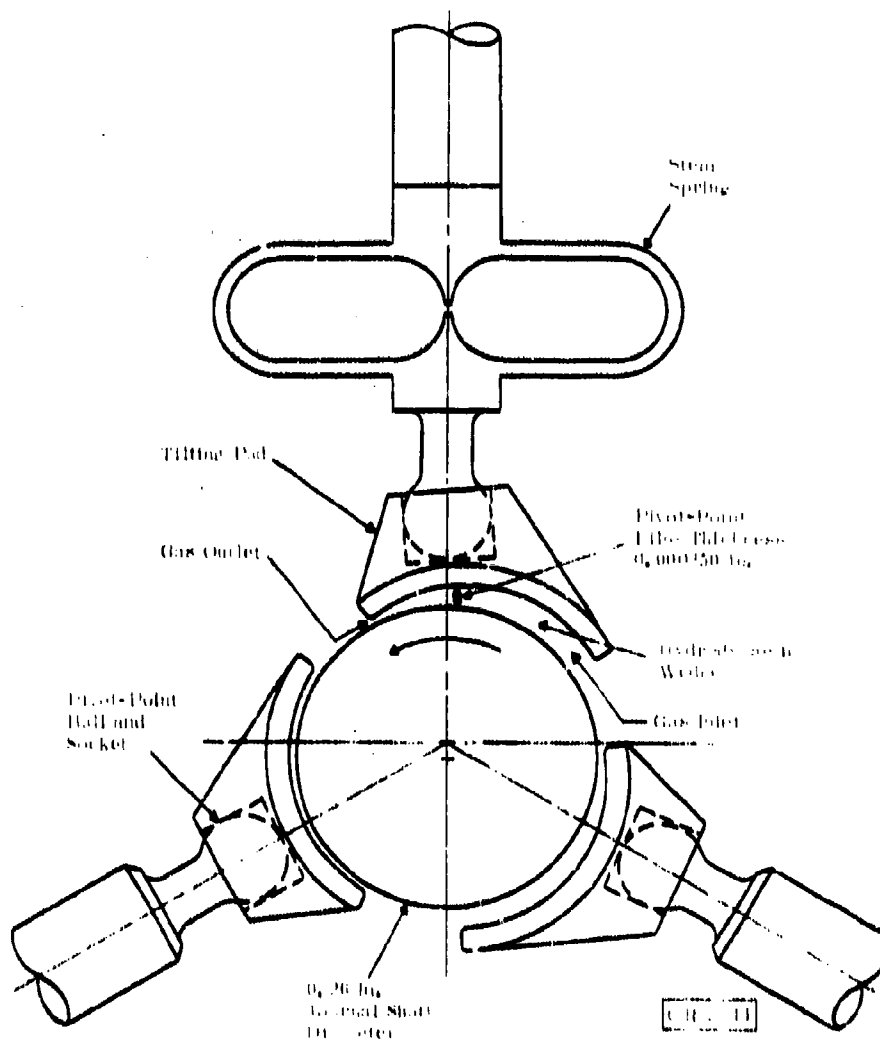


Figure 46. Cryogenic Turboalternator Tilting-Pad Journal Bearing

A double-acting hydrodynamic thrust bearing with a gimballed system mount was selected because of:

- Confidence in the ultimate success
- Prior manufacturing and cryogenic test experience
- Suitability for any attitude plus *g*-loading
- Suitability for complete self-alignment

A spiral-grooved inward pumping geometry (shown in Figures 47 and 48) was selected for the turboalternator designs because a stable configuration could be obtained that operated with a greater load capacity and less power loss than any other configuration.

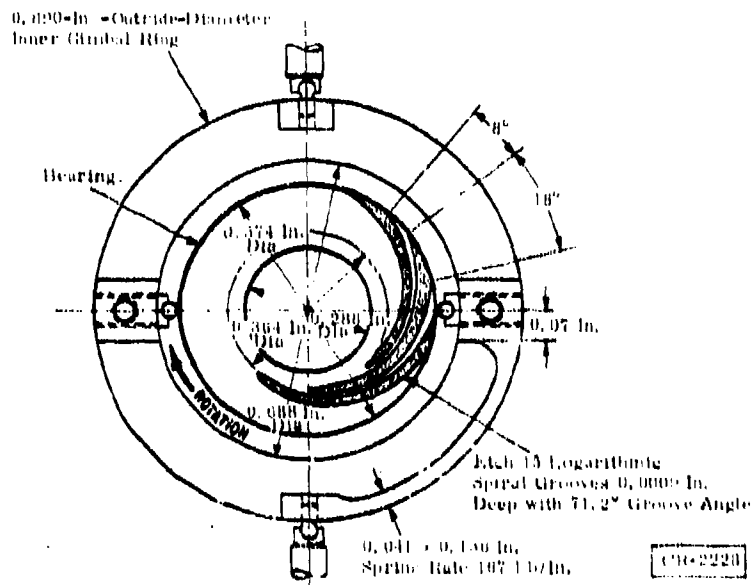


Figure 47. Gimbal-Mounted Spiral-Groove Thrust Bearing

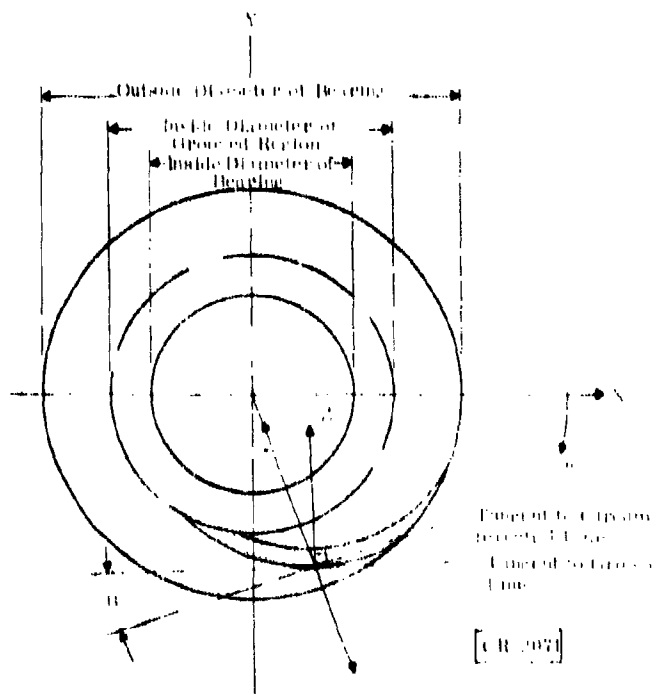


Figure 48. Spiral-Groove Thrust Bearing (Schematic Diagram)

JOURNAL BEARING DESIGN**PROCEDURE**

The procedure for journal bearing design consists of the following steps:

- Set up criteria for selection.
- Select bearing parameters and performance characteristics for preliminary design.
- Determine first bending critical speed of rotating assembly.
- Determine the stability and response of the rotor/journal bearing combination.

Many of the selection criteria are based upon engineering judgment, based upon past experience. For example, the principal journal bearing design goal is to maintain a fluid film separation of the bearing surfaces in the cryogenic environment. All that is required is a nonzero minimum film thickness, but there are two other film thicknesses that are usually considered. One is the pivot film thickness chosen as a design goal in advance of thermal distortion data. The second film thickness is chosen as the absolute minimum acceptable film thickness, which should take into account basic equation accuracy, numerical solution accuracy, and anticipated manufacturing tolerances. Similar considerations apply to critical speeds and other aspects of the design.

The criteria used in designing the journal bearings are:

- Pivot film thickness at 2-g steady-state load without bearing surface distortion will be 100 microinches.
- Absolute minimum film thickness will be 50 microinches.
- Power loss must be low.
- Shoe pitch, roll, and radial translational natural frequencies, with undistorted bearing surfaces, must be 25 percent above or 5 percent below the operating speed extremes.
- First bending critical speed must be 25 percent above the operating speed range.
- Whirl threshold speed must be above the operating speed range.
- Maximum nondimensional pivot film thickness (H/P) will be 0.75, for pad stability.
- Minimum nondimensional pivot film thickness will be 0.20, to limit bearing friction.
- Maximum pivot point stress (hertz) will be 100,000 psi.

The journal bearings were designed with a selector computer program, JSELECT (Ref. 4, App. VI), that contained the following:

- Coefficient of nondimensional polynomials for single-pad load, power loss, radial stiffness, and pitch axis stiffness versus bearing number (Λ) at constant nondimensional pivot film thicknesses (HP) of 0.20, 0.25, 0.30, 0.40, 0.50, 0.60, and 0.75.
- Logic to compute internally coefficients of nondimensional polynomials for single pad load, power loss, radial stiffness, and pitch axis stiffness and load versus HP at constant Λ .
- Coefficients of nondimensional polynomials for pad inertia versus shaft mass for constant Λ at the threshold of translatory whirl instability.
- A routine based on beam theory for computing two rigid-body natural frequencies and the first bending critical speed of a system consisting of four bars, three masses, and two bearings.
- A routine for computing the increase in journal diameter due to centrifugal force.
- Logic for testing film thicknesses relative to input criteria.
- Logic for testing the proximity of the following frequencies relative to the end points of an operating speed range:
 - Shaft rigid-body translations and rotations
 - Shoe radial translation
 - Shoe pitch axis rotation
 - Translatory self-excited whirl
- Logic for varying the machined-in clearance, preload, and preload spring stiffness if frequency or film thickness tests are not passed.
- Logic for computing performance characteristics if the machined-in clearance, preload, and preload spring stiffness are specified.
- Logic to determine the pivot ball radius so the hertz stress will be 100,000 psi.

The original pad data contained in the selector program were produced by a numerical solution of the transient Reynolds equation. Since the results are based on a disturbance from equilibrium, both steady-state and stability data were obtained simultaneously. All pad design data are based on a pad

are length of 100 degrees, with a pivot location of 65 percent and a length-to-diameter ratio of one.

PERFORMANCE

The JSELECT journal bearing selector program was used to design the tilting-pad journal bearings for the turboalternator. Initially, a target maximum speed of 250,000 rpm for room-temperature operation was used as input. With this high maximum speed, it was found that maximum rigid-body critical speed for the 2-g operation was too close to the cold temperature design operating speed of 90,000 rpm. The reason for this is that the high, 250,000-rpm speed required a stiffer gas bearing at the lower, 90,000-rpm design speed. The variations of the maximum rigid-body critical speeds are as shown in Table 15 for the three levels of g-loading of interest. Then, the stiffness of the shaft was reduced from 7,000 pound-inches². With only this change, the maximum rigid-body critical speed was reduced by only about 1000 rpm.

Table 15

DESIGNS WITH A MAXIMUM OPERATING SPEED OF 250,000 RPM
EI = 7000 lb-in.²

G-Loading	0.0		1.0		2.0	
Design bearing number (A)	0.250	1.150	0.250	--	0.25	1.150
Maximum rigid-body critical speed (rpm)	75,200	105,400	85,200	--	96,200	127,800
						CR-2280

As shown on page 144 of Reference 4, the spring rate of typical finished turboalternator shafts of the subject design are 50,000 and 38,000 lb-in. Using the simple beam formula likened to conditions of the test, the shaft stiffness is:

$$EI = \frac{SL^3}{48}$$

- where E - Youngs modulus (psi)
- I - Second moment of area (inch⁴)
- S - Shaft spring rate (lb/in.)
- L - Span between supports (inch)

The corresponding shaft stiffness values, EI, are 7410 and 5640 pound-inches². Hence, the 6000 value appeared to be a reasonable average and was used for all subsequent design runs.

It was therefore decided to lower the maximum operating speed to 200,000 rpm. The 2-g operating range of bearing numbers was first investigated, and

the lowest bearing loss was determined. The results are shown in Table 16, where a bearing number of 0.350 provides the lowest journal bearing power loss of 0.1542 watt. The maximum shaft rigid-body critical speed is comfortably below the design point of 90,000 rpm.

Table 16
DESIGN SPEED PERFORMANCE AT 2.0 G

Bearing Number Lambda (nd)	Single Bearing Power Loss (watts)	Maximum Shaft Rigid-Body Critical Speed (rpm)	Fixed Pivot-Pad Film Thickness (in.)	Spring-Mounted Pivot-Pad Film Thickness (in.)
0.4000	0.1500	85,043	165	241
0.3500	0.1542	81,531	168	245
0.3000	0.1580	80,035	167	239
0.2500	0.1637	80,350	164	236

CR-2281

Complete design runs were then made for the three g-loadings of interest:

<u>Run Number</u>	<u>G-Loading</u>
4791001	2.0
4791002	1.0
4791003	0.0

A summary of these performance runs is given in Table 17. The three runs are printed completely in Figures 49, 50, and 51.

Pertinent performance parameters from these three computer runs are given in Figures 52 and 53 as a function of the g-loading. Figure 53 shows the variations of bearing power loss and pivot film thickness for the two extremes in operating conditions of speed and temperature. Figure 52 shows that the highest calculated rigid-body critical speed is safely under the design speed, and the spring-pad radial translational critical speed is well above the maximum operating speed. The pad-pitch critical frequencies are shown operating reasonably above the respective operating and design speeds.

Next, an analysis was conducted to evaluate the effects of the spring pad, spring rate, and film thicknesses. Figure 54 shows the results of computer runs of constant values of nondimensional spring-pad film thickness for varying values of spring-pad spring rate. This nondimensional film thickness is the ratio of the actual film thickness to the operating machined-in radial clearance. Also shown are the 1-g design values. The results indicate that

Table 17
GAS BEARING PERFORMANCE SUMMARY

Characteristic	Design Condition	Maximum Speed Condition
<u>Operating Conditions</u>		
Speed (rpm)	90,000	200,000
Temperature (°R/°C)	22, 5/14, 0	585/325
Viscosity of helium (lb-sec/in. ²)	1.1×10^{-10}	31.0×10^{-10}
Ambient pressure (psia)	17.22	17.22
<u>Rotor</u>		
Weight (pound)	0.5070	
First bending critical speed (rpm)	359,000	
Wheel free hold speed (rpm)	600,100	
Rigid body critical speeds (rpm):		
Vertical	33,000, 17,000	
Transverse	40,000, 74,000	
Effective EI (lb-in.)	6,000	
Journal wall thickness (inch)	0.020	
Distance between journals (inch)	1.95	
<u>1st Operation</u>		
<u>Journal Bearings</u>		
Bearing number, Z (nd)	0, 3503	2, 604
Power loss, both journals (watts)	0, 2954	5, 34
Minimum pivot clearance (in.)	185	242
Bearing vertical stiffness (lb/in.)	919	1573
Bearing transverse stiffness (lb/in.)	1584	2692
Spring Loaded Shafts		
Load (pound)	0, 0611	0, 2144
Pivot fillet thickness (in.)	235	262
First critical frequency (rpm)	130084	263880
Transition critical frequency (rpm)	308332	608220
Fixed-Pivot Shafts		
Load (pound)	0, 0875	0, 2407
Pivot fillet thickness (in.)	143	242
First critical frequency (rpm)	200735	200047
<u>2nd Operation</u>		
<u>Journal Bearings</u>		
Power loss, both journals (watts)	0, 3084	3, 60
Minimum pivot clearance (in.)	108	231
Bearing vertical stiffness (lb/in.)	975	1659
Bearing transverse stiffness (lb/in.)	1928	3174
<u>0.5th Operation</u>		
<u>Journal Bearings</u>		
Power loss, both journals (watts)	0, 2804	3, 30
Minimum pivot clearance (in.)	201	251
Bearing vertical stiffness (lb/in.)	893	1520
Bearing transverse stiffness (lb/in.)	1314	2697

G E 2203

JSELCTU 14:42EST 12/19/72

*****GAS-LUBRICATED JOURNAL BEARINGS*****

DESIGN SPECIFICATIONS

DESIGN RUN NUMBER 4791001

DESIGN SPEED (RPM)	90000.0
TEMP. AT DESIGN SPD (R)	85.20
AMBIENT PRESS, DESIGN SPD (PSIA)	17.22
VISCOSITY, DESIGN (LB*SEC/IN**2)	0.9100E-09
MAX. SPEED (RPM)	200000.0
TEMP. AT MAX SPD (R)	585.00
AMBIENT PRESS, MAX SPD (PSIA)	17.22
VISCOSITY, MAX (LB*SEC/IN**2)	0.3100E-08
JOURNAL DIA. (IN)	0.261
ROTOR WEIGHT (LB)	0.0526
LEFT OVERHUNG WT. (LB)	0.0074
WT. BETWEEN BRGS. (LB)	0.0396
RIGHT OVERHUNG WT. (LB)	0.0057
LEFT WT. TO LEFT BRG. (IN)	0.2450
LEFT BRG. TO CO (IN)	1.3800
CO TO RIGHT BRG. (IN)	0.5700
RT BRG TO RT OVERHUNG WT (IN)	0.1650
G LOADING	2.0000
JOURNAL WALL THICKNESS (IN)	0.1305
YOUNG*INERTIA, (LB*IN**2)	0.6000E+04
PERCENT OF RAD FOR PAD THICK	0.1530
PAD LENGTH (IN)	0.2610
POISSONS RATIO (ND)	0.2600
YOUNGS MODULUS (PSI)	0.3000E+08
WT DEN OF J. MAT. (LB/IN**3)	0.2800
WT DEN OF PAD MAT (LB/IN**3)	0.2800
ANGLE BETWEEN PIVOTS (DEG)	120.0000
MINIMUM PIVOT FILM TK. (IN)	0.000100

T
FIX= T

SPRING STIFFNESS (LB/IN)	0.9556E+03
MACHINED IN CLEARANCE (IN)	0.000382
STARTING PIVOT FILM THICK.(ND)	0.643000
BALL RADIUS (IN)	0.014000
SOCKET RADIUS (IN)	0.014300

ONLY ONE PRELOAD IS BEING CONSIDERED

Figure 40. Design for 2.0-g Gas-Lubricated Journal Bearings (Sheet 1 of 4)

LAMBDA LOOP

LAMBDA, DES. SPD.	0.350
LAMBDA, MAX. SPD.	8.694
CLEARANCE, DES. SPD. (IN)	0.00038123
CLEARANCE, MAX. SPD. (IN)	0.00037817
WHIRL SPEED (RPM), DESIGN	1041163.12
WHIRL SPEED (RPM), MAXIMUM	696180.04

THIS SECTION INCREASES FLUTTER FREQ
ENTERING PRELOAD LOOP

*****GAS LUBRICATED JOURNAL BEARINGS*****

CONDITIONS AT DESIGN SPEED

LAMBDA (ND)	0.3502
AMBIENT PRESSURE (PSIA)	17.22
CLEARANCE (IN)	0.000381
JOURNAL DIAMETER (IN)	0.261002
BRG. TRANSVERSE STIFF. (LB/IN)	1928.08
BRG. VERTICAL STIFF. (LB/IN)	979.48
BRG. POWER LOSS (WATTS)	0.1542

SHOES WITH FIXED PIVOTS

LOAD (LB)	0.1056
PIVOT FILM THICKNESS (IN)	0.000168
PITCH STIFFNESS (IN-LB/RAD)	3.1133
PITCH CRITICAL FREQ. (RPM)	230567.7

SHOES WITH SPRING MTD. PIVOTS

LOAD (LB)	0.0529
PIVOT FILM THICKNESS (IN)	0.000245
PITCH STIFFNESS (IN-LB/RAD)	0.8220
PITCH CRITICAL FREQ (RPM)	118476.5
TRANS. CRITICAL FREQ (RPM)	380516.4
STIFF OF PRELOAD SPRING (LB/IN)	955.6
PIVOT SOCKET RADIUS (IN)	0.0143
PIVOT BALL RADIUS (IN)	0.0140

Figure 49. Design for 2.0-g Gas-Lubricated Journal Bearings (Sheet 2 of 4)

****GENERAL CONDITIONS****

WHIRL SPEED LIMIT (RPM)	696180.0
FIRST BENDING CRIT. SPD. (RPM)	359878.2
SHAFT RIGID BODY CRIT SPD (RPM)	81530.1
SHAFT RIGID BODY CRIT SPD (RPM)	58231.4
SHAFT RIGID BODY CRIT SPD (RPM)	47410.6
SHAFT RIGID BODY CRIT SPD (RPM)	34075.0
SHOE PITCH INERTIA (IN-LB-SEC ²)	0.5340E-08
WEIGHT OF SHOE (LB)	0.000359
THICKNESS OF SHOE (IN)	0.0200
MACHINED-IN CLEARANCE (IN)	0.000382
START-UP CLAMPING FORCE (IN)	0.
START-UP CLEAR ON TOP SHOE (IN)	0.00053

*******GAS LUBRICATED JOURNAL BEARINGS*******

****CONDITIONS AT MAXIMUM SPEED****

LAMBDA (ND)	2.694
AMBIENT PRESSURE (PSIA)	17.22
CLEARANCE (IN)	0.000378
JOURNAL DIAMETER (IN)	0.261008
BEARING X-STIFFNESS (LB/IN)	3173.931
BEARING Y-STIFFNESS (LB/IN)	1659.158
BEARING POWER LOSS (WATTS)	1.80

SHOES WITH FIXED PIVOTS

LOAD (LB)	0.2584
PIVOT FILM THICKNESS (IN)	0.000231
PITCH STIFFNESS (IN LB/RAD)	5.4367
PITCH CRITICAL (RPM)	304696.2

SHOES WITH SPRING MTD. PIVOTS

LOAD (LB)	0.2088
PIVOT FILM THICKNESS (IN)	0.000270
PITCH STIFFNESS (IN LB/RAD)	3.8173
PITCH CRITICAL (RPM)	255316.2
TRANSLATION CRITICAL (RPM)	502798.2

Figure 48. Design for 2.0-g Gas-Lubricated Journal Bearings (Sheet 3 of 4)

LIST

12NPTS 14141EST 12/19/72
 100 1
 150 4791001
 200 90000. 25.2 17.22 9.1E-10 200000. 585.
 300 17.22 31.E-10 .261 .0074 .0396 .0057
 400 .245 1.38 .570 .165 .05265 2.0
 500 .1305 .28 .28 .26 30.E6 6000.
 600 .153 .261 .0001
 700 0 1
 800 T
 900 .000382 955.6 .643 .0140 .0143

Figure 49. Design for 2.0-g Gas-Lubricated Journal Bearings (Sheet 4 of 4)

JSELCTU 08124EST 12/20/72
 *****GAS LUBRICATED JOURNAL BEARINGS*****

DESIGN SPECIFICATIONS

DESIGN RUN NUMBER 4791002

DESIGN SPEED (RPM)	90000.0
TEMP. AT DESIGN SPD (R)	25.20
AMBIENT PRESS, DESIGN SPD (PSIA)	17.22
VISCOSITY, DESIGN (LB*SEC/IN**2)	0.9100E-09
MAX. SPEED (RPM)	200000.0
TEMP. AT MAX SPD (R)	585.00
AMBIENT PRESS, MAX SPD (PSIA)	17.22
VISCOSITY, MAX (LB*SEC/IN**2)	0.3100E-08
JOURNAL DIA. (IN)	0.261
ROTOR WEIGHT (LB)	0.0526
LEFT OVERHUNG WT. (LB)	0.0074
WT. BETWEEN BRGS. (LB)	0.0396
RIGHT OVERHUNG WT. (LB)	0.0057

Figure 50. Design for 1.0-g Gas-Lubricated Journal Bearings (Sheet 1 of 4)

LEFT WT. TO LEFT BRG. (IN)	0.2450
LEFT BRG. TO CG (IN)	1.3800
CG TO RIGHT BRG. (IN)	0.5700
RT BRG TO RT OVERHUNG WT (IN)	0.1650
G LOADING	1.0000
JOURNAL WALL THICKNESS (IN)	0.1305
YOUNG*INERTIA, (LB*IN**2)	0.6000E+04
PERCENT OF RAD FOR PAD THICK	0.1530
PAD LENGTH (IN)	0.2610
POISSONS RATIO (ND)	0.2600
YOUNGS MODULUS (PSI)	0.3000E+08
WT DEN OF J. MAT. (LB/IN**3)	0.2800
WT DEN OF PAD MAT (LB/IN**3)	0.2800
ANGLE BETWEEN PIVOTS (DEG)	120.0000
MINIMUM PIVOT FILM TK. (IN)	0.000100

T
FIX= T

SPRING STIFFNESS (LB/IN)	0.9556E+03
MACHINED IN CLEARANCE (IN)	0.000382
STARTING PIVOT FILM THICK.(ND)	0.590000
BALL RADIUS (IN)	0.014000
SOCKET RADIUS (IN)	0.014300

ONLY ONE PRELOAD IS BEING CONSIDERED

LAMBDA LOOP

LAMBDA, DES. SPD.	0.350
LAMBDA, MAX. SPD.	2.694
CLEARANCE, DES. SPD. (IN)	0.00038123
CLEARANCE, MAX. SPD. (IN)	0.00037817
WHIRL SPEED (RPM), DESIGN	1041163.12
WHIRL SPEED (RPM), MAXIMUM	696180.04

THIS SECTION INCREASES FLUTTER FREQ
ENTERING PRELOAD LOOP

*****GAS LUBRICATED JOURNAL BEARINGS*****

CONDITIONS AT DESIGN SPEED

LAMBDA (ND)	0.3502
AMBIENT PRESSURE (PSIA)	17.22
CLEARANCE (IN)	0.000381

Figure 50. Design for 1.0-g Gas-Lubricated Journal Bearings (Sheet 2 of 4)

JOURNAL DIAMETER (IN)	0.261002
BRG. TRANSVERSE STIFF. (LB/IN)	1583.65
BRG. VERTICAL STIFF. (LB/IN)	918.76
BRG. POWER LOSS (WATTS)	0.1477

SHOES WITH FIXED PIVOTS

LOAD (LB)	0.0875
PIVOT FILM THICKNESS (IN)	0.000185
PITCH STIFFNESS (IN-LB/RAD)	2.3596
PITCH CRITICAL FREQ. (RPM)	200725.0

SHOES WITH SPRING MTD. PIVOTS

LOAD (LB)	0.0611
PIVOT FILM THICKNESS (IN)	0.000225
PITCH STIFFNESS (IN-LB/RAD)	1.1459
PITCH CRITICAL FREQ (RPM)	139883.8
TRANS. CRITICAL FREQ (RPM)	398321.9
STIFF OF PRELOAD SPRING (LB/IN)	955.6
PIVOT SOCKET RADIUS (IN)	0.0143
PIVOT BALL RADIUS (IN)	0.0140

GENERAL CONDITIONS

WHIRL SPEED LIMIT (RPM)	696180.0
FIRST BENDING CRIT. SPD. (RPM)	359699.6
SHAFT RIGID BODY CRIT SPD (RPM)	73935.4
SHAFT RIGID BODY CRIT SPD (RPM)	56392.3
SHAFT RIGID BODY CRIT SPD (RPM)	43091.0
SHAFT RIGID BODY CRIT SPD (RPM)	33018.4
SHOE PITCH INERTIA (IN-LB-SEC ²)	0.5340E-08
WEIGHT OF SHOE (LB)	0.000359
THICKNESS OF SHOE (IN)	0.0200
MACHINED-IN CLEARANCE (IN)	0.000382
START-UP CLAMPING FORCE (IN)	0.
START-UP CLEAR ON TOP SHOE (IN)	0.00053

*****GAS LUBRICATED JOURNAL BEARINGS*****

CONDITIONS AT MAXIMUM SPEED

LAMBDA (ND)	2.694
AMBIENT PRESSURE (PSIA)	17.22
CLEARANCE (IN)	0.000378

Figure 50. Design for 1,0-g Gas-Lubricated Journal Bearings (Sheet 3 of 4)

JOURNAL DIAMETER (IN)	0.261008
BEARING X-STIFFNESS (LB/IN)	2892.058
BEARING Y-STIFFNESS (LB/IN)	1572.722
BEARING POWER LOSS (WATTS)	1.77

SHOES WITH FIXED PIVOTS

LOAD (LB)	0.2407
PIVOT FILM THICKNESS (IN)	0.000242
PITCH STIFFNESS (IN LB/RAD)	4.9265
PITCH CRITICAL (RPM)	290047.1

SHOES WITH SPRING MTD. PIVOTS

LOAD (LB)	0.2144
PIVOT FILM THICKNESS (IN)	0.000262
PITCH STIFFNESS (IN LB/RAD)	4.0771
PITCH CRITICAL (RPM)	263860.2
TRANSLATION CRITICAL (RPM)	508219.6

LIST

12NPTS 08:35EST 12/20/72

100 1
 150 4791002
 200 90000. 25.2 17.22 9.1E-10 200000. 585.
 300 17.22 31.E-10 .261 .0074 .0396 .0057
 400 .245 1.38 .570 .165 .05265 1.0
 500 .1305 .28 .28 .26 30.E6 6000.
 600 .153 .261 .0001
 700 0 1
 800 T
 900 .000382 955.6 .590 .0140 .0143

Figure 50. Design for 1.0-g Gas-Lubricated Journal Bearings (Sheet 4 of 4)

JSELCTU 17:00EST 12/19/78

*****GAS LUBRICATED JOURNAL BEARINGS*****

DESIGN SPECIFICATIONS

DESIGN RUN NUMBER 4791003

DESIGN SPEED (RPM)	90000.0
TEMP. AT DESIGN SPD (R)	25.20
AMBIENT PRESS, DESIGN SPD (PSIA)	17.22
VISCOSITY, DESIGN (LB*SEC/IN**2)	0.9100E-09
MAX. SPEED (RPM)	200000.0
TEMP. AT MAX SPD (R)	585.00
AMBIENT PRESS, MAX SPD (PSIA)	17.22
VISCOSITY, MAX (LB*SEC/IN**2)	0.3100E-08
JOURNAL DIA. (IN)	0.261
ROTOR WEIGHT (LB)	0.0526
LEFT OVERHUNG WT. (LB)	0.0074
WT. BETWEEN BRGS. (LB)	0.0396
RIGHT OVERHUNG WT. (LB)	0.0057
LEFT WT. TO LEFT BRG. (IN)	0.2450
LEFT BRG. TO CG (IN)	1.3800
CG TO RIGHT BRG. (IN)	0.5700
RT BRG TO RT OVERHUNG WT (IN)	0.1650
G LOADING	0.
JOURNAL WALL THICKNESS (IN)	0.1305
YOUNG*INERTIA, (LB*IN**2)	0.6000E+04
PERCENT OF RAD FOR PAD THICK	0.1530
PAD LENGTH (IN)	0.2610
POISSONS RATIO (ND)	0.2600
YOUNGS MODULUS (PSI)	0.3000E+08
WT DEN OF J. MAT. (LB/IN**3)	0.2800
WT DEN OF PAD MAT (LB/IN**3)	0.2800
ANGLE BETWEEN PIVOTS (DEG)	120.0000
MINIMUM PIVOT FILM TK. (IN)	0.000100

T
FIX= T

SPRING STIFFNESS (LB/IN)	0.9556E+03
MACHINED IN CLEARANCE (IN)	0.000382
STARTING PIVOT FILM THICK. (ND)	0.930000
BALL RADIUS (IN)	0.014000
SOCKET RADIUS (IN)	0.014300

ONLY ONE PRELOAD IS BEING CONSIDERED

Figure 51. Design for 0.0-g Gas-Lubricated Journal Bearings (Sheet 1 of 3)

LAMBDA LOOP

LAMBDA, DES. SPD.	0.350
LAMBDA, MAX. SPD.	2.694
CLEARANCE, DES. SPD. (IN)	0.00038123
CLEARANCE, MAX. SPD. (IN)	0.00037817
WHIRL SPEED (RPM), DESIGN	1041163.12
WHIRL SPEED (RPM), MAXIMUM	696180.04

THIS SECTION INCREASES FLUTTER FREQ
ENTERING PRELOAD LOOP

*****GAS LUBRICATED JOURNAL BEARINGS*****

CONDITIONS AT DESIGN SPEED

LAMBDA (ND)	0.3502
AMBIENT PRESSURE (PSIA)	17.22
CLEARANCE (IN)	0.000381
JOURNAL DIAMETER (IN)	0.261002
BRG. TRANSVERSE STIFF. (LB/IN)	1313.77
BRG. VERTICAL STIFF. (LB/IN)	892.76
BRG. POWER LOSS (WATTS)	0.1442

SHOES WITH FIXED PIVOTS

LOAD (LB)	0.0743
PIVOT FILM THICKNESS (IN)	0.000201
PITCH STIFFNESS (IN-LB/RAD)	1.7740
PITCH CRITICAL FREQ. (RPM)	174045.2

SHOES WITH SPRING MTD. PIVOTS

LOAD (LB)	0.0743
PIVOT FILM THICKNESS (IN)	0.000202
PITCH STIFFNESS (IN-LB/RAD)	1.7491
PITCH CRITICAL FREQ (RPM)	172618.3
TRANS. CRITICAL FREQ (RPM)	422994.4
STIFF OF PRELOAD SPRING (LB/IN)	955.6
PIVOT SOCKET RADIUS (IN)	0.0143
PIVOT BALL RADIUS (IN)	0.0140

GENERAL CONDITIONS

WHIRL SPEED LIMIT (RPM)	696180.0
FIRST BENDING CRIT. SPD. (RPM)	359627.7
SHAFT RIGID BODY CRIT SPD (RPM)	67372.7

Figure 51. Design for 0.0-g Gas-Lubricated Journal Bearings (Sheet 2 of 3)

SHAFT RIGID BODY CRIT SPD (RPM)	55595.1
SHAFT RIGID BODY CRIT SPD (RPM)	39342.5
SHAFT RIGID BODY CRIT SPD (RPM)	32562.5
SHOE PITCH INERTIA (IN-LB-SEC ²)	0.5340E-08
WEIGHT OF SHOE (LB)	0.000359
THICKNESS OF SHOE (IN)	0.0200
MACHINED-IN CLEARANCE (IN)	0.000382
START-UP CLAMPING FORCE (IN)	0.
START-UP CLEAR ON TOP SHOE (IN)	0.00053

*****GAS LUBRICATED JOURNAL BEARINGS*****

CONDITIONS AT MAXIMUM SPEED

LAMBDA (ND)	2.694
AMBIENT PRESSURE (PSIA)	17.22
CLEARANCE (IN)	0.000378
JOURNAL DIAMETER (IN)	0.261008
BEARING X-STIFFNESS (LB/IN)	2696.998
BEARING Y-STIFFNESS (LB/IN)	1520.435
BEARING POWER LOSS (WATTS)	1.75

SHOES WITH FIXED PIVOTS

LOAD (LB)	0.2270
PIVOT FILM THICKNESS (IN)	0.000251
PITCH STIFFNESS (IN LB/RAD)	4.5255
PITCH CRITICAL (RPM)	277993.8

SHOES WITH SPRING MTD. PIVOTS

LOAD (LB)	0.2270
PIVOT FILM THICKNESS (IN)	0.000253
PITCH STIFFNESS (IN LB/RAD)	4.4550
PITCH CRITICAL (RPM)	275819.6
TRANSLATION CRITICAL (RPM)	317811.9

LIST

I2NPTS 17:11EST 12/19/72

100 1
150 4791003
200 90000. 25.2 17.22 9.1E-10 200000. 585.
300 17.22 31.E-10 .261 .0074 .0396 .0057
400 .245 1.38 .570 .165 .05265 0.0
500 .1305 .28 .28 .24 30.E6 6000.
600 .153 .261 .0001
700 0 1
800 T
900 .000382 955.6 .530 .0140 .0143

Figure 51. Design for 0.0-g Gas-Lubricated Journal Bearings (Sheet 3 of 3)

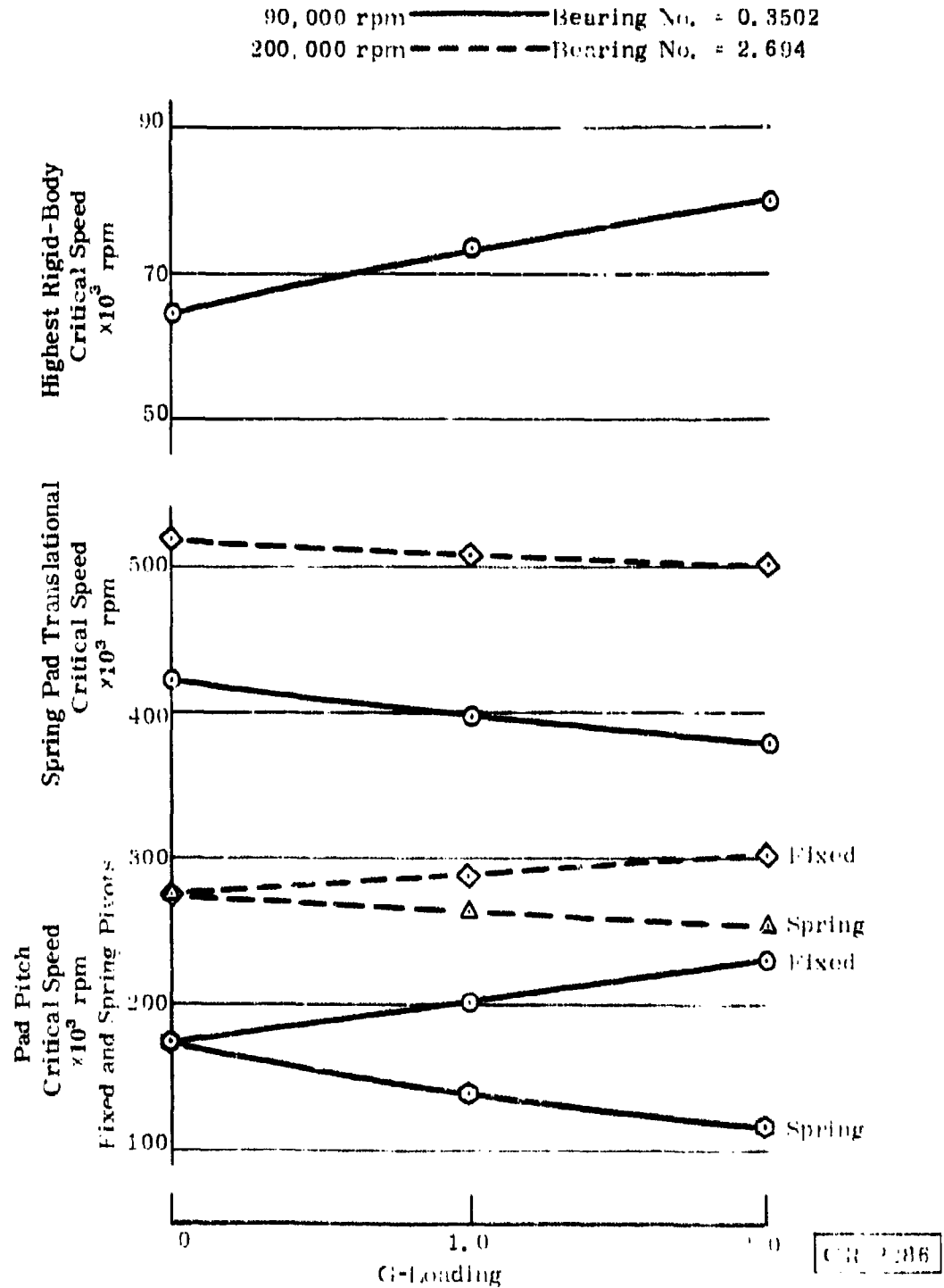
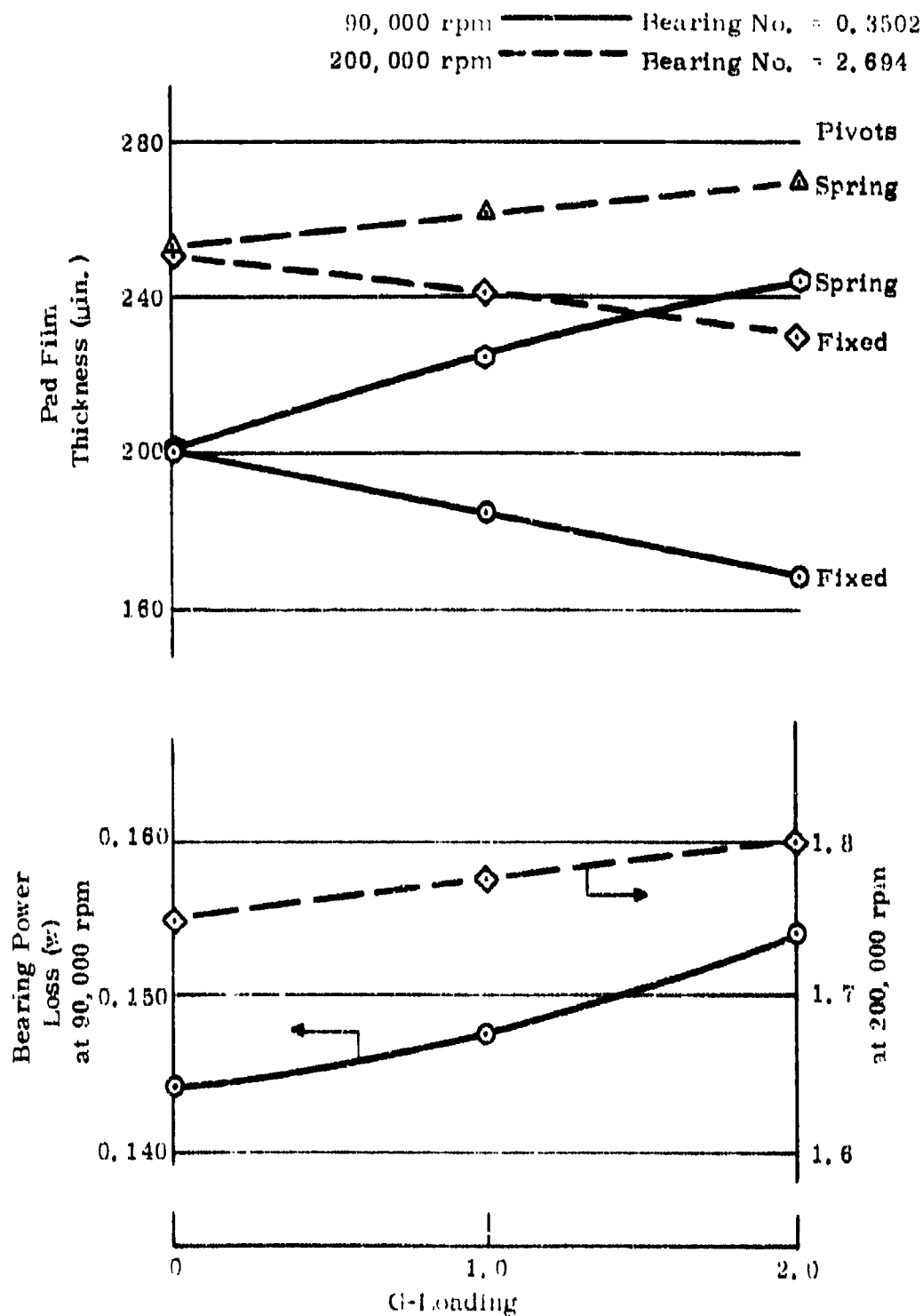


Figure 52. Journal Bearing Performance as a Function of G-Loading



CR-2287

Figure 53. Journal Bearing Performance as a Function of G-Loading

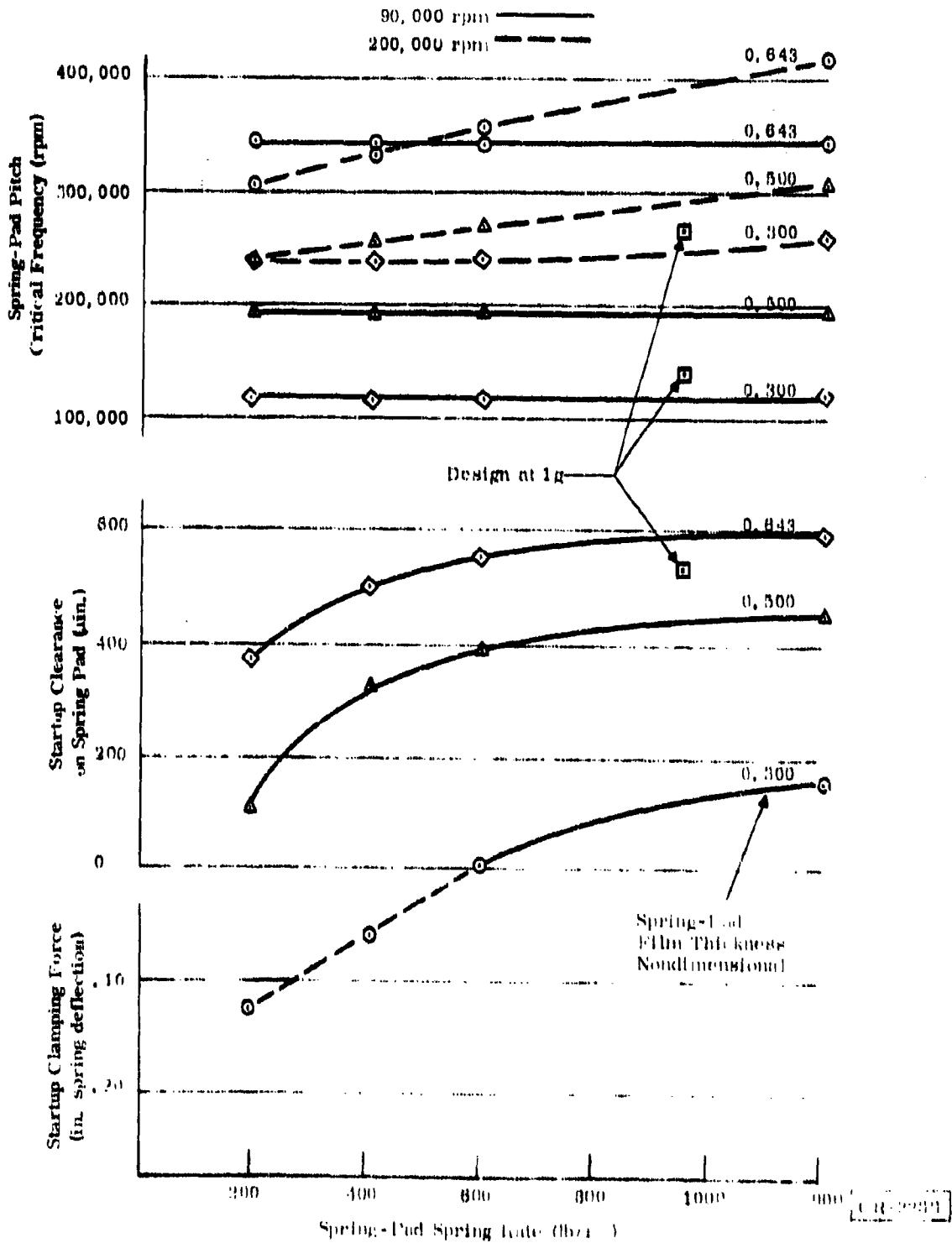


Figure 54. Journal Bearing Design Clearance and Pad Frequency Versus Spring-Pad Spring Rate

the spring-pad spring rate is not too sensitive above a value of 600 pounds per inch. There is a decrease in the spring-pad pitch critical frequency, but this is of no significant consequence.

Probably the most critical problem with varying the spring rate to a softer spring is the practical aspect of setting the initial desired bearing clearances.

A complete summary of the selected design is shown in Table 18.

A comparison with a similar previous design shows the Wright-Patterson Air Force Base contract design uses a 584-microinch ground in clearance, as

Table 18
TURBOALTERNATOR TILTING-PAD JOURNAL
GAS-BEARING DESIGN SUMMARY

Characteristic	Design Parameter
Type	3-shoe tilting pad
Pad wrap angle (deg)	100
Pad pivot location (% from leading edge)	65
Pad material and weight density (lb/in. ³)	304, 0.28
Pad coating and surface finish (rms)	Nitride, 4
Diameter (inch)	0.261
Pad length (inch)	0.261
Angle between pivots (deg)	120
Journal material and weight density (lb/in. ³)	304, 0.28
Journal wall thickness (inch)	0.1305
Cold machined-in clearance (inch)	0.000382
Ball material, coating, and surface finish (rms)	304, Nitride*, 4
Socket material, coating, and surface finish (rms)	304, Nitride*, 4
Preload spring stiffness (lb/in.)	956.0
Shoe pitch inertia (in.-lb-sec ²)	0.534×10^{-6}
Nominal weight of shoe (pound)	3.59×10^{-4}
Nominal thickness of shoe (inch)	0.020

*Subject to change

CR-2279

compared to the 382-microinch clearance for the present design. This would lead to lower bearing number and higher bearing power loss, as was seen from the trend of Table 16.

THRUST BEARING DESIGN

PROCEDURE

The process of establishing the selection criteria for the thrust bearing was essentially the same as for the journal bearing; the design-goal film thickness corresponding to the maximum load was assigned in advance of thermal distortion data.

The design criteria used in selecting the thrust bearing are:

- Maximum design load of 2.0 g
- Minimum film thickness of 100 microinches with parallel, undistorted bearing surfaces at maximum load
- Stable operation with minimum possible gimbal pivot friction and damping from zero net load to maximum load
- Low power loss
- Minimum outside diameter
- Maximum gas film moment
- No rigid-body natural frequencies in speed or load range
- Maximum stiffness over operating range

The general thrust-bearing design procedure consists of the following principal steps:

- Set up criteria for selection.
- Optimize load capacity with respect to film thickness for axially stable face geometries.
- Determine bearing and gimbal-ring moments of inertia and pivot friction characteristics necessary to provide stability with a misaligned thrust runner for both axial translation of the rotor and angular rotation of the gimbal ring.

The spiral-groove thrust bearing selector program for uniform clearance, STBSUC (Ref. 4, App. IX), was used to obtain design and performance parameters. This same program was used to compute the film righting moment for the spiral-groove bearings, at a load of approximately 2 g.

The moment was then checked, using the nonuniform clearance program, SPGRTH (Ref. 4, App. VIII). Pivot characteristics were computed so that the pivot friction moment equaled the film moment with collar misalignment at maximum load.

Program STBSUC, the spiral-groove thrust bearing selector program for uniform clearance, was used first to evaluate the thrust bearing design. The program is based on analytical expressions for computing the load capacity of a spiral-groove bearing with a uniform film thickness. In addition, the power loss, axial stiffness, and tilt stiffness are computed; several other parameters, such as the Reynolds number, are computed and listed as an aid in the design selection. When the bearing design parameters have been selected, a plotting program is used to compute and plot performance characteristics for a double-acting bearing.

The principal parameters for the bearing design study are:

- Ratio of outside diameter to inside diameter
- Design film clearance at which the load is to be optimized

For a small value of optimized film clearance, the load-versus-clearance curve will have a steep slope, maximizing the film thickness at high load at the expense of the film thickness at a lower loading. This film thickness is normally selected as a compromise between the film-thickness safety margin at maximum load and stiffness at normal operating conditions.

The design parameters are usually selected so that:

- The Mach number is less than 0.8 at the outside diameter.
- Minimum number of grooves is less than the maximum number of grooves. The minimum number is based on minimizing groove entrance effects; the maximum number is based on manufacturing considerations.
- Relative swash amplitude is less than $0.15 \times$ film thickness.
- Reynolds number is less than 1500.
- The bearing number λ is less than 50.
- Convective and transient inertias are much less than one.
- Steady-state and dynamic local compressibility are much less than one.
- Thrust-runner tip speed is less than 800 feet per second.

Based on the comparison of the load capacity predicted by this program with available experimental data, the theoretical load capacity and stiffness are multiplied by 0.75 as a safety factor.

PERFORMANCE

The principal dimensions of the thrust face were established. In order to evaluate the sensitivity of the depth of groove on this design, a set of three different groove-depth designs were considered. A range of the three

designs for which the groove depth was varied and the corresponding optimum clearance of each groove depth is shown on Figure 55. Also shown is the referenced drawing tolerance range established.

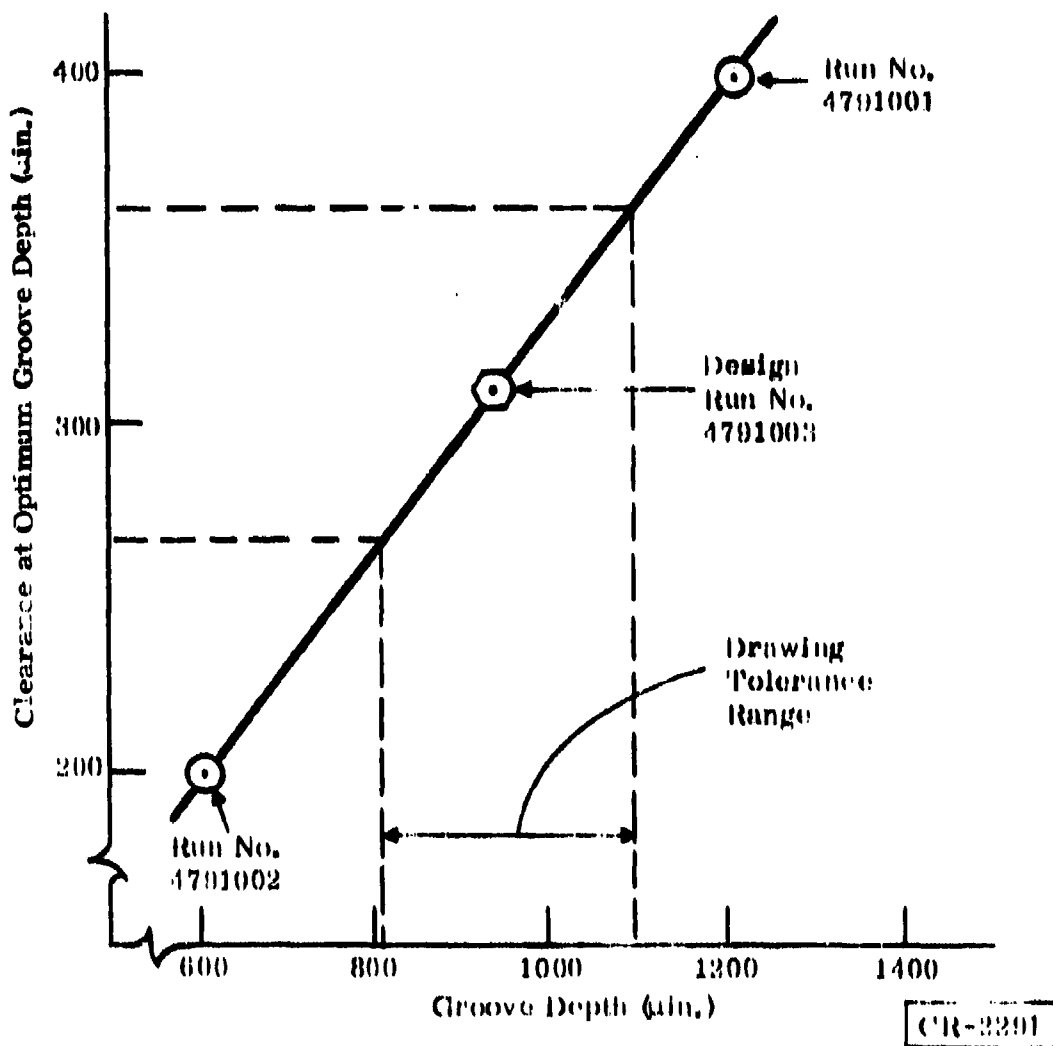


Figure 55. Thrust Bearing Groove Depth Versus Clearance

The selected design run number is 4791003, shown on Figure 56. The output of this computer program run represents the design speed performance expected from one thrust bearing face only. The following input is printed with the output:

- Title indicating the gas used as the lubrication.
- Ratio of outside diameter to inside diameter.
- Shaft rotational speed (rpm).

STURIN 15:26EST 12/21/72

100 1
 200 4791003
 300 .00031 90000. .287 25.2 17.22 .003
 400 .289 .73 1.93 71.2 .010 9.4E-6
 500 9.4E-6 .05265 2.0 0.0
 600 1 25 25

READY
 OLD STRSUCU

READY
 RUN

STRSUCU 15:27EST 12/21/72

HELIUM-LUBRICATED SPIRAL GROOVE THRUST BEARING

RATIO OF OD TO ID = 2.0000

INPUT

DESIGN RUN NUMBER 4791003

SPEED, RPM	0.9000E+05	GROOVE LT/BRO WIDTH	0.7300E+00
TEMPERATURE, DEG. R	0.2520E+02	GROOVE/RIDGE WIDTH	0.1930E+01
BEARING ID, IN.	0.2870E+00	GROOVE ANGLE, DEG	0.7120E+02
AMBIENT PRESS., PSIA	0.1722E+02	EXP COEFF. BRO, IN/IN F	0.9400E-05
SWASH ANGLE, DEG	0.3000E-02	EXP COEFF. RUN, IN/IN F	0.9400E-05
WT DEN BRO MAT, LB/IN3	0.2890E+00	MIN ALLOW. RIDGE W, IN	0.1000E-01
SHAFT WEIGHT, LB	0.5265E-01	CLEAR AT OPT ORV. D, IN	0.3100E-03

OUTPUT

MACH NO. AT OD	0.2897E+00	MIN. NO. GROOVES	28
GIMBAL MTD BRO TK., IN	0.6250E-01	VISCOSITY, LB-SEC/IN2	0.4020E-09
MAX NO. OF GROOVES	39	BEARING OD, IN.	0.5740E+00
MOLECULAR MFP, IN.	0.2163E-06	BRO. INER. IN-LB-SEC2	0.2367E-06
GROOVE DEPTH, IN.	0.9455E-03	TIP SPEED, FT/SEC	0.2254E+03

Figure 56. Helium-Lubricated Spiral-Groove Thrust Bearing, Design Run No. 4791003. Ratio of Outside to Inside Diameter 2.0 (Sheet 1 of 3)

	25	50	75
CLEARANCE, MICROINCHES			
LOAD, LB	0.1339E+00	0.1261E+00	0.1155E+00
POWER, WATTS	0.7328E+00	0.3840E+00	0.2635E+00
RELATIVE SWASH AMPLITUDE	0.1928E+01	0.3806E+00	0.2191E+00
MAX DISTORTION TO CLEAR RAT.	0.5002E+00	0.1282E+00	0.5747E-01
AXIAL FREQUENCY, CPM	0.9725E+04	0.1548E+05	0.1666E+05
TILT FREQUENCY, CPM	0.3553E+05	0.5655E+05	0.6086E+05
AXIAL STIFFNESS LB/IN	0.1415E+03	0.3584E+03	0.4151E+03
TILT STIFFNESS IN-LB/RAD	0.3277E+01	0.8303E+01	0.9615E+01
EFFECT. VIS. LB-SEC/IN**2	0.3822E-09	0.3919E-09	0.3952E-09
REYNOLDS NO.	0.6647E+02	0.1329E+03	0.1994E+03
LAMBDA	0.8700E+02	0.2175E+02	0.9667E+01
CONVECTIVE INERTIA RATIO	0.1480E-03	0.5920E-03	0.1332E-02
TRANSIENT INERTIA RATIO	0.9428E+00	0.1579E+01	0.1786E+01
LOCAL COMPRESS. RATIO, SS	0.6751E+00	0.1688E+00	0.7501E-01
LOCAL COMPRESS. RATIO, DYN	0.1637E-01	0.6513E-02	0.3115E-02

	100	125	150
CLEARANCE, MICROINCHES			
LOAD, LB	0.1039E+00	0.9204E-01	0.8035E-01
POWER, WATTS	0.2023E+00	0.1652E+00	0.1402E+00
RELATIVE SWASH AMPLITUDE	0.1551E+00	0.1733E+00	0.1068E+00
MAX DISTORTION TO CLEAR RAT.	0.7245E-01	0.2083E-01	0.1449E-01
AXIAL FREQUENCY, CPM	0.1710E+05	0.1720E+05	0.1687E+05
TILT FREQUENCY, CPM	0.8264E+05	0.8283E+05	0.6163E+05
AXIAL STIFFNESS LB/IN	0.4397E+03	0.4424E+03	0.4256E+03
TILT STIFFNESS IN-LB/RAD	0.1019E+02	0.1025E+02	0.9861E+01
EFFECT. VIS. LB-SEC/IN**2	0.3969E-09	0.3979E-09	0.3986E-09
REYNOLDS NO.	0.2659E+03	0.3323E+03	0.3988E+03
LAMBDA	0.5437E+01	0.3480E+01	0.2417E+01
CONVECTIVE INERTIA RATIO	0.2368E-02	0.3700E-02	0.5328E-02
TRANSIENT INERTIA RATIO	0.1929E+01	0.2028E+01	0.2084E+01
LOCAL COMPRESS. RATIO, SS	0.4219E-01	0.2700E-01	0.1875E-01
LOCAL COMPRESS. RATIO, DYN	0.1804E-02	0.1159E-02	0.7987E-03

	175	200	225
CLEARANCE, MICROINCHES			
LOAD, LB	0.6932E-01	0.5927E-01	0.5040E-01
POWER, WATTS	0.1222E+00	0.1087E+00	0.9799E-01
RELATIVE SWASH AMPLITUDE	0.2894E-01	0.9661E-01	0.9827E-01
MAX DISTORTION TO CLEAR RAT.	0.1066E-01	0.8168E-02	0.6458E-02
AXIAL FREQUENCY, CPM	0.1623E+05	0.1536E+05	0.1436E+05
TILT FREQUENCY, CPM	0.5929E+05	0.5612E+05	0.5246E+05
AXIAL STIFFNESS LB/IN	0.3939E+03	0.3530E+03	0.3085E+03
TILT STIFFNESS IN-LB/RAD	0.9125E+01	0.8177E+01	0.7146E+01
EFFECT. VIS. LB-SEC/IN**2	0.3991E-09	0.3995E-09	0.3997E-09
REYNOLDS NO.	0.4653E+03	0.5317E+03	0.5982E+03
LAMBDA	0.1776E+01	0.1359E+01	0.1074E+01
CONVECTIVE INERTIA RATIO	0.7252E-02	0.9471E-02	0.1199E-01
TRANSIENT INERTIA RATIO	0.2097E+01	0.2075E+01	0.2025E+01
LOCAL COMPRESS. RATIO, SS	0.1378E-01	0.1055E-01	0.8334E-02
LOCAL COMPRESS. RATIO, DYN	0.5574E-03	0.4040E-03	0.2984E-03

Figure 56. Helium-Lubricated Spiral-Groove Thrust Bearing, Design Run No. 4791003, Ratio of Outside to Inside Diameter 2.0 (Sheet 2 of 3)

	250	275	300
CLEARANCE, MICRONS			
LOAD, LB	0.4271E-01	0.3616E-01	0.3064E-01
POWER, WATTS	0.3941E-01	0.3234E-01	0.2641E-01
RELATIVE SHAKE AMPLITUDE	0.1031E+00	0.1107E+00	0.1208E+00
MAX DISTORTION TO CLEAR RAT.	0.5234E-02	0.4328E-02	0.3638E-02
AXIAL FREQUENCY, CPM	0.1330E+03	0.1224E+03	0.1122E+03
TILT FREQUENCY, CPM	0.4859E+03	0.4472E+03	0.4099E+03
AXIAL STIFFNESS LB/IN	0.2646E+03	0.2241E+03	0.1822E+03
TILT STIFFNESS IN-LB/RAD	0.6130E+01	0.5192E+01	0.4361E+01
EFFECT. VIS. LB-SEC/IN**2	0.4000E-09	0.4002E-09	0.4003E-09
REYNOLDS NO.	0.6647E+03	0.7311E+03	0.7976E+03
LAMBDA	0.8700E+00	0.7191E+00	0.6042E+00
CONVECTIVE INERTIA RATIO	0.1460E-01	0.1791E-01	0.2131E-01
TRANSIENT INERTIA RATIO	0.1257E+01	0.1277E+01	0.1791E+01
LOCAL COMPRESS. RATIO, SS	0.6751E-02	0.5579E-02	0.4698E-02
LOCAL COMPRESS. RATIO, DYN	0.2239E-03	0.1703E-03	0.1311E-03

	325	350	375
CLEARANCE, MICRONS			
LOAD, LB	0.2601E-01	0.2215E-01	0.1892E-01
POWER, WATTS	0.7135E-01	0.6609E-01	0.6318E-01
RELATIVE SHAKE AMPLITUDE	0.1333E+00	0.1484E+00	0.1659E+00
MAX DISTORTION TO CLEAR RAT.	0.3101E-02	0.2674E-02	0.2330E-02
AXIAL FREQUENCY, CPM	0.1020E+03	0.9370E+03	0.8560E+03
TILT FREQUENCY, CPM	0.3743E+03	0.3423E+03	0.3127E+03
AXIAL STIFFNESS LB/IN	0.1574E+03	0.1313E+03	0.1096E+03
TILT STIFFNESS IN-LB/RAD	0.3646E+01	0.3042E+01	0.2539E+01
EFFECT. VIS. LB-SEC/IN**2	0.4004E-09	0.4006E-09	0.4007E-09
REYNOLDS NO.	0.3641E+03	0.3305E+03	0.2970E+03
LAMBDA	0.5144E+00	0.4437E+00	0.3867E+00
CONVECTIVE INERTIA RATIO	0.2501E-01	0.2901E-01	0.3330E-01
TRANSIENT INERTIA RATIO	0.1704E+01	0.1619E+01	0.1536E+01
LOCAL COMPRESS. RATIO, SS	0.3994E-02	0.3444E-02	0.3000E-02
LOCAL COMPRESS. RATIO, DYN	0.1022E-03	0.8046E-04	0.6403E-04

	400
CLEARANCE, MICRONS	
LOAD, LB	0.1623E-01
POWER, WATTS	0.5942E-01
RELATIVE SHAKE AMPLITUDE	0.1862E+00
MAX DISTORTION TO CLEAR RAT.	0.2049E-02
AXIAL FREQUENCY, CPM	0.7825E+03
TILT FREQUENCY, CPM	0.2859E+03
AXIAL STIFFNESS LB/IN	0.9159E+02
TILT STIFFNESS IN-LB/RAD	0.2122E+01
EFFECT. VIS. LB-SEC/IN**2	0.4007E-09
REYNOLDS NO.	0.1063E+04
LAMBDA	0.3390E+00
CONVECTIVE INERTIA RATIO	0.3749E-01
TRANSIENT INERTIA RATIO	0.1457E+01
LOCAL COMPRESS. RATIO, SS	0.2637E-02
LOCAL COMPRESS. RATIO, DYN	0.5145E-04

Figure 56. Helium-Lubricated Spiral-Groove Thrust Bearing, Design Run, No. 4701003, Ratio of Outside to Inside Diameter 2.0 (Sheet 3 of 3)

- Gas temperature ($^{\circ}\text{R}$) used in computing the viscosity.
- Bearing inside diameter (inch).
- Ambient pressure (psia).
- Thrust-runner swash angle, peak-to-peak (deg).
- Weight density of the bearing material ($\text{lb}/\text{in.}^3$) used in calculating the moment of inertia for tilt frequency output.
- Shaft weight (pound) used in computing axial frequency output.
- Groove-length/bearing-width ratio (nondimensional) measured radially.
- Groove/ridge-width ratio (nondimensional) measured at constant radius.
- Groove angle (deg) measured between tangent-to-groove and radial coordinates.
- Coefficient of thermal expansion for bearing material ($\text{in.}/\text{in.}^{\circ}\text{F}$) used to compute dishing due to bearing film shear heating.
- Coefficient of thermal expansion for thrust-runner material ($\text{in.}/\text{in.}^{\circ}\text{F}$) used to compute dishing due to bearing film shear heating.
- Minimum allowable ridge width (inch) and minimum thickness of ridge used to compute maximum bearing number.
- Clearance at which load capacity is to be optimized (inch).

The output consists of a group of overall performance factors which include the following:

- Mach number (nondimensional), based on helium and the thrust bearing outside diameter, used to indicate the potential of compressibility effects at the tip of the thrust bearing.
- Viscosity ($\text{lb-sec}/\text{in.}^2$), based on appropriate gas at input temperature.
- Molecular mean-free path (inch), based on the appropriate gas used to compute the effective viscosity.
- Minimum number of grooves, computed on the basis that the pressure ripple across the grooves is 10 percent of the pressure rise along the grooves and related to the assumption that the edge correction is negligible.
- Maximum number of grooves, which manufacturing and structural considerations have based on an input quantity that limits the ridge wall thickness.
- Estimated moment of inertia of the bearing, with respect to a diameter, through the midplane ($\text{in.}^2\text{-lb-sec}^2$).

- Assumed thickness of the thrust disk, based on dividing the annular width of the thrust disk by 2.5.
- Bearing outside diameter obtained from the inside diameter and the ratio of outside diameter to inside diameter.
- Groove depth (inch).
- Thrust-runner tip speed (ft/sec).

Individual performance items are then tabulated in 16 columns, for one thrust face only, with a heading for the land film clearance in microinches:

- Load capacity (lb), including the 0.75 safety factor referred to above.
- Power loss (watts).
- Relative swash amplitude (nondimensional). This is the ratio of calculated swash amplitude to the maximum swash amplitude at contact. The calculated swash amplitude is based on the swash angle, the film tilt stiffness and the moment of inertia of the bearing, calculated on the basis of an assumed thickness-to-diameter ratio.
- Maximum distortion-to-clearance ratio (nondimensional). Distortion is due to bearing viscous shear heating and is assumed to flow axially, causing the thrust disk to take the shape of a cap of a sphere.
- Axial frequency (cycles/minute), which is natural frequency based on the axial film stiffness and weight of the rotor.
- Tilt frequency (cycles/minute), or natural frequency based on the film tilt stiffness and bearing moment of inertia.
- Axial stiffness (lb/in.), again including the 0.75 safety factor.
- Tilt stiffness of the gas film (lb/rad).
- Effective viscosity (lb-sec/in.²). This quantity is used in calculating bearing performance and is based on the film thickness, viscosity, and molecular mean-free path. The mean-free path effect reduces the viscosity and therefore the load capacity, becoming more pronounced as the film thickness decreases.
- Reynolds number (nondimensional). This is the ratio of inertia to viscous forces, indicating whether the assumption of laminar flow used in the present analysis is valid. The value should be less than 1500.
- Convective inertia ratio (nondimensional). This is based on the groove width and tangential velocity, indicating whether the assumption of negligible inertia effect is valid. The ratio should be very much less than one.

- Transient inertia ratio (nondimensional), based on the nominal bearing gap and axial oscillation, indicating whether the assumption of negligible inertia effect is valid. The ratio should be very much less than one.
- Local compressibility ratio, steady-state (nondimensional) based on the tangential velocity, indicating whether the assumption of quasi incompressibility is valid. In this analysis, a sectionally linear pressure profile is assumed. To be valid, the magnitude of the circumferential pressure fluctuation must be small compared to the local pressure level. This ratio should be very much less than one.
- Local compressibility ratio, dynamic (nondimensional), based on axial oscillation and referring to the assumption defined above. This ratio should be very much less than one.

Figure 57 shows the corresponding design computer run for a single thrust bearing face at the maximum speed conditions of 200,000 rpm and 585° R.

STURIN 09:45ST 03/27/73

```

100 1
200 4791004
300 .000311 200000. 0.287 585.0 17.22 0.003
400 0.289 0.13 1.93 71.2 .010 9.4E-6
500 9.4E-6 0.00265 2.0 0.0
600 1 100 25
    
```

READY
OLD STBSUCU

READY
RUN

STBSUCU 09:45ST 03/27/73

HELIUM LUBRICATED SPIRAL GROOVE THRUST BEARING

RATIO OF OD TO ID = 2.0000

INPUT

DESIGN RUN NUMBER 4791004

SPEED, RPM	0.2000E+06	GROOVE LT/RIG WIDTH	0.7700E+00
TEMPERATURE, DEG. F	0.5850E+03	GROOVE RIDGE WIDTH	0.1930E+01
BEARING ID, IN.	0.2870E+00	GROOVE ANGLE, DEG	0.7120E+02
AMBIENT PRESS., PSIA	0.1722E+02	EXP COEFF. RHO, IN/IN F	0.9400E-05
SWASH ANGLE, DEG	0.1000E-02	EXP COEFF. RUN, IN/IN F	0.9400E-05
WT DRG RIG MAT, LB/IN ³	0.2890E+00	MIN ALLOW. RIDGE h, IN	0.1000E-01
SHAFT WEIGHT, LB	0.5265E-01	CLEAR AT OPT ORV. D, IN	0.3110E-03

Figure 57. Helium-Lubricated Spiral-Groove Thrust Bearing, Design Run No. 4791004. Ratio of Outside to Inside Diameter 2.0 (Sheet 1 of 3)

OUTPUT

NACH NO. AT NO	0.1336E+00	MIN. NO. GROOVES	28
GIMBAL MTD RRG TK. IN	0.6250E-01	VISCOSITY, LR-SEC/IN ²	0.3066E-08
MAX NO. OF GROOVES	39	BEARING OD, IN.	0.5740E+00
MOLECULAR MFP, IN.	0.7500E-05	RRG. INER. IN-LR-SEC ²	0.2367E-06
GROOVE DEPTH, IN.	0.9486E-03	TIP SPEED, FT/SEC	0.5009E+03
CLEARANCE, MICROINCHES	100	125	150
LOAD, LR	0.1209E+01	0.1142E+01	0.1043E+01
POWER, WATTS	0.5255E+01	0.4571E+01	0.4057E+01
RELATIVE SWASH AMPLITUDE	0.2423E+00	0.3788E-01	0.5750E-01
MAX DISTORTION TO CLEAR RAT.	0.8779E-01	0.6001E-01	0.4766E-01
AXIAL FREQUENCY, CPM	0.3048E+05	0.4527E+05	0.5109E+05
TILT FREQUENCY, CPM	0.1114E+06	0.1654E+06	0.1867E+06
AXIAL STIFFNESS LR/IN	0.1390E+04	0.3066E+04	0.3905E+04
TILT STIFFNESS IN-LR/RAD	0.3220E+02	0.7102E+02	0.9046E+02
EFFECT. VIS. LR-SEC/IN**2	0.2088E-09	0.2231E-09	0.2337E-08
REYNOLDS NO.	0.3337E+01	0.4172E+01	0.5006E+01
LAMBDA	0.9214E+02	0.5897E+02	0.4095E+02
CONVECTIVE INERTIA RATIO	0.2972E-04	0.4644E-04	0.6688E-04
TRANSIENT INERTIA RATIO	0.1949E-01	0.3034E-01	0.3585E-01
LOCAL COMPRESS. RATIO, SS	0.7150E+00	0.4576E+00	0.3178E+00
LOCAL COMPRESS. RATIO, DYN	0.2445E-01	0.2324E-01	0.1822E-01
CLEARANCE, MICROINCHES	175	200	225
LOAD, LR	0.9309E+00	0.8174E+00	0.7099E+00
POWER, WATTS	0.3657E+01	0.3335E+01	0.3071E+01
RELATIVE SWASH AMPLITUDE	0.4601E-01	0.4109E-01	0.3936E-01
MAX DISTORTION TO CLEAR RAT.	0.3320E-01	0.2611E-01	0.2107E-01
AXIAL FREQUENCY, CPM	0.4288E+05	0.5234E+05	0.5042E+05
TILT FREQUENCY, CPM	0.1932E+06	0.1912E+06	0.1842E+06
AXIAL STIFFNESS LR/IN	0.4183E+04	0.4098E+04	0.3903E+04
TILT STIFFNESS IN-LR/RAD	0.5599E+02	0.5495E+02	0.5411E+02
EFFECT. VIS. LR-SEC/IN**2	0.2419E-09	0.2484E-09	0.2538E-08
REYNOLDS NO.	0.5841E+01	0.6675E+01	0.7509E+01
LAMBDA	0.3009E+02	0.2304E+02	0.1820E+02
CONVECTIVE INERTIA RATIO	0.9103E-04	0.1189E-03	0.1505E-03
TRANSIENT INERTIA RATIO	0.3881E-01	0.3015E-01	0.4038E-01
LOCAL COMPRESS. RATIO, SS	0.2335E+00	0.1787E+00	0.1412E+00
LOCAL COMPRESS. RATIO, DYN	0.1385E-01	0.1050E-01	0.7990E-02
CLEARANCE, MICROINCHES	250	275	300
LOAD, LR	0.6121E+00	0.5259E+00	0.4510E+00
POWER, WATTS	0.2850E+01	0.2601E+01	0.2499E+01
RELATIVE SWASH AMPLITUDE	0.3955E-01	0.4110E-01	0.4373E-01
MAX DISTORTION TO CLEAR RAT.	0.1737E-01	0.1466E-01	0.1239E-01
AXIAL FREQUENCY, CPM	0.4772E+05	0.4463E+05	0.4143E+05
TILT FREQUENCY, CPM	0.1743E+06	0.1631E+06	0.1514E+06
AXIAL STIFFNESS LR/IN	0.3405E+04	0.2980E+04	0.2567E+04
TILT STIFFNESS IN-LR/RAD	0.7991E+02	0.5983E+02	0.5947E+02
EFFECT. VIS. LR-SEC/IN**2	0.2592E-09	0.2620E-09	0.2652E-08
REYNOLDS NO.	0.8744E+01	0.9178E+01	0.1001E+02
LAMBDA	0.1474E+02	0.1218E+02	0.1024E+02
CONVECTIVE INERTIA RATIO	0.1859E-03	0.2238E-03	0.2675E-03
TRANSIENT INERTIA RATIO	0.3986E-01	0.3205E-01	0.3755E-01
LOCAL COMPRESS. RATIO, SS	0.1143E+00	0.9458E-01	0.7944E-01
LOCAL COMPRESS. RATIO, DYN	0.6125E-02	0.4774E-02	0.3693E-02

Figure 57. Helium-Lubricated Spiral-Groove Thrust Bearing - Design Run
No. 4791004. Ratio of Outside to Inside Diameter 2.0 (Sheet 2 of 3)

CLEARANCE, MICROINCHES	325	350	375
LOAD, LB	0.3870E+00	0.1325E+00	0.2864E+00
POWER, WATTS	0.2357E+01	0.2232E+01	0.2121E+01
RELATIVE SWASH AMPLITUDE	0.4731E-01	0.5177E-01	0.5709E-01
MAX DISTORTION TO CLEAR RAT.	0.1067E-01	0.9280E-02	0.8148E-02
AXIAL FREQUENCY, CPM	0.3827E+05	0.3525E+05	0.3243E+05
TILT FREQUENCY, CPM	0.1308E+06	0.1288E+06	0.1185E+06
AXIAL STIFFNESS LB/IN	0.2191E+04	0.1859E+04	0.1573E+04
TILT STIFFNESS IN-LB/RAD	0.5075E+02	0.4306E+02	0.3644E+02
EFFECT, VIS. LB-SEC/IN**2	0.2680E-03	0.2704E-03	0.2726E-03
REYNOLDS NO.	0.1085E+02	0.1168E+02	0.1252E+02
LAMBDA	0.8724E+01	0.7522E+01	0.6522E+01
CONVECTIVE INERTIA RATIO	0.3140E-03	0.3641E-03	0.4180E-03
TRANSIENT INERTIA RATIO	0.3609E-01	0.3454E-01	0.3309E-01
LOCAL COMPRESS. RATIO, SS	0.6769E-01	0.5836E-01	0.5084E-01
LOCAL COMPRESS. RATIO, DYN	0.2906E-02	0.2708E-02	0.1850E-02
CLEARANCE, MICROINCHES	400	425	450
LOAD, LB	0.2474E+00	0.2144E+00	0.1864E+00
POWER, WATTS	0.2022E+01	0.1933E+01	0.1852E+01
RELATIVE SWASH AMPLITUDE	0.6328E-01	0.7036E-01	0.7836E-01
MAX DISTORTION TO CLEAR RAT.	0.7211E-02	0.6427E-02	0.5765E-02
AXIAL FREQUENCY, CPM	0.2982E+05	0.2744E+05	0.2527E+05
TILT FREQUENCY, CPM	0.1090E+06	0.1003E+06	0.9232E+05
AXIAL STIFFNESS LB/IN	0.1331E+04	0.1126E+04	0.9522E+03
TILT STIFFNESS IN-LB/RAD	0.3032E+02	0.2609E+02	0.2113E+02
EFFECT, VIS. LB-SEC/IN**2	0.2745E-03	0.2762E-03	0.2777E-03
REYNOLDS NO.	0.1375E+02	0.1418E+02	0.1502E+02
LAMBDA	0.5759E+01	0.5101E+01	0.4550E+01
CONVECTIVE INERTIA RATIO	0.4756E-03	0.5369E-03	0.6019E-03
TRANSIENT INERTIA RATIO	0.3154E-01	0.3010E-01	0.2874E-01
LOCAL COMPRESS. RATIO, SS	0.4469E-01	0.3954E-01	0.3531E-01
LOCAL COMPRESS. RATIO, DYN	0.1495E-02	0.1219E-02	0.1001E-02
CLEARANCE, MICROINCHES	475		
LOAD, LB	0.1627E+00		
POWER, WATTS	0.1778E+01		
RELATIVE SWASH AMPLITUDE	0.8731E-01		
MAX DISTORTION TO CLEAR RAT.	0.5200E-02		
AXIAL FREQUENCY, CPM	0.2330E+05		
TILT FREQUENCY, CPM	0.8513E+05		
AXIAL STIFFNESS LB/IN	0.8121E+03		
TILT STIFFNESS IN-LB/RAD	0.1881E+02		
EFFECT, VIS. LB-SEC/IN**2	0.2791E-03		
REYNOLDS NO.	0.1585E+02		
LAMBDA	0.4084E+01		
CONVECTIVE INERTIA RATIO	0.6706E-03		
TRANSIENT INERTIA RATIO	0.2745E-01		
LOCAL COMPRESS. RATIO, SS	0.3169E-01		
LOCAL COMPRESS. RATIO, DYN	0.8284E-03		

Figure 57. Helium-Lubricated Spiral-Groove Thrust Bearing, Design Run No. 4791004. Ratio of Outside to Inside Diameter 2.0 (Sheet 3 of 3)

With an 800-microinch total clearance for the two thrust faces, a combined thrust bearing performance run is shown in Figure 58 for the 948-microinch groove depth. The various performance factors, such as load, power, axial stiffness, and tilt stiffness, are shown as a function of the

HELIUM-LUBRICATED SPIRAL GROOVE THRUST BEARING

Ratio of Outside to Inside Diameter = 2.00

Run No. 4

APPROXIMATE WEIGHT BY WEIGHT LENGTHS WIDTH 3.7300E 03
 LEAD, IN 0.7520E 02 GROOVE/PIECE -18TH 0.1930E 01
 AXIAL STIFFNESS LB/IN 0.1720E 02 GROOVE ANGLE, DEG 0.3120E 02
 TAPER, IN/IN 0.3740E 03 INITIAL CLEAR, IN 6.2500E-04
 CLEARANCE, IN 0.2070E 03 TOTAL AXIAL CLEAR, IN 0.8000E-03
 CLEARANCE, IN 0.3100E-03

PARAMETER	UNIT	VALUE	UNIT	VALUE	UNIT	VALUE
LEAD, IN		0.7520E 02		0.1895E 00		6.1005E 00
AXIAL STIFFNESS LB/IN		0.1720E 02		0.2013E 00		0.2113E 00
TAPER, IN/IN		0.3740E 03		0.4362E 03		0.4534E 03
CLEARANCE, IN		0.2070E 03		0.1018E 02		0.1064E 02
CLEARANCE, IN		0.3100E-03		0.1018E 02		0.1064E 02

PARAMETER	UNIT	VALUE	UNIT	VALUE	UNIT	VALUE
LEAD, IN		0.7520E 02		0.1895E 00		6.1005E 00
AXIAL STIFFNESS LB/IN		0.1720E 02		0.2013E 00		0.2113E 00
TAPER, IN/IN		0.3740E 03		0.4362E 03		0.4534E 03
CLEARANCE, IN		0.2070E 03		0.1018E 02		0.1064E 02
CLEARANCE, IN		0.3100E-03		0.1018E 02		0.1064E 02

PARAMETER	UNIT	VALUE	UNIT	VALUE	UNIT	VALUE
LEAD, IN		0.7520E 02		0.1895E 00		6.1005E 00
AXIAL STIFFNESS LB/IN		0.1720E 02		0.2013E 00		0.2113E 00
TAPER, IN/IN		0.3740E 03		0.4362E 03		0.4534E 03
CLEARANCE, IN		0.2070E 03		0.1018E 02		0.1064E 02
CLEARANCE, IN		0.3100E-03		0.1018E 02		0.1064E 02

Figure 58. Helium-Lubricated Spiral-Groove Thrust Bearing,
 Ratio of Outside to Inside Diameter = 2.00
 Design Run No. 4791003

loaded side clearance of the bearing. The information for the computer programs is shown graphically in Figures 59, 60, and 61 for the three different groove-depth designs that were considered.

The designs from these bearing performance runs are compared in Table 19 for the three groove-depth designs. Shown in this table are the significant performance factors for 1-g, 2-g, and 0-g operation. It can be seen that the largest groove depth, of 1220 microinches, is not satisfactory to meet the criteria

Table 19
THRUST BEARING DESIGN COMPARISON

Speed (rpm)	90,000		
Temperature (°R/°K)	22.5/14.0		
Viscosity of helium (lb-sec/in. ²)	9.1×10^{-10}		
Ambient pressure (psia)	17.22		
Rotor weight (pound)	0.0507		
Design groove depth (μin.)	Computer Run Numbers		
	4791001	4791002	4791003
1220	610	948	
<u>1-g Operation</u>			
Load (pound)	0.0507	0.0507	0.0507
Power loss, both faces (watt)	0.170	0.145	0.150
Land clearance (μin.)	170	240	210
Axial stiffness (lb/in.)	230.0	45.0	36.0
Tilt stiffness (in.-lb/rad)	5.8	10.0	8.4
<u>2-g Operation</u>			
Load (pound)	0.1014	0.1014	0.1014
Power loss, both faces (watt)	--	0.200	0.235
Land clearance (μin.)	below 100	140	100
Axial stiffness (lb/in.)	--	118	45.0
Tilt stiffness (in.-lb/rad)	--	34.0	10.5
<u>0-g Operation</u>			
Load (pound)	0.0	0.0	0.0
Power loss, both faces (watt)	0.1153	0.1282	0.1196
Land clearance (μin.)	400	400	400
Axial stiffness (lb/in.)	183.4	183.0	183.2
Tilt stiffness (in.-lb/rad)	3.70	3.77	4.24

CR-2290

Speed - 80,000 rpm
 Temperature - 25.2° R
 Dwg. No. 423D435
 Design Run No. 4791001

Ambient pressure - 17.20 psia
 Outside diameter - 0.574 in.
 Inside diameter - 0.287 in.
 Total axial clearance - 0.8 mil

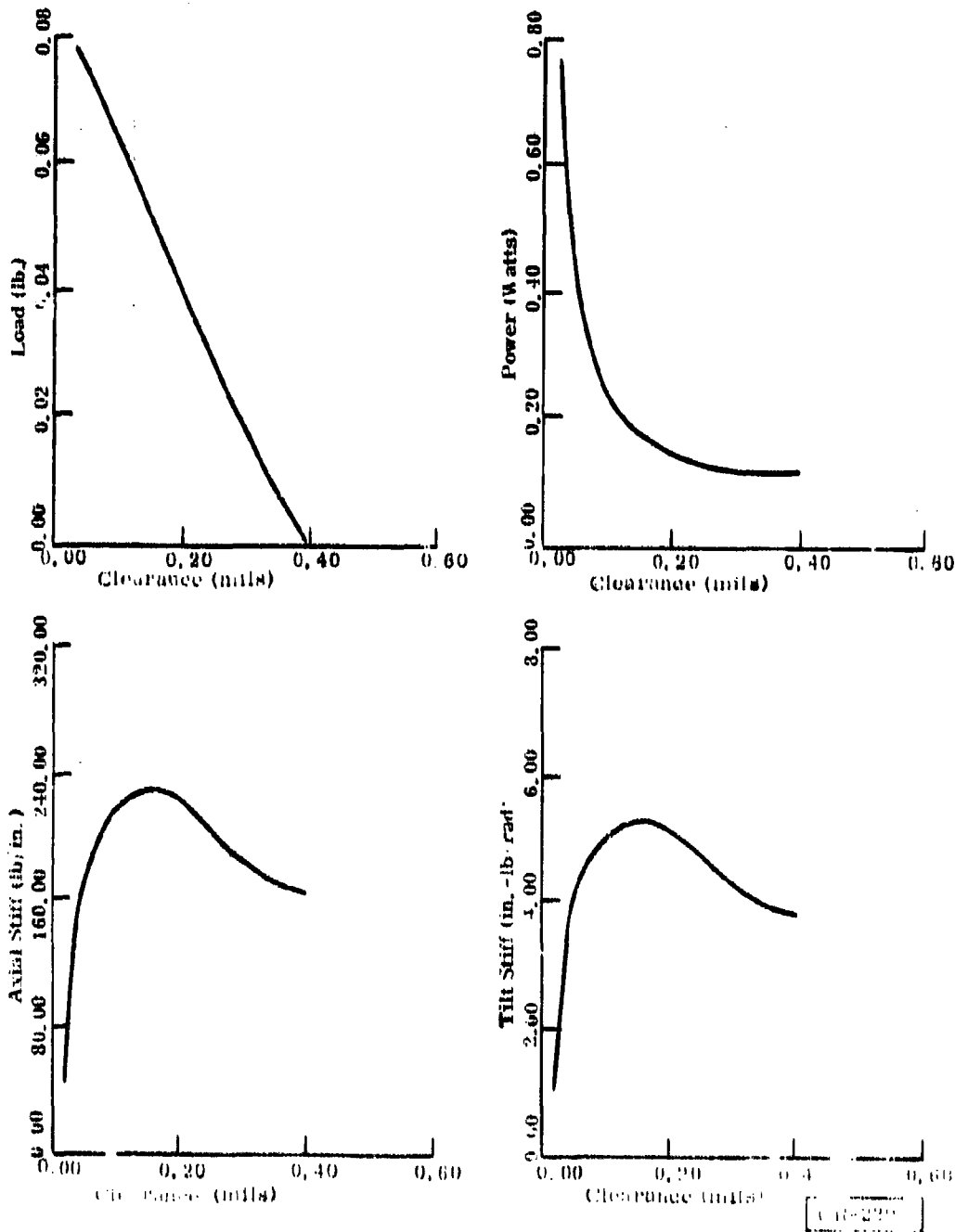


Figure 50. Helium-Lubricated, Spiral-Groove Thrust Bearing, 1220-Microlinch Groove Depth, Performance as a Function of Loaded Side Clearance

Speed = 90,000 rpm
 Temperature = 25.2°R
 Dwg. No. 423D435
 Design Run No. 4791002

Ambient pressure = 17.220 psia
 Outside diameter = 0.574 in.
 Inside diameter = 0.287 in.
 Total axial clearance = 0.8 mil

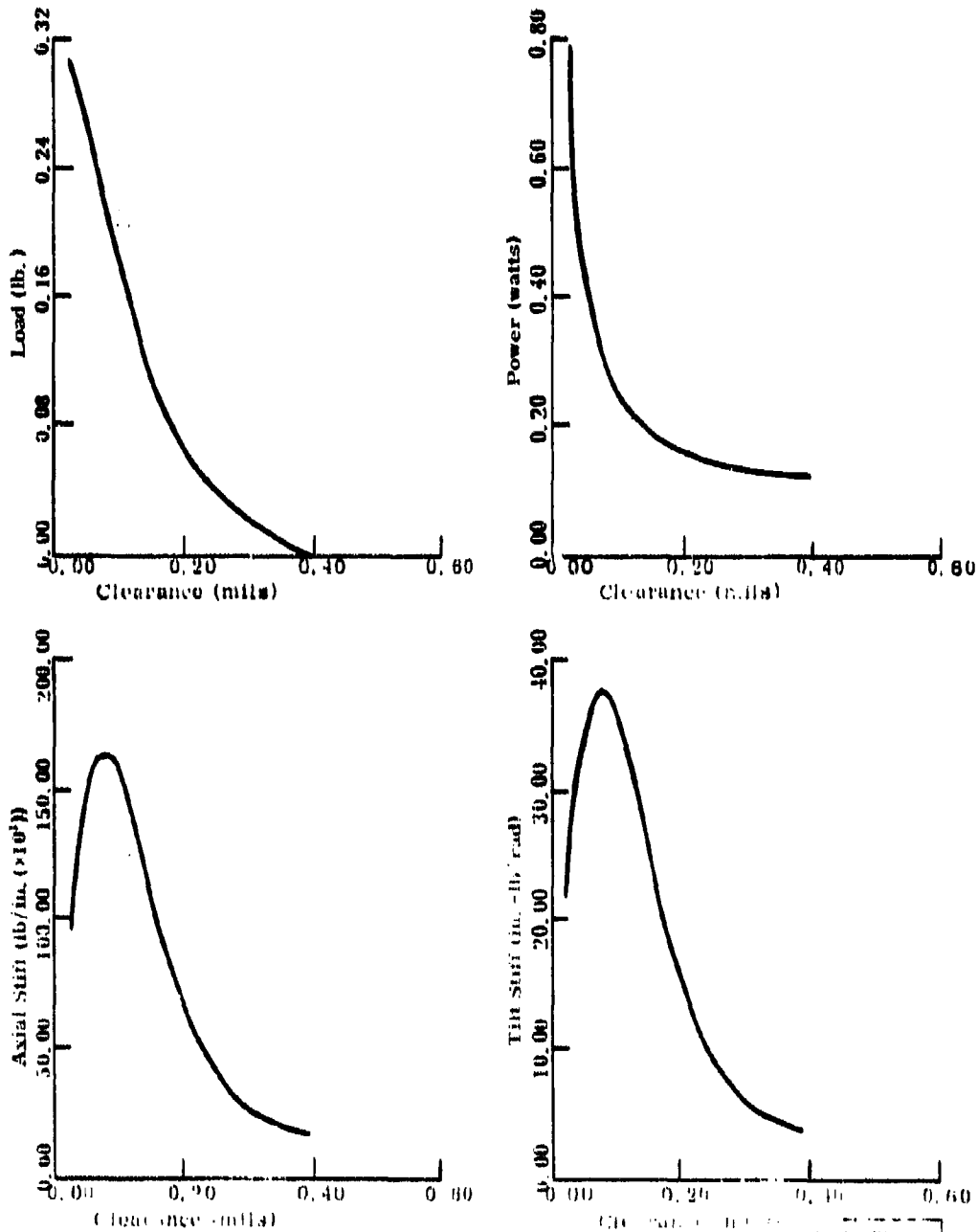


Figure 80. Helium-Lubricated, Spiral-Groove Thrust Bearing, 610-Microinch Groove Depth, Performance as a Function of Loaded Side Clearance

Speed = 90,000 rpm
 Temperature = 25.2°R
 Dwg. No: 423D435
 Design Run No. 4791003

Ambient pressure = 17.220 psia
 Outside diameter = 0.574 in
 Inside diameter = 0.287 in
 Total axial clearance = 0.8 mil

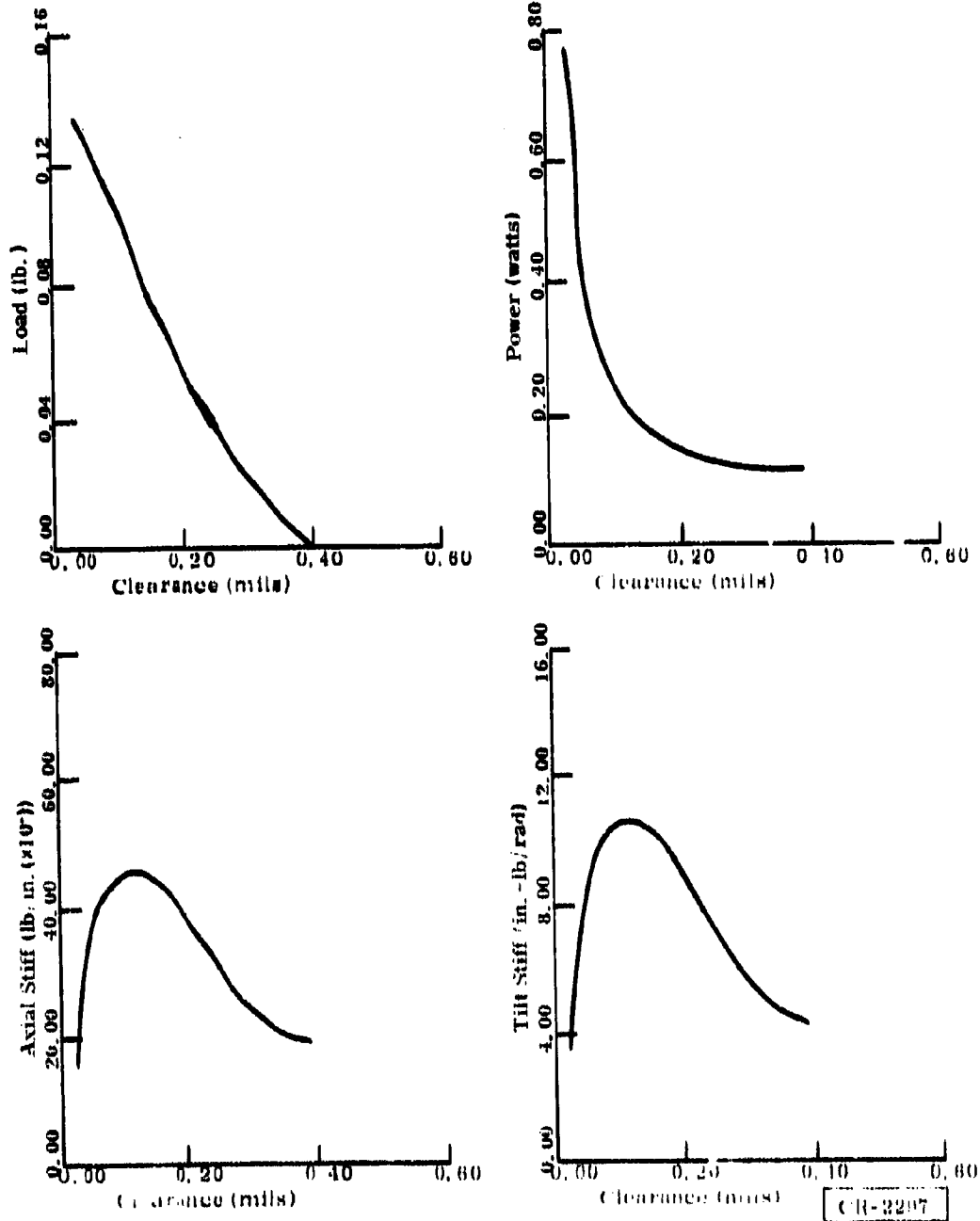


Figure 61. Helium-Lubricated, Spiral-Groove Thrust Bearing, 948-Microinch Groove Depth, Low-Temperature Performance as a Function of Loaded Side Clearance

of a minimum thickness of 100 at the 2-g operating condition. The other two designs are satisfactory, and there is little difference between them as far as the performance features are concerned. However, the design with a groove depth of 610 microinches should be considered a very limited design since the tolerance on maintaining this type of groove depth is more serious than maintaining a groove-depth tolerance around the larger, 948-microinch, clearance. It can be concluded that the existing thrust bearing design drawing, 423D435, will adequately suit the turboalternator thrust bearing design. Table 20 shows the complete geometry of the thrust bearing design.

Table 20
TURBOALTERNATOR SPIRAL-GROOVE THRUST
BEARING DESIGN SUMMARY

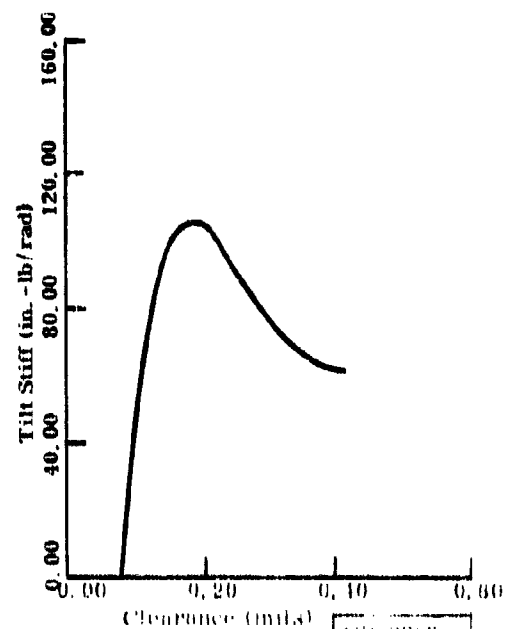
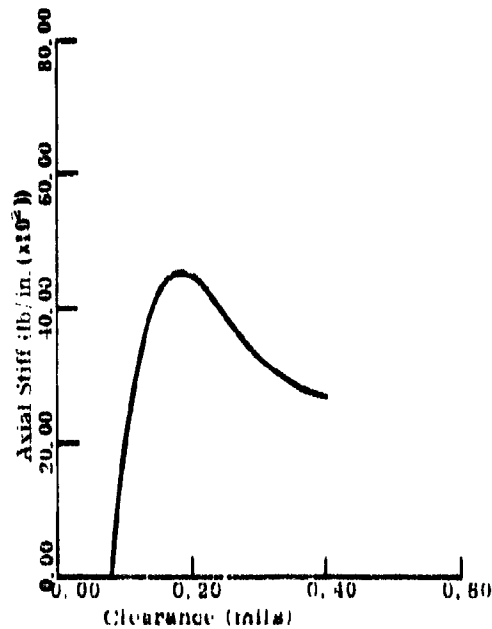
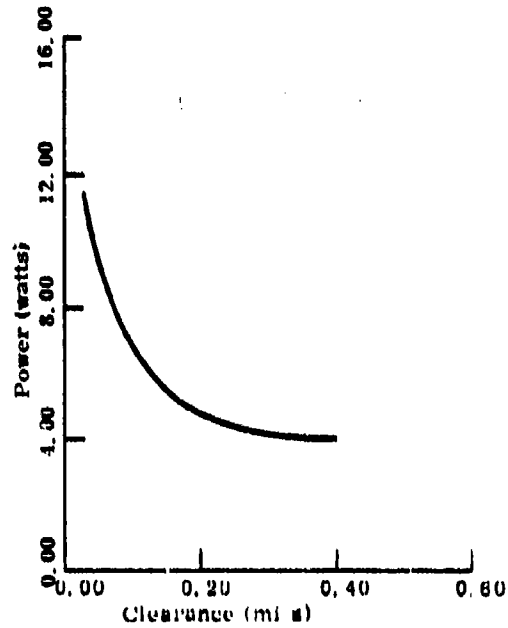
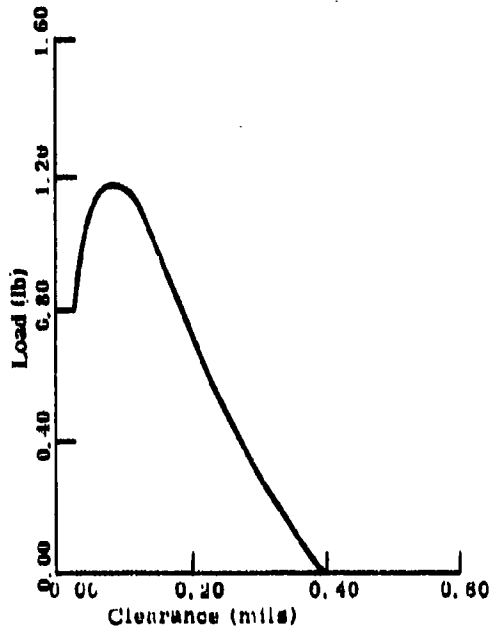
Characteristic	Design Parameter
Outside diameter (inch)	0.574
Inside diameter (inch)	0.287
Inside diameter, grooved region (inch)	0.364
Number of grooves	15
Groove angle (deg)	71.2
Groove width to ridge width at constant radius (nd)	1.93
Groove width (deg)	15.809
Ridge width (deg)	8.191
Depth of groove (inch)	0.000948
Collar swash angle (deg)	0.003
Total axial clearance (inch)	0.0008
Bearing material, coating, and surface finish (rms)	Beryllium copper, none, 8
Collar material, coating, and surface finish (rms)	304L, NITRIDE, 4

CR-2289

Figure 62 shows the performance to be expected for the high-speed operation of 200,000 rpm and 585°R under the maximum-speed and maximum-temperature operating conditions.

Speed = 200,000 rpm
 Temperature 585.0°R
 Dwg. No. 423D435
 Design Run No. 4791004

Ambient pressure = 17.220 psia
 Outside diameter = 0.574 in.
 Inside diameter = 0.287 in.
 Total axial clearance = 0.8 mil



CP 2208

Figure 62. Helium-Lubricated, Spiral-Groove Thrust Bearing, 048-Microinch Groove Depth, Room-Temperature Performance as a Function of Loaded Side Clearance

Appendix III

TURBOALTERNATOR ASSEMBLY PROCEDURES

This manual provides detailed assembly and disassembly procedures for the turboalternator development by General Electric Corporate Research and Development in Schenectady, New York, under Contract No. DAAK02-71-C-0026. All instructions and procedures described are based on techniques that were successfully employed by Corporate Research and Development during the course of the development program.

Special assembly tools are shown in Figure 63. All part numbers refer to turboalternator assembly drawing 588E477 as shown in Figure 19 and to the photograph of parts in Figure 64, unless otherwise specified.

PRELIMINARY CLEANING AND HANDLING

1. After manufacturing, inspect all parts under a microscope to ensure complete deburring and satisfactory surface finishes on all critical areas.
2. Ultrasonically clean the electric stator in a solution of Freon* and vacuum-bake at 120°F for 8 hours. Install a liquid nitrogen cold trap in the vacuum line between the vacuum pump and the furnace, to prevent oil migration. Ultrasonically clean all other parts several times in clean solutions of chloroethene to ensure removal of oil and grease films and any particles clinging to the surfaces.

CLEAN ROOM ASSEMBLY

1. Perform all final cleaning operations, assembly procedures, and initial testing in a clean room to ensure maximum cleanliness of the complete assembly.
2. Prior to entering the clean room, ultrasonically clean all parts and seal them in clean plastic. This step includes cleaning and sealing of tools, fixtures, and so forth used in the assembly procedures.
3. Final-clean the turboalternator parts in a clean room area, in a solution of Freon.
4. Assemble the turboalternator inside pressurized clean benches within the clean room area. Air through the clean benches is filtered to 99.95 percent of 0.3-micron particles.

*Freon, a precision cleaning agent manufactured by E. I. DuPont de Nemours and Company, Inc.

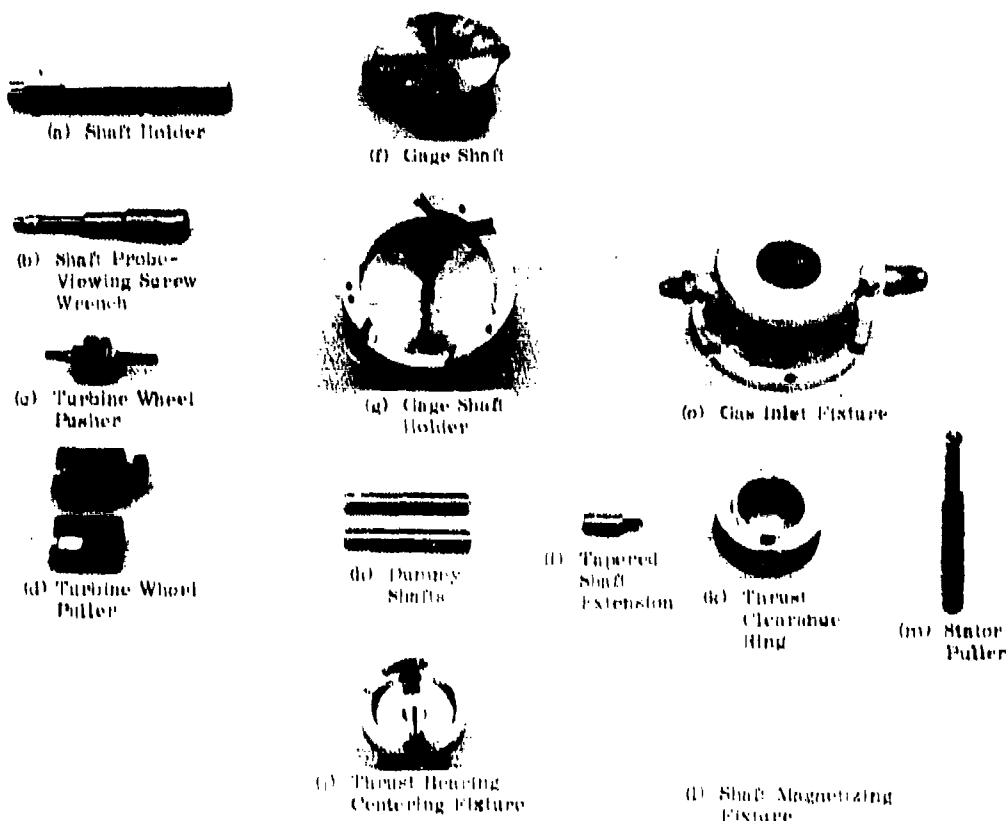


Figure 63. Turboalternator Assembly Tools and Fixtures

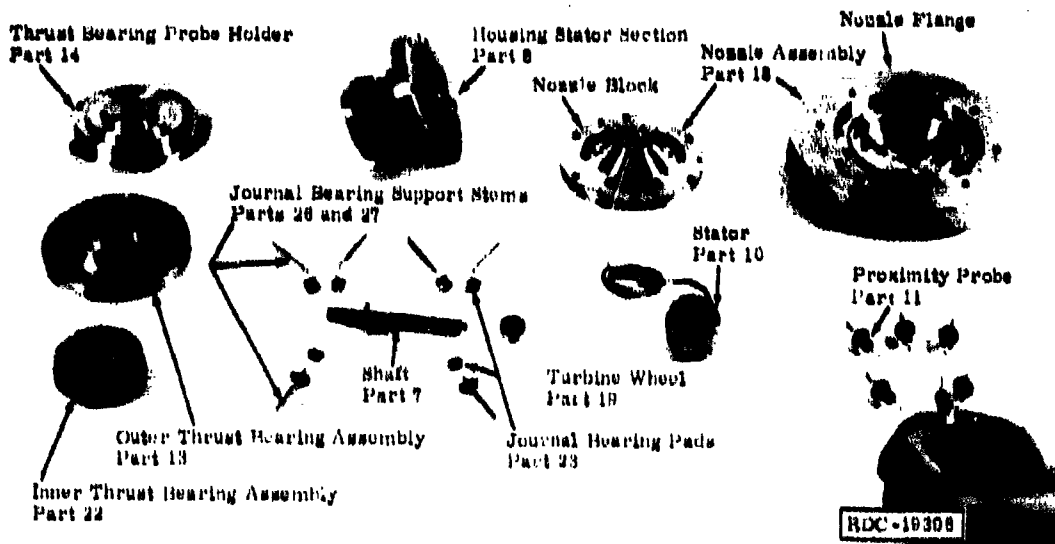


Figure 64. Turboalternator Parts

CAUTION

Handle all parts carefully during assembly to prevent damage to critical surfaces and dimensions.

CAUTION

Use no lubricants in any portion of the assembly because most lubricants are very volatile at room temperature and will cause serious contamination in the refrigerator system.

INITIAL WHEEL-TO-SHAFT ASSEMBLY

Assemble the turbine wheel (Part 19) onto the unmagnetized shaft (Part 7) as follows:

NOTE: Inspect finishes of turbine wheel bores prior to assembly to ensure that the chemical conversion coating and lubricative plating were not damaged in previous assemblies.

1. Scribe lines at each end of the shaft on the outer diameter, along the axis of the shaft and along a line on the back of the turbine wheel adjacent to the shaft, for realignment after the balancing operation.
2. Install the thrust end of the shaft in the brass shaftholder (a) and tighten the clamping screw. Place the turbine wheel (Part 19) on the opposite end of the shaft, aligning the scribed lines. Thread the wheel pusher assembly (c) into the end of the shaft, using the threads in the inside diameter of the shaft grinding center. (For details of the wheel pusher assembly, see Figure 65.) Then, after rechecking the alignment of the scribed lines, tighten the wheel pusher assembly by holding the end of the threaded rod (Part 8, Figure 65) with a wrench on the flats and tighten the nut (Part 11, Figure 65), forcing the turbine wheel onto the shaft.

Normally, a torque on the order of 1.0 in. -lb is required to push the 0.5-inch-diameter aluminum turbine wheel onto the shaft with 0.0004-inch interference, wheel-to-shaft fit. A sudden increase in the torque value indicates the turbine wheel has been pushed completely onto the shaft and the stop on the inside diameter of the turbine wheel is touching the end of the shaft.

3. Remove the wheel pusher assembly from the shaft and insert the special hexhead cap screw (Part 32) in the threaded shaft center. This hexhead cap screw, with the top ground flat, is used for the viewing surface of the thrust proximity probe during final assembly and testing. Using the socket wrench (b), torque the hexhead cap screw to 5.5 in. -lb by holding the shaft holder at the opposite end of the shaft.

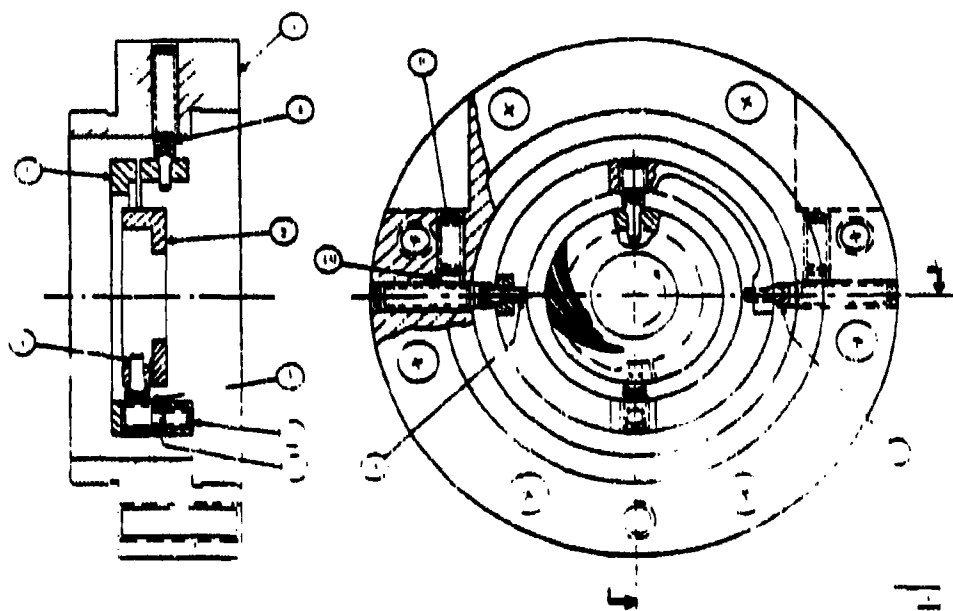


Figure 87. Turboalternator Inner Thrust Bearing Assembly

assembled, accurately center the gimbal ring and thrust bearing and adjust the tipping force of the gimbals.

4. Center the gimbal by using a No. 48 drill, 0.076 inch in diameter, to measure the spacing between the gimbal ring and the mounting flange. Adjust the pivot screws accordingly.
5. Use a No. 54 drill, 0.055 inch in diameter, as a guide to adjust the spacing for centering the thrust bearing in the gimbal.
6. Position the inner thrust bearing assembly on its test fixture (j). When the thrust bearing is properly centered, the assembly will slip easily onto the fixture.
7. Adjust the thrust bearing pivot screws and the gimbal pivot screws until a 1.5- to 2.0-g breakaway force is measured on a force gage when pressed against the outer edge of the gimbal ring and the thrust bearing at the midpoint between pivots. Then lock the pivot screws in position by tightening the locking set screws (Parts 8 and 9).
8. Recheck the centering of the thrust bearing on the test fixture (j) after adjusting the correct tipping force.

NOTE: The gimbal rings and thrust bearings are designed with a spring at the pivot sections to maintain the tipping force over a wide range of temperatures.

OUTER THRUST BEARING ASSEMBLY (PART 13)

The same procedures are followed in the assembly of the outer thrust bearing, as outlined above, for the inner thrust bearing. Test fixture j, used to center the thrust bearing, is designed to accept both thrust bearings. For details of this assembly see Figure 68.

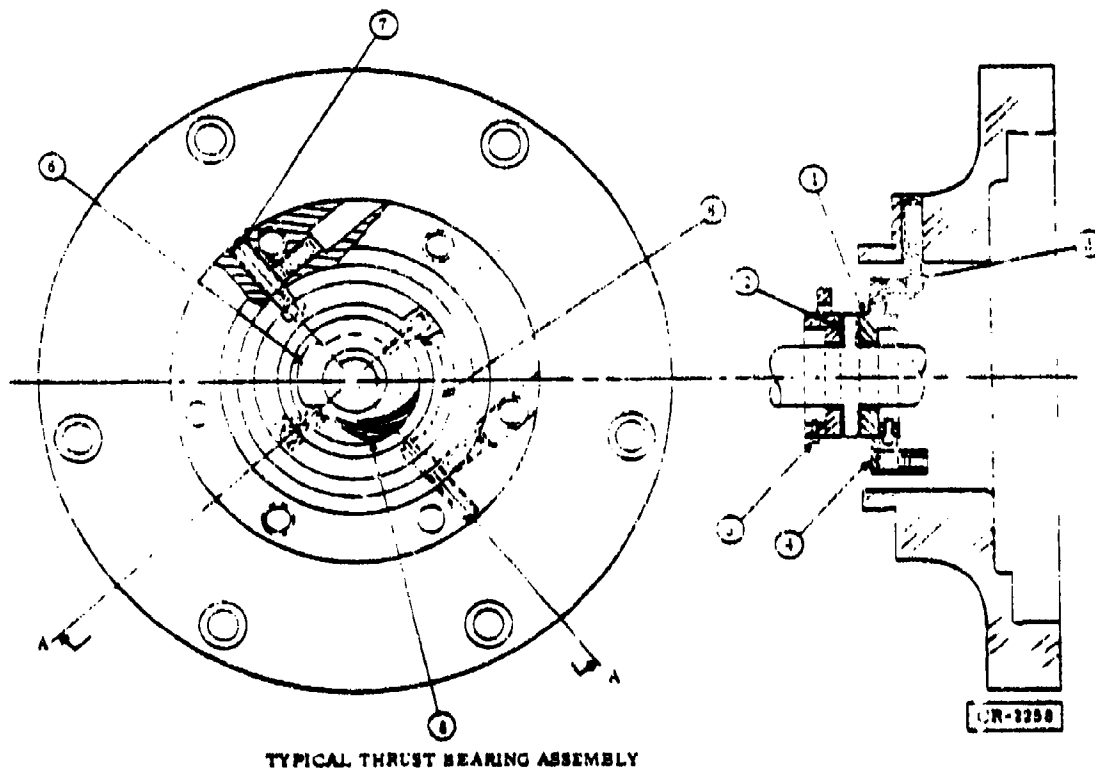


Figure 68. Turboalternator Outer Thrust Bearing Assembly

PRELIMINARY JOURNAL BEARING ASSEMBLY
AND STATOR INSTALLATION

1. Assemble the journal bearing support clamps and stems (Parts 26 and 27) onto the housing sections (Parts 8 and 13). The spring stems in bearing stem support assemblies (Part 27) must be inserted from the inside diameter of the housing before the stem clamps are attached to the housing. The other journal bearing support stems can be inserted through the stem clamps from the outside of the housing sections.
2. Position the journal bearing stems off center to allow clearance for the installation of the gage shaft (f) into the stator section of the housing (Part 8), from the nozzle end. The nozzle-to-housing

rabnet fit dimensions on the housing are used to position the gage shaft vertically and to center the gage shaft into the housing. Assemble the gage shaft holder (g) to the housing nozzle flange with three screws (Part 49). Then gradually tighten the centering screw in the gage shaft holder to position the gage shaft securely into the housing.

3. Assemble the three journal bearing pads (Part 23) into the housing. Check the pad orientation before assembly (Figure 69). Hold the two solid stems in the assemblies (Part 28) firmly, so the pads are against the gage shaft and tighten the stem clamps securely. Position the spring stem assembly (Part 27) so the pad is held gently against the gage shaft, without applying pressure from the spring. Tighten the spring stem clamp securely.

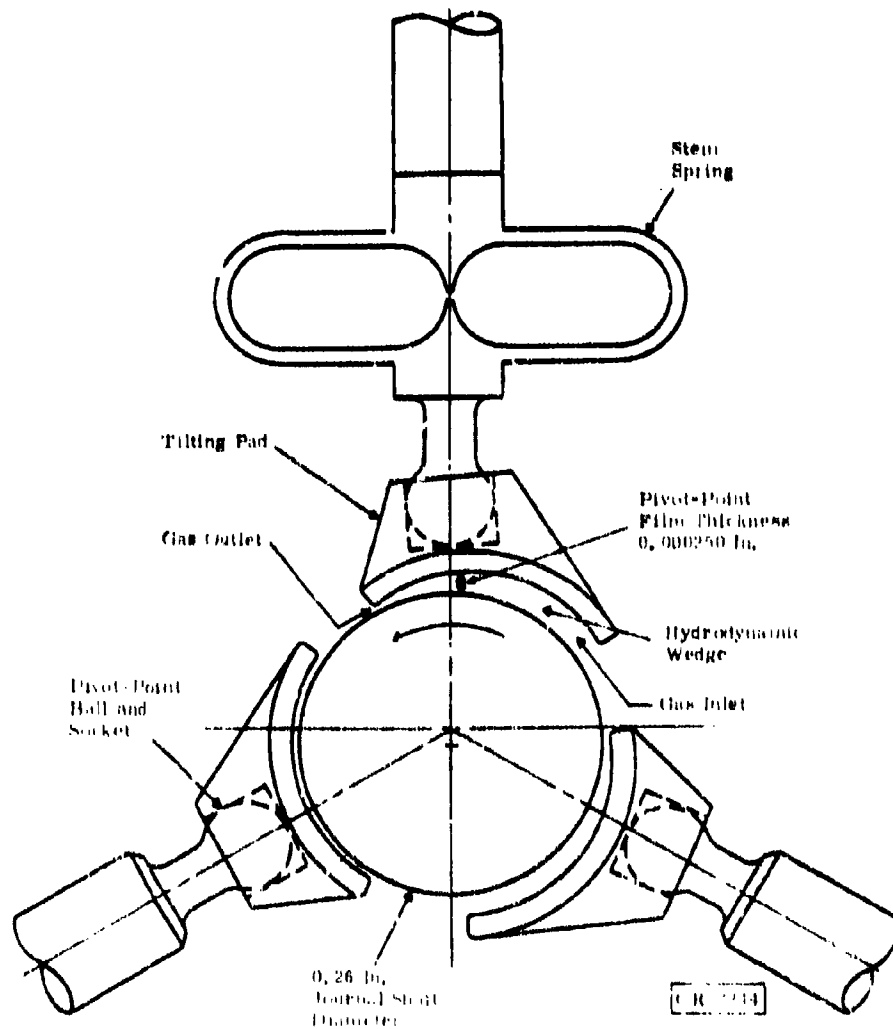


Figure 69. Cryogenic Turboalternator Tilting-Pad Journal Bearing, Viewing Shaft from Thrust End

4. Remove the gage shaft holder and gently tap on the end of the gage shaft with the back end of the brass shaft holder (c) to loosen the gage shaft from the housing. Do not allow the gage shaft to drop out of the housing. Insert a dummy shaft (h) through the housing and gently push the gage shaft out as the dummy shaft is inserted. The ends of the shafts must be held together during this operation to prevent the pads from dropping off. Tape the dummy shaft to the housing so it will not drop out.
5. To install the stator (Part 10), the stator leads must first be fed through the housing and out through the hole in the housing wall. Orient the stator above the housing so the leads can be drawn through as the stator is inserted into the housing. Press on the stator shell to be certain that the stator is bottomed in the housing. Then tighten the set screw (Part 46), to secure the stator in position.
6. Assemble the journal bearing pads in the outer thrust sections of the housing (Part 13) in a manner similar to that described above; however, it is necessary to temporarily remove the thrust bearing and gimbal assembly from this section of the housing by loosening one of the pivot screws in the housing section. Insert the same gage shaft (f) from the thrust bearing probe holder end (Part 14) using the housing rabbet fit dimension again to center the gage shaft. Mount the gage shaft holder to the outer thrust bearing flange and tighten the centering screw in the holder, to position the gage shaft. Install the pads and stems as outlined previously, using the same procedures to remove the gage shaft and install the dummy shaft (h). Then reinstall the thrust bearing and gimbal assembly over the dummy shaft. Readjust the pivot screw previously loosened, to give the 1.5- to 2.0-g tipping force and the pivot locking screw reset. Partially remove the dummy shaft from the assembly, but position it to hold the journal bearing pads in place and allow retesting of the centering of the thrust bearing with the bearing test fixture (j).

SHAFT HOUSING ASSEMBLY

1. After completion of the rotating assembly balancing operation, install the brass shaft holder (a) onto the thrust end of the shaft and tighten the clamping screw. Hold the shaft securely by the shaft holder and remove the probe viewing screw (Part 32) from the shaft, using the socket wrench (b). Remove the shaft holding fixture from the shaft.
2. Remove the 0.5-inch-diameter turbine wheel from the shaft, using wheel puller (d). Disassemble the halves of the wheel puller assembly (Parts 1 and 2 of Figure 70) and reassemble them around the turbine wheel, as shown in Figure 70. Hold assembled Parts 1 and 2 of the wheel puller (d) with a wrench on the flats, as the pulling force is applied by tightening the screw, Part 7 of Figure 70. Normally, a torque of 3 to 4 in.-lb is required to remove the wheel.

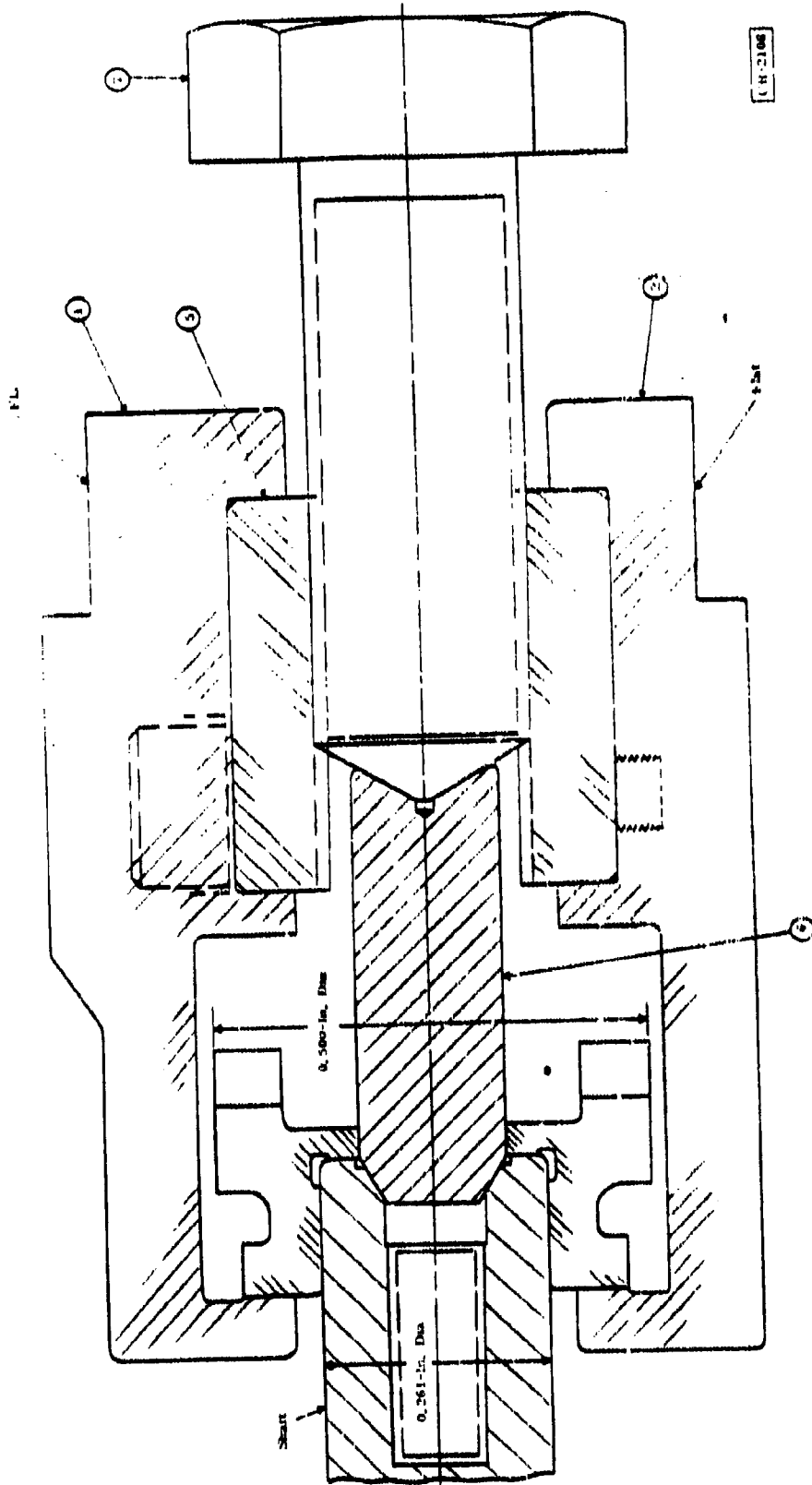


Figure 70. First-Stage Wheel Puller (dj)

3. Place the preassembled, inner thrust bearing assembly (Part 22) onto the previously assembled housing section (Part 8) with the journal bearings and stator installed.
4. Thread the tapered shaft extension (l) into the end of the shaft at the turbine end. Insert the tapered extension and shaft through the inner thrust bearing assembly. Position the end of the shaft extension against the end of the dummy shaft and gently remove the dummy shaft as the shaft is installed. Keep the two shaft ends together so the journal bearing pads do not drop off the stems.
5. Remove the tapered shaft extension and, using wheel pusher c, install the 0.5-inch-diameter turbine wheel and probe viewing screw (Part 32). * After completing the above assembly, remove the shaft holding fixture (a).

NOZZLE ASSEMBLIES

Preassemble the nozzle assembly (Part 18) on the bench. Do not assemble the gas inlet and discharge cylinder (Part 15) at this time. Ensure that the c-seals are centered in the seal grooves before the inner and outer nozzle sections are assembled. Orient the offset mounting holes in the nozzle sections for correct alignment during assembly. Torque the six No. 4-40 0.5-inch-long assembly screws to 5.5 in.-lb, to ensure a metal-to-metal seal at the inner section adjacent to the nozzle channels.

PRELIMINARY THRUST BEARING SHIMMING

Depth micrometers are used to measure the shaft position to obtain the axial shim requirements (Figure 71). Table 21 lists the clearance specifications and the required depth micrometer measurements and calculations to determine the thickness of the shims. The following procedures are used:

1. Place the partially assembled turboalternator in a vertical position, thrust end up, on a stand with a cutout to clear the turbine wheel. Press down on the inner thrust bearing mounting flange to be certain it is fully seated onto the housing.

NOTE: Threaded holes have been provided in the outer flanges of the thrust bearing assemblies (Parts 13 and 22) for jack-out screws, if required.

2. Position the thrust clearance ring (k) onto the inner thrust bearing mounting flange (Figure 72). Measure and record Distance A from the top of the thrust clearance ring to the top of the shaft thrust runner.

*Described above under "Initial Wheel-to-Shaft-Assembly."

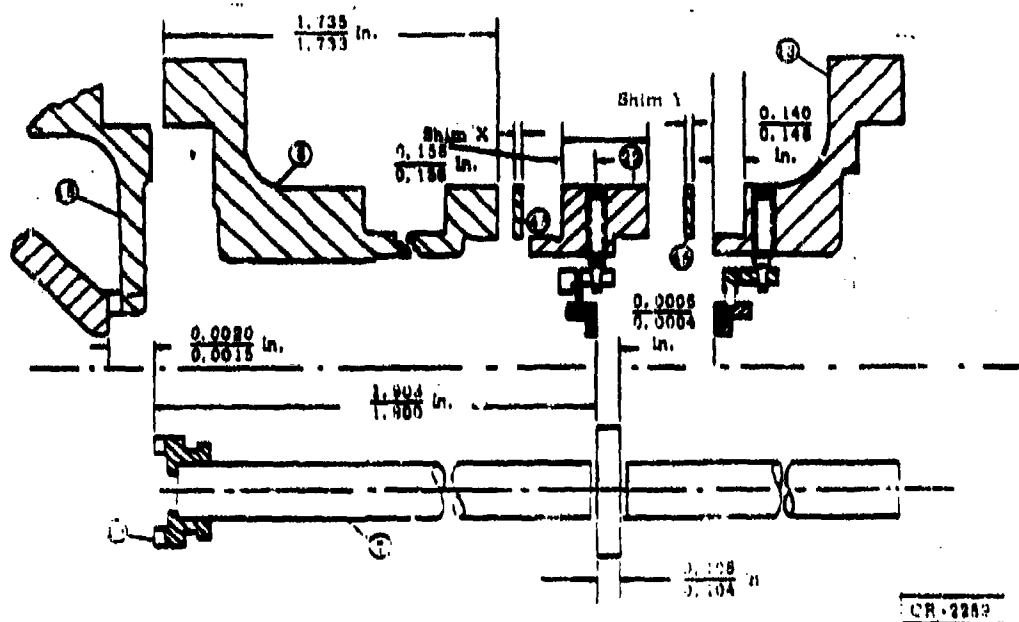


Figure 71. Turboalternator Dimensions for Shimming Thrust Bearing Position

Table 21

AXIAL SHIMMING MEASUREMENTS FOR TURBOALTERNATOR

Specifications	Distance (inch)
Wheel-to-nozzle clearances	0.0015-0.0020
Shaft total axial travel between thrust bearings	0.0004-0.0008
<u>Inner Thrust Bearing Shim</u>	Operator inserts assembly measurements here _____ _____ _____
A. Distance from top of thrust clearance ring (k) to top of shaft thrust runner	
B. Repeat Measurement 1 with nozzle installed	
C. Inner shim (X) required: $X = (A - B) + 0.0015$	_____
<u>Outer Thrust Bearing Shim</u>	_____ _____ _____
D. Repeat Measurement A with nozzle assembled and inner thrust shims (X) installed.	
E. Distance from top of thrust clearance ring (k) to outer thrust bearing surface	
F. Outer shim (Y) required: $Y = (0.732 - E) - (D - 0.6605) + 0.005$	_____

8. Thread the tapered shaft extension (1) into the thrust end of the shaft. Install the outer thrust bearing assembly by positioning the dummy shaft against the end of the shaft extension and slide the outer thrust bearing assembly onto the shaft.
9. Remove the tapered shaft extension and insert the three outer bearing shims, of thickness y , calculated above, between the inner and outer thrust bearing mounting flanges, 120 degrees apart.
10. With the outer thrust bearing in position, turn the shaft from the thrust end to be certain the turbine wheel and shaft are free to rotate. Then gradually tighten the thrust-end assembly screws (part 40). Do not overtighten the screws; they should be just snug enough to hold the shims in place.

INSTALLATION OF THRUST PROXIMITY PROBES

1. Mount the turboalternator assembly onto a support stand, turbine end down. Three lengths of 4-40 threaded rod can be used in place of three alternate nozzle assembly screws to attach the turboalternator to the support. The turboalternator support should be mounted on two indexing tables so the turboalternator can be rotated from a vertical to a horizontal position and can be rotated radially about the axis of the shaft. Figure 73 is a typical test station showing oscilloscopes, the Wayne-Kerr instruments, and a turboalternator mounted on two indexing tables.
2. Adjust the indexing tables to position the turboalternator vertically, with the turbine end down.
3. Install the thrust proximity probe (Part 11) into the nozzle block by carefully turning the probe in until it touches the end of the shaft; then back it out slightly, and tighten the jam nut.

CAUTION

Care must be exercised in carrying out this procedure, to avoid damaging the probe Textolite threads.

4. Connect a 10-foot lead between the probe and the Wayne-Kerr instrument (Model PM100B).
5. Clip the ground lead from the Wayne-Kerr instrument to the turboalternator housing.
6. Connect an oscilloscope to the Wayne-Kerr recorder output through the filter circuit, shown in the instruction manual for Wayne-Kerr instruments.

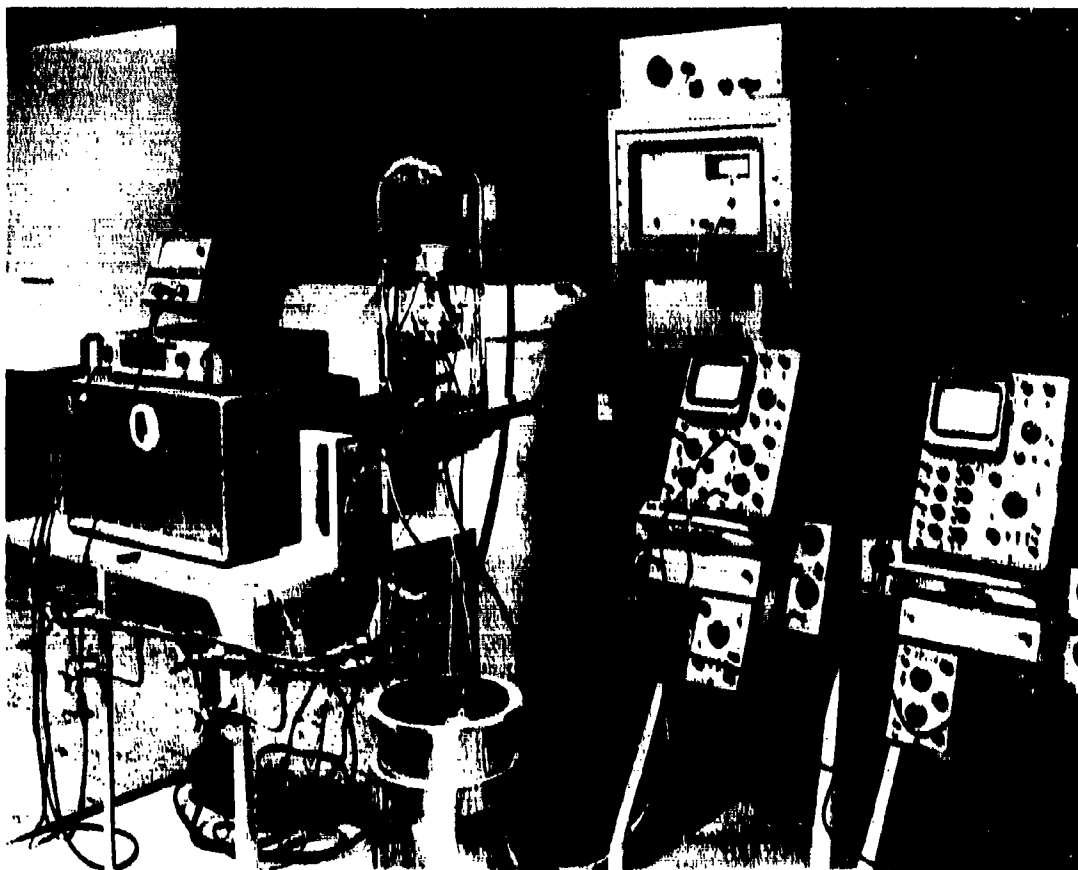


Figure 73. Open-Cycle Test Station for Turboalternator

NOTE: All of the individual oscillators in each Wayne-Kerr instrument must be disconnected and rewired to provide operation from a separate, single, 50 kHz supply; otherwise, the individual oscillators will operate out of phase and will cause heating and erratic signals.

7. Set the oscilloscope Y-axis sensitivity to 0.2 d-c V/cm and the X-axis to a sweep of 2 ms/cm. Adjust Y-axis gain control to 4.0 cm for 1 volt of d-c input.
8. Switch the Wayne-Kerr instrument to the CHECK position. Short the oscilloscope Y-axis input and adjust the zero position to a point that is 1 cm down from the top of the screen scale.
9. Switch the Y-axis input on the oscilloscope to the d-c position and adjust the Wayne-Kerr set adjustment to give a 4.0 cm deflection on the oscilloscope.

10. Switch the Wayne-Kerr instrument back to the READ position. The thrust proximity probe is then ready to be used, and after the adjustments outlined above, the sensitivity of the oscilloscope is 400 $\mu\text{in}/\text{cm}$.
11. Readjust the thrust probe position so the output signal from the Wayne-Kerr instrument appears at the middle of the oscilloscope screen.
12. Measure the total thrust bearing clearance by noting the thrust probe signal level on the oscilloscope after the above setting. Then rotate the turboalternator 180 degrees vertically and note the thrust probe output signal on the oscilloscope with the shaft resting on the outer thrust bearing. Change the outer thrust bearing shim height (Y) as required to meet the specified total axial shaft travel of 0.0004 to 0.0006 inch, and record the actual shim thickness on Line F of Table 21, for future reference.
13. The thrust proximity probe is also used to measure the clearance between the turbine wheel and the nozzle. Reposition the turboalternator vertically, with the turbine end down. Temporarily increase the thickness of the three shims (Y) by 0.001 inch, and remeasure the total travel of the shaft between thrust bearings with the thrust probe. Then gradually decrease the thickness of the three inner thrust bearing shims (x) in steps of 0.001 inch. As the value of the inner thrust shims decreases, the thrust probe may have to be backed out so it does not touch the shaft.

A thickness of the shims (x) is obtained where the turbine wheel just touches the nozzle, lifting the shaft off the inner thrust surface, reducing the total travel of the shaft. Once the above condition is obtained the thickness of shims (x) can be calculated to provide a 0.0015-0.0020-inch clearance between the turbine wheel and nozzle, beyond the inner thrust bearing surface. Record the actual shim thickness on Line C, for future reference.
14. Install shims x and y of the corrected values to meet the axial clearance specifications. Align the scribe marks on the outside of the housing at the thrust end to align the journal bearing support stems at each end of the housing assembly and tighten the thrust assembly screws (Part 40).

FINAL JOURNAL BEARING PAD ADJUSTMENTS

1. Adjust the indexing table to position the turboalternator horizontally and rotate the turboalternator until the pad stems between the shaft orbit proximity probe mounting holes are pointing directly up. In this position, the turboalternator shaft is resting between the bottom pads.

2. Install the four proximity probes (Part 11) adjacent to the shaft, two in the housing at the turbine end and two in the inner thrust-bearing mounting flange. Tighten the probes with the jam nuts.

CAUTION

Care must be exercised in carrying out this procedure, to avoid damaging the probe Textolite threads.

3. Connect the 10-foot leads between the probes and the Wayne-Kerr instruments. The probes and Wayne-Kerr instruments are identified by looking down on the turboalternator from the turbine end. The first probe on the left is X_1 , and the corresponding probe on the right is Y_1 . At the thrust end, the probe on the left is X_2 and the probe on the right is Y_2 .
4. Check to ensure that the ground lead is connected to the turboalternator housing.
5. Each of the probe output signals from the four Wayne-Kerr instruments must be filtered and connected to an oscilloscope with dual-trace amplifiers for both the X axis and the Y axis. Connect the output from Probe X_1 to the X axis and the output from Probe Y_1 to the Y axis of one trace, and X_2 and Y_2 to the X axis and Y axis of the other trace.
6. Set the scope sensitivity on all four channels to 0.2 d-c V/cm and adjust the four channels to 4.6 cm for 1 volt of d-c input.
7. Switch all four Wayne-Kerr instruments to the CHECK position. Adjust the four channels to give a deflection of 4.6 cm by adjusting the Wayne-Kerr set adjustments and switching the scope between the shorted input and the d-c input.
8. Switch the Wayne-Kerr instruments back to the READ position.
9. Short the scope inputs, and adjust the two zero positions to points that are 1 cm down from the top and 2 cm in from the right. Switch the scope inputs to the DC position. The orbit probes are then ready to be used, and after the above adjustments, the scope sensitivity is 400 μ in/cm.
10. Readjust the four probe positions so the scope signals are just on the bottom left corner of the screen. This adjustment is made with the turboalternator in the position described in Step 1.
11. The shaft clearances are measured by rotating the turboalternator assembly 120 degrees to the right and left of the position described above for setting the probes and plotting the probe readings in the three positions. An accurate method of recording the three positions is to take a triple exposure of the turbine end only, and then of the

thrust end only, with a scope camera. Cut a section of the scope grid from a photo and use this section to measure the lengths of the triangle legs formed by the three points, in centimeters. The legs of the triangles should be approximately equal. Substitute the average value of the triangle legs in the following equation to determine the mean bearing pivot-point radial clearances in microinches:

$$C' = 115.6 \times (\text{the length of the average leg in centimeters})$$

The radial clearance, C' , of the shaft should be 240 ± 25 microinches. Greater differences in the radial clearances will require adjustment of the spring stems and pads (Part 27) monitored by the proximity probes and the oscilloscope to obtain the proper clearance. During the adjustment of the journal bearing pads, the support stems can only be moved minute distances or the journal bearing pads may drop off the stems. In this case, the journal bearings must be reset to the gage shaft, as outlined above under "Preliminary Journal Bearing Assembly and Stator Installation."

TURBOALTERNATOR OPERATION

Preliminary turboalternator performance tests are made in an open-cycle test station (Figures 73 and 74). Figure 75 is a cutaway view of the turboalternator assembly for open-cycle testing; a schematic diagram of the station is shown in Figure 76. High-pressure gas (helium or nitrogen) is supplied from gas cylinder banks and is expanded across the turbine to atmospheric pressure. Liquid nitrogen temperature tests are performed by precooling helium gas with a cooling coil immersed in liquid nitrogen.

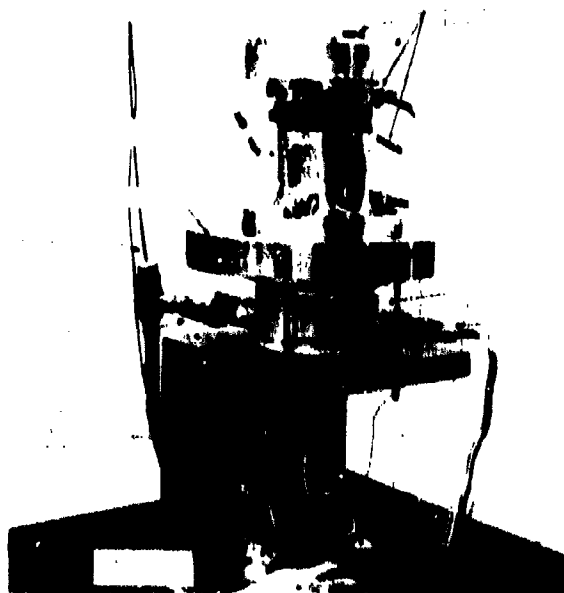
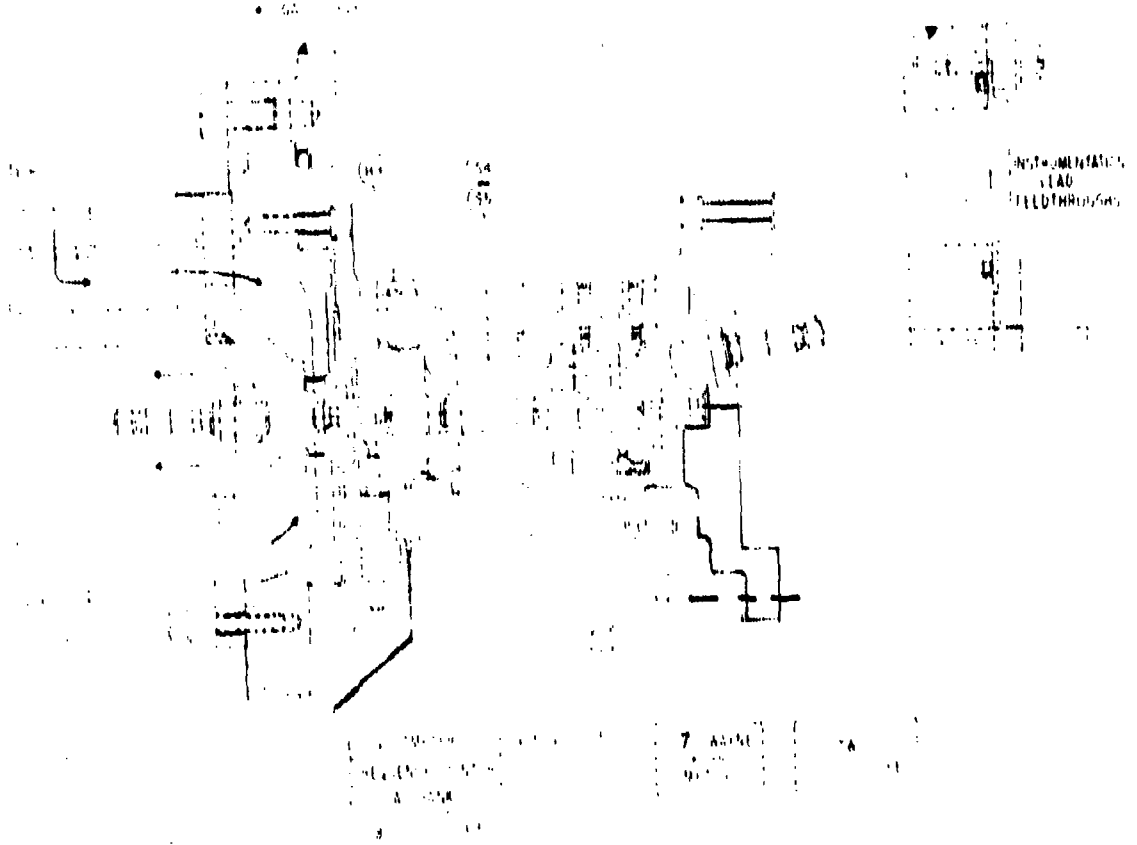


Figure 74. Turboalternator Assembly on Open-Cycle Test Stand



- (C) Alternator Frequency (hertz)
- (F) Flowmeter Pressure (psig)
- (P) Nozzle Inlet Pressure (in. mercury)
- (J) Flowmeter Reading
- (H) Housing Pressure (in. water)
- (R) Load Resistance per Phase (ohms)
- (V1) Voltage, Line to Neutral (volts)
- (V2) Voltage, Line to Neutral (volts)
- (V3) Voltage, Line to Neutral (volts)
- (B1) Shunt Voltage (volts)
- (B2) Shunt Voltage (volts)
- (B3) Shunt Voltage (volts)
- (T0) Gas Temperature at Flowmeter
- (T1) Gas Temperature into Nozzle
- (S4) Alternator Winding Temperature
- (S5) Alternator Winding Temperature

Figure 75. Principal Turboalternator Instrumentation

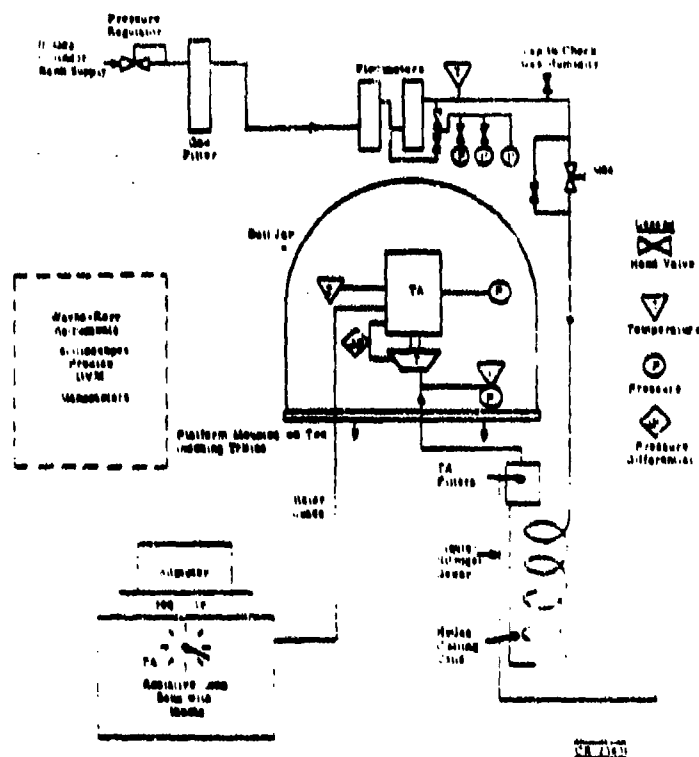


Figure 76. Open-Cycle Turboalternator Test Station

Figures 73 and 74 show a two-stage turboalternator mounted on two indexing tables in the open-cycle test station.

The inlet gas flow instrumentation for testing two-stage turboalternators is shown in Figure 77 along with a moisture analyzer and temperature-measuring instrumentation. The moisture analyzer is used to monitor the moisture content of the helium gas supply prior to low temperature tests, to reduce the possibility of ice crystals hindering the operation of the turboalternator.

Water and mercury manometers, not shown in the above figures, are used to measure the housing and nozzle pressures.

A temporary nozzle gas inlet fixture (c) is attached to the nozzle assembly. The same size-c seals used in the nozzle assembly and the gas connections are also used to assemble the gas inlet fixtures onto the nozzles. Attach the gas inlet fixtures to the nozzles by using three 4-40 threaded rods to replace alternator screws in the nozzle assemblies. Tighten three 4-40 nuts against the gas inlet fixture flanges to compress the c-seals. The threaded rods at the turbine end should be of sufficient length to attach the turboalternator to the support stand on the indexing tables. Two gas connections are provided in the gas inlet fixture. The larger connection is for the gas inlet flow, and the smaller connection is used to measure the nozzle inlet pressure on a mercury manometer.

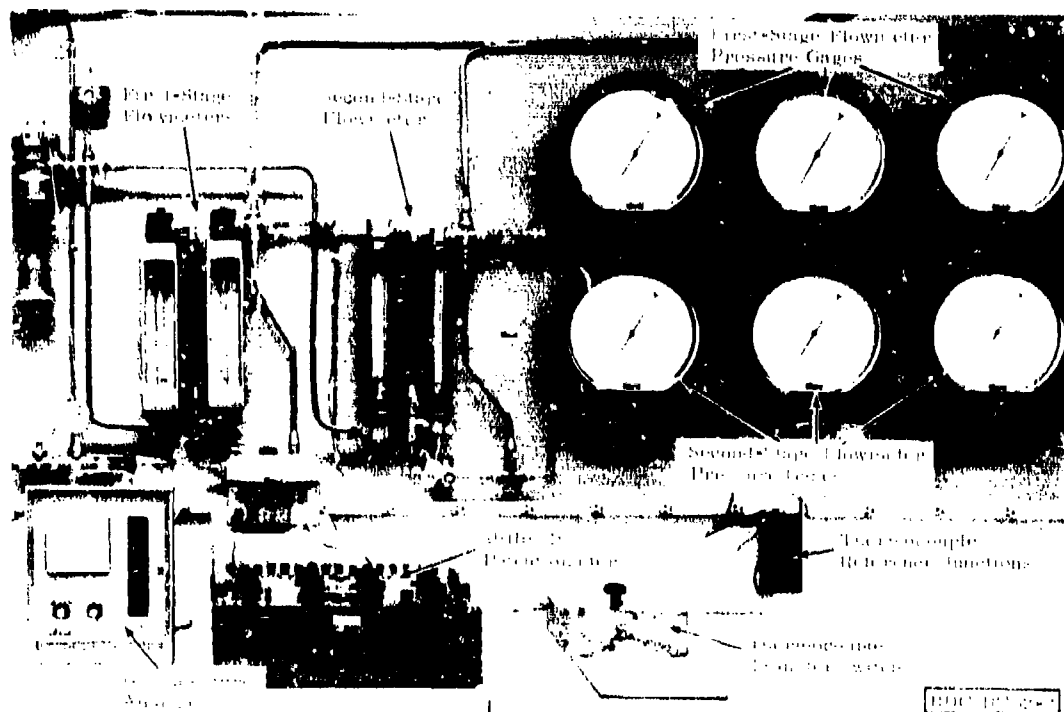


Figure 77. Open-Cycle Turboalternator Inlet Gas Instrumentation

The sealed turboalternator housing cover is not installed during this preliminary test.

Install proximity probes (Part 11) in the outer thrust bearing section of the housing (Part 13) and in the thrust bearing probe holder (Part 14). Adjust the probes to an approximate distance of 0.0030 to 0.0035 inch from the leading edge of the journal bearing pad and the outer gimbal ring, with the turboalternator in a horizontal position. Connect the probe output signals to an oscilloscope, in the manner in which the thrust proximity probe was connected. Use the pad probe and thrust gimbal probe to monitor the operation; their sensitivities and accuracies are not comparable to the other proximity probes, because of the viewing surface and angles involved in the measurements. Therefore, use the two probe signals as an indication only.

The turboalternator is operated as follows:

1. Adjust the index of dial to position the turboalternator in a vertical position. Connect the compressed helium gas to the nozzle and bleed with the adjustment in the line.

2. Turn the flow control valve to allow the helium gas flow to the nozzle. The flow rate should be approximately 100 to 150 gpm. The pressure should be 100 to 150 psia. The flow rate should be adjusted to the desired value.

one of the shaft orbit proximity probes can be used to monitor the speed by connecting the probe output signal to another scope and calculating the speed from the oscilloscope sweep rate.

3. Check to ensure the proper operation of the turboalternator by monitoring the proximity probe signals on the oscilloscopes. The orbits should be quite small in diameter (approximately 1/3 cm or smaller on the oscilloscope screen) and uniform. If the shaft is hitting, the orbits and the thrust signals will be quite distorted and will continually vary in size and amplitude. In this case, the thrust and orbit measurements made with the proximity probes will have to be repeated in order to correct a shim adjustment or a shift in a pad position. The pad probe and thrust gimbal signals should be uniformly once per oscillation.

MAGNETIZING SHAFT MAGNET

The measurements and adjustments outlined above under "Installation of Thrust Proximity Probe" and "Final Journal Bearing Pad Adjustment" cannot be made with the shaft magnet magnetized, because the force of the magnet's field would not allow the shaft to float freely when measuring the clearances. Therefore, the turboalternator must be disassembled to remove and magnetize the shaft. The assembly procedure must therefore be reversed to remove the shaft for magnetizing. Keep the shims identified while the parts are disassembled, and use the dummy shafts to hold the pads in position as the shaft is removed.

NOTE: If it is necessary to completely disassemble the turboalternator, use a hole gage to assist in the removal of the stator. Adjust a 0.3- to 0.4-inch gage to the smallest diameter and insert it through the stator. Increase the diameter of the hole gage and gently lift the stator out of the housing.

1. Place the shaft, with the turbine wheel removed, in a plastic container (c) to protect the critical shaft surfaces from the metal field yoke on the magnetizing coil.
2. Subject the shaft magnet to a uniform field of 25 kG, in a plane perpendicular to the length of the shaft, to fully magnetize the magnet.
3. Reassemble the turboalternator using the same procedures. Now all of the critical clearances have been adjusted. Install the correct shims during assembly.

The turboalternator is now ready for open cycle tests.

SHAFT BALANCE EQUIPMENT

The turboalternator shafts (Part 7) are balanced on a modified Model MV-6 balancer (Figure 78), manufactured by Micro Balancing, Inc., in Farmingdale, New York.

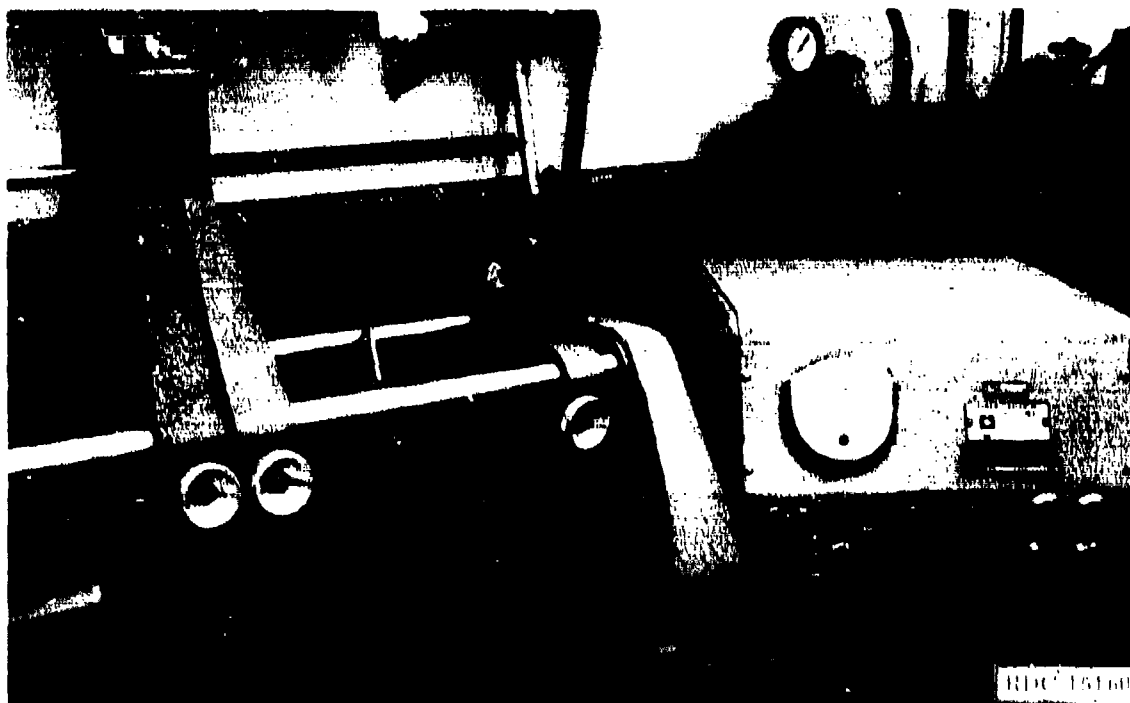


Figure 78. Modified Model MV-6 Balancer

After reviewing the particular balancing requirements of the turboalternator with the representatives of Micro Balancing, Inc., the following modifications were made to provide a maximum unbalance displacement in each plane of approximately 2.0 μm :

- Balancing speed of the shaft was changed to 6000 rpm, which required an additional filter in the electronics of the Model MV-6 balancer.
- Heavy duty, 1/8-inch-wide, Mylar recording tape was used for the drive belt between the shaft and the motor.
- Shaft cradle and support hardware (Figure 79) were redesigned to reduce weight to a minimum. The cradle support plate is supported by three balls instead of the usual four. The vibration transducers are placed as close together as possible, and nylon rods 1/16 inch in diameter are used for bearings in the V-blocks, to reduce friction.

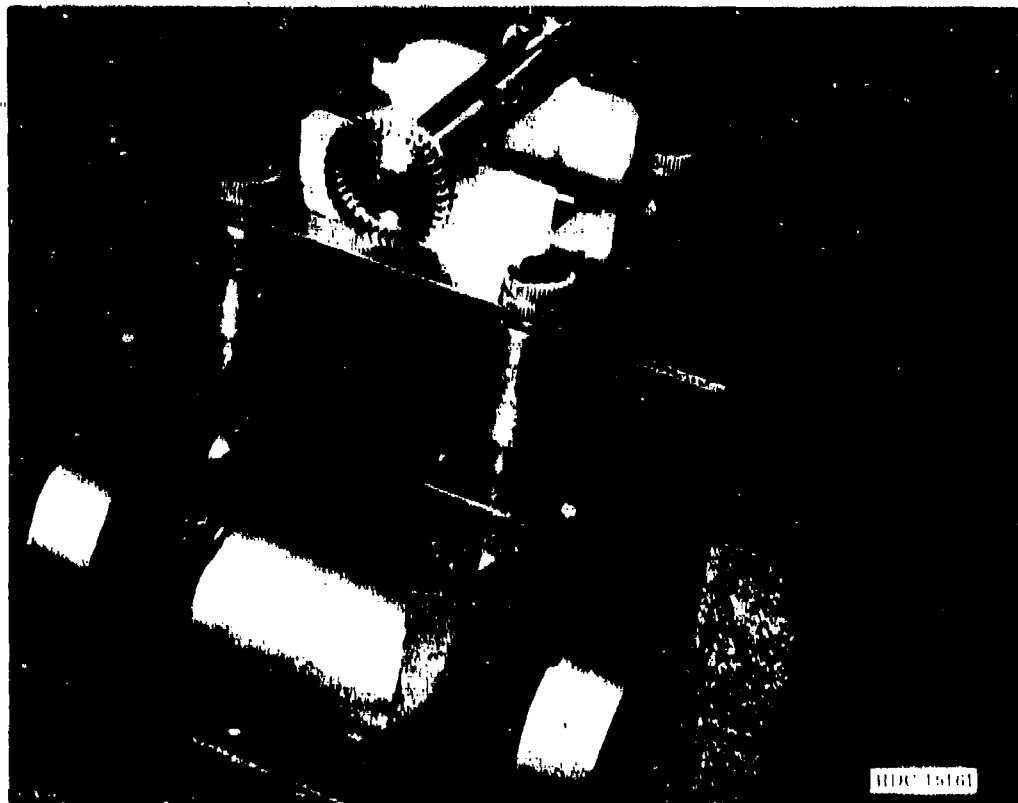


Figure 79. Balancing Cradle Assembly

PARTS LIST FOR ASSEMBLY DRAWINGS

Tables 22 through 24 list parts for the 14" K radial impulse turboalternator and for inner and outer thrust gimbal assemblies.

Table 22

PARTS LIST FOR SINGLE-STAGE
RADIAL IMPULSE TURBOALTERNATOR

Qty	Part No.	Name	Drawing No./Description
1	1	Assembly	
1	2	Shaft and wheel material specification	5431 63NP-1
1	3	Assembly fixtures	483166-1, 1, 2, 3, 4, 5, 12
1	4	Wheel spacer and washers	493164-1, 2, 4
1	5	Crack nut	5431 101P-1
1	6	Crack nut holder	5431 101P-2, 3
1	7	Wash	5007 642P-1
1	8	Flushing water oration	5009 645P-1
1	9	Stator nut	Stator No. 801K, 0.400 to 0.400, 1.00. Standard Tool Company
1	10	Stator	42316310-1
1	11	Probe	42316400-1
1	12	Probe	42316400-2
1	13	Water thrust gland assembly	PI-48316400-1
1	14	Front bearing probe holder	4831662P-1
1	15	Exhaust and discharge cylinder	48316600-1
1	16	Exhaust bearing	48316600-1
1	17	Cover - Turbine section	PI-48316600-1
1	18	Neutral capability	PI-48316600-1
1	19	Turbine wheel	48316610-1
1	20	Exhaust fixture	48316600-1
1	21	Exhaust thrust gland assembly	PI-48316600-1
1	22	Bearing pad	5431 63NP-2
1	23	Bearing stem support assembly	PI-48316600-1
1	24	Bearing stem support assembly	PI-48316600-1 (bearing)
1	25	Plate	48316600
1	26	Seal - probe	PI-48316600-1
1	27	Seal - probe cover	PI-48316600-1
1	28	Seal	Part No. 812A04-0019-2, Pressure Seals, Inc., Holliston, MA or equal
1	29	Seal	Part No. 811B04-0022-2, Pressure Seals, Inc., Holliston, MA or equal
1	30	Seal	Part No. 811B04-0023-2, Pressure Seals, Inc., Holliston, MA or equal
1	31	Seal	Part No. 814A-0043-2, Pressure Seals, Inc., Holliston, MA or equal
1	32	Seal	Part No. 814A-0044-2, Pressure Seals, Inc., Holliston, MA or equal
1	33	Seal	Part No. 814A-0045-2, Pressure Seals, Inc., Holliston, MA or equal
1	34	Seal, live pocket lead	4.40 x 1.00 long material - stainless steel, All Metal Seal Products Co., or equal
1	35	Seal	
1	36	Seal	
1	37	Seal	
1	38	Seal	
1	39	Seal	
1	40	Seal	
1	41	Seal	
1	42	Seal	
1	43	Seal	
1	44	Seal	
1	45	Seal	
1	46	Seal	
1	47	Seal	
1	48	Seal	
1	49	Seal	
1	50	Seal	
1	51	Seal	
1	52	Seal	
1	53	Seal	
1	54	Seal	
1	55	Seal	
1	56	Seal	
1	57	Seal	
1	58	Seal	
1	59	Seal	
1	60	Seal	
1	61	Seal	
1	62	Seal	
1	63	Seal	
1	64	Seal	
1	65	Seal	
1	66	Seal	
1	67	Seal	
1	68	Seal	
1	69	Seal	
1	70	Seal	
1	71	Seal	
1	72	Seal	
1	73	Seal	
1	74	Seal	
1	75	Seal	
1	76	Seal	
1	77	Seal	
1	78	Seal	
1	79	Seal	
1	80	Seal	
1	81	Seal	
1	82	Seal	
1	83	Seal	
1	84	Seal	
1	85	Seal	
1	86	Seal	
1	87	Seal	
1	88	Seal	
1	89	Seal	
1	90	Seal	
1	91	Seal	
1	92	Seal	
1	93	Seal	
1	94	Seal	
1	95	Seal	
1	96	Seal	
1	97	Seal	
1	98	Seal	
1	99	Seal	
1	100	Seal	

Table 23
PARTS LIST FOR INNER THRUST GIMBAL ASSEMBLY
(Group No. G1)

Qty	Part No.	Name	Drawing No. /Description
1	1	Housing -- Inner gimbal	423D436P-1
1	2	Thrust bearing	423D436P-1
1	3	Inner gimbal ring	543C174P-1
2	4	Pivot screw	664B311P-1
2	5	Pivot screw	664B311P-2
4	6	Pivot stem	664B317P-1
--	7	--	--
2	8	Set screw, hex socket	No. 0-80 x 3/32 long, cup point, stainless steel
2	9	Set screw, hex socket	No. 2-56 x 1/8 long, cup point, stainless steel
2	10	Copper slug	1/16 dia x 1/32 long, copper, B11B34C
2	11	Copper slug	1/32 dia x 1/32 long, copper, B11B34C

CR-2250

Table 24
PARTS LIST FOR OUTER THRUST GIMBAL ASSEMBLY
(Group No. G1)

Qty	Part No.	Name	Drawing No. /Description
1	1	Housing -- outer gimbal	588E446P-1
1	2	Thrust bearing	423D436P-2
1	3	Outer gimbal ring	543C175P-1
2	4	Pivot screw	664B311P-1
2	5	Pivot screw	664B311P-2
4	6	Pivot stem	664B317P-1
-	7	--	--
2	8	Set screw, hex socket	No. 0-80 x 3/32 long, cup point, type 304 stainless steel
4	9	Set screw, hex socket	No. 2-56 x 1/8 long, cup point, type 304 stainless steel
2	10	Copper slug	1/16 dia x 1/32 long, copper, B11B34C
2	11	Copper slug	1/32 dia x 1/32 long, copper, B11B34C

CR-2251

Appendix IV

SPECIFICATIONS FOR A SET OF SEVEN CRYOGENIC HEAT EXCHANGERS

This appendix includes a listing of the specifications that accompanied the purchase order to Kinergetics Incorporated on 20 November 1972. There were two sets of modifications of these specifications. The first set was sent on 17 July 1974. These modifications instructed the vendor to conduct thermal and pressure drop tests on only the warmer two balanced flow heat exchangers, instead of on all four, as had been previously stipulated. The vendor was also instructed to conduct a test that would determine whether plugging of the colder heat exchangers would occur as a result of condensation of impurities picked up by the helium gas in the warmer heat exchangers. The second set of modifications was sent on 23 December 1974 and instructed the vendor to block off the coldest heat exchanger and to cut a hole that would vent this exchanger to the jacket.

SPECIFICATIONS

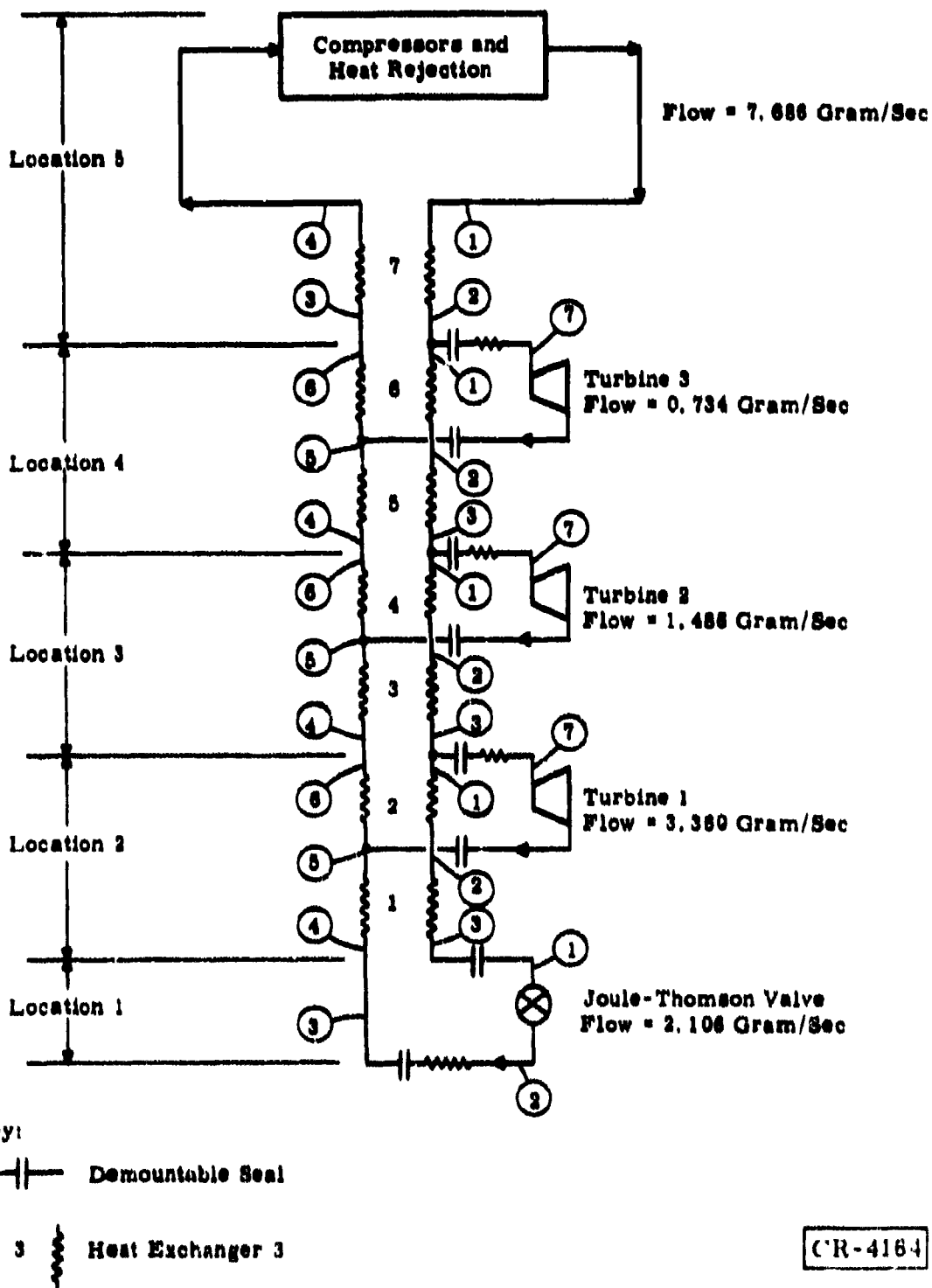
A set of seven cryogenic heat exchangers is required for a three-stage, Claude cycle, cryogenic refrigeration system (Figure 80). The refrigerant is helium gas.

The vendor is required to design, construct, and pressure-drop test the heat exchanger system. Thermal performance testing by the vendor is to be quoted as a separate option. While carrying out this work, the vendor shall be called upon to coordinate with General Electric engineers to assure compatibility of the heat exchanger system with the rest of the cryogenic refrigeration system.

The heat exchanger system shall be provided by the vendor under a subcontract with the General Electric Company. The prime contract is between the General Electric Company and the U. S. Army. As a subcontractor, the heat exchanger vendor shall be subject to the terms and conditions of the prime contract.

The subcontract shall be on a fixed cost, guaranteed performance basis. The performance guarantee is required for the performance parameters tested by the vendor.

In the heat exchanger system, weight is important; the vendor shall design for minimum weight. In replying to this request for proposal, the vendor shall provide his estimate of the weight and size of the heat exchanger, based upon an initial design. It is recognized that the weight and size may change somewhat as minor design modifications are made for compatibility with the rest of the refrigeration system.



CR-4164

Figure 80. Claude Cycle System (Schematic Diagram)

Specifications for the heat exchanger system and testing procedures are given below.

THERMAL PERFORMANCE AND PRESSURE DROP

Specifications for thermal performance and pressure drop are expressed in terms of temperatures, pressures, and flow rates throughout the heat exchanger system, as indicated in Figures 80 and 81. Note: The required thermal effectiveness of all balanced flow heat exchangers is 98.5 percent; however, the vendor shall design for 99.0 percent, to be conservative, and the heat exchanger vendor shall be responsible for pressure drops only within the heat exchanger cores and headers. The General Electric Company shall be responsible for pressure drops in the connecting tubing.

<u>LOC.</u>	<u>P(ATM)</u>	<u>TEMP(K)</u>	<u>LOC.</u>	<u>P(ATM)</u>	<u>TEMP(K)</u>
1 1	2.800	5.747	1 2	1.180	4.406
1 3	1.174	4.400	2 2	2.814	12.57
2 1	2.828	13.84	2 4	1.174	4.400
2 3	2.800	5.747	2 6	1.157	12.95
2 5	1.162	12.45	3 2	2.842	49.27
2 7	2.814	14.00	3 4	1.157	12.95
3 1	2.856	54.35	3 6	1.139	32.73
3 3	2.828	13.84	4 2	2.871	155.3
3 5	1.145	46.73	4 4	1.139	32.73
3 7	2.842	55.00	4 6	1.122	163.5
4 1	2.885	166.1	5 2	2.885	166.1
4 3	2.856	54.35	5 4	1.100	332.4
4 5	1.122	153.8			
4 7	2.871	170.0			
5 1	2.914	335.0			
5 3	1.122	163.5			

Notes:

1. Pressures are given in atmospheres (absolute).
2. Temperatures are given in degrees Kelvin.
3. Locations 1 through 5 are identified in Figure 80. "Location," above, is the cycle station. For example, Location 5-4 is the inlet to the compressor, where the pressure is 1.100 atmospheres and the temperature is 332.4°K.

Figure 81. Pressure and Temperatures Throughout System

STRUCTURE

In addition to transferring heat, the heat exchanger system is the principal structural member of the cryogenic refrigerator. To minimize heat leaks and facilitate system construction, it is desirable not to rely on external support members, but rather to suspend the cryogenic components, such as turboalternators, on the heat exchangers. The final arrangements

and support of the cryogenic components shall be worked out in coordination meetings with engineers from the vendor's firm, the General Electric Company, and the U. S. Army.

General Configuration

The heat exchanger system shall be constructed either as a single unit or as two units. For example, Exchangers 1, 2, 3, and 4 could be constructed as a single unit, with a uniform cross section, and Exchangers 5, 6, and 7 could be constructed as another unit, with a different cross section. A rigid connection between the two units shall be provided, with the colder unit supported entirely by the warmer unit.

Attachment to Flange

The warm end of Heat Exchanger 7 shall be attached to a room temperature flange. The vendor shall provide a header capable of being rigidly attached to the flange in a manner to be worked out with General Electric and U. S. Army engineers. This header is preferably the only means of support for the entire set of heat exchangers and other cryogenic components.

Support of Components

If possible, the turboalternators and a radiation shield shall be supported by the heat exchangers. The vendor shall provide rigid piping connections to the heat exchangers, and tabs or protrusions on the headers, where needed, to provide this support.

The total weight of each of the three turboalternators is estimated to be 10 pounds. The center of gravity of the turboalternators is estimated to be 5 inches from the edge of the heat exchangers. The weight of the radiation shield, to be supported at the warm end of Location 3 (Figure 80), is estimated to be between 4 and 6 pounds.

The General Electric Company will select the piping sizes, with regard to pressure drop and strength, and will be responsible for mounting the components on the heat exchangers. The vendor shall be responsible for the strength of the heat exchanger and the strength of the mounting protrusions and piping connections to the exchangers.

Turbines and Joule-Thomson valves shall be mounted to the heat exchanger by means of demountable vacuum-type seals. These seals shall permit removal of the turbine packages from the heat exchanger during system development. Half of each seal (one flange) shall be mounted directly on the heat exchanger headers. The flanges mounted on the heat exchanger headers shall be the flat flanges (the grooved flanges will be provided by the General Electric Company and will be attached to the turbine packages).

Structural Heat Leak

If the vendor requires external structural members for support of the heat exchanger, the turboalternators, or the radiation shield, the heat leaks through these members shall be used to calculate a corrected thermal performance of the heat exchangers. The corrected thermal performance must still meet the thermal performance specifications described above under "Thermal Performance and Pressure Drop."

LEAKAGE

The heat exchangers shall be bubble tight, from stream to stream. Bubble tightness is defined on page 181 under "External Leakage."

The heat exchanger must be leak tight to the outside, as measured by a helium mass spectrometer leak detector. Leakage test procedures are specified below.

DESIGN LIFE

The design life of the heat exchangers shall be 5000 hours, with 100 cooldown and warmup cycles required during refrigeration system testing. The vendor shall give consideration to any degradation of materials that might affect performance during that period.

CLEANLINESS

Cleanliness procedures shall be observed during assembly. Heat exchanger parts shall be degreased and ultrasonically cleaned before assembly.

Assembly shall be performed in a Class A, or better, clean room. The exchangers shall be packaged for shipping in a clean heat-sealed plastic bag, with dry nitrogen packaged inside.

TESTING PROCEDURES -- THERMAL

Thermal performance testing shall be an optional item to be quoted separately by the vendor. If the General Electric Company elects to have thermal performance testing performed by the vendor, then the General Electric Company and the U.S. Army will review test plans, testing methods, apparatus, and instrumentation with the vendor and will give approval before testing begins.

Cryogenic Tests

The four balanced flow exchangers shall be tested individually by the vendor, between room temperature and liquid nitrogen temperature, with helium gas. The flow rates shall be varied, and thermal effectiveness mea-

measurements shall be obtained at two Reynolds numbers above and two Reynolds numbers below the design Reynolds number.

Data Extrapolation

Data for balanced flow heat exchangers shall be extrapolated to the actual operating temperature, accounting for average fin thermal conductivity, longitudinal heat conduction, and average helium density, thermal conductivity, and viscosity. Heat transfer data obtained in balanced flow exchanger tests shall be used to predict unbalanced flow exchanger performance at operating conditions.

Errors in both the experiments and the data extrapolations must be sufficiently small to assure achieving the thermal performance goals. A simplified analysis of errors shall be conducted by the vendor.

TESTING PROCEDURES -- PRESSURE DROP

Pressure drop testing shall be performed by the vendor even though thermal tests may not be performed by the vendor.

Flow Tests

The vendor shall test both streams of each of seven exchangers with nitrogen gas flowing at room temperature and near atmospheric pressure. Pressure drops shall be measured with Reynolds numbers at two points below and two points above the design Reynolds number.

Similar tests shall be made with one stream of one heat exchanger using helium gas at room temperature and near atmospheric pressure, as a test of the extrapolation method.

Data Extrapolation

The vendor shall extrapolate pressure drop results to actual operating conditions for all exchangers, taking into account average gas density and viscosity.

THERMAL CYCLING

Before leakage testing, all exchangers shall be cycled between room temperature and liquid nitrogen temperature at least three times. Each cycle must be accomplished in less than one hour. The cycling may be accomplished by submerging the exchangers in liquid nitrogen.

TESTING PROCEDURES -- LEAKAGE

Stream-To-Stream Leakage

Stream-to-stream leakage shall be measured in all heat exchangers at once, with the exchangers at a temperature below 100°K. With all ports of the exchangers blocked, except for one port on each side, the exchangers shall be pressurized on one side with helium gas at 20 psig. With the other side at about atmospheric pressure, the leakage gas shall be collected and measured. An acceptable leakage level shall be a mass flow rate less than 1×10^{-6} atm-cm³/sec, which corresponds approximately to bubble tightness.

External Leakage

Leaks through the exchanger outer walls shall be measured by means of a helium mass spectrometer having a sensitivity of at least 10⁻¹¹ torr-liters/sec. With the exchangers at room temperature, the inside shall be connected to the leak detector and evacuated. Helium shall be introduced in a plastic bag outside the exchanger to indicate the existence of leaks, and any leak shall be located by local probing. The test shall be repeated with the exchanger below 100°K. Any leakage indicated by the leak detector shall be repaired.

WITNESS TESTING

At least one series of heat transfer tests (if performed by the vendor) and pressure drop tests shall be witnessed by a General Electric and/or a U. S. Army representative. One-week notice of these tests shall be given by the vendor.

DESIGN REVIEW

A design review shall be held with General Electric and U. S. Army representatives at Ft. Belvoir, Virginia, and approval must be given before construction starts.

SCHEDULE

It is anticipated that the subcontract will begin on 15 February 1971. With this as the starting date, the following schedule of completion dates is offered as a guide:

<u>Task</u>	<u>Completion Date</u>
Coordinate with General Electric on system and structural requirements. One trip by vendor to Schriever AFB, Colorado.	29 February 1971

Prepare initial design and review with General Electric.	15 March 1972
Prepare final design and review with General Electric and U. S. Army (one trip by vendor to Ft. Belvoir, Virginia).	14 April 1972
Fabricate heat exchanger system.	15 June 1972
Complete pressure drop and heat transfer tests (General Electric visit to vendor).	14 July 1972
Ship deliverable items.	17 July 1972

DELIVERABLE ITEMS

The following items are to be delivered under the contract.

<u>Item</u>	<u>Description</u>
1	One (1) set of seven cryogenic heat exchangers
2	Three (3) copies of a letter report, including a brief description of test apparatus and procedures, results of heat transfer testing (if performed) and pressure-drop testing (both basic test results and extrapolations to actual operating conditions), and a summary of structural calculations
3	Three (3) sets of heat exchanger system drawings (outline and detailed drawings are required).

KI Ref FP-2025

FINAL TECHNICAL REPORT

GENERAL ELECTRIC PURCHASE ORDER NO. 002-207165

November 1972 through April 1975

Prepared By

M. A. Elkan

Kinergetics Incorporated
6029 Reseda Boulevard
Tarzana, CA 91356

TABLE OF CONTENTS

<u>Section</u>		<u>Page</u>
I	Introduction	1
II	Exchanger System Configuration	1
III	Stress Analysis of Port Tubes	4
IV	Test Procedure and Results	9
V	Summary and Conclusions	24

LIST OF ILLUSTRATIONS

<u>Figure</u>		<u>Page</u>
1	Heat Exchanger Section	2
2	Basic Exchanger Construction	3
3	Layout - Cryogenic RPX (KI Drawing 3700)	5
4	Photograph of Heat Exchanger	6
5	Schematic of Heat Exchanger System	11
6	Schematic of Pressure Drop Measurement Test System	12
7	Test System Pressure Drop	13
8	Thermal Effectiveness Test System Schematic	17
9	Helium Flow vs. Nitrogen Boil-Off	22
10	Helium Flow vs. N ₂ Boil-Off for G.E. and Air Force	23

LIST OF TABLES

<u>Table</u>		<u>Page</u>
1	Pressure Drop Measurements (Nitrogen at 70° F)	15
2	Thermal Effectiveness Test Data at Five Flow Points	16
3	Mass Flow Rate, Nitrogen Boil-Off, Thermal Effectiveness	21

I. INTRODUCTION

This report describes the test apparatus, procedures, and results of heat transfer testing and pressure drop testing of the heat exchanger fabricated to General Electric Specification No. GL-12913. The exchanger system is part of a three-stage Claude cycle cryogenic refrigeration system. The refrigerant is helium gas.

Due to problems in the thermal performance test system, the 98.5 percent design effectiveness of the warm end, balanced section of the heat exchanger was not directly demonstrated in testing. The degree of vacuum required in the vacuum test chamber, to minimize external heat leaks during testing, could not be attained. A helium leak in the helium flow circuit in the chamber is suspected as the cause. The inadequate vacuum and possible helium leak combined with an extrapolation of the cool-down flow vs. liquid nitrogen boil-off data point to a large heat leak in the exchanger test system. The pressing nature of the schedule did not leave time to pursue a cure of the problem.

The cold end balanced flow section in the exchanger was bonded in place but is inoperative. It is sealed off from the remaining operative six sections of the heat exchanger. Difficulties encountered with leakage in this section during assembly of the heat exchanger and time limitations were factors in the decision to install the section as a "dummy" in the system.

II. EXCHANGER SYSTEM CONFIGURATION

The heat exchanger system consists of a set of seven heat exchanger sections, four balanced-flow and three unbalanced-flow, alternately mounted in series. Each section is composed of a sandwich of alternating .0075 dia. mesh copper screen parts and thermoplastic sheet parts which have been heated and pressed to force the thermoplastic through the screen voids. The flow passages are formed by precutting holes of the desired size, shape, and location in the thermoplastic sheets. Figure 1 is a photograph of a completed section, and Figure 2 indicates the construction concept. The fused thermoplastic forms solid walls which separate the gas flows from each other and from the outside atmosphere. Heat is transferred to and from the gas by passage over the wire mesh. Heat transfer between passages is accomplished by conduction through the screen wires, which run unbroken through the plastic separating walls. At the same time, the plastic forms an effective insulator to conduction in the longitudinal direction. Flow imbalance compensation is obtained by varying the flow area in the center portion of the exchanger as discussed by Cowans [1].

The exchanger system is effectively clamped together in the longitudinal direction by an Inconel bolt which runs down the open center. This clamp greatly strengthens the

1. K. W. Cowans, ADVANCES IN CRYOGENIC ENGINEERING, VOL. 19, Plenum Press, New York (1974), p 437.

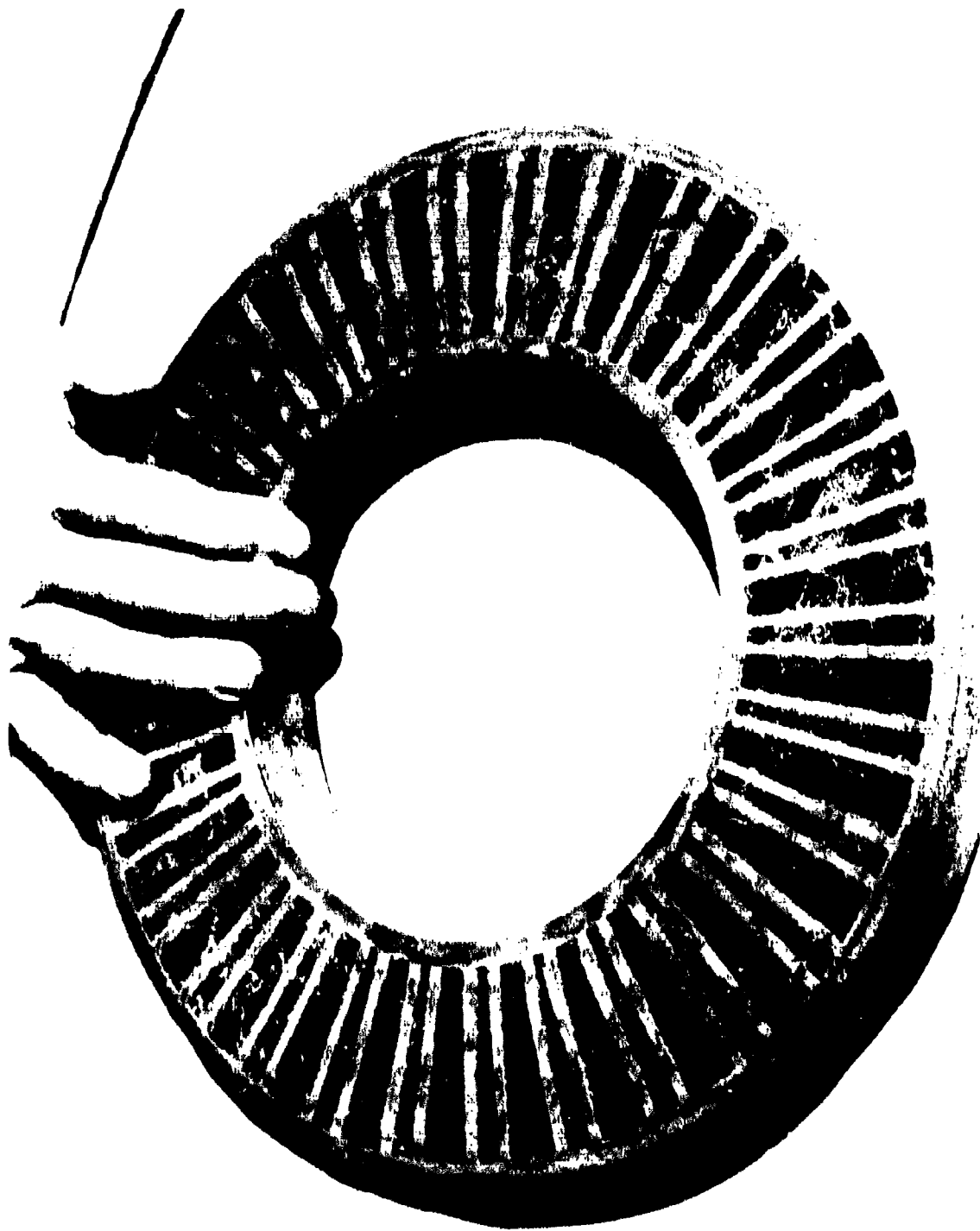
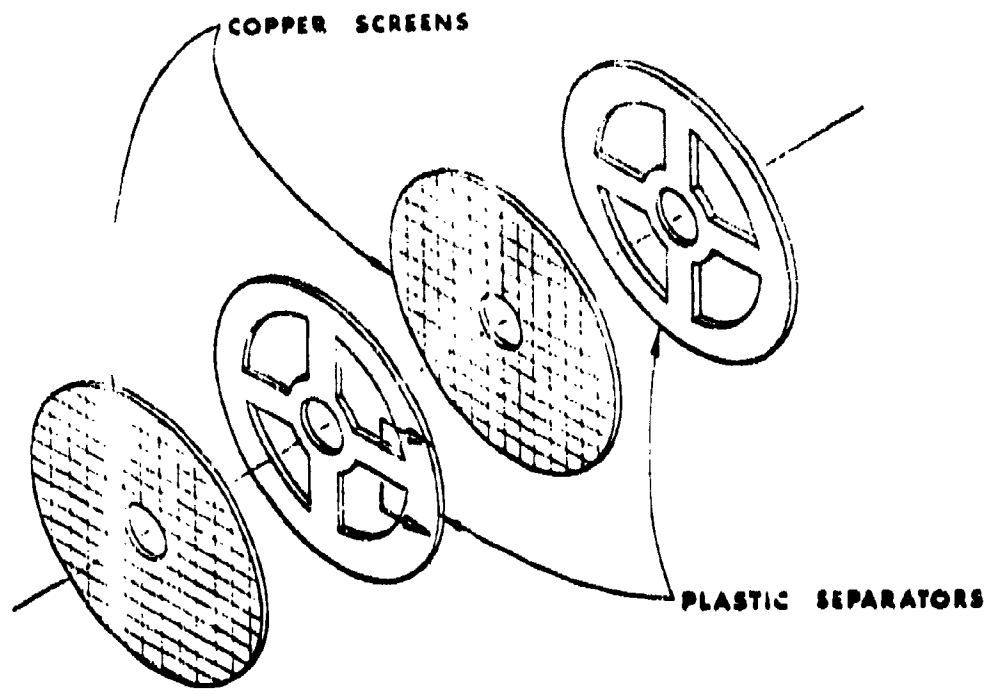
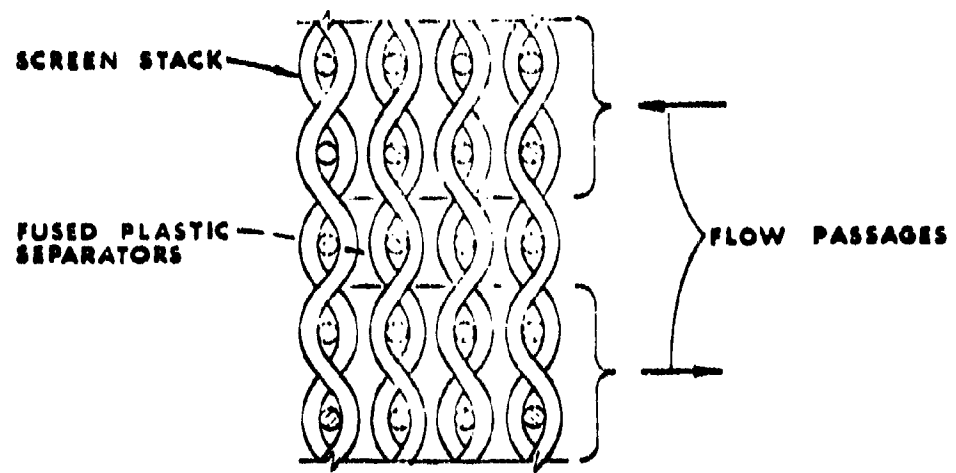


FIGURE 1 - HEAT EXCHANGER SECTION



EXPLODED VIEW



CROSS SECTION

FIGURE 2 - BASIC EXCHANGER CONSTRUCTION

exchanger and helps to prevent leakage at all bonded joints. The bolt is a 2.5 inch diameter Inconel 718 rod, threaded on the warm end. The flanged cold end is carried in a stainless steel cap structure which transfers the load to the exchanger body. The threaded end carries a nut and washer which transfer loads to a set of three Belleville springs. It was originally intended to use five Belleville springs, but it was not possible to start the nut on the bolt threads with the five in place because the exchanger was slightly longer than anticipated. The next lowest odd number of springs had to be used. These springs are carried in the warm end manifold structure, and the loads are transferred to the exchanger body through this structure.

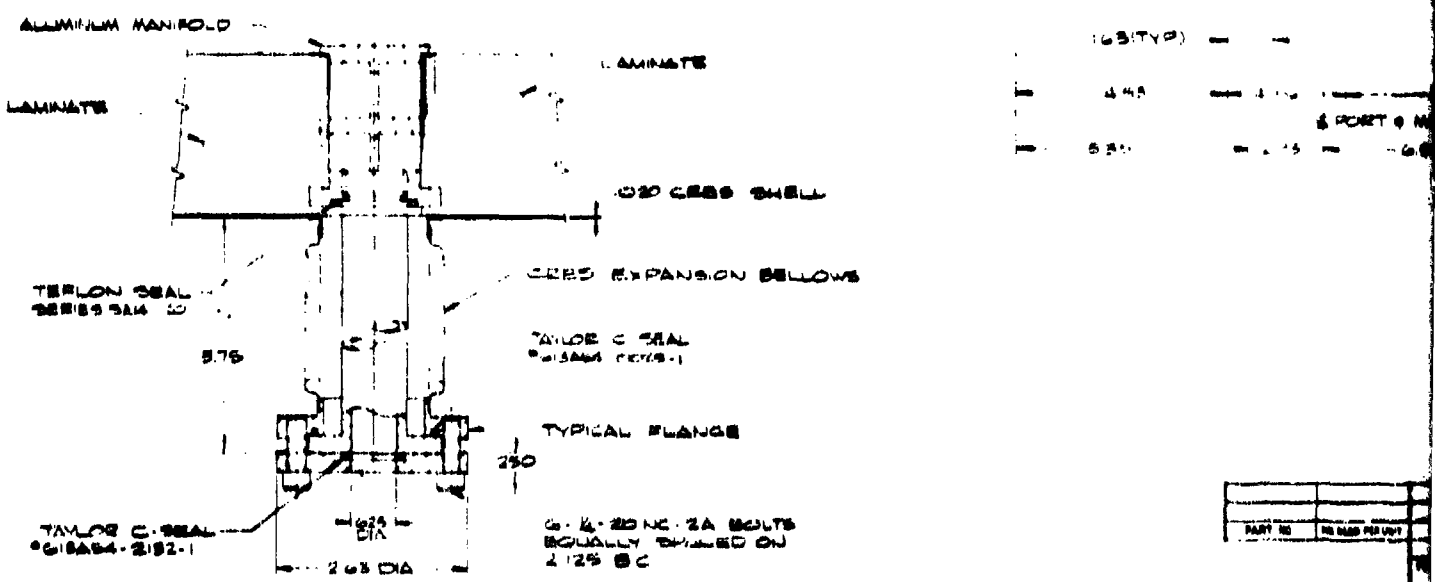
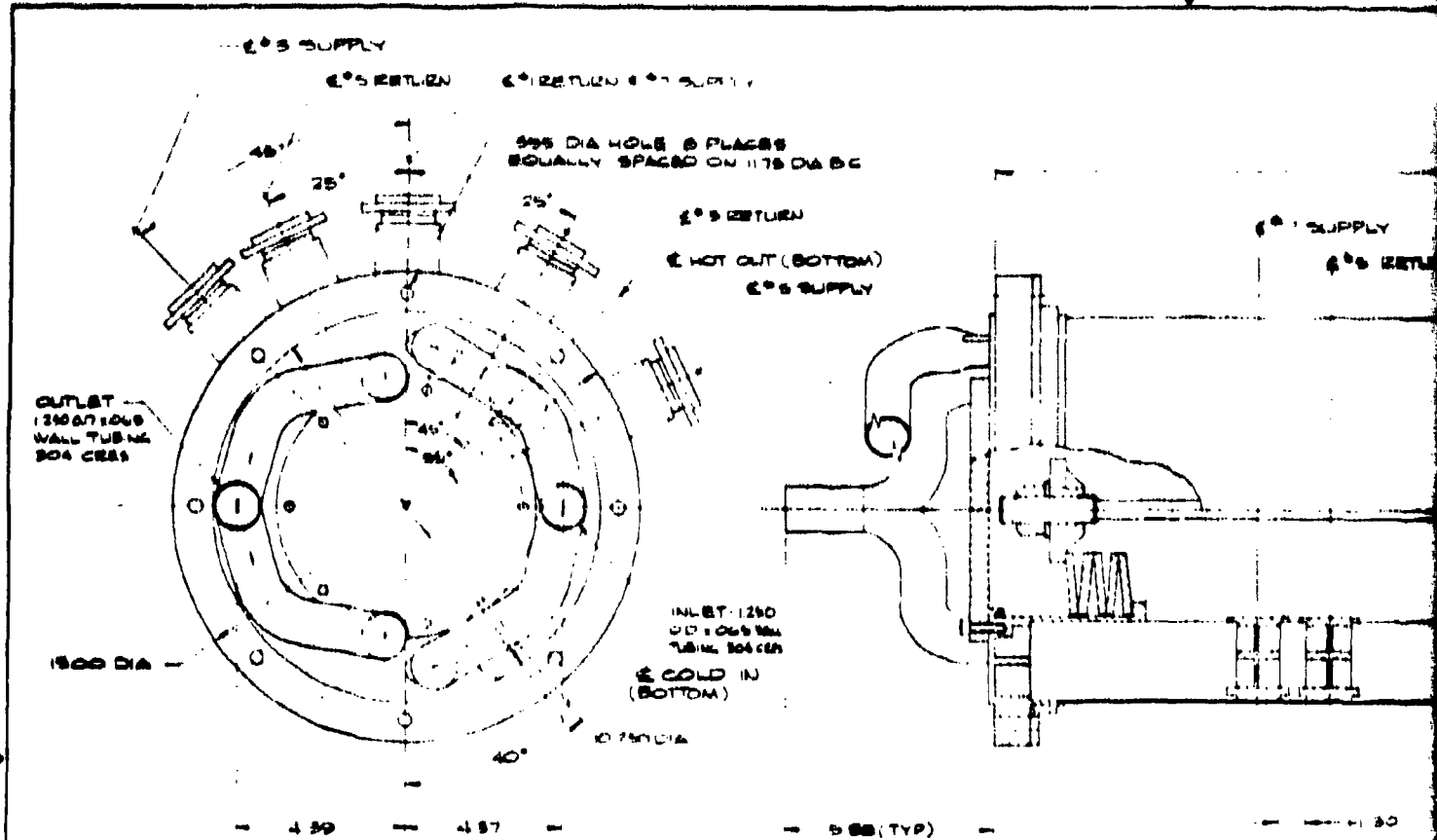
The heat exchanger is enclosed in a stainless steel cylindrical shell of .050 inch wall thickness with a flat .25 inch thick end plate welded on one end and a flange, with a bolt hole pattern, welded on the other end. The can is bolted to the warm end manifold of the exchanger and uses a neoprene O-ring between the flanges for sealing. There is a nominal .050 inch gap between the exchanger outer surface and the inside shell wall which has been partially filled with seven one-inch wide strips, spaced along the length of the exchanger and bonded around the circumference of the exchanger, of a furry, compliant cotton material which retains its compliance at liquid nitrogen temperatures. This material serves to impede thermal conduction currents between the cold and warm end of the exchanger. Holes are cut in the shell to provide for the supply and return port flanges, which emerge from the manifold and connect to the cryogenic system turbines and other auxiliaries. Special lateral movement bellows have been designed not only to provide for longitudinal movement of the heat exchanger body with respect to the outer shell, but also to retain any leaking helium within the shell. Each port flange has a bellows with one end welded to the outer shell and the other end to the flange on the end of the port tube (see detail in Figure 3). Therefore, when the heat exchanger body expands or contracts longitudinally due to temperature changes, the bellows deflect laterally.

The Belleville springs are sized and deflected to provide a clamping load varying from 15,800 lb warm to 12,000 lb cold. The load variation occurs because of approximate 0.126 inch differential between the exchanger body and the bolt during cool-down.

The exchanger weighs approximately 250 lb and can be seen as a layout in Figure 3 and in a photograph in Figure 4.

III. STRESS ANALYSIS OF PORT TUBES

The design criterion relative to port tube strength in the heat exchanger states that each port tube shall be able to withstand a bending torque of 170 newton-meters (125 ft-lb) at the exchange core wall, and a force in line with the pipe of 1110 newtons (250 lb) in either direction. The port tube is illustrated in the KI drawing package in drawing #3711. The length of the tube from the flange end to the exchanger core is 3.965 inches, the outer diameter is .875 inch, and the inner diameter is .635 inch. The following is a calculation of the stress in the tube due to the bending torque applied (assuming elastic bending theory is applicable).



TYPICAL FLANGE DETAIL
SCALE 1/1

PART NO	REVISION

REVISIONS			
LTB	ECO	DESCRIPTION	DATE
A		REVISED AND REDRAWN	7 MAR 71
B		REVISED TO PARALLEL CONNECTION	10 MAR 71

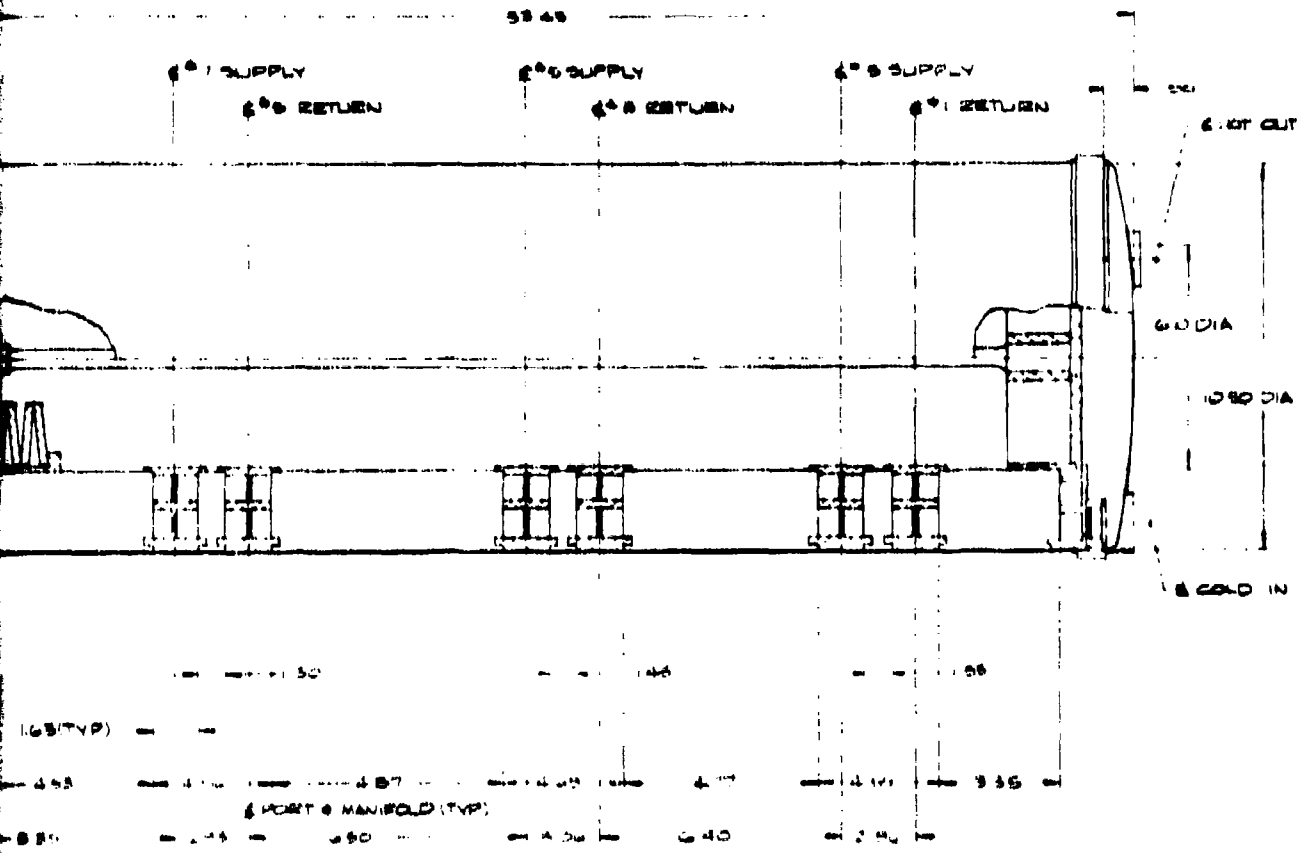


FIGURE 3

QTY RECEIVED	QTY ORDERED	ITEM NO	IDENTIFYING NO.	DESCRIPTION	MATERIAL	SPECIFICATION
LIBRARY OF MATERIAL						
UNLESS OTHERWISE SPECIFIED			DRAWN TO REF. 7029			
DRILL TOLERANCES			DRAWN TO REF. 7029			
.000 TO .125 ± .001			DRAWN TO REF. 7029			
.125 TO .375 ± .001			DRAWN TO REF. 7029			
.375 TO .125 ± .001			DRAWN TO REF. 7029			
.125 TO .125 ± .001			DRAWN TO REF. 7029			
MACH FINISH			OR BETTER			
BREAK SHARP EDGES 8:10			REMOVE ALL BURRS			
FINISH APPLY ALL 8:10 FINISH			DIMENSIONS ARE PER UNAS 1-11			
DIMENSIONS ARE IN INCHES			UNLESS OTHERWISE SPECIFIED			
FOL. AS + 51			ALL ± .010			
12.1 ± .010			AND ± .005			
			(SEE NOTE ON ALL DRAWINGS)			
PART NO		MFG. PART NO		MATERIAL		SPECIFICATION
				MINERALTES INC.		TAYLOR & HOBSON 5111
				LAYOUT CRYOGENIC RPX 7 SECTION		
D		51210		1.4700		
ALL		RIGHT		SHEET		OF

L5700 A

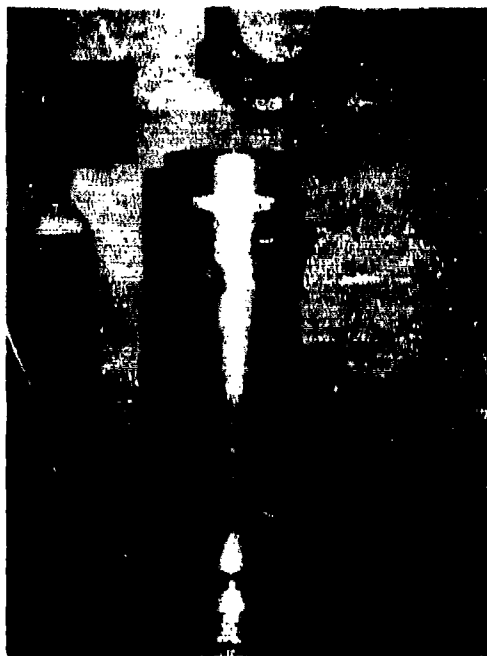


FIGURE 4 - PHOTOGRAPH OF HEAT EXCHANGER

$$\sigma = \frac{My}{I}$$

where:

σ = stress in tube due to bending (lb/in²)

M = bending torque (ft-lb)

y = distance from neutral axis to outermost wall (in)

I = moment of inertia (in⁴)

for this particular case:

$$M = 125 \text{ ft-lb} = 1500 \text{ in-lb}$$

$$y = .875/2 \text{ in}$$

$$I = \frac{\pi}{4} (R^4 - R_o^4) = \frac{\pi}{4} \left[\left(\frac{.875}{2} \right)^4 - \left(\frac{.635}{2} \right)^4 \right] = .0208 \text{ in}^4$$

$$\sigma = \frac{(1500 \text{ in-lb}) (.4375 \text{ in})}{.0208 \text{ in}^4} = 31,561.1 \text{ lb/in}^2$$

This bending stress is acceptable for the material being used, stainless steel 304, which has a yield stress of approximately 35,000 lb/in². Should the bending stress exceed 35,000 lb/in², plastic elongation may occur. Only gross plastic elongation would be critical to the design.

The stress in the header pipe due to a 1110 newton (250 lb) force in line with the pipe is analyzed as follows.

For the case of tension or compression:

$$s = \frac{F}{A}$$

where:

s = stress in the pipe due to tension or compression (lb/in²)

F = tensile force (lb)

A = cross-sectional area of pipe (in²)

for this case:

$$F = 250 \text{ lb}$$

$$A = \pi (R^2 - R_o^2) = \pi \left[\frac{.675}{2}^2 - \frac{.635}{2}^2 \right] = .285 \text{ in}^2$$

$$s = \frac{250 \text{ lb}}{.285 \text{ in}^2} = 878.34 \text{ lb/in}^2$$

The stress due to compression or tension is well below the yield stress.

For the case of buckling due to compression:

$$P_E = \frac{\pi^2 E I}{L_e^2}$$

where:

P_E = elastic buckling load (lb)

E = modulus of elasticity (lb/in²)

I = moment of inertia (in⁴)

L_e = effective length of the tube (in)

for this case:

$$E = 29 \times 10^6 \text{ lb/in}^2$$

$$I = .0208 \text{ in}^4$$

$$L_e^* = 0.7 L = 0.7 (3.965 \text{ in}) = 2.7755 \text{ in}$$

$$P_E = \frac{\pi^2 (29 \times 10^6 \text{ lb/in}^2) (.0208 \text{ in}^4)}{(2.7755 \text{ in})^2} = 7.7282 \times 10^5 \text{ lb}$$

The force required to buckle the pipe is far in excess of 250 lb.

* The header tube is best represented as a pinned-fixed column in which case the effective length is given as .7L.

IV. TEST PROCEDURE AND RESULTS

The test specifications called for four separate performance tests:

- 1) External leakage
- 2) Stream-to-stream leakage
- 3) Pressure drop
- 4) Thermal effectiveness

The following sections describe the procedures used and the results obtained.

1. External Leakage

Leaks through the exchanger shell were measured by means of a helium mass spectrometer having a sensitivity of 1.5×10^{-9} Torr liters/sec. With the exchanger at room temperature, the inside was connected to a diffusion pump and leak detector and evacuated. The system was evacuated for a period of three days with the best helium background reading, on the leak detector, being 4400 divisions. Bagging the exchanger assembly and filling the bag with helium gas produced no significant change in the background reading. The calibrated helium leak of 3.7×10^{-8} std cc/sec corresponded to 80 divisions on the leak detector. Therefore, the 4400 divisions would correspond to a helium leak no larger than 2.04×10^{-6} std cc/sec. It is postulated that the high helium background reading is due to outgassing of the exchanger, since it had been stream-to-stream leak tested with helium upon completion of assembly.

A second external leakage test was to be performed upon completion of the thermal performance tests, by which time the exchanger would have experienced several cool-down cycles. The test was to involve pressurizing the exchanger with helium gas and using a helium sniffer, connected to the leak detector, around the outside to detect leakage through the shell. This test was not performed due to the request to ship the exchanger.

2. Stream-to-Stream Leakage

Stream-to-stream leakage was measured in all heat exchangers at once, with the temperature below 100° K and also at room temperature. Directly upon completion of the thermal performance test, while the exchanger system was still cold, the vacuum chamber was opened. With positive helium pressure on the system, one of the bellows hoses was detached from the exchanger port and both openings were capped. This physically separated the high pressure side of the exchanger from the low pressure side. The high pressure side was then pressurized to 20 psig. The low pressure side of the exchanger rose at a

rate of 10 psi/21 sec until equilibrium with the high pressure side was reached. This leak corresponds to less than 1.8 percent of the operating helium flow rate.

The same test was made, without changing the test arrangement, after the exchanger had reached room temperature. The high pressure side was pressurized to 20 psig and valved off. The low pressure side of the exchanger showed no increase in pressure, although the high pressure side decayed at a rate of approximately 8 psi/minute.

It appears that a relatively small stream-to-stream leak, at room temperature, opens up at operating temperatures. The pressure decay on the high pressure side was due to a leak in the adjoining helium circuit outside of the exchanger. The exchanger itself was then separated from the adjoining hoses and LN₂ dewar and both high and low pressure streams were pressure decay tested at room temperature. In each case, the stream to be tested was pressurized to 20 psig of helium gas and valved off from the source. Decay on both sides was less than .2 psi/minute.

Preliminary room temperature stream-to-stream pressure decay leak tests had been performed on both the high and low pressure streams of the exchanger upon completion of assembly. The low pressure side decayed at a rate of approximately .2 psi/minute and the high pressure side decayed at a rate of approximately .12 psi/minute. Both leak rates were considered acceptable.

3. Pressure Drop

Pressure drop measurements were made on both streams on various combinations of two (balanced and unbalanced) of the six operating exchanger sections with nitrogen gas at room temperature. Each exchanger section could not be tested individually, except for #7, due to the design of the exchanger system, which does not provide an inlet and outlet for each stream of each section (Figure 5). For each section combination, pressure drops were measured at Reynolds numbers two points below and two points above the design Reynolds number.

The procedure was to flow gas from a compressed nitrogen bottle into the exchanger section(s) with a pressure gauge and a laminar flow meter in the system (see Figure 6). The pressure drop through the section(s) and downstream of the test system was indicated by the inlet pressure gauge. The pressure drop through the section(s) alone was found by subtracting the downstream test system pressure drop, at the given flow rate, from the overall pressure drop read on the inlet pressure gauge. Data was taken separately for pressure drop vs. flow in the downstream test system alone (Figure 7).

Pressure drop measurements were made prior to the external leakage test, in which the can was evacuated. It was decided not to make the one required pressure drop test, using helium gas, until later in the program because the introduction of helium gas into the exchanger would reduce sensitivity of the leak detector to be used in the external leakage test.

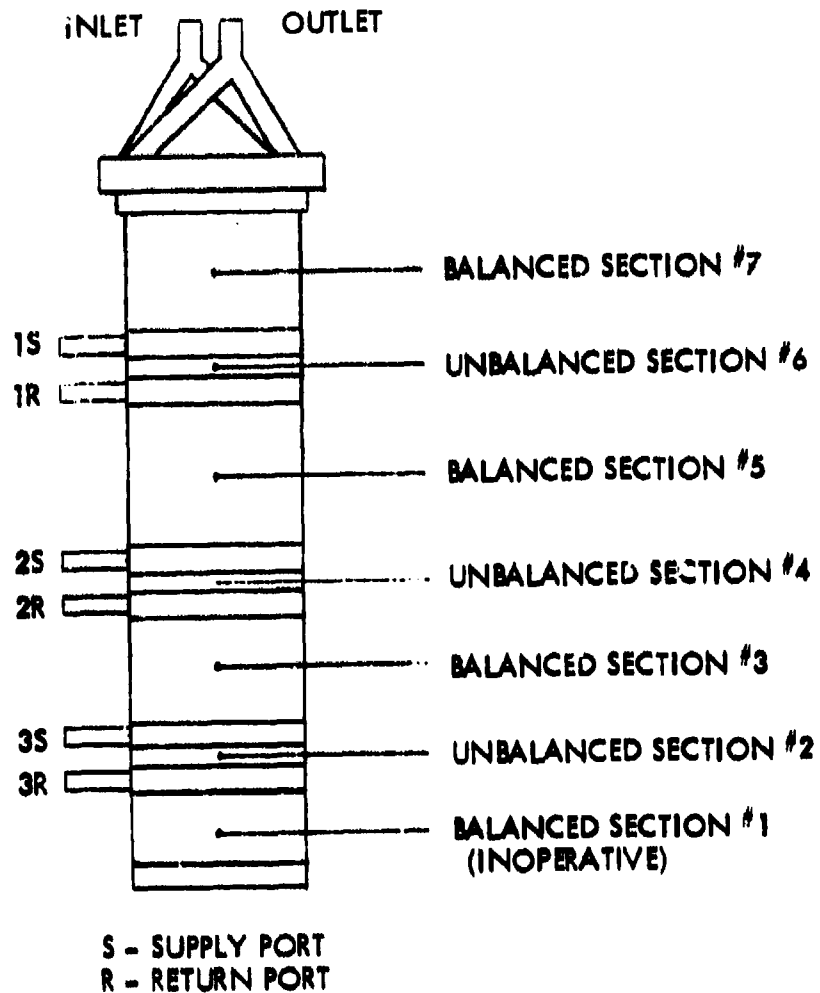


FIGURE 5 - SCHEMATIC OF HEAT EXCHANGER SYSTEM

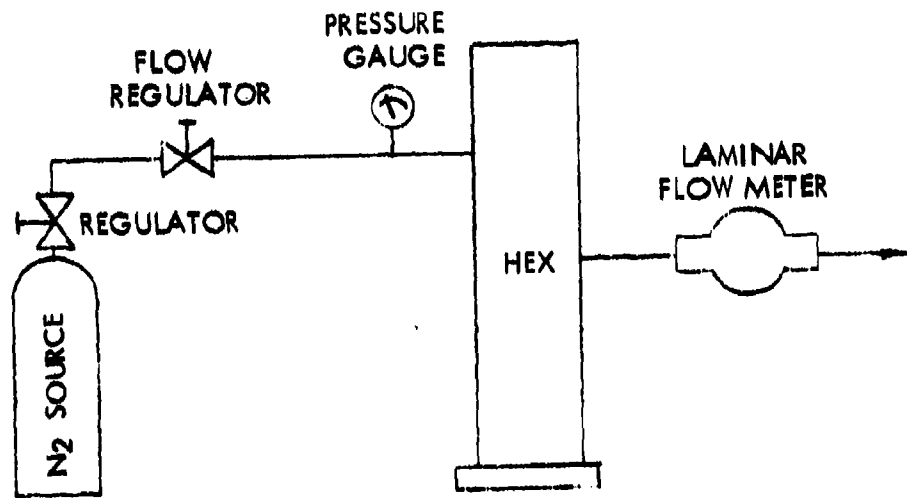


FIGURE 6 - SCHEMATIC OF PRESSURE DROP MEASUREMENT TEST SYSTEM

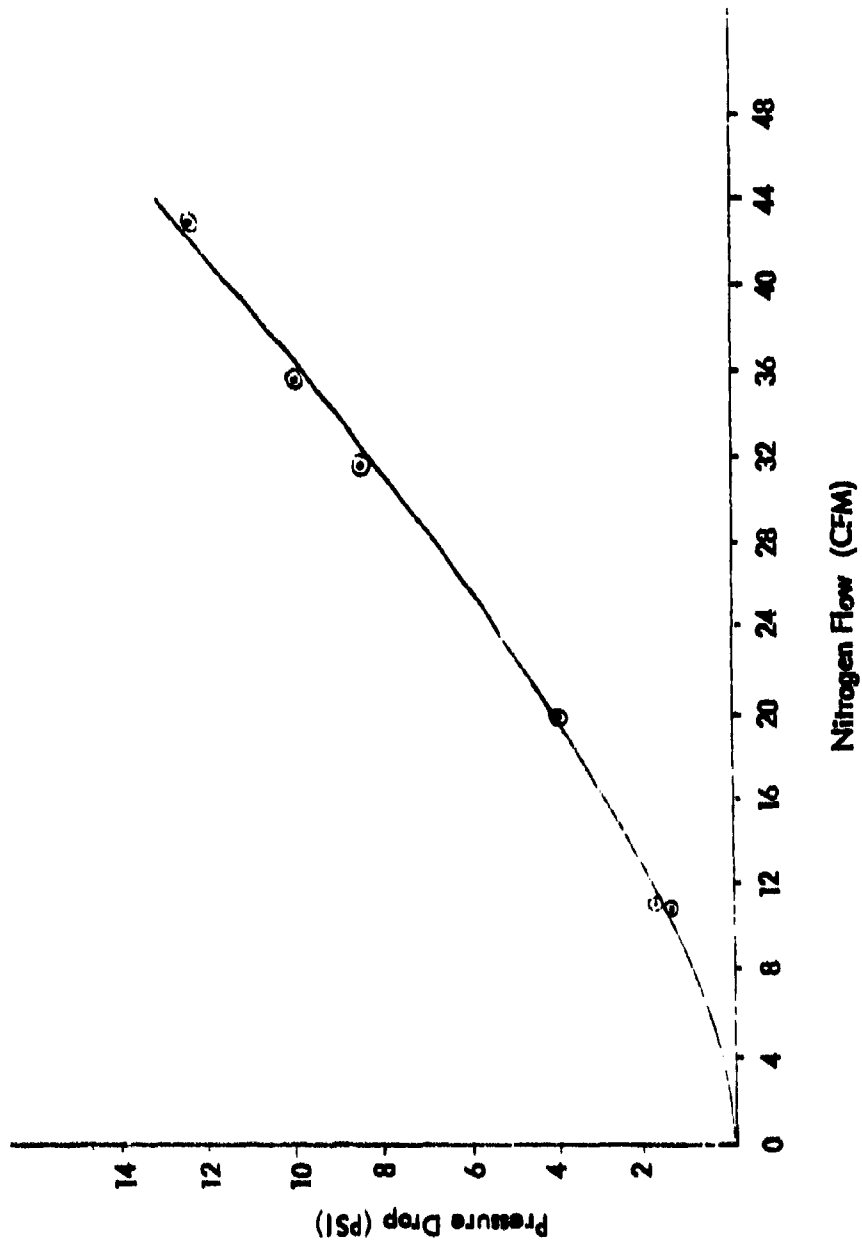


FIGURE 7 - TEST SYSTEM PRESSURE DROP

The set of pressure drop measurements performed was determined to be invalid because the pressure drop through the testing system was much greater than that through the exchanger section(s). After it was determined that the data was invalid, it was decided to continue on to the external leakage test and come back to the pressure drop measurements after completion of all other tests. The order to stop work and ship the exchanger was received before the pressure drop measurements could be remade. Table 1 presents the data taken on the first attempt.

The following equation, taken from the Hagen-Poiseville equation for laminar flow, would be used to extrapolate pressure drop test data (N_2 subscript) to actual operating conditions (He subscript).

$$\Delta P_{He} = \frac{\Delta P_{N_2} - \Delta P_{T.S.}}{QN_2} \frac{\dot{m}_{He}}{\rho_{He}} \frac{\mu_{He}}{\mu_{N_2}}$$

where:

ΔP_{He} = pressure drop through section(s) at operating conditions

ΔP_{N_2} = pressure drop through section(s) at test conditions

$\Delta P_{T.S.}$ = pressure drop through the test system alone

QN_2 = volumetric flow through test system

\dot{m}_{He} = operating mass flow rate

ρ_{He} = average density of helium gas in section(s) under operating conditions

μ_{He} = average viscosity of helium gas in section(s) under operating conditions

μ_{N_2} = average viscosity of nitrogen gas in section(s) under test conditions

4. Thermal Performance Test

The raw test data for the warmest balanced section is presented in Table 2. Included is the system flow rate, pressure, and nitrogen boil-off flow rate. This data was taken with a vacuum, in the test chamber, varying from 8×10^{-3} Torr to 25×10^{-3} Torr. The cool-down was started with a vacuum of 3×10^{-4} Torr, but this vacuum rose to the above range after 1-1/2 hours into the cool-down. Apparently, a leak in the system opened up at this point. A schematic of the testing system is shown in Figure 8.

Section(s)	Parting Arrangement		Q _{NR} Flow at Reynolds No. (cfm)	Test Data (Q _i - CFM, ΔP _i - PSI)										
	Flow In	Flow Out		Q ₁	ΔP ₁	Q ₂	ΔP ₂	Q ₃	ΔP ₃	Q ₄	ΔP ₄	Q ₅	ΔP ₅	
Low Pressure Side	3 & 2	3R	2R	42.5	30.0	11.5	35.6	14.00	42.5	15.40	47.0	15.6	52.1	19.75
	4 & 5	2R	1R	22.0	11.5	2.5	15.0	5.50	22.2	7.50	28.0	11.0	36.8	13.25
	6 & 7	1R	Outlet	13.5	8.0	.5	10.6	.75	13.5	1.75	14.5	2.0	20.0	4.25
	7 - 2	3R	Outlet	—	11.1	2.5	12.8	4.00	28.2	11.50	36.6	17.5	48.0	19.25
High Pressure Side	4 - 3	2S	3S	42.5	28.8	14.0	40.5	20.00	43.7	22.20	47.0	24.5	53.5	27.50
	6 - 5	1S	2S	22.0	12.0	7.5	15.0	9.75	22.4	15.00	30.0	24.0	35.2	27.00
	7	Inlet	1S	13.5	7.5	1.25	10.0	2.00	13.2	5.50	15.0	5.75	21.0	7.75
	7 - 3	Inlet	3S	—	9.3	4.0	12.6	6.25	27.0	14.50	40.5	23.0	47.0	26.00

Equipment:

F7 Meriam SDMC2-2
 M3 Dwyer, #8 to -8 in. H₂O
 P47 U. S. Gauge AW-2926 ABO1

Table 1 - Pressure Drop Measurements (Nitrogen at 70° F)

Helium Flow Reading (In·H ₂ O)	System (1) Pressures (psi)	Nitrogen Boil-Off (2) (% of F4)
2.50	14.6 / 11.2	43
3.20	14.6 / 10.2	50
3.53	14.3 / 9.7	48
3.9	14.4 / 9.2	52
4.35	14.1 / 8.7	52

109° K at #1 supply port, 20×10^{-3} Torr vacuum.

Equipment:

Flow Meters - F4 Fisher and Porter Flowrator Model 10A27350,
tube No. FP-3/4-27-G-10/80

Pressure

Gauges - P29, U. S. Gauge BU-2579-A
P47, U. S. Gauge AW-2926AB01

Vacuum

Gauges - VAC3, CVC Type G PH-100C
VAC4, Thermocouple vacuum gauge NRC 802-A

Thermocouple

Bridge - T1, Leeds and Northrup, Model 8693

- (1) See Figure 8 for location of pressure gauges.
(2) Flowmeter R4, maximum flow 11.0 scfm air @ STP.

**Table 2 - Thermal Effectiveness Test Data
at Five Flow Points**

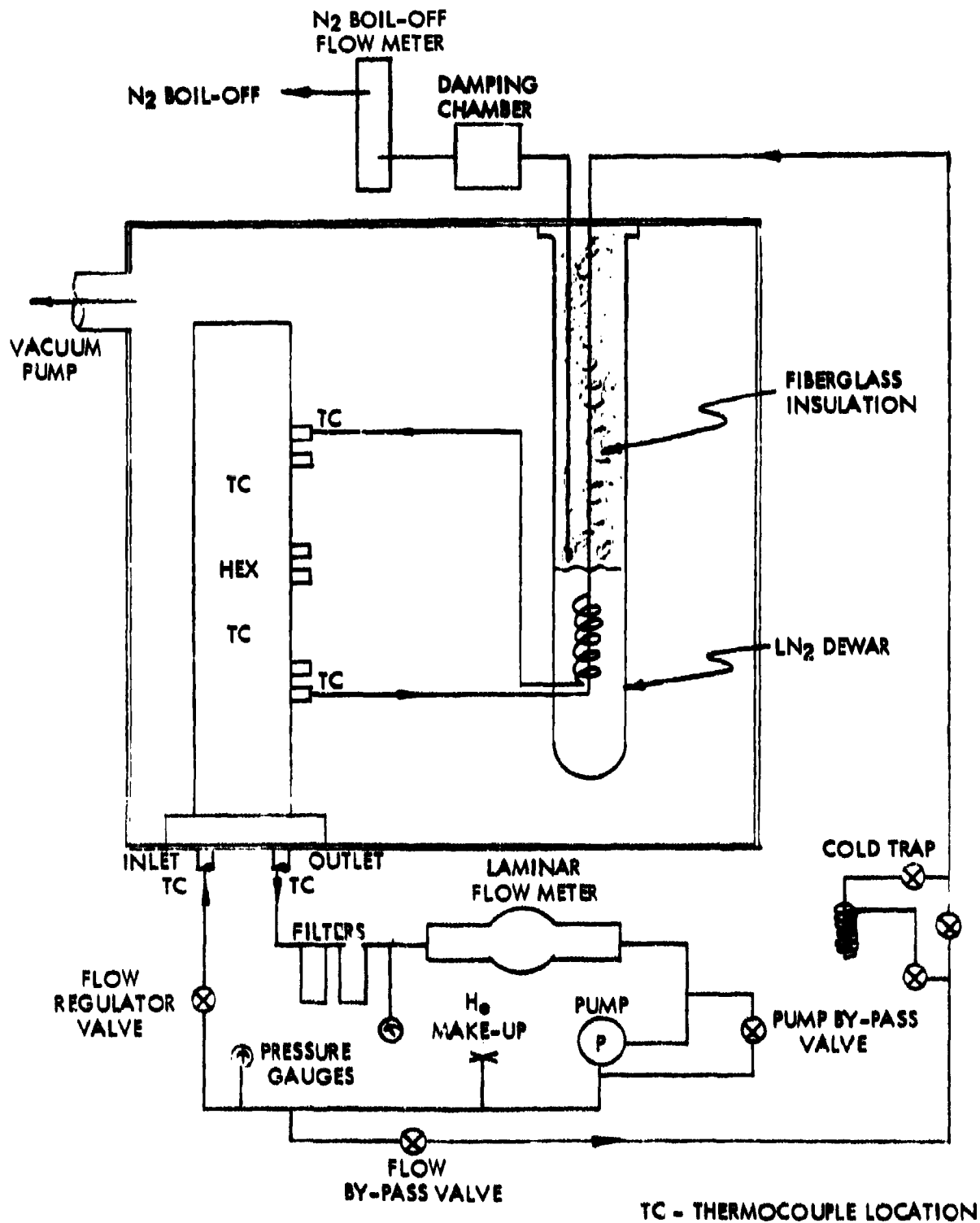


FIGURE 8 - THERMAL EFFECTIVENESS TEST SYSTEM SCHEMATIC

To obtain exchanger thermal effectiveness, the data is reduced as follows:

- 1) The Meriam flowmeter curves are entered at the appropriate differential pressure to obtain the corresponding scfm of air. This value is then corrected for helium viscosity ($\times .912$) and multiplied by the density of helium, calculated at 100°F and the system outlet pressure, to obtain the helium mass flow rate.
- 2) The N_2 flowmeter readings are multiplied by 11 scfm (the maximum flow rate) and the density of nitrogen at room conditions to obtain the N_2 boil-off mass flow rate.
- 3) The temperature difference across the gas flows (δT) is then found by comparing the heat capacity of the helium flow to the N_2 mass flow times the latent heat of LN_2 , i.e.,

$$\dot{m}_{\text{N}_2} \lambda_{\text{N}_2} = \dot{m}_{\text{He}} C_{p\text{He}} \delta T$$

or:

$$\delta T = \frac{\dot{m}_{\text{N}_2} \lambda_{\text{N}_2}}{\dot{m}_{\text{He}} C_{p\text{He}}}$$

- 4) The effectiveness is calculated by the equation:

$$e = \frac{\Delta T}{\Delta T + \delta T}$$

where ΔT is the temperature difference between the gas entering the warm end and the gas leaving the cold end.

A sample calculation of the data reduction procedure is shown on the following page. Table 3 shows the reduced data for the five flow points observed during the test.

The calculated effectiveness of the exchanger, extrapolated to operation conditions, is almost 93 percent. The design effectiveness was 99 percent and the required effectiveness is 98.5 percent. A linear extrapolation of the five helium flow vs. nitrogen boil-off points shows a 32 percent boil-off at zero flow (Figure 9). This, along with the poor vacuum of 25×10^{-3} Torr under which the test was run, is indicative of a large heat leak in the testing system. Correction of the boil-off data for the maximum flow point recorded (4.35 inches H_2O @ 52 percent boil-off) gives an efficiency of 97.11 percent. It is believed that the linear extrapolation is conservative and that a concave curve, which opens upward, would be a closer approximation. This belief is given substance upon making reference to a graph of helium flow vs. nitrogen boil-off for a similar high efficiency heat exchanger constructed several years ago by KI for General Electric (G.E. P.O. 002-206289) (Figure 10).

Effectiveness Data Reduction

(typical)

Data Point 1:

H₂ flow reading 2.5 inches H₂O, p = 14.6 psig

N₂ flow reading 43 percent

Helium Mass Flow

$$Q_{\text{air}} (\text{scfm}) = 2.5 \left(\frac{100 \text{ scfm}}{8 \text{ in H}_2\text{O}} \right) = 31.25$$

viscosity correction factor is .912

$$\text{for } \mu_{\text{He}} = 1.98 \times 10^{-4} \text{ poise}$$

$$\mu_{\text{air}} = 1.80 \times 10^{-4} \text{ poise}$$

$$Q_{\text{He}} (\text{scfm}) = .912 \times 31.25 = 28.5$$

$$\dot{m}_{\text{He}} = Q_{\text{He}} \rho_{\text{He}} = \frac{\left(28.5 \frac{\text{ft}^3}{\text{min}} \right) \left(1.11869 \times 10^{-5} \frac{\text{lb}_m}{\text{in}^3} \right)}{60 \frac{\text{sec}}{\text{min}}} \left(1728 \frac{\text{in}^3}{\text{ft}^3} \right) (454)$$

$$\dot{m}_{\text{He}} = 4.168 \text{ gm/sec}$$

$$\rho_{\text{He}} = \frac{29.3}{386.3 \times 565 \times 12}$$

Nitrogen Mass Flow

$$Q_{\text{N}_2} (\text{scfm}) = .43 (11.0 \text{ scfm}) = 4.73$$

$$\dot{m}_{\text{N}_2} = Q_{\text{N}_2} \rho_{\text{N}_2} = \left(4.73 \frac{\text{ft}^3}{\text{min}} \right) \left(.0753 \frac{\text{lb}_m}{\text{ft}^3} \right) \left(60 \frac{\text{min}}{\text{sec}} \right) (454 \frac{\text{gm}}{\text{lb}_m})$$

$$\dot{m}_{\text{N}_2} = 2.695 \text{ gm/sec}$$

$$\rho_{\text{N}_2} = \frac{14.7 \times 144}{55.16 \times 510}$$

Effectiveness Data Reduction

(continued)

δT and ΔT

$$\dot{m}_{H_2} C_p \delta T = \dot{m}_{N_2} \Delta h_{N_2}$$

$$\delta T = \frac{\dot{m}_{N_2} \Delta h_{N_2}}{\dot{m}_{H_2} C_p}$$

$$\Delta h_{N_2} = 1310 \frac{\text{cal}}{\text{mole}} = 195.83 \frac{\text{watt} \cdot \text{sec}}{\text{gm}}$$

$$C_p = 1.25 \frac{\text{BTU}}{\text{lb}_m \cdot ^\circ\text{F}} = 2.9042 \frac{\text{watt} \cdot \text{sec}}{\text{gm} \cdot ^\circ\text{F}}$$

$$\therefore \delta T = \frac{2.695 \times 195.83}{4.168 \times 2.9042} = 43.59 \text{ } ^\circ\text{F}$$

$$\Delta T = 118^\circ \text{F} - (-260^\circ \text{F}) = 378^\circ \text{F}$$

Effectiveness:

$$\epsilon = \frac{\Delta T}{\Delta T + \delta T}$$

$$\epsilon = \frac{378}{378 + 43.59} = .8966$$

\dot{m}_{He} Helium Mass Flow (gm/sec)	\dot{m}_{N_2} Nitrogen Mass Flow (gm/sec)	Effectiveness (%)
4.1687	2.695	89.66
5.3360	3.134	90.82
5.6753	3.008	91.80
6.2380	3.259	92.09
6.7700	3.259	92.826

Table 3 - Mass Flow Rate, Nitrogen Boil-Off, Thermal Effectiveness

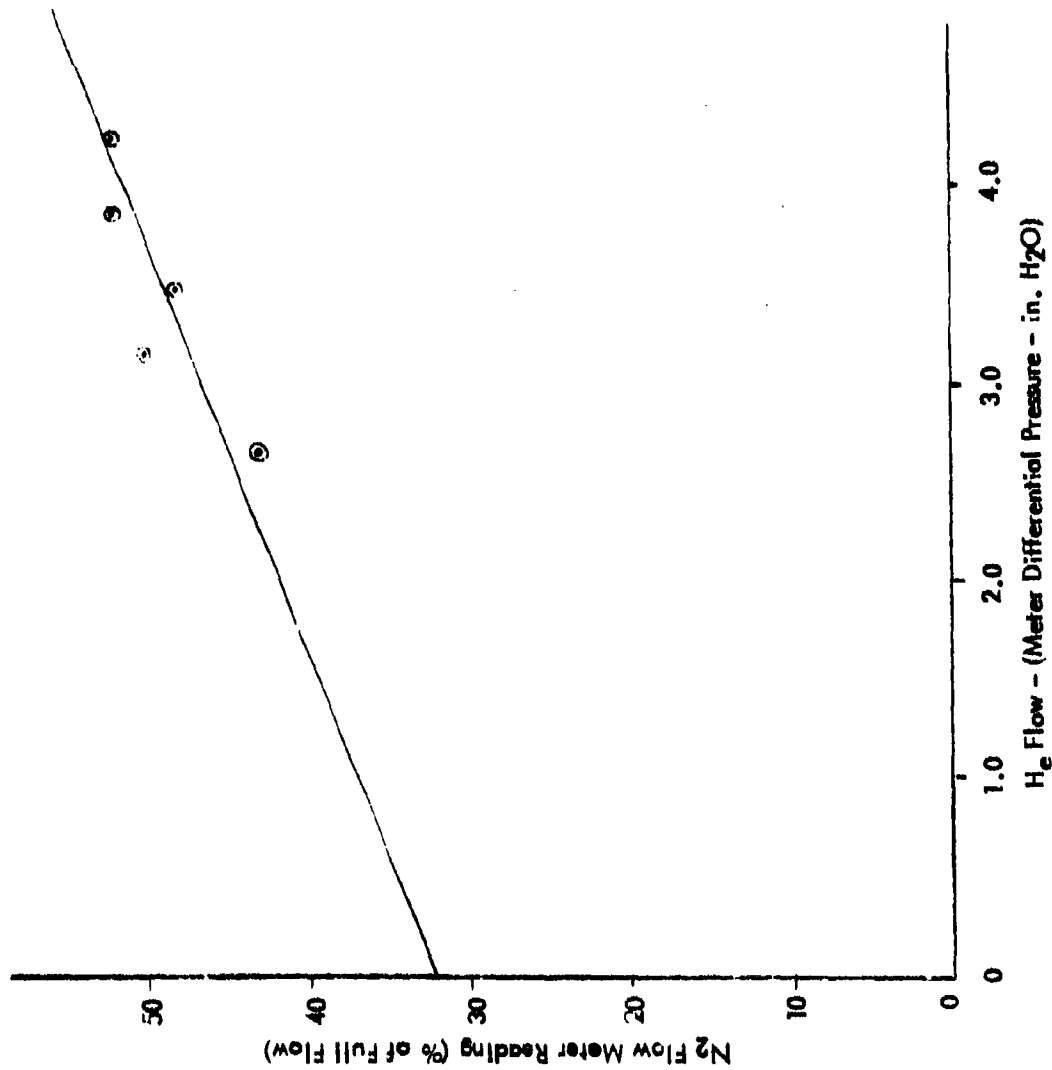


FIGURE 9 - HELIUM FLOW VS. NITROGEN BOIL-OFF

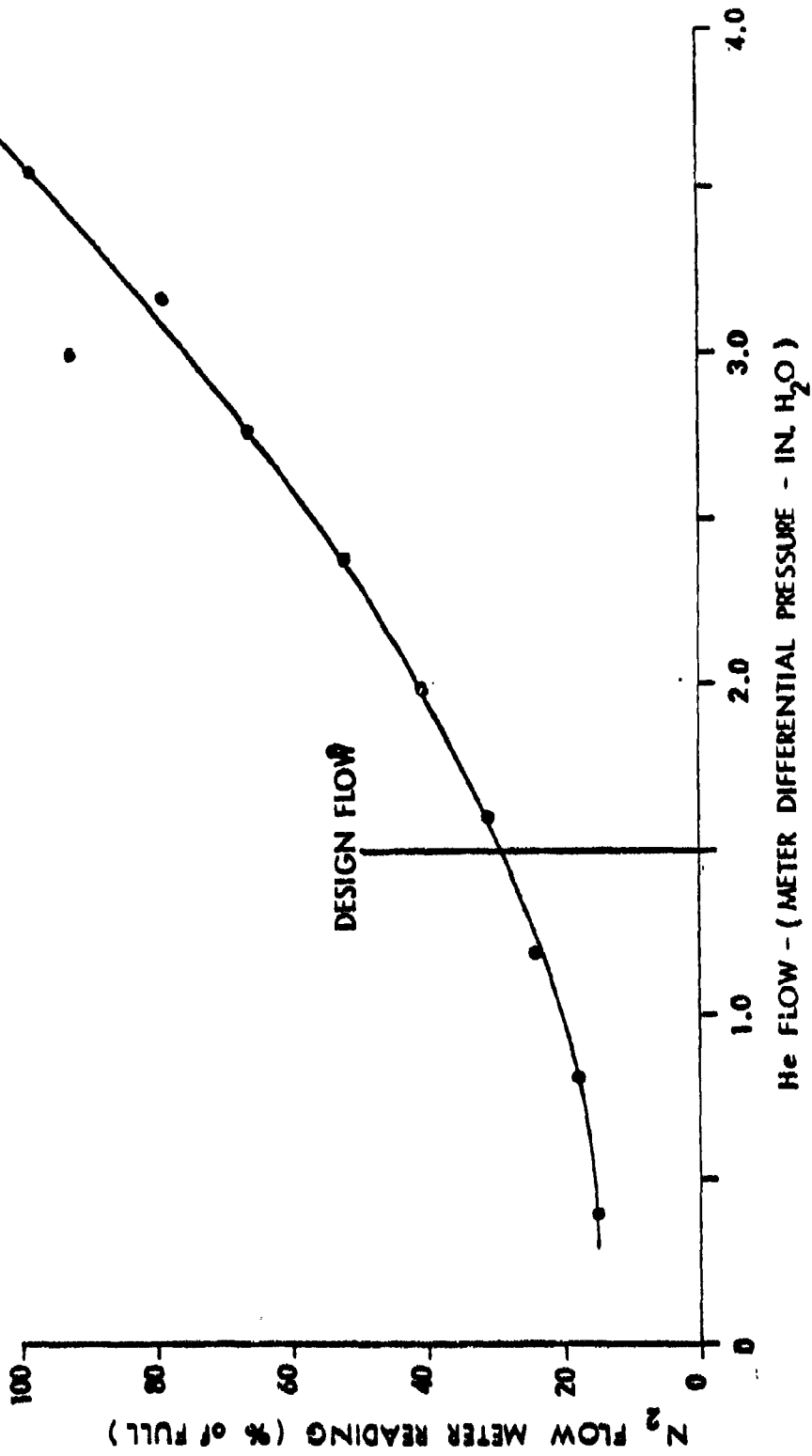


FIGURE 10 - HELIUM FLOW vs. N₂ BOILOFF
FOR G.E. AND AIR FORCE

V. SUMMARY AND CONCLUSIONS

Problems with the thermal testing system and time limitations were the main causes of the apparently inconclusive data on the performance of the heat exchanger. It is believed that the 93 percent effectiveness of the exchanger, which was determined from the one thermal performance test made, is due to leakage within the vacuum chamber, which can introduce severe heat leaks, and is not inherent in the heat exchanger itself. Extrapolation of the Helium flow vs. Nitrogen boil-off data points lend credence to this view. External leakage tests revealed no gross vacuum leaks, but the tests were made at room temperature and after the system had been exposed to helium gas. The background indicated by the helium leak detector was relatively high, due to helium and outgassing in the heat exchanger; this prohibited detection of medium and small leaks. Stream-to-stream leakage was small enough to have only minimal effects on the performance.

Future testing of the refrigeration system by General Electric will hopefully reveal the effectiveness which the heat exchanger is capable of attaining. Much knowledge has been gained in the design and construction of compact, high effectiveness, cryogenic heat exchangers through this program. It is believed that the state-of-the-art has been advanced by this heat exchanger.

Appendix VI

HEAT EXCHANGER ANALYSIS

RELATING RESULTS TO DESIGN CONDITIONS

To simplify testing, the data presented in this report were taken at temperatures slightly lower than the design condition temperatures. The data were taken at Reynolds numbers above and below the design condition Reynolds numbers.

HEAT TRANSFER DATA

The flow in the heat exchanger is in the laminar regime, but because each layer of screen must form a new boundary layer, the heat exchanger has developing laminar flow. The following correlation approximates the curves for stacked screens at low Reynolds numbers (Ref. 7, pp. 129-130):

$$St = Pr^{-0.66} Re^{-0.45} = NTU A_s/A_f$$

where:

$$St = h/Gc$$

$$Pr = uc/K$$

$$Re = GD/K$$

K = Thermal conductivity

$$u = \text{Viscosity} = 5.023 \times 10^{-6} \times T^{0.647} \text{ g/cm/sec}$$

c = Specific heat

h = Convective heat transfer coefficient

G = Mass flux

A_s = Heat transfer surface area

A_f = Flow cross section

D = Hydraulic diameter

NTU = Number of Transfer Units

The Prandtl number is a weak function of the absolute temperature, so the temperature dependence of the convective heat transfer coefficient is determined primarily by the viscosity. The following proportionality can then be used to scale heat transfer data taken at conditions other than the design conditions:

$$NTU \propto T^{0.66} / G^{0.45}$$

PRESSURE DROP DATA

Because the flow is laminar, the friction factor is proportional to the inverse of the Reynolds number:

$$f \propto 1/Re$$

$$\Delta P \propto Gu/\rho$$

$$\Delta P \propto GT^{1.647}$$

where:

$$Re = GD/u$$

$$f = \Delta P/4(L/D) (G^2/2\rho Af^2)$$

$$\Delta P = \text{Pressure drop}$$

$$L = \text{Length}$$

$$\rho = \text{Density}$$

The pressure drop is therefore generated at the warm end of the heat exchanger. The pressure drop can be scaled to design conditions by the ratio of the warm end temperatures raised to the 1.647th power.

DATA REDUCTION COMPUTER PROGRAM

The thermocouple measurements in millivolts, the pressure drop across the nozzle flowmeter, the pressure at the entrance of the nozzle, and the barometric pressure are inputs to a computer program that calculates the mass flow, temperatures, effectiveness, and NTU for each data point. The following paragraphs list the program and explain the variables. A sample run is also presented, which represents the initial data point in Table 8.

The program was originally designed to include the thermocouple measurements ΔT_1 and ΔT_2 in Figure 35. Because of the shorting of these thermocouples, the program was altered to ignore these readings. In the sample run, these thermocouples read zero.

Following is the nomenclature for Program HEDRI:

<u>Line</u>	<u>Symbol and Explanation</u>
170	TEST = test number; MO, DAY, YR = month, day, and year of the test.
180	MV1 MV6 = thermocouple millivolt readings (numbers 1, 2, 3, and 4 correspond to the thermocouples in Figure 35. Number 5 is the difference couple labeled ΔT_1 ; number 6 is the difference couple labeled ΔT_2).

<u>Line</u>	<u>Symbol and Explanation</u>
180	BAROM = barometric pressure in mm of mercury; P11N = pressure upstream of flow nozzle (psig); DPIN = Pressure drop across flow nozzle (in. water).
187	MVNOZ = thermocouple millivolt reading at the flow nozzle.
200	D1 = diameter of pipe upstream of flow nozzle (cm); D2 = diameter of flow nozzle throat (cm).
210	M = molecular weight of gas (g/mole).
220	CP = specific heat of gas (J/g°K).
230	MU = gas viscosity (poise).
240	TTAB = number of entries in temperature-millivolt table.
250	DTTAB = number of entries in temperature difference-difference-couple millivolt table.
550	DTLAV = lengthwise average temperature difference between heat exchanger. (This average is based upon four differences: the differences between absolute thermocouple readings at the two ends, and the difference couple readings at the two ends).
580	P1 = absolute pressure upstream of flow nozzle (bar).
600	DP = flow nozzle pressure drop (dynes/cm ²).
610	RHO = gas density upstream flow nozzle (g/cm ³).
620	ARSQ = area ratio squared.
630	A2 = area of flow nozzle throat.
640	MDOT = mass flow rate through nozzle, assuming nozzle coefficient = 1.0
650	NRE = Reynolds number, based on the mass flow rate.
660	CV = nozzle coefficient, based upon curve fit of American Society of Mechanical Engineers data.
670	MDOT = new mass flow rate, based upon nozzle coefficient.
700	EFF = thermal effectiveness.
710	NTUA = apparent NTU.
720	HT = heat transferred from stream to stream.

Figure 82 is a sample data run, which represents the initial data point.

HEDN1

08/18/75

```

1000 ----HEAT EXCH DATA REDUCTION----
101
1100 ----NOZZLE FLOW METER----
111
1200 ----REF. JUNCTIONS 1A4 AT 273.15 K AND 2A3 AT 77.35 K----
130 INTEGER TEST,MO,DAY,YR,1,TTAB,DITAB
135 REAL MV1,MV2,MV3,MV4,MV5,MV6,MVN0Z,PIIN,MU,NRE,MD0T,NTUA,MVA
140 DIMENSION MVA(20),TA(20),DTA(10),DMVA(10)
150 DATA (MVA(I), I=1,18)/0.,.0429,.219,.408,.610,.815,1.052,1.29,
151A 1.541,1.804,2.365,2.973,3.621,4.310,5.04,5.81,6.621,7.472/
154 DATA (TA(I), I=1,18)/77.35,80.,90.,100.,110.,120.,130.,140.,
155A 150.,160.,180.,200.,220.,240.,260.,280.,300.,320./
157 DATA (DTA(I), I=1,8)/77.,100.,140.,180.,220.,260.,300.,340./
158 DATA (DMVA(I), I=1,8)/60.,51.5,40.5,34.,29.8,26.7,24.1,22.1/
159
1600 ----INPUTS----
170 READ, TEST,MO,DAY,YR
180 READ, MV1,MV2,MV3,MV4,MV5,MV6
190 READ, BAR0M,PIIN,DPIN
195 MV1=MV1+5.5463; MV4=MV4+5.5463
196 PIIN=PIIN*2.306
197 MVN0Z=MV4
200 D1=6.35; D2=2.0252
210 M=4
220 CP=5.2
230 MU=200E-6
240 TTAR=18
250 DTTAR=8
251
3100 ----PRINT INPUTS----
320 PRINT,"TEST NO.",TEST
330 PRINT,"DATE: ",MO,"/",DAY,"/",YR
340 PRINT,"MILLIVOLT READINGS: 1,2,3,4,5,6"
350 PRINT,MV1,MV2,MV3,MV4,MV5,MV6
360 PRINT,"NOZZLE TEMP (MV)=" ,MVN0Z
370 PRINT,"BAR0M PRESS (MMHG)=" ,BAR0M
380 PRINT,"PRESS UPSTREAM NOZZLE (IN HG)=" ,PIIN
390 PRINT,"NOZZLE DELTA P (IN. HG)=" ,DPIN
400 PRINT,"NOZZLE DIA (CM): (1)=" ,D1," (2)=" ,D2
410 PRINT,"MOL WT (G/MOLE)=" ,M
420 PRINT,"SPEC HT (J/G K)=" ,CP
430 PRINT,"VISC (POISE)=" ,MU
431
4500 ----TEMPERATURES----
460 CALL INTERP(MVN0Z,TN0Z,MVA,TA,TTAB)
470 CALL INTERP(MV1,T1,MVA,TA,TTAB)
480 CALL INTERP(MV2,T2,MVA,TA,TTAB)
490 CALL INTERP(MV3,T3,MVA,TA,TTAB)
500 CALL INTERP(MV4,T4,MVA,TA,TTAB)
510 CALL INTERP(.5*(T2+T3),DTDM,DTA,DMVA,DTTAB)

```

Figure 82. Sample Data Run (Sheet 1 of 3)

HEDR1 08/18/75

```

520 D16=D1DM*MVA
530 CALL INTERPC(.5*(11+14),DTDM,D1A,DMVA,D11AR)
540 D15=D1DM*MV5
550 D1LAV=(11-12+14-13)*.5
560 D1EAV=(11-14+12-13)*.5
561
5800 -----FLOW RATE-----
590 P1=(P1IN+25.4+PAKQM)/750.
600 DP=DP1N+2490
610 RHO=P1*MZ(R3.14*INQZ)
620 ARSO=(DP/PI)*4
630 AP=.7854*D2*DP
640 MDOT=AP*(P.*RHO*DP*(1.-ARSO))*5
650 NRE=MDOT*(.7854*D2*MI)
660 CV=.7115*NRE*.02909
670 MDOT1=CV*MDOT
671
6900 -----THERMAL PERFORMANCE-----
700 FFF=D1LAV*(D1LAV+D1EAV)
710 NIUA=FFF*(1.-FFF)
720 HI=(CP*MDOT1+D1LAV)
721
7400 -----PRINT OUTPUT-----
750 PRINT,"INPUT"
760 PRINT,"T1=",11," DEG F"
770 PRINT,"T2=",12
780 PRINT,"T3=",13
790 PRINT,"T4=",14
800 PRINT,"TEMPERATURE DIFFERENCES"
810 PRINT,"DIFF COUPLE 5=",115," 12-13=",12-13
820 PRINT,"DIFF COUPLE 6=",117," 11-14=",11-14
830 PRINT,"EFF=",FFF
840 PRINT,"NUA=",NIUA
850 PRINT,"NRE=",NRE
860 PRINT,"NOZZLE COEF=",CV," OK FOR 2000<NRE<60000"
870 PRINT,"MASS FLOW (G/SEC)=",MDOT
880 PRINT,"HEAT TRANS (KAL/H)=",HI
930 STOP
935 END
936
9400 -----INTERPOLATION SHEET-----
950 SUBROUTINE INTERPC(XVAL,YVAL,AA,YA,NIAP)
960 DIMENSION XA(30),YA(30)
970 IF(XVAL-XA(1))94,90,90
980 90 1=2
990 91 IF(XVAL-XA(1))93,93,93
1000 92 1=1+11 IF(1-NIAP)91,91,91
1010 93 YVAL=YA(1-1)+(XVAL-XA(1-1))*(YA(1)-YA(1-1))/(XA(1)-XA(1-1))
1020 RETURN
1030 94 PRINT,"OUTSIDE RANGE OF THERMOCUPLE TABLE"

```

Figure 82. Sample Data Run (Sheet 2 of 3)

HEDR1 08/18/75

1040 STOP
1040 END

HEDR1 15:16 08/18/75

?1,7,22,75
?1.1852,0.7567,0.2438,0.6173,0.0,0.0
?750.07,1.5,9.7

TEST NO. 1
DATE: 7/ 22/ 75
MILLIVOLT READINGS: 1,2,3,4,5,6
6.7315000E+00 7.5670000E-01 2.4380000E-01 6.1636000E+00
0. 0.
NOZZLE TEMP (MV) = 6.1636000E+00
BAROM PRESS (MMHG) = 7.5007000E+02
PRESS UPSTREAM NOZZLE (IN HG) = 3.4590000E+00
NOZZLE DELTA P (IN. H2O) = 9.7000000E+00
NOZZLE DIA (CM): (1) = 6.3500000E+00 (2) = 2.0282000E+00
MOL WT (G/MOLE) = 4
SPEC HT (J/G K) = 5.2000000E+00
VISC (POISE) = 2.0000000E-04
OUTPUT
T1 = 3.0259695E+02 DEG K
T2 = 1.1715610E+02
T3 = 9.1312169E+01
T4 = 2.8872010E+02
TEMPERATURE DIFFERENCES
DIFF COUPLE 5 = 0. T2-T3 = 2.5843928E+01
DIFF COUPLE 6 = 0. T1-T4 = 1.3876850E+01
FFF = 9.0600180E-01
APPAR. NTU = 9.6385012E+00
NRE = 3.0571199E+04
NOZZLE COEF = 9.4084347E-01 BK FOR 2000 < NRE < 60000
MASS FLOW (G/SEC) = 9.3582964E+00
HEAT TR NS (WATT) 9.3153120E+03

PROGRAM STOP AT 930

Figure 82. Sample Data Run (Sheet 3 of 3)

EFFECT OF HELIUM LEAKAGE, THERMAL RADIATION, AND AXIAL CONDUCTION ON HEAT EXCHANGER PERFORMANCE

STREAM-TO-STREAM LEAKAGE

If radiation and conduction are ignored and if there is no leakage to the casing, the control system shown in Figure 83 can represent heat exchanger 7.

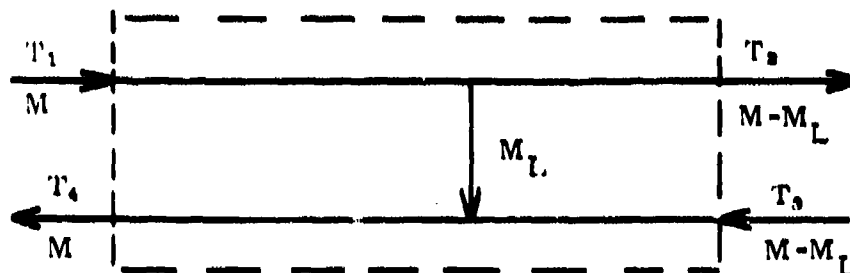


Figure 83. Stream-to-Stream Leakage

In Figure 83:

- M_L = Stream-to-stream leakage
- M = Heat exchanger mass flow
- T_1 = Temperature of the gas from the compressor
- T_2 = Temperature of the high pressure gas leaving the heat exchanger
- T_3 = Temperature of the gas returning from the nitrogen dewar
- T_4 = Temperature of the low pressure gas leaving the heat exchanger
- C = Specific heat of the gas

$$(M - M_L)C(T_3 - T_2) + MC(T_1 - T_2) = 0$$

$$\frac{M_L}{M} = 1 - \frac{T_1 - T_4}{T_2 - T_3}$$

LEAKAGE TO CASING

The casing of the heat exchanger is connected to the warm end of the low pressure stream. A leak to the casing therefore bypasses the low pressure stream. Assuming the radiation and conduction are negligible and assuming there is no stream-to-stream leakage, the control system shown in Figure 84 represents the heat exchanger.

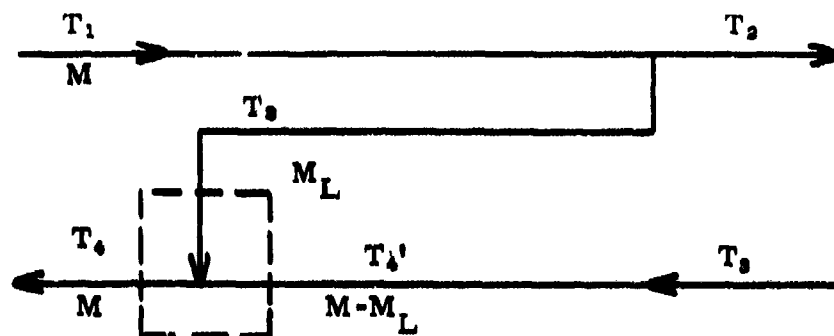


Figure 84. Leakage to Casing

In Figure 84:

T_4' = Low pressure stream temperature before mixing

M_L = Leakage to the casing

T_1, T_2, T_3, T_4 = Temperatures as defined in Figure 83

An energy balance for the above control system yields the following relationship between the mass flows and temperatures:

$$M_L CT_3 + (M - M_L) CT_4' = MCT_4$$

$$\frac{M_L}{M} = \frac{(T_4' - T_4)}{(T_4' - T_3)}$$

The following approximation can be made to simplify the above equation:

$$T_4' \leq T_1$$

This approximation approaches an equality as the effectiveness of the heat exchanger (without a leak) increases and as the size of the leak increases. This equation essentially notes the fact that a heat exchanger with unbalanced flow will have a pinch at one end. This approximation can be combined with the previous equation to yield the following equation for calculation of the leakage to the casing of the heat exchanger:

$$\frac{M_L}{M} \leq \frac{(T_1 - T_4)}{(T_1 - T_3)}$$

THERMAL RADIATION AND AXIAL CONDUCTION

The control system in Figure 85 shows the effect of thermal radiation and axial conduction on the performance of the heat exchanger. It is assumed that the leakage in the heat exchanger can be neglected.

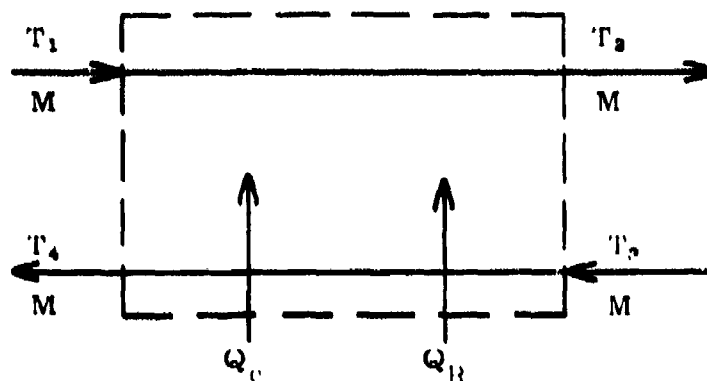


Figure 85. Radiation and Conduction

where:

Q_R = Radiation to the heat exchanger

Q_C = Conduction down the heat exchanger

T_1, T_2, T_3, T_4 = Temperatures as defined in Figure 83

The following energy balance can then be written to show the effect of thermal radiation and axial conduction on the temperatures in the heat exchanger:

$$MC(T_1 - T_4) + MC(T_3 - T_2) + Q_R + Q_C = 0$$

$$\frac{Q_R + Q_C}{MC} = (T_3 - T_2) - (T_1 - T_4)$$

Thermal radiation and axial conduction appear as a difference in the temperature differences at the warm and cold ends of the heat exchanger. If it were not for the leakage in the heat exchanger, this would provide a method for exact calculation of the thermal radiation and axial conduction. The last data point in Table 8 has the least amount of leakage because the axial compression of the heat exchanger had been increased and the pressure difference between streams is small. The difference in the stream-to-stream temperatures at either end of the heat exchanger for this case is 1.4°K. This is in part caused by leakage, but it does provide an upper bound on the effect of radiation and conduction. This would decrease the effectiveness of the heat exchanger by 0.35 percent.

Appendix VII

REFERENCES

1. D. B. Colyer and W. R. Oney, High-Speed Cryogenic Alternator Development, Phase I Final Report, U.S. Army Mobility Equipment Research and Development Center Contract No. DAAK02-68-C-0320, Fort Belvoir, Va., July 1970.
2. R. B. Fleming, R. K. Terbush, and D. B. Colyer, Development of a Single Stage Cryogenic Turborefrigerator, Phase II Final Report, U.S. Army Mobility Equipment Research and Development Center Contract No. DAAK02-68-C-0320, Fort Belvoir, Va., March 1972.
3. D. B. Colyer et al., Design and Development of Cryogenic Turbo Refrigerator Systems, Phase A Final Report, Report No. AFFDL-TR-71-117, Air Force Flight Dynamics Laboratory Contract No. F33615-71-C-1003, Air Force Flight Dynamics Laboratory, Wright-Patterson Air Force Base, Ohio, December 1971.
4. D. B. Colyer et al., Design and Development of Cryogenic Turbo Refrigerator Systems, Phase B Final Report, Report No. AFFDL-TR-72-154, Air Force Flight Dynamics Laboratory Contract No. F33615-71-C-1003, Air Force Flight Dynamics Laboratory, Wright-Patterson Air Force Base, Ohio, April 1973.
5. D. B. Colyer et al., Design and Development of Cryogenic Turbo Refrigerator Systems, Phase C Final Report, Report No. AFFDL-74-93, Air Force Flight Dynamics Laboratory Contract No. F33615-71-C-1003, Air Force Flight Dynamics Laboratory, Wright-Patterson Air Force Base, Ohio, April 1974.
6. P. G. Wapato, Investigation of Thermodynamic Cycles and Components for Turbo-Type Refrigerators, AirResearch Manufacturing Company Draft, U.S. Air Force Contract No. F33615-68-C-1549, Wright-Patterson Air Force Base, Ohio, August 1970.
7. W. M. Kays and A. L. London, Compact Heat Exchangers, McGraw-Hill Book Company, New York, N. Y., 1964.
8. R. McFee, "Optimum Input Leads for Cryogenic Apparatus," The Review of Scientific Instruments, Vol. 30, No. 2, February 1959, pp. 98-102.

Preceding page blank